Independent review of the climate risk method for the NSW Regional Water Strategies Program

Independent Expert Panel

2 April 2020

APPENDICES

Note: The draft Methods Paper and background reports that the Panel reviewed for this report were not public at the time of the review.

CC BY

www.chiefscientist.nsw.gov.au/reports

APPENDICES

CONTENTS

Appendix 1: Statement of requirements
Appendix 2: DPIE-Water Methods Paper
Appendix 3: Macquarie region paper
Appendix 4: Lachlan region paper
Appendix 5: Bega region paper
Appendix 6: DPIE-Water presentation
Appendix 7: Additional advice provided by DPIE-Water: climate data used
Appendix 8: Additional advice provided by DPIE-Water: data assessment and headwater calibration guidelines
Appendix 9: National and state initiatives
Appendix 10: Climate data and information
Appendix 11: Strategic water planning under climate uncertainty
References

APPENDIX 1: STATEMENT OF REQUIREMENTS

Independent Expert Panel – Independent Review of Climate Risk Method for Regional Water Strategies

Background

The Regional Water Strategies (RWS) are investigating the resilience of NSW's water resources in the context of future climate variability and climate change.

Water management planning for river systems dominated by agricultural water use in NSW has previously been based on observed climate data from 1890. This time period is insufficient to accurately assess the risk of failure of water infrastructure, or potential impacts to identified water dependent assets. The RWS aims to improve the understanding of risk in these systems through the use of techniques to reconstruct a past climatic sequence using paleoclimate data analysis and utilize this past sequence to produce 10,000 years of plausible past climate sequences using stochastic data generation techniques.

The Department of Planning, Industry and Environment's (DPIE) Water Group used the above methods in the now completed Greater Hunter Regional Water Strategy. It is proposed to apply this method for RWS now being developed across the remainder of regional NSW. In addition, the remaining strategies will also incorporate NARCliM data to overlay the potential impacts of human induced climate change.

The Independent Expert Panel's purpose is to provide expert advice on the suitability of the methods used to produce these extended climatic sequences, and the applicability of the use of these datasets in determining long-term water security solutions for towns, industry, environment and Aboriginal communities across NSW.

The Panel will make recommendations about improvements to methods to incorporate new climate change data and consider the applicability of overlaying the paleo informed climate sequences with NARCliM climate change information.

Scope

Inclusions:

- Panel statement on expected future climatic characteristics related to water security across NSW's twelve regions for a period up to the next 40 years.
- Review of the suitability of the methods used to produce stochastically generated rainfall and evaporation data to characterise past climate.
- Review of the suitability of using downscaled rainfall and potential evapotranspiration data from climate models and other sources, to characterise future climate.
- Review of the suitability of combining paleoclimate informed stochastic datasets with NARCliM 1.0 climate model data to characterise future climate.
- Review of suitability of DPIE methods to produce plausible future climate characteristics, and application to hydrological models, including quality assurance methods
- Recommendations for improvements to DPIE methods that can be applied in short and medium terms.

Exclusions:

- Review of DPIE hydrological models
- Review of decision-making tools used to inform RWS options analysis datasets

Requirements

A panel including four internationally recognised climate experts will be established to review the method used by DPIE-Water to incorporate climate risk into the analysis underpinning Regional Water Strategies. This method involves integrating stochastic rainfall and evaporation data (that has been calibrated with observational records, paleo-climate and/or East Coast low frequency) with climate change data to conduct hydrological modelling to better understand future climate risks to water resources. The Panel may be called on again, during the Regional Water Strategies development process, to consider if the methods developed should be amended to include new information as a result of the release of NARCliM 1.5 - which will become available from late 2019.

APPENDIX 2: DPIE-WATER METHODS PAPER

Developing climate data sets for use in climate risk assessment for Regional Water Strategies

WATER BRANCH - WATER MODELLING UNIT

Developing climate data sets for use in climate risk assessment for Regional Water Strategies

Version History

Version	Author(s)	Comments	Date
1.0	Richard Beecham	Initial draft for comment	03/04/2019
2.0	Richard Beecham	First draft for discussion	29/09/2019

Executive Summary

Contents

Executive Summary 3

Introduction 5

- Purpose of method 6
- Purpose of paper 6

Regional Water Strategies 7

- Adaptation to climate risk 7

Modelling framework 8

- Modelled assessment of water security 8

Climate data for risk assessment 10

- Historic data characteristics 10
- Enhanced data sets 10
  - Rationale 10
  - Statistically extended data sets of climate variability 12
  - Paleo-climatological extension of climate variability 12
  - Developing these extended statistical data sets of variability 12
- Climate change 16
  - Climate models 16
  - Discussion of outcomes from climate models 17
  - Incorporating change into climate risk data sets 18
  - Factoring in climate change 20
- Quality assurance 21

References 22

Introduction

Water planning in NSW is driven by community expectations and by climatic conditions in different regions.

Much of the water related development and planning took place based on a lived experience of climate conditions, i.e., what our communities going back several generations have experienced, and recorded in hydro-climatic data.

This hydro-climatic data is used as input to computer models of our river systems. This data combined with modelled representations of the physical and management features of our river systems can be used to test arrangements to share water across different consumptive use sectors and to the environment. The rules for distribution are guided by legislation and policy, with input from the community. The models are used in this process to determine overall water availability under different sharing and infrastructure scenarios.

The climate we have used to determine current sharing arrangements is characterised in the data collected on rainfall and temperature going back to the late nineteenth century, and evaporation since the 1970s. However, with recent experience of droughts, concerns are increasing that changes in climate arising from increased greenhouse gas emissions may make droughts more severe.

Using observed climate alone is increasingly considered insufficient to characterise climatic risk to water security, and hence we need to augment observed climate for water security investigations.

In a world where there were minimal anthropogenic influences on climate, this would mean we would at a minimum need to represent climate variability better, most notably the likelihood of extended droughts longer than those we have observed since the late 19th Century. However, the effects of greenhouse gas emissions means that the future climate cannot be characterised solely by the past. It will be different, the challenge is to understand how it will be different, and we need to use contemporary climate change science for this purpose.

The climate data will be used in established computer models of NSW river systems to test our existing water sharing arrangements and identify any notable vulnerabilities in important water security related outcomes, such as urban centres running out of water for extended periods, insufficient water to maintain ecosystem health, and decline in reliability of water supply for agriculture. These impacts will be assessed within a risk framework of consequence and likelihood, and measures formulated and tested to reduce these vulnerabilities.

The climate data we will develop will still include significant uncertainty. We need to understand and communicate this uncertainty and impacts on modelled water security outcomes, and consider this alongside other sources of physical and behavioural uncertainty affecting water availability and water use in our river systems.

The development of these methods for modelling climate variability and climate change are a major enhancement compared to historical practice, and provide a better basis to understand climate risk to water security. We have also designed these methods to allow for improvement in data and methods as science and policy evolves.

Purpose of method

We want to develop climate risk data sets that will better inform risks to water security using a more comprehensive understanding of climate variability and plausible change.

The climate risk data sets need:

(i) a more comprehensive representation of climate variability than is provided by the current practice of using historically recorded datasets, and

(ii) to consider plausible changes in climate.

To provide the comprehensive representation of past climate variability, we are developing stochastic datasets based on the statistical characteristics of past climatic conditions over the past 1000 years, reconstructed using indirect measures of climatic conditions going back several centuries, known as paleo-climate data.

The development of datasets to show plausible future changes in climate are informed by ongoing global climate modelling investigations. We acknowledge there are different levels of confidence in the direction and magnitude of these changes, and challenges in formulating these results into suitable inputs to our river system models.

The level of confidence in climate change outcomes varies across NSW. Some regions show a high level of agreement in modelled outcomes between different climate models, with results supported by meteorological principles and observations. However, for other regions, there is considerable variability in modelled outcomes between different climate models, and observations of recent climate are within ranges of natural variability.

Challenges in utilising existing climate model data within our models include the spatial resolution of the data combined with the comparative short length of the data sets at daily time steps. We intend to use these results accordingly, and communicate confidence levels in modelled datasets to decision makers.

The method does not include the water modelling that will be undertaken using these climatic sequences, nor of the assessment of river system vulnerabilities and options.

Purpose of paper

This short paper describes how we are developing the climatic risk data sets for Regional Water Strategies. This is as a draft initially for the purpose initially of enabling a review of the method by an Independent Expert Panel, and then as a basis to communicate the rationale to the community as part of the Regional Water Strategy program.

The paper is not intended to be highly technical; however, information that is more technical is contained in the references used to develop this paper, and to implement the methods.

Regional Water Strategies

The NSW Government is developing twelve regional water strategies to determine the best solutions for long-term water resource resilience – including policy, planning and infrastructure solutions. The objective of the Regional Water Strategy Program is to deliver resilient water resources for towns and communities, the environment, Aboriginal communities and industry.

In order to build this resilience, the strategies will be evidence based to provide a better understanding of current and future water needs. This will include improved data and knowledge about the risks arising from climate variability and change, to improve our ability to deal with extreme events.

Typically, the largest risks to water security, where available water is insufficient to meet critical demands, is during extreme droughts. The vulnerability of water dependent sectors to extreme droughts is y clearly a concern, especially for critical human water needs, high value permanent plantations, and key environmental assets. Managed river systems in NSW have allocation rules that operate to share water between the environment and different classes of water access entitlements. The decision on how these rules operate has been based on an understanding of climatic conditions such as have been experienced in the period when we have good records of rainfall, which extend back to the 1890s.

However, this vulnerability is much greater if we were to have a drought more severe than those that have occurred since 1890. We know that this is not only possible, it is probable, and could well occur sometime in the near future. Due to the short period of past climatic data, the risk of experiencing such a drought is not well understood. The Regional Water Strategy has committed to fully assessing these vulnerabilities through a deeper understanding of climate risks that will affect the water security.

The method proposed to assess the resilience of the modelled water management outcomes of water systems to more extreme variability and climate change is to test it with a wider range of plausible climate data sets than the one used to develop the water management arrangements (NWC, 2010). For a given scenario, the hydrologic models would be used with multiple input data sets, generating multiple output data sets.

If more critical outcomes such as urban water security fail too frequently based on results from these data sets, this indicates that there may be a problem with the resilience of these outcomes, and further measures should be considered to improve these. Where solutions are being proposed to address water security issues identified, these also need to be assessed that not only they are able to operate effectively during the observational record, but also that they are effective during more extreme drought periods.

Adaptation to climate risk

Future climate is subject to significant uncertainty, and this would be the case in eastern Australia regardless of global warming by virtue of our high variability. Decision making under uncertainty has long been a consideration in water resource management. However, we have strong signs that a better representation of plausible future climate is required.

While this report discusses primarily relevant science that informs climate risk, we acknowledge that other sources of uncertainty such as economic and societal also affect decision making, perhaps in a more significant way (Dessai, 2009; NWC, 2010). Methods to deal with science and other sources of uncertainty are discussed in these references and references therein. Further bottom-up methods are also of interest, (Brown et al. 2011; Cully et al. 2016)

Modelling framework

Modelled assessment of water security

The tool by which this will happen is the water models that DPIE Water has built, used and maintained to inform water policy and planning proposals and decisions of changes to water availability and use. The water models are complex, and consider the interactions between many different biophysical and management processes. This is shown as simply as possible at Figure 1. These have been developed for all regulated, and many unregulated river systems in NSW.

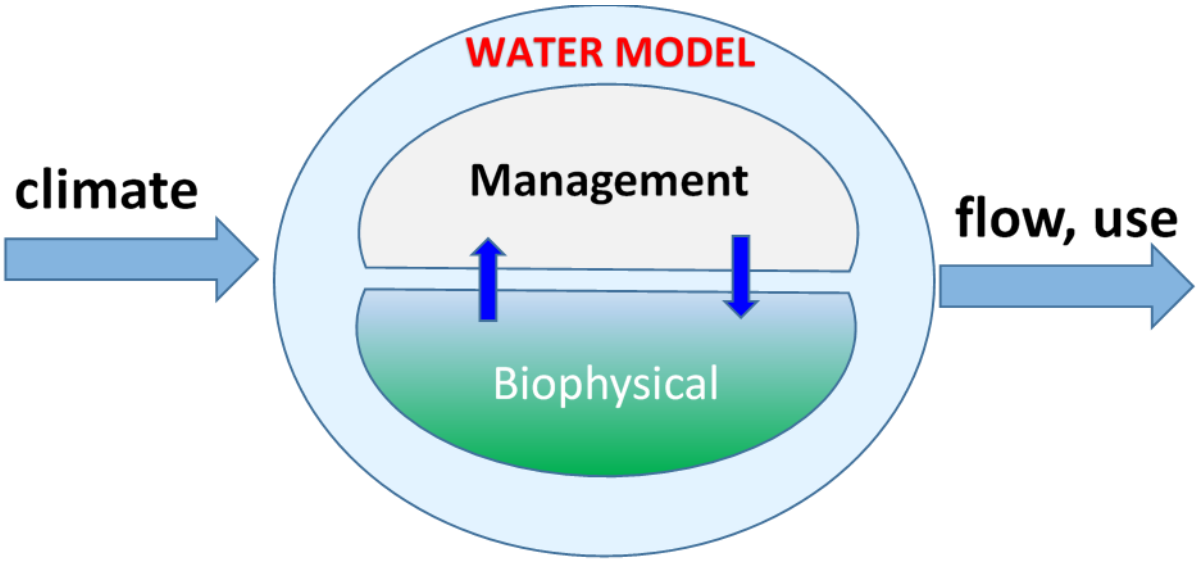

Figure 1 . Simplified illustration of water models used to inform Regional Water Security program

For simplicity Figure 1 indicates the model only produces outputs daily time series of flow and use, although in reality the models can produce a vast array of results at most locations in the river system, including volumes in storage, allocations, crop areas etc. These results are used produce metrics of direct relevance to understanding water security.

Examples of metrics include frequency, magnitude, and maximum intervals between flow events producing environmental benefits, or the percent of time water cannot meet urban water demand, or reliability of supply for the irrigation sector. An example of an integrating indicator would consider the volume in a large headwater storage, which would have a causal link to each of these sector specific metrics.

Figure 2 shows an example of modelled volume of water stored in a headwater storage over a period of sixteen years, with changes caused by inflows, evaporation, and releases of water to meet downstream environmental and consumptive demands. The particular sequences shows the storage partially filling at intervals, with periods where the storage is empty. These low volume periods would indicate periods of low water security caused in part by dry conditions. A metric of the percent of time a storage is empty, assessed over a significant period of climate variability would help us understand vulnerability in water security for urban supply provided by this storage, with different metrics providing information for other categories of user or environmental outcomes.

Further analysis of the impacts of climate change may produce a different metric, depending on the magnitude of change of either rainfall and/or potential evapotranspiration. While such results are not available at the time of writing, an example of sensitivity to climatic changes in the inflows responsible for increases to storage, is shown at Figure 3. This example shows reduced

inflow from higher evapotranspiration alone, as would be expected with the same rainfall falling on a drier soil. This is reduced further with lower rainfall, as less rain falls on a much drier soil.

The water security related impacts would be calculated when all such inflows are routed through the water model. This example would show an increase in the metric of percent of time a headwater storage is empty, with corresponding impacts on other water security related metrics.

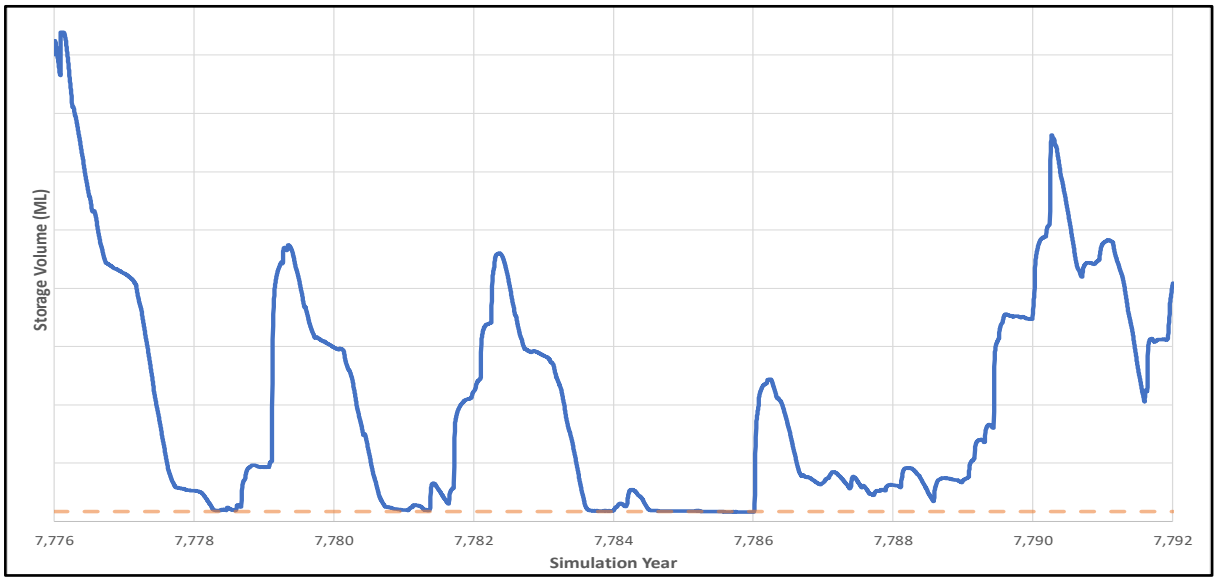

Figure 2 . Modelled volume of water stored behind a headwater dam for 16 year period

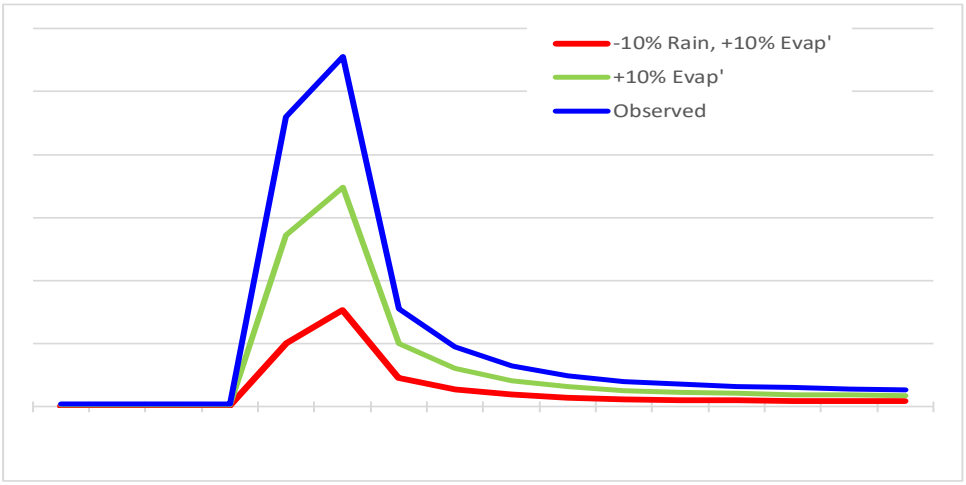

Figure 3 . Modelled sensitivity analysis of changes in flow from historic climate, with 10% increase in potential evapotranspiration, and combined with 10% decrease in rainfall

Climate data for risk assessment

Historic data characteristics

Areally extensive rainfall data has been collected since the late nineteenth century, and is stored primarily on the Bureau of Meteorology's databases. Standardised evaporation measurements have been collected since the early 1970s. This data is accessible through the Queensland Government's SILO database, which has infilled missing data to provide consistent, complete data across Australia for all climate variables since the late 19th century.

The observed rainfall is characterised by variability over different time scales. Figure 5 shows normalised annual rainfall totals at a site in central west NSW, and the cumulative departure from the mean of this data (also known as a residual mass curve (RMC)). The annual totals are colour coded by terciles to help in interpretation of inter-annual variability. The RMC allows for visualisation of multi-decadal variability.

The positive or negative gradients for segments of the RMC indicate periods of above or below average rainfall respectively. The rain totals in Figure 5 show a decade of positive gradient in the RMC, followed by five decades of negative gradient, then about five further decades of positive gradient. The respective average for these multi-decadal periods are 10% lower or higher than the long term average respectively. The actual totals show clustering of wet and dry years during these multi-decadal periods, interspersed by dry and wet years respectively. This characteristic is typical of much of NSW, with regional differences, particularly in the south.

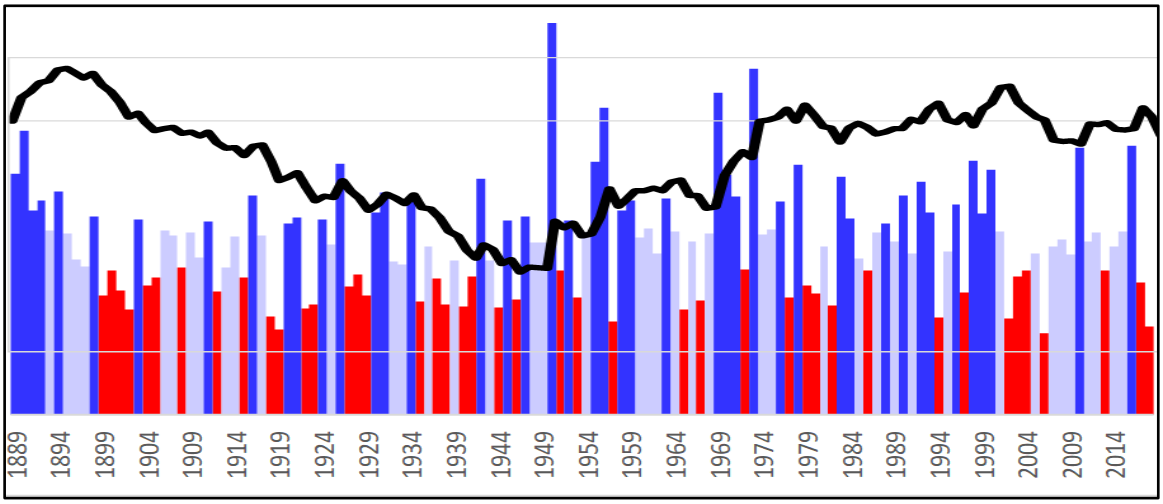

Figure 4. Climate variability in central west NSW. Annual rainfall totals are colour coded as terciles, with red and dark blue indicating driest and wettest 1/3 of years respectively. The thick black line is the cumulative departure from the mean of these annual totals.

Enhanced data sets

Rationale

The starting point to develop enhanced data sets to assess climate risk is to understand the key climatic drivers operating in the region of interest, and to base our characterisation of future climate on this. This is consistent with the approach promoted by Kiem and Verdon-Kidd (2013) for flood hazard assessment. They key drivers take the form of weather systems operating in and around Australia that either independently or in combination are responsible for rain (Figure 4). The base diagram (http://www.bom.gov.au/watl/about-weather-and-climate/australian-climate-influences.shtml) has been extended to include the Inter-decadal Pacific Oscillation (IPO), a large-scale multi-decadal driver that may amplify or attenuate the impact of the other

drivers on rainfall. For example, the rainfall patterns shown in Figure 5 can be explained in large part by different phases of IPO and El Nino / La Nina.

The prevalence of these systems is in turn dependent in part on the distribution of oceanic temperature anomalies and their interaction with the atmospheric circulation pattern. This prevalence of these systems has a natural variability. However, increasing greenhouse gas emissions could change that variability. In some cases, how these will change is understood reasonably well from climate change science outcomes including modelling, e.g. Southern Annular Mode or SAM). However, in some cases the direction and magnitude of change remains uncertain.

The relative importance of these key climatic drivers varies depending different parts of NSW. By characterising NSW as either north or south, and as either inland or coastal, we can summarise the dominant drivers:

A. Northern inland – IPO and El-Niño Southern Oscillation (ENSO)

B. Northern coastal - IPO and ENSO

C. Southern inland – IPO, SAM and Indian Ocean Dipole (IOD)

D. Southern coastal – East Coast Lows (ECLs).

For northern NSW, we will be using predominately the data based signals, as changes to IPO and ENSO based on climate change science is still uncertain. However, the climate science indicates some consensus in the direction and magnitude of projected in ECL from an analysis of NARCliM outputs (Pepler et al, 2016) and in SAM based on outputs from a high emission scenario simulations Phase Five of the Coupled Model Intercomparison Project (CMIP5) models (Lim et al, 2016).

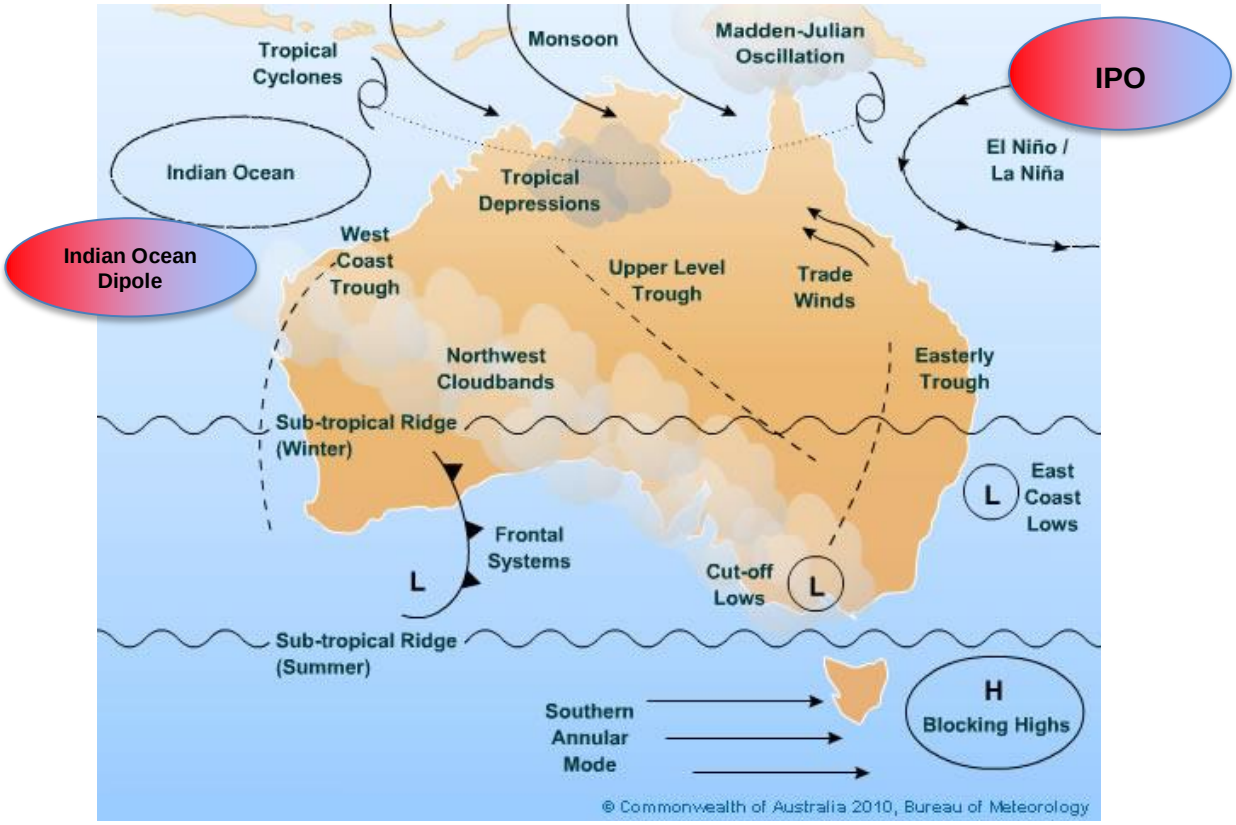

Figure 5. Australian climate influences, modified from Bureau of Meteorology 2010 (http://www.bom.gov.au/watl/about-weather-and-climate/australian-climate-influences.shtml)

Statistically extended data sets of climate variability

Given that natural variability of wet and dry periods is an important characteristic of NSW's climate, we decided that this is important to include in climate risk assessment, and to develop a more comprehensive understanding of climate variability through statistical means.

The complexity of extending climate data starts with simple statistical generation from what could be considered random climate variability. The complexity can be increased by explicitly considering major climate drivers of natural variability and change, and climatic persistence.

The simple statistical generation of extended climate sequences for climate risk analysis has been used to analyse water security for decades, using the statistical properties of observed rainfall and combining this with a random component to generate alternate sequences with similar statistical characteristics. From a sample of tens to hundreds of years of rainfall data, thousands to tens of thousands of years of data can be generated and analysed. The clustering of wet or dry years show in Figure 5, also known as persistence, can be incorporated statistically to produce more extreme sequences.

Paleo-climatological extension of climate variability

The uncertainty associated with the data generated stochastically generated is affected by how representative the sample data set is of long-term climate. While inter-annual variability has a sample of ~130 years of data to work with, we only have 2-3 of the multi-decadal phases represented, and this is a very small sample to work with of this important characteristic.

Palaeo-climatological studies using surrogate biophysical features in the region have been able to characterise climate going back several centuries (see Gel et al, 2009) to the last millennium (Vance et al, 2013). While these data sets are relative rather than quantitative, they clearly indicate different patterns of wet and dry periods, including multi-decadal droughts in the 11th to 14th centuries CE.

This degree of persistence is well outside of the range of variability within our historical data alone. However, we can use this as a complementary data set to characterise the variability of the multi-decadal cycles, within which the inter-annual variability is affected.

Developing these extended statistical data sets of variability

The expertise to undertake this work resides primarily outside this government department, but is available within climate research units at various universities. This work has been outsourced for the Regional Water Strategy, to generate extended climate sequences for all climate stations used in our water models using the historical data set alone, and to repeat this incorporating and extended paleo-climatological record of IPO to develop the multi-decadal variability.

The methods stratify historical data based on its occurrence in the negative or positive phase of the corresponding observational IPO, and develop multisite statistics from these separated data sets for rainfall and potential evapotranspiration, and generate separate sets of stochastic data. A parallel generation of IPO phase is generated using a longer sample of IPO phases developed from palaeo-climatological studies. The observational, palaeo-climatological and a 1000-year sample of generated IPO phases is show at Figure 6.

Following that, the separate stochastically generated data sets of rainfall for a corresponding length of time are spliced depending on whether the IPO is in positive or negative phase.

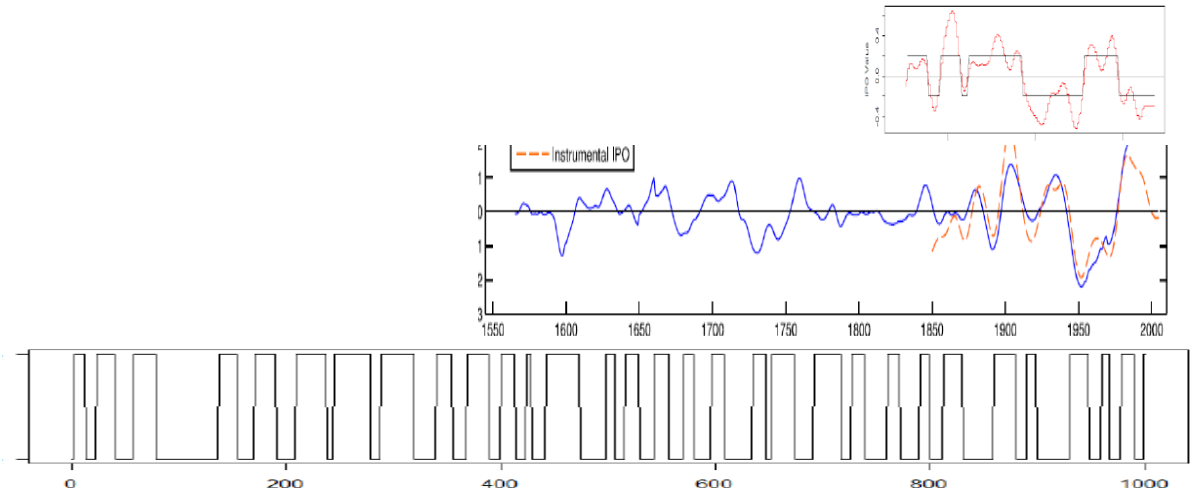

Figure 6. Observational (top), palaeo-climatological (middle) and generated (bottom) IPO phases (after Leonard et al, 2019)

We have completed this work for the Macquarie Valley (Leonard et al, 2019) and the Lachlan Valley (Verdon-Kidd, 2019). A similar project was also undertaken for the Bega Valley on the south coast of NSW (Kiem, 2019). Work is underway on other tributaries of the northern Murray Darling Basin, with those for the Border Rivers Valley, Gwydir Valley, Namoi-Peel Valley, and Barwon Darling River system all the subject of Regional Water Strategies. Inflows from Queensland tributaries are being modelled based on similar data sets.

The climate generation for these river systems need to be undertaken concurrently so that wet and dry periods, including multi-decadal cycles, are in harmony. This is particularly important where there is currently or potentially a hydraulic connection between river systems, such as happens with all northern tributaries flowing into the Barwon-Darling. This may also be important in considering relative contributions from northern and southern river systems for the Basin Plan.

An example of the complete 10,000-year sequence of annual rainfall is shown at Figure 2. As the detail of the annual totals is hard to discern for this much data, a 50 year moving average has been included as the black line to show the variability of relatively wet and relatively dry periods.

Annual rainfall totals for parts of this 10,000 year sequence have been included in Figure 3. The historical time annual time series is the graph at the top, followed by the 130-year sequence with the lowest mean and 130-year sequence, which includes the lowest 10-year mean. Each of these three graphs includes a line showing the 10-year moving average of annual total rainfall. The drought severity in the sequence with the lowest 10 year mean are likely to show modelled results with far less secure water supplies than anything we have experienced or planned for.

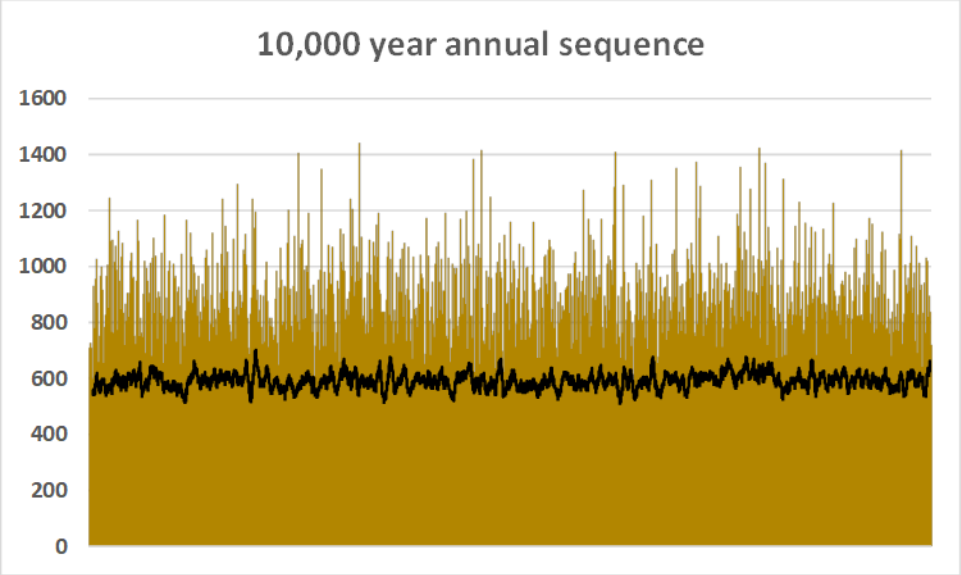

Figure 7 . 10,000-year sequence of generated annual rainfall totals including 50-year moving average

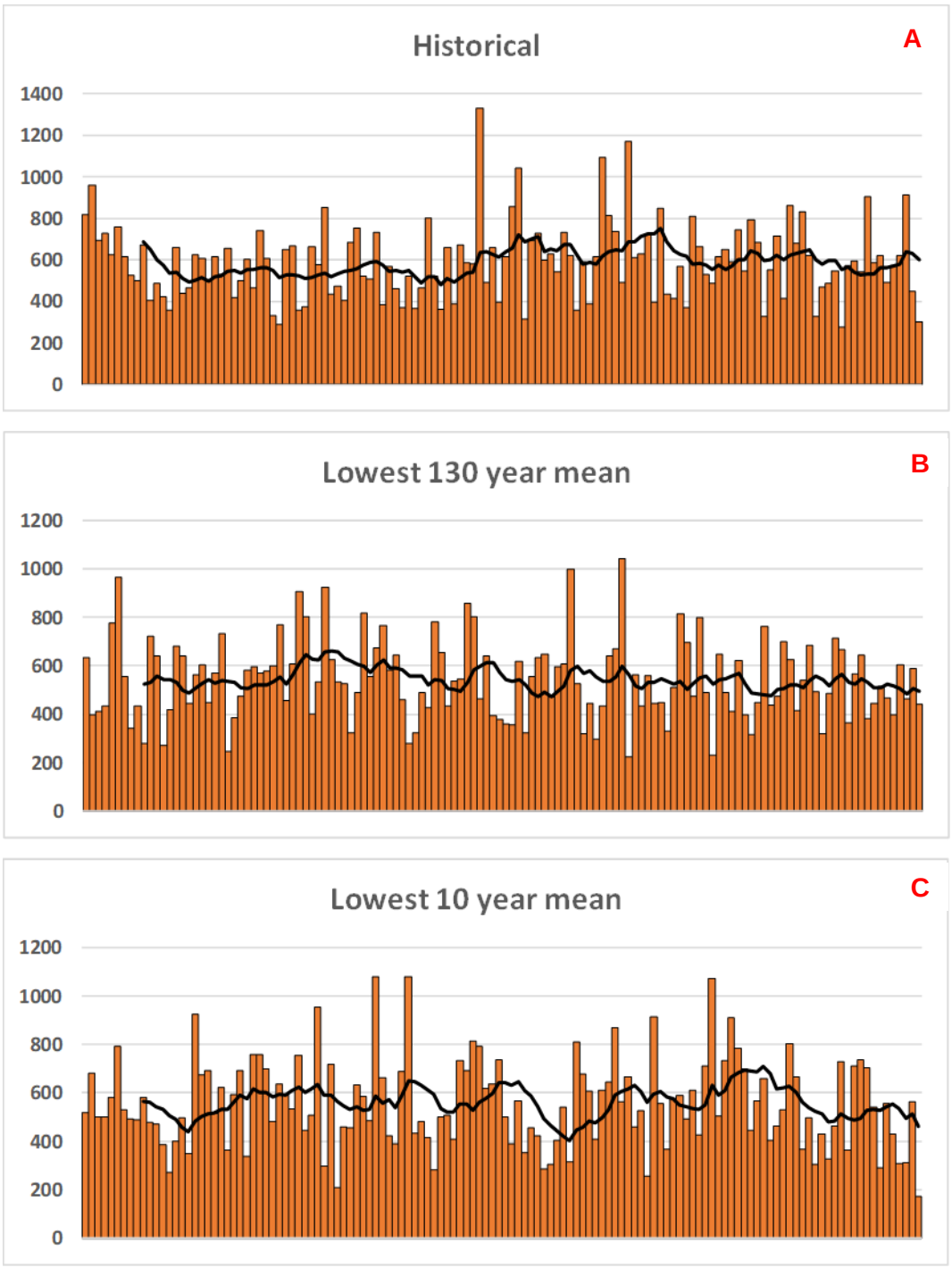

Figure 8. Three 130 year sequences of annual rainfall totals, including (A) historical since 1890-2019; (B) the 130 year sequence with the lowest mean from the 10,000 year generated sequence; and (C) the 130 year sequence which includes the lowest mean 10 year sequence. All three 130 sequences include black lines showing 10 year moving averages.

Climate change

The statistically extended data sets incorporating palaeo-climate information provide a comprehensive representation of climate variability under stationary conditions. We understand that climate change means that the stationarity assumption is not valid, and that future climate will be different. We discuss below what that difference may be, and how we intend to factor this difference into the climate risk data sets.

The differences we are interested in are in both of the primary climatic variables used in water balance modelling, that is: (i) rainfall, and (ii) potential evapotranspiration. The characteristics of rainfall are of particular interest as they affect water availability. These characteristics include daily and seasonal distributions, and inter-annual and multi-decadal variability. With potential evapotranspiration, because of its lower variability and its spatial coherence, we are mostly interested its changes in seasonal means.

The primary sources of information would be observational changes, and climate models. However, because of the high natural variability, it is statistically difficult to attribute climate change as a causal factor for observational change, although it could be considered as an additional line of evidence. For this reason, there is a reliance on climate models for information on likely changes. These also have considerable uncertainties, and the challenge is working with those uncertainties.

Climate models

Most of the predictions about how climate will change in the future come from Global Climate Models (GCMs). These are physically based simulation models, mathematically representing the interactions between the physics and chemistry of the entire major atmospheric, oceanic and land based processes that affect climate. To do this, the GCMs discretise the globe into three-dimensional layers from the deep ocean to the top of the atmosphere (Figure 9).

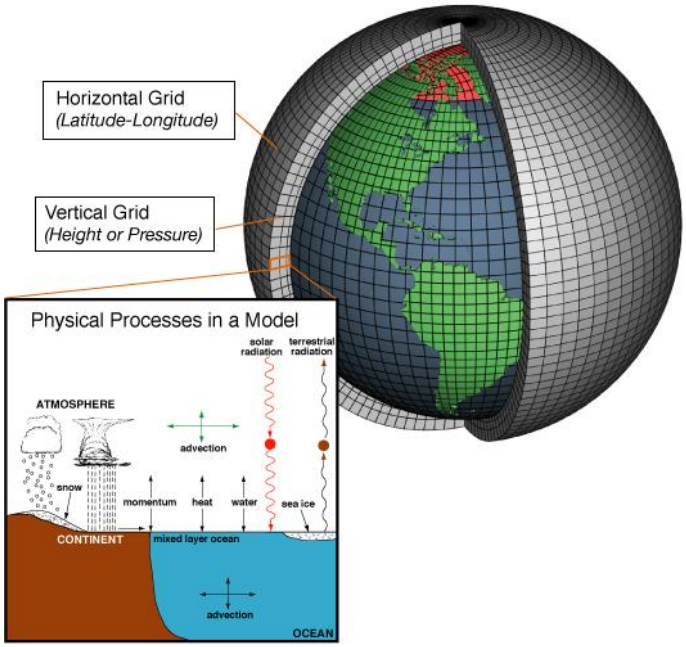

Figure 9. Simple schematic of a Global Climate Model (GCM)
https://www.climate.gov/file/atmosphericmodelschematicpng

These large, complex, computationally intensive models (41 as reported by IPCC (2014) are developed by major research institutions around the world, and form the basis of the periodic assessments undertaken by the United Nations' International Panel on Climate Change (IPCC).

Fuller descriptions of the range of models, including assessments of their ability to make realistic projections of climate, is beyond the scope of this paper, but can be accessed through IPCC (2014) and references therein.

Discussion of outcomes from climate models

The main challenges using the information from these models for climate risk assessment include (i) developing an understanding of the uncertainty in projected changes; and (ii) being able to formulate these changes to use as inputs to our water models.

The level of skill of GCMs in simulating climate parameters can inform the uncertainty in projections of change. This skill is assessed by comparing modelled results with observations. Higher skills scores indicate higher confidence that projected changes are robust. Further information on uncertainty can come from comparing the different GCMs. If all the models are in agreement, at least in terms of direction of change, again, we have higher confidence that projected changes are robust. For example, GCMs have a high level of skill in simulating temperature, and therefore projected simulated increases in temperature are likely to be robust. There is universal agreement between the models that temperature will increase, although there is some variation in the amount by which it will change. Other scientific lines of evidence support this change, most notably physics, and observations of increasing global temperatures.

GCMs generally have less skill in modelling all aspects of rainfall variability based on comparisons with observations. While these may for example be able to reproduce well enough a probability density distribution of daily rainfall compared to observations (Perkins et al, 2007), the models are not able to reproduce important characteristics that affect water security such as inter-annual and multi-decadal distribution. This is a factor affecting uncertainty in projections in rainfall under global warming, with a large range of projections for NSW (Figure 10).

There is relatively little agreement in northern NSW on the magnitude and direction of change of seasonal rainfall, with most projections falling within the range of natural variability.[1] There is a larger degree of consensus between models of significant reductions in winter and spring rainfall in the southern inland region of NSW, particularly the Murrumbidgee and Murray Rivers. Lines of evidence, including physics and atmospheric observations (Timbal and Drosdowsky, 2012), also support this drying.

A further change is projected in the southern coastal region of NSW, not so much from GCMs directly, as the resolution is too coarse for this, but from an analysis of NARCliM results showing a change in the frequency and seasonality of East Coast Low weather systems important for water security (Pepler et al, 2016).

There is evidence from modelled results, and supported by physics, of an increase in rainfall intensity particularly for high rainfall days. For example, a summer rainfall event that may have been 100 mm under historical conditions may in the future be 120 mm, meaning that some medium to major floods may be larger.

The other important climatic factor in determining water availability is potential evapotranspiration. These results from GSMs are fortunately far more reliable, partly because this are closely related to temperature.

[1] https://www.climatechangeinaustralia.gov.au/en/climate-projections/explore-data/summary-data-explorer/#

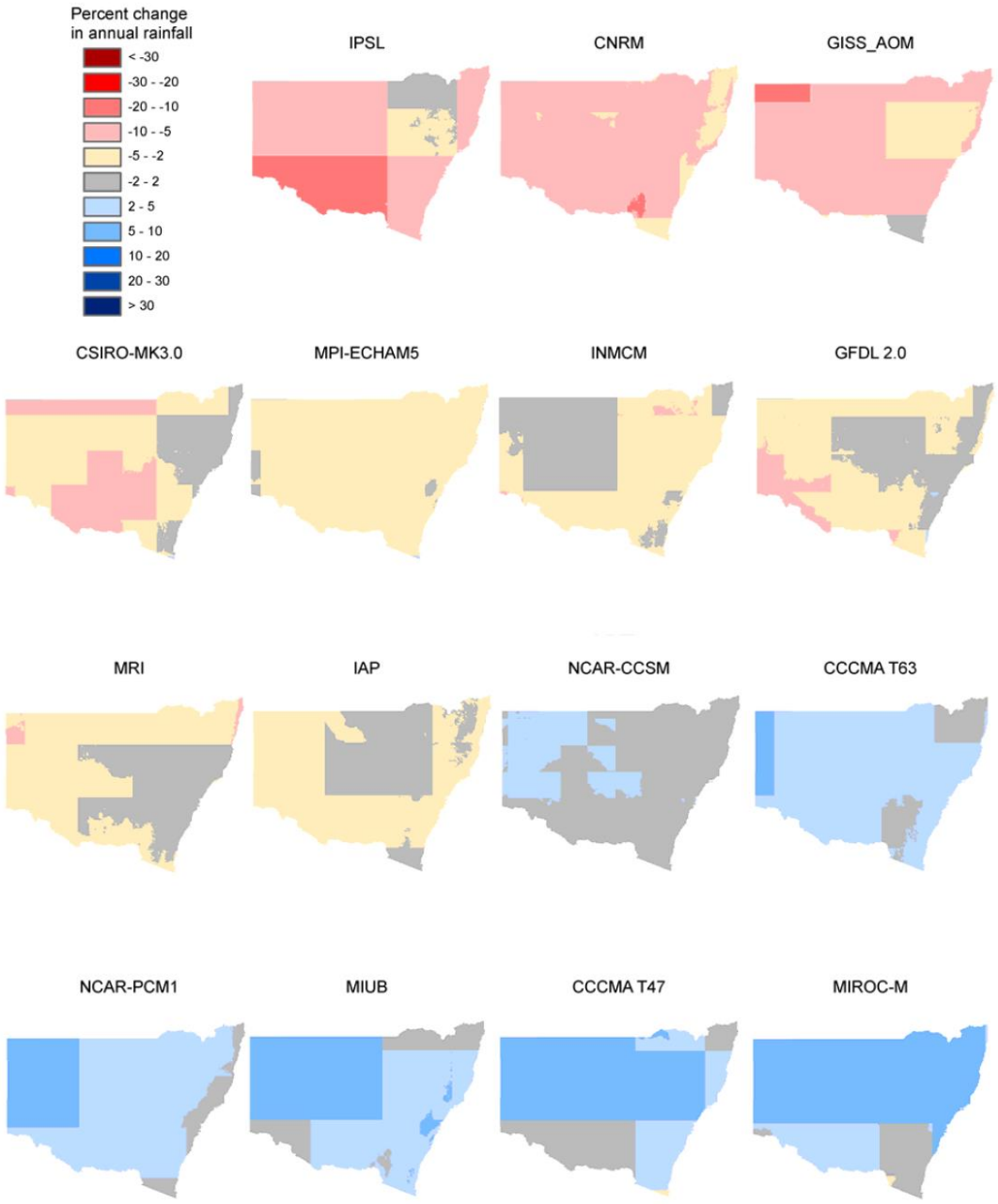

Figure 10. Percent change in mean annual rainfall across NSW and ACT regions (2030 relative to 1990) based on climate change projections from 15 GCMs for the medium global warming scenario.

Incorporating change into climate risk data sets

A limitation of directly using results from GCMs is the coarse spatial resolution of the results, compared to what water models need. Different methods known as downscaling have been developed to enable this, including factoring, statistical and dynamical (NWC, 2010). Dynamical downscaling has been deployed on a subset of the Coupled Model Intercomparison Project phase 3 (CMIP3) models for the NARCliM Project (Evans et al, 2014). The dataset produced by this project includes 4 GCMs re-modelled through finer resolution grids using 3 different Regional Climate Models (RCMs), producing a suite of 12 modelled results.

The GCM outputs for 3 different 20 year climate periods were used, 1990-2009, 2020-2039, and 2060-2079. The modelled results are at daily or sub-daily -step for suite of climate variables, including rain and potential evapotranspiration. The dynamical downscaling results have been

shown to significantly improve the performance of modelled outputs compared to the parent GCMs for the NCEP/NCAR re-analysis data set (see Fei et al, (2016; Fita et al (2016)). The spatial representation of rainfall more closely aligns with the observational pattern compared as demonstrated in (Figure 11).

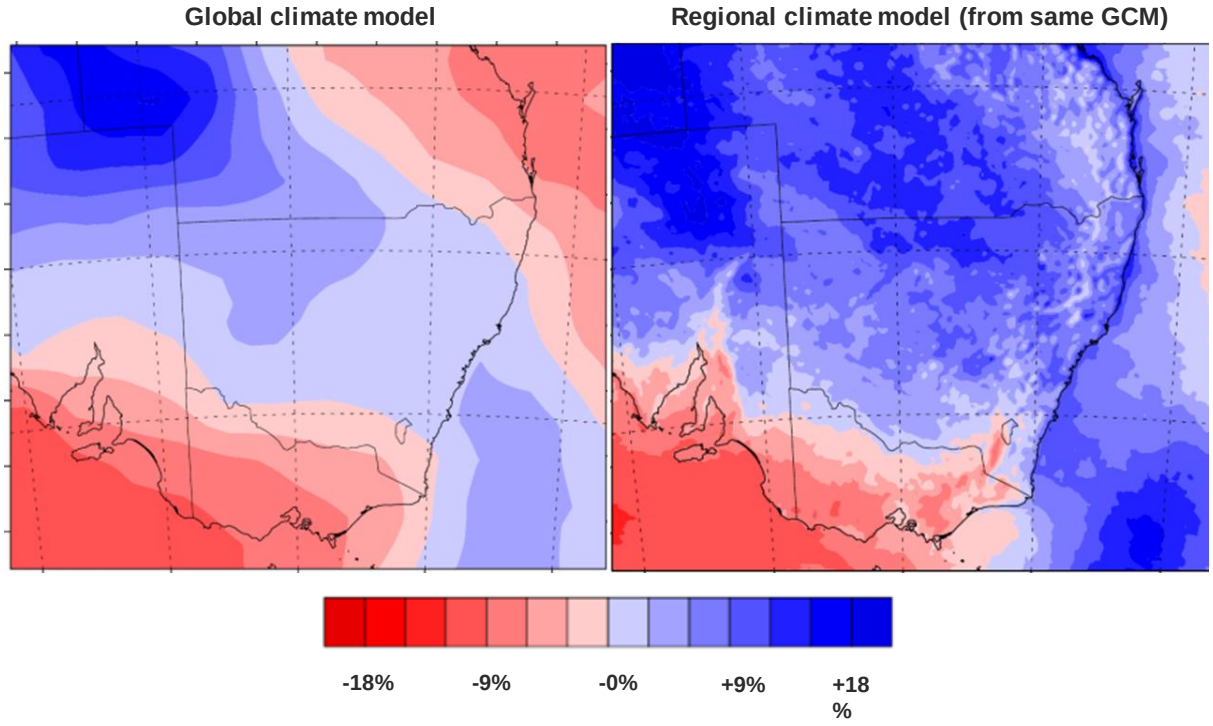

Figure 11. Improvements in spatial variability of rainfall based on NARCliM results

The results from the NARCliM project represent a significant improvement compared to the driving GCM. Consideration was given to using these NARCliM data sets directly. However, there are two significant reasons why this was not selected as the sole source of climate risk data.

The dynamical downscaling does not fully address limitations and uncertainties of the driving GCM (Fei et al, 2016). Therefore, the uncertainties in the skill of GCM to replicate important rainfall characteristics such as inter-annual and multi-decadal variability remain an issue. Dessai et al (2009) caution on an over-reliance on a small set of modelling results as under-representing the uncertainty in projections, and does not provide sufficient confidence for robust adaptive responses.

The other factor is the shortness of the modelled outputs, and the limitations this present in assessing water security. Notwithstanding the GCM/RCM limitations in reproducing longer scale variability, use of 20-year data sets in a region with the variability in rainfall experienced in NSW presents a large likelihood of mis-representing climate risk to water security. This is demonstrated using an analysis of observed data, a ‘perfect’ model of climate.

Selection of any 20-year period of observed annual rainfall, using the same data as shown in Figure 4, results in a mean rainfall (Table 1) ranging from 516 mm/y to 682 mm/y, or from 88% to 116% of the mean of all 20-year periods. Based on results of elasticity or runoff (Vaze et al, 2008), this equates to a 30-50% difference in mean water availability. A similar result for five-year samples, which are the scale that drought severity could be considered, produce a wider range of variability.

The comparison, of 20-year periods lagged by 30 years as a basis for reporting projected percentage changes in rainfall is also problematic, as shown in Figure 11 and reported Table 1. These calculations based on the same data set show that depending on the start date of the 'baseline' period, the rainfall 30 years later could be either 26% more or 13% less. The influence of using short duration rainfall records as a basis for concluding on changes in a variable climate needs further investigation.

Table 1. Statistics of means and ratios of means over different periods for a ~130 year sample of observed annual rainfall in Central West NSW.

Statistic	Ratio different 20 y periods	5 year moving average (mm/y)	20 y moving average (mm/y)
Mean	1.04	589	588
Maximum	1.26	861 *(+46%)*	682 *(+16%)*
Minimum	0,87	422 *(-28%)*	516 *(-12%)*

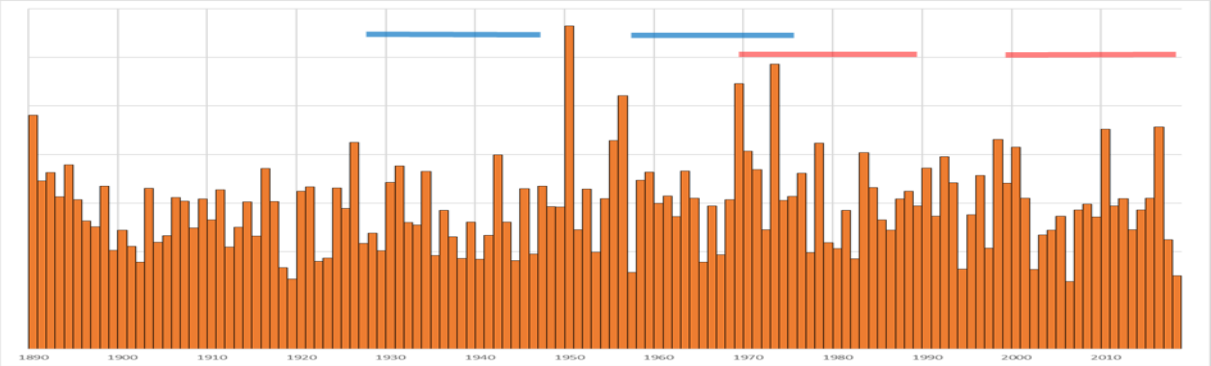

Figure 12. Impact of sampling ratios of 20-year rainfall totals of different periods within an observed rainfall time series. Blue bars indicate a 16% increase, whereas red bars indicate a 12% reduction.

Factoring in climate change

The advantages conferred by the dynamical downscaling approach of the NARCliM project are a significant advantage to using this data set for inclusion of change. The conclusions of Fei et al (2016) regarding the improvement compared to the driving GCM, and the more coherent spatial variability provide a sound basis for using these results compared to other methods.

This does not supersede the climate risk arising from variability. Therefore, the challenge is how to combine these. The changes we want to include are rainfall at all temporal scales, daily, seasonal, inter-annual, and multi-decadal.

The dynamically downscaled results are most reliable at daily and season scales. The comparative shortness of the data sets, and the limitations of GCMs to represent longer variability changes, means that the information is not there to work with to use dynamically downscaled results to vary these rainfall characteristics. However, inter-annual and multi-decadal variability is well represented in the stochastic data.

We decided that best use of the NARCliM rainfall data at this stage is to stress-test our water systems. For this reason, we have selected the GCM/RCM combination that had the lowest near future rainfall compared to the present day. The ratios of this data at the location of each of our rainfall stations used in the water models was calculated from the bias-corrected NARCliM

data sets, and used to re-factor the stochastic data set. The potential evapotranspiration results from the same NARCliM scenario was also used to factor the stochastically generated potential evapotranspiration results.

We understand that this tacitly accepts the same limitations discussed with using these ratios. However, the purpose of this change factoring is to provide a lower bound estimate of water availability to test the vulnerability of water security outcomes. The limitation identified does not preclude model results being used to test this objective, in this case the model developed is fit for purpose to answer the question being asked of it.

This method of generating stochastic data from historic and palaeo-climatic data sets, and then factoring by NARCliM results was (or will be) applied to three of the four regions. The important exception is for the south coast regions in NSW, where the change analysis was based on NARCliM derived changes to East Coast Low seasonal frequency, which were applied initially based on the availability of the East Coast Low synoptic database (Pepler et al, 2016) first, and then stochastic data generated from the perturbed data set

Quality assurance

Given the importance of this data set, we are undertaking due diligence by putting in place an additional quality control step in addition to the quality control processes undertaken by the suppliers of the data. This is so we can confirm the expectations of the data set are met for the stochastic data, and to understand the characteristics of the data set as it affects hydrologic regime. This additional quality control step is undertaken by DPIE independently, with any concerns identified raised with suppliers.

Analysis undertaken to date has been provided as feedback to improving the stochastic data sets. Further analysis will be undertaken to test the outcomes from using the NARCliM data sets, including testing of the nascent NARCliM 1.5 data set, which when finished will have a longer period of simulations, and potentially a means to better understand projected changes to inter-annual and multi-decadal variability.

References

Brown, C., Y. Ghile, M. Laverty, and K. Li, (2012), Decision scaling: Linking bottom-up vulnerability analysis with climate projections in the water sector, *Water Resources Research*, v. 48, pp 1-12: W09537, doi:10.1029/2011WR011212.

Culley, S., Noble, S., Yates, A., Timbs, M., Westra, S., Maier, H. R., Giuliani, M., and A. Castelletti (2016), A bottom-up approach to identifying the maximum operational adaptive capacity of water resource systems to a changing climate, *Water Resource Reseach*, v. 52, pp. 6751-6768, doi:10.1002/2015WR018253.

Dessai, S., Hulme, M, Lempert, R. and R. Pielke, Jr., (2009), Climate prediction: a limit to adaptation? pp. 64-78 **in** *Adapting to Climate Change: Thresholds, Values, Governance*, eds. W.N. Adger, I. Lorenzoni and K.L. O'Brien. Cambridge University Press (Cambridge).

Dey, R, Lewis, SC, Arblaster, JM, Abram, NJ. (2019). A review of past and projected changes in Australia's rainfall. *WIREs Climate Change*. https://doi.org/10.1002/wcc.577

Evans, J.P., Ji, F., Lee, C., Smith, P., Argueso, D., and L. Fita (2014). Design of a regional climate modelling projection ensemble experiment – NARCliM. *Geoscientific Model Development*, v. 7, no. 2, pp 621-629.

Fei, J., Evans, J., Teng, J., Scorgie, Y., Argueso, D., and A. Di Luca, (2016). Evaluation of long-term precipitation and temperature Weather Research and Forecasting simulations for southeast Australia. *Climate Research.* v. 67. pp 99-115.

Fita, L., Evans, J. P., Argüeso, D., King, A. and Y. Liu, (2016). Evaluation of the regional climate response in Australia to large-scale climate modes in the historical NARCliM simulations. *Climate Dynamics*, v. 49, nos. 7-8, pp 2815-2829.

Gell, P., Gergis, J., Mills, K., Baker, P., De Deckker, P, Finlayson, M.,5, Hesse, P., Jones, R. Kershaw, P., Pearson, P., Treble, P., Barr, C., Brookhouse, M., Drysdale, R. Haberle, S. Karoly, D., McDonald, J., Reid, M., Thoms, M., and J. Tibby (2009), *Palaeoclimate studies relevant to natural resource management in the Murray Darling Basin*. Report prepared for Murray Darling Basin Authority.

IPCC, (2013): *Climate Change 2013: The Physical Science Basis. Contribution of Working Group I to the Fifth Assessment Report of the Intergovernmental Panel on Climate Change* Cambridge University Press, Cambridge, United Kingdom and New York, NY, USA, 1535 pp.

Kiem, A.S., (2019). *Incorporating changes in East Coast Low (ECL) behaviour into stochastically generated hydroclimatic data for the Bega River region, New South Wales, Australia*. Report prepared for NSW Department of Industry by University of Newcastle, (unpublished).

Kiem, A.S. and Verdon-Kidd, D.C. (2013): The importance of understanding drivers of hydroclimatic variability for robust flood risk planning in the coastal zone. *Australian Journal of Water Resources*, 17(2), 126-134, doi:10.7158/W13-015.2013.17.2.

Leonard, M., Westra, S. and B. Bennett (2019). *Multisite Rainfall and Evaporation Data Generation for the Macquarie Water Infrastructure Project*, report prepared for NSW Department of Industry, University of Adelaide (unpublished).

Lim, E.-P., H. H. Hendon, J. M. Arblaster, F. Delage, H. Nguyen, S.-K. Min, and M. C. Wheeler (2016), The impact of the Southern Annular Mode on future changes in Southern Hemisphere rainfall, *Geophysical. Research. Letters.,* v. 43, pp. 7160–7167, doi:10.1002/2016GL069453

NWC (National Water Commission) (2010). *Incorporating Climate Change in Water Resource Planning*. Waterlines Report Series (May 2010).

Olson, R., Evans, J.P., Di Luca, A. and D. Argüeso, (2016), The NARCliM project: model agreement and significance of climate projections. *Climate Research*, v. 69, no. 3, pp 209-227.

Pepler, A.S., Di Luca, A., Ji, F., Alexander, L.V., Evans, J.P. and S.C. Sherwood, (2016): Projected changes in east Australian mid-latitude cyclones during the 21st century. *Geophysical. Research. Letters*. doi: 10.1002/2015GL067267

Perkins, S., Pitman, A.J., Holbrook, N.J., and J. McAneney. (2007). Evaluation of the AR4 Climate Models' Simulated Daily Maximum Temperature, Minimum Temperature, and Precipitation over Australia Using Probability Density Functions. *Journal of Climate*, v. 20, pp 4356-4376.

Pitman, A.J. and S.E. Perkins, 2008, Regional projections of future seasonal and annual changes in rainfall and temperature over Australia based on skill-selected AR4 models, Earth Interactions, 12, Paper No. 12, 1-50, doi: 10.1175/2008EI260.1.

Timbal B and Drosdowsky W (2012) The relationship between the decline of South Eastern Australia rainfall and the strengthening of the sub-tropical ridge, *International Journal of Climatology*, doi:10.1002/joc.3492.

Vance, T.R., Roberts, J.L., Plummer, C.T., Kiem, A.S. and van Ommen, T.D. (2015): Interdecadal Pacific variability and eastern Australian mega-droughts over the last millennium. *Geophysical Research Letters*, v.42, no. 1, pp. 129-137, doi:10.1002/2014GL062447

Vaze J.,Teng J., Post D., Chiew F, Perraud J-M., and D. Kirono, (2008), *Future climate and runoff projections (~2030) for New South Wales and Australian Capital Territory*, NSW Department of Water and Energy, Sydney

Verdon-Kidd, D.C., (2019), *Development of multi-site rainfall and evaporation data for the Lachlan Regional Water Strategy*. Report prepared for the NSW Department of Industry by University of Newcastle (unpublished).

Victorian Department of Environment Land Water and Planning (DELWP) (2016). *Guidelines for Assessing the Impact of Climate Change on Water Availability in Victoria*. 75p. (Victorian Government).

APPENDIX 3: MACQUARIE REGION PAPER

Multisite rainfall and evaporation data generation for the Macquarie Water Infrastructure Project by Michael Leonard, Seth Westra and Bree Bennett

Multisite Rainfall and Evaporation Data Generation for the Macquarie Water Infrastructure Project

Michael Leonard, Seth Westra, and Bree Bennett

DOCUMENT STATUS RECORD

Project Title: Multisite Rainfall and Evaporation Data Generation for the Macquarie Water Infrastructure Project
Client: New South Wales Department of Industry, Crown Lands and Water
Document Number: 2019/01
File Name: MacquarieRiver_StochasticGeneration_FinalReport_20190114.docx

Issue No.	Date of Issue	Description	Signatures	
			Authors	Approved
01	15/01/2019	Final Report	ML, BB, SW	SW

Disclaimer:

1. The Intelligent Water Decisions research group has taken all reasonable steps to ensure that the information contained within this report is accurate at the time of production. In some cases, we may have relied upon the information supplied by the client.
2. This report has been prepared in accordance with good professional practice. No other warranty expressed or implied is made as to the professional advice given in this report.
3. The Intelligent Water Decisions maintains no responsibility for the misrepresentation of results due to incorrect usage of the information contained within this report.
4. This report should remain together and be read as a whole.
5. This report has been prepared solely for the benefit of the client listed above. No liability is accepted by the Intelligent Water Decisions with respect to the use of this report by third parties without prior written approval.

Contact Details:

Intelligent Water Decisions research group
School of Civil, Environmental and Mining Engineering
University of Adelaide

Physical:
Engineering North Building
North Terrace Campus
University of Adelaide, Adelaide.

Postal:
University of Adelaide, Adelaide, 5005

Telephone: (08) 8313 5451
Fax: (08) 8313 4359

Executive Summary

The production of long 'stochastic' timeseries of climate variables such as rainfall and evapotranspiration is often used to supplement the historical climate record when conducting drought risk assessments. While historical data provides one realized set of climatic conditions, stochastic models enable the generation of extended synthetic climatic conditions which are just as plausible as those occurring in the past.

To this end, ten thousand years of jointly simulated stochastic data has been generated for 100 rainfall sites and 45 evaporation sites in the Macquarie River catchment, with seven different model variants developed to simulate the stochastic sequences with different assumptions regarding the role of natural climate variability and anthropogenic climate change. The 'historical' climate runs comprise 'Model A', which is the base model without climate partitioning, 'Model B' which accounts for shifts based on the instrumental record of the Interdecadal Pacific Oscillation (IPO), and 'Model C', which includes paleoclimate information to improve the estimation of the dwell time in each IPO phase. While all three model variants reflect the historical climate, 'Model C' is identified as the best representation of historical observations.

The performance of 'Model C' is evaluated in detail relative to historical rainfall and evaporation over the period from 1890 to 2018, and a high level summary is provided in Table 1 for rainfall sites and Table 2 for evaporation sites. The labels 'Overall Good', 'Overall Fair' and 'Overall Poor' are detailed in Section 2.5, and arise from the consistent application of a defined set of tests to all sites and a set of 20 relevant variables. Of the statistics presented here, 12 are identified as 'Overall Good', seven are identified as 'Overall Fair' and one is identified as 'Overall Poor'. An intermediate level summary can be found in the Section 3.1, and plots for each site can be found in the Annex documentation corresponding to each statistic.

Table 1 Rainfall evaluation summary of performance, Paleoclimatic IPO model variant, 100 sites 129 years length, 77 replicates. Traffic light criterion specified by systematic evaluation method (Section 2.5). Detailed plots for each site in Annex documentation.

Statistic	Evaluation of Model Performance	Detailed Statistics
Distribution of Annual Total Rainfall	**OVERALL – GOOD**	Annex A
Distribution of 2-year Rainfall Totals	**OVERALL – GOOD**	Annex A
Distribution of 5-year Rainfall Totals	**OVERALL – GOOD**	Annex A
Distribution of 10-year Rainfall Totals	**OVERALL – GOOD**	Annex A
Mean of Monthly Rainfall Totals	**OVERALL – GOOD**	Annex B
Standard Deviation Monthly Rain Totals	**OVERALL – FAIR**	Annex B
Distribution of Annual Proportion Wet Days	**OVERALL – POOR**	Annex C
Mean of Monthly Proportion Wet Days	**OVERALL – GOOD**	Annex D
Std. Dev. Monthly Prop. Wet Days	**OVERALL – FAIR**	Annex D
Annual 1-day Rainfall Maximum Distrib.	**OVERALL – GOOD**	Annex E
Annual 2-day Rainfall Maximum Distrib.	**OVERALL – FAIR**	Annex E
Annual 3-day Rainfall Maximum Distrib.	**OVERALL – FAIR**	Annex E

Table 2 Evaporation evaluation summary of performance, Paleoclimatic IPO model variant, 45 sites 129 years length, 77 replicates. Traffic light criterion specified by systematic evaluation method (Section 2.5). Detailed plots for each site in Annex documentation.

Distribution of Annual Total Evaporation	**OVERALL – GOOD**	Annex F
Distribution of 2-year Evaporation Totals	**OVERALL – GOOD**	Annex F
Distribution of 5-year Evaporation Totals	**OVERALL – GOOD**	Annex F
Distribution of 10-year Evaporation Totals	**OVERALL – GOOD**	Annex F
Mean of Monthly Evaporation Totals	**OVERALL – GOOD**	Annex G
Standard Deviation Monthly Evaporation Totals	**OVERALL – FAIR**	Annex G

The outcomes of the stochastic modelling, and anticipated implications for water security assessments, can be summarised as follows

- **Multi-year annual totals rainfall/evaporation** – the model reproduces these statistics well, which is critical for application to drought assessment.
- **Monthly totals rainfall/evaporation** – the mean of the monthly totals are considered good, and the standard deviations are considered fair. Discrepancies in simulated data are discussed in the report and show for a representative rainfall site that the fair classification of the standard deviation of monthly totals is due to occasional simulated wet months that inflate the standard deviation. For evaporation, some months may have a standard deviation which is 2mm lower than observed. For a reported example at one site, the observations range from 85 mm to 115 mm (90% interval) while the simulations range from 88 mm to 112 mm.
- **Proportion of wet days** – this statistic is classified as 'Overall Poor' in the annual distribution, but 'Overall Good' for mean of monthly proportions and 'Overall Fair' for the standard deviations of monthly proportions. Interpreting this performance, the proportion of wet days is unbiased, but lacks variability at the annual scale. For the driest year on record from a representative site, this translates to an extra 10 wet days in the median simulation compared to the observation. However, the process of rainfall amounts compensates for this lack of variability (by simulating less rainfall per wet day in these situations) so that rainfall totals are unbiased and there is good reproduction of the variability of annual totals.
- **Annual maxima** – the annual maximums are 'Overall Good' for 1-day maximums and 'Overall Fair' for 2-day or 3-day maximums. Where there is fair performance, it is shown that the observed values are not far outside the border of the 90% confidence interval of simulated extremes. The performance of these statistics is mostly relevant to flood studies, for catchments that have a response time in the order of several days.

Compared to single-site rainfall models, the class of models that are able preserve multisite statistics from daily to inter-annual scales across both rainfall and evaporation variables is not large. Based on the performance summary, the model outlined in this report was able to account for key attributes of the multisite rainfall and evaporation observations for the historical record. The project scope also includes the requirement to develop stochastic rainfall representing future climate conditions; for this purpose, four model variants ('Model D' to 'Model G') were developed, corresponding to conditions of 20-year time slices centred on 2030, 2050, 2070 and 2090. RCP4.5 was identified as a representative set of projections and median scaling factors derived from the CSIRO Climate Futures Tool were applied to the generated stochastic data. The scaling factors indicate from a 3% increase (summer 2050) to a 10% decrease in rainfall

(winter 2090), and for evaporation, an increase between 3% (2030 all seasons) and 8% (autumn/winter 2090).

The generated daily timeseries of 10,000 years length are recommended for use in hydrological modelling studies of the Macquarie River catchment. 'Model C' is recommended for use as the best representation of the historical climate as it includes information from paleoclimate records on the IPO. 'Model D' to 'Model G' are recommended for studies that consider potential additional effects of climate change in addition to baseline variability, noting that these are generated using median projections and do not simulate the full range of potential climatic changes that may occur in the future.

Contents

Executive Summary i
Contents iv
List of Annex Documents v
List of Figures vi
List of Tables ix
Acknowledgements x
1 Introduction 1
1.1 Project Scope 1
1.2 Background 2
2 Methodology 5
2.1 Observation Data 5
2.1.1 Rainfall data 5
2.1.2 Evaporation data 6
2.1.3 Instrumental records of low-frequency climatic variability 9
2.1.4 Paleo records of low-frequency climatic variability 9
2.1.5 Analysis of IPO partitioned rainfall data 10
2.1.6 Analysis of IPO partitioned evaporation data 12
2.1.7 Future climate 13
2.2 Model Specification – Base model 14
2.2.1 At-site rainfall model 15
2.2.2 At-site evaporation model 17
2.2.3 Multi-site rainfall model 21
2.2.4 Multi-site evaporation model 22
2.2.5 Joint simulation of rainfall and evaporation 23
2.3 Extended Model Specification – Climatic Variability and Future Climate 25
2.3.1 IPO Dwell-time distribution from instrumental and paleoclimatic record 25
2.3.2 Future changes as a result of anthropogenic climate change 25
2.4 Model Calibration 27
2.4.1 Step 1. Rainfall – Single site rainfall distribution 27
2.4.2 Step 2. Rainfall – Single site temporal correlation 27
2.4.3 Step 3. Rainfall – Spatial correlation 27
2.4.4 Step 4. Evaporation – Single site evaporation distribution 27
2.4.5 Step 5. Evaporation – Single site temporal correlation 27
2.4.6 Step 6. Evaporation – Spatial correlation 27
2.4.7 Step 7. Rainfall-Evaporation – Spatial correlation 28

2.4.8 Step 8. Space-time correlation 28
2.4.9 Step 9. IPO calibration 28
2.4.10 Step 10. Future Trends 28
2.5 Model Evaluation 28
2.5.1 Evaluation of distribution quantiles 28
2.5.2 Evaluation of distribution of monthly totals 29
2.5.3 Pooling performance over multiple sites 29
3 Results 32
3.1 Model Evaluation Summary 32
3.2 Detailed Evaluation of Distributions 33
3.2.1 Multi-Year Annual Rainfall Totals (1-, 2-, 5-, and 10-years) 33
3.2.2 Mean and Standard Deviation of Monthly Rainfall Totals 35
3.2.3 Annual Wet Day Proportion 36
3.2.4 Monthly Wet Day Proportion (Mean and Standard Deviation of) 38
3.2.5 Annual Rainfall Maximums (1-, 2-, and 3-day) 39
3.2.6 Multi-Year Annual Evaporation Totals (1-, 2-, 5-, and 10-years) 39
3.2.7 Mean and Standard Deviation of Monthly Evaporation Totals 43
4 Discussion and Recommendations 44
4.1 Model Summary 44
4.2 Summary of Model Evaluation 44
4.3 Summary of Future Climate Outputs 46
4.4 Recommendations 46
5 References 47
6 Appendix A – Finalised list of sites 48
7 Appendix B – Traffic Light Comparison for 'Model A' (base), 'Model B' (instrumental IPO) and 'Model C' (paleoclimatic IPO) 50

List of Annex Documents

ANNEX A – Annual Rainfall Totals, incl. Multi-Year Annual Rainfall Totals (2-, 5-, and 10-years)
ANNEX B – Monthly Rainfall Totals (Mean and Standard Deviation of)
ANNEX C – Annual Wet Day Proportion
ANNEX D – Monthly Wet Day Proportion (Mean and Standard Deviation of)
ANNEX E – Annual Rainfall Maximums (1-, 2-, and 3-day)
ANNEX F – Annual Evaporation Totals, incl. Multi-Year Annual Evaporation Totals (2-, 5-, and 10-years)
ANNEX G – Monthly Evaporation Totals (Mean and Standard Deviation of)

List of Figures

Figure 1 Elevation Profile of the Macquarie River (MDB, 2018) 4
Figure 2 Location of Rainfall Sites (See Appendix A for Site Details)..... 5
Figure 3 Distribution of average rainfall at 100 rainfall sites (left) spatial gradient of annual totals (right) variation in monthly totals throughout the year..... 6
Figure 4 Location of Evaporation Sites (See Appendix A for Site Details) 7
Figure 5 (left) Morton Wet evaporation (middle) IQQM evaporation and (right) FAO56 evaporation. Top row shows the spatial distribution, middle row shows monthly averages for each year on record, bottom row shows distribution of daily evaporation for representative site. IQQM data has a different spatial distribution, higher seasonal variation and 'blocky' daily distribution. 8
Figure 6 Representative sample of 'IQQM' evaporation data for site E32. It appears the data has been generated from a model which assumes the same value for almost all days within a given month but a different value for each repeated month (e.g. compare January to January). There are random shifts for some days, which are likely due to a model which correlates evaporation to wet days (assumed inference).9
Figure 7 Timseries of Interdecadal Pacific Oscillation (red) showing positive and negative states (black) 9
Figure 8 Comparison of the instrumental IPO timeseries to the combined paleo IPO timeseries, Figure 1 from Henley et al. (2011)..... 10
Figure 9 Distribution of dwell-times for phases of the IPO, solid lines represent the estimated distribution from the instrumental IPO record, dashed lines represent the estimated distribution from paleoclimatic IPO reconstructions (from Henley et al, 2011) 10
Figure 10 Annual rainfall totals at 100 sites sorted in ascending order. Each vertical bar represents 1 site. The IPO negative state (blue symbols) receives ~90 mm more rainfall than the IPO positive state (red symbols)..... 11
Figure 11 Yearly timeseries of annual total rainfall. Black lines show years corresponding to changes in the IPO state. (top) the annual rainfall is shown for each site where the sites have been sorted by their long-term average so that the wettest site appears at the top of the figure and the driest site appears at the bottom. (bottom) barplot of the arithmetic average across all sites..... 11
Figure 12 Annual evaporation totals at 45 sites, separated by evaporation type and each group sorted in ascending order. Each vertical bar represents 1 site. The IPO negative state (blue symbols) receives marginally less evaporation, approximately 17 mm less than the IPO positive state. 12
Figure 13 Yearly timeseries of annual total evaporation (Morton Wet sites only). Black lines show changes in the IPO state. (top) the annual evaporation is shown for each site where the sites have been sorted by their long-term average so that the most evaporative site appears at the top. (bottom) barplot of the arithmetic average across all sites. 12
Figure 14 Scatterplot of annual average rainfall and evaporation for 45 sites. The totals are stratified by the IPO. 13
Figure 15 Projected change in seasonal precipitation for 2090 (2080-99). Graphs show change in (from left) summer, autumn, winter and spring. Anomalies are given in % relative to 1995 (1986-2005) under RCP2.6 (Green), RCP4.5 (blue) and RCP8.5 (purple). Natural climate variability is represented by the grey bar. Plot reproduced from Climate Change in Australia website (CSIRO and Bureau of Meteorology, 2015)..... 13
Figure 16 Projected change in seasonal evapotranspiration for 2090 (2080-99). Graphs show change in (from left) summer, autumn, winter and spring. Anomalies are given in % relative to 1995 (1986-2005) under RCP2.6 (Green), RCP4.5 (blue) and RCP8.5 (purple). Natural climate variability is represented by the grey bar. Plot reproduced from Climate Change in Australia website (CSIRO and Bureau of Meteorology, 2015)..... 14
Figure 17 Schematic of latent variable concept 15
Figure 18 Distribution of lag-1 daily autocorrelation parameter across 100 rainfall sites for each month.... 16

Figure 19 Distribution of rainfall. Observed (red symbol) versus 100 simulated replicates (grey lines) monthly means (left) and monthly standard deviations (right) 16
Figure 20 Distribution of daily evaporation for a representative site (which one) for each month 17
Figure 21 Schematic of method used to reproduce skewness in distribution of daily evaporation 17
Figure 22 Daily evaporation for a representative site (top) fitted mean trend, (bottom) residuals after removing the mean 18
Figure 23 Fitted trends to mean-corrected residuals (top) positive and (bottom) negative 18
Figure 24 Standardised residuals of evaporation 19
Figure 25 Autocorrelation of standardised residuals for a representative site, x axis represents daily lags .. 20
Figure 26 Example simulation from single-site model of evaporation. Grey symbols are observations, red symbols are simulation. Solid purple shows the simulated mean, solid blue/green show the lower/upper 95% interval and dashed blue/green show the lower/upper 99.7% interval 20
Figure 27 Distribution of rainfall. Observed (red symbol) versus 100 simulated replicates (grey lines) monthly means (left) and monthly standard deviations (right) 20
Figure 28 Rainfall sample correlation values with distance for a representative site and month 21
Figure 29 Rain-Rain correlation matrix for 100 sites 21
Figure 30 Structure of evaporation correlations (left) shows sample correlation with distance for a representative site. Banding of the correlation is evident due pairing of to the different types of evaporation: Mwet-Mwet (black); Mwet-IQQM (orange); Mwet-FAO56 (magenta); IQQM-IQQM (blue); IQQM-FAO56 (green) and FAO56-FAO56 (red). (right) A key for the different pairings of evaporation type in the structure of the covariance matrix 22
Figure 31 Evap-Evap correlation matrix for 45 sites 22
Figure 32 Rainfall-Evaporation sample correlation values with distance for a representative site and month, observations (black) and fitted correlation function (red) 23
Figure 33 Nested block-correlation matrix joint simulation of 100 rain sites and 45 evaporation sites. Rain-Rain correlation is the bottom left block (Figure 29); Evap-Evap as the top-right block (Figure 31) and the off-diagonal blocks showing negative correlations obtained from the Rain-Evap function (Figure 32). 24
Figure 34 Nested block-correlation matrix joint simulation of 145 sites and two timesteps, lower left block time (t, t) and upper right block (t+1, t+1) are nested matrices from Figure 26 of static spatial correlations, the off-diagonal blocks represent the lag-1 in time (t, t+1) cross-correlations between pairs of sites. The off-diagonals are rescaled from the spatial correlations by a constant autocorrelation parameter across all sites (space-time separable covariance structure). 24
Figure 35 Example simulation of 1000 years IPO states from the alternating renewal model with parameters from the IPO instrumental record. 25
Figure 36 Change factors for projected rainfall RCP4.5 shown for multiple time periods and seasons, CSIRO Climate Futures 26
Figure 37 Change factors for projected evaporation RCP4.5 shown for multiple time periods and seasons, CSIRO Climate Futures 26
Figure 38 Flow chart of performance classification of simulation into three categories (GOOD, FAIR, POOR) using criteria specified according to two tests. Example A shows >90% observations inside the simulated 90% confidence interval (GOOD). Example B shows <90% observations inside the simulated 90% confidence interval. Example C shows >90% of sample statistic intervals overlapping with the simulated 90% confidence interval (FAIR). Example D shows an example failing both tests (POOR). Examples use 129 data points. 30
Figure 39 Flow chart of performance classification of simulation into three categories (GOOD, FAIR, POOR) using criteria specified according to two tests. Example A shows >90% observations inside the simulated 90% confidence interval (GOOD). Example B shows <90% observations inside the simulated 90% confidence interval. Example C shows >90% of sample statistic intervals overlapping with the simulated 90% confidence interval (FAIR). Example D shows an example failing both tests (POOR). 31

Figure 40 Distribution of annual rainfall totals for 1-, 2-, 5- and 10-year totals for a representative location simulation shows 90% confidence interval, performance tag GOOD (see Section 2.5) 34
Figure 41 Distribution of (left) means of monthly totals; (right) standard deviations of monthly totals. Whiskers of grey box plot extend to the 90% interval. Red shows the observed mean/standard deviation along with error bars showing the standard error of each observed statistic. Performance tag GOOD for the means; performance tag FAIR for the standard deviations 35
Figure 42 Paired comparison of full distribution of monthly totals for one representative site R1 50018 and one replicate. Grey monthly boxplot has 129 years of simulated data from one replicate and red monthly boxplot has 129 years of observations. 35
Figure 43 Distribution of the proportion of wet days within a given year. Four representative sites are shown for different performance outcomes, GOOD, FAIR and POOR (see Section 2.5) 37
Figure 44 Distribution of (left) means of monthly proportions of wet days (right) standard deviations of monthly proportions of wet days. Whiskers of grey box plot extend to the 90% interval. Red shows the observed mean/standard deviation along with error bars showing the standard error of each observed statistic. Three representative sites are shown R78, R79, R80 for different performance outcomes (see Section 2.5) 38
Figure 45 Frequency analysis of extremes (left) annual maximum daily rainfall (middle) annual maximum 2-day rainfall (right) annual maximum 3-day rainfall. Four representative sites R25-R28 are shown for different performance outcomes (see Section 2.5) 40
Figure 46 Distribution of annual evaporation totals for 1-, 2-, 5- and 10-year totals for a representative location with 'FAIR' / 'GOOD' performance (see Section 2.5), simulation shows 90% confidence interval ... 41
Figure 47 Distribution of annual rainfall totals for 1-, 2-, 5- and 10-year totals for a representative location with 'POOR' performance (see Section 2.5), simulation shows 90% confidence interval 42
Figure 48 Distribution of monthly evaporation totals (left) means of monthly totals (right) standard deviations of monthly totals. Whiskers of grey box plot extend to the 90% interval. Red shows the observed mean/standard deviation along with error bars showing the standard error of each observed statistic. Two representative sites are shown (see Section 2.5) 43

List of Tables

Table 1 Rainfall evaluation summary of performance, Paleoclimatic IPO model variant, 100 sites 129 years length, 77 replicates. Traffic light criterion specified by systematic evaluation method (Section 2.5). Detailed plots for each site in Annex documentation. i
Table 2 Evaporation evaluation summary of performance, Paleoclimatic IPO model variant, 45 sites 129 years length, 77 replicates. Traffic light criterion specified by systematic evaluation method (Section 2.5). Detailed plots for each site in Annex documentation. ii
Table 3 Cases of simulated data outputs. 'Model C' (*) is intended as the primary output for evaluation of historical climate conditions 2
Table 4 Aggregate performance categorisation criteria from Bennett et al. (2018) 29
Table 5 Rainfall evaluation summary of performance, 'Model C' Paleoclimatic IPO model variant, 100 rainfall sites 129 years length, 77 replicates. Traffic light criterion specified by systematic evaluation method (Section 2.5). The x-axis shows the percentage of sites in each category of 'Good' (green), 'Fair' (yellow) or 'Poor' (red). Detailed plots for each site in Annex documentation. 32
Table 6 Evaporation evaluation summary of performance, 'Model C' Paleoclimatic IPO model variant, 45 evaporation sites 129 years length, 77 replicates. Traffic light criterion specified by systematic evaluation method (Section 2.6). The x-axis shows the percentage of sites in each category of 'Good' (green), 'Fair' (yellow) or 'Poor' (red). Detailed plots for each site in Annex documentation. 33
Table 7 Observed versus simulation comparison for four representative sites. The number of wet days in the driest year (per 129 record length). The simulation is summarised by the median and the 90% limits. . 36
Table 8 List of 100 rainfall sites used in the study 48
Table 9 List of 45 evaporation sites used in the study (31 unique locations since E32-E45 are co-located). The Mwet label indicates data following the Morton Wet equation, -evt/evg labels indicate the IQQM evaporation data and FAO56 indicates the sites using reference crop data 49
Table 10 Rainfall evaluation summary of performance for 3 different model variants 50
Table 11 Evaporation evaluation summary of performance for 3 different model variants. 50

Acknowledgements

We acknowledge Forugh Dorani and Dushmanta Dutta from the NSW Department of Industry, as well as Owen Droop from ODHydrology for the provision of data and constructive conversations on the relevant modelling requirements. A/Prof. Mark Thyer provided considerable guidance and invaluable discussions on the climatic modelling elements of this project.

1 Introduction

Water in the Macquarie Valley is needed for many demands, including irrigation, stock, domestic use, town supply, ecological, and recreational demands. The valley supports a diversity of agricultural activity, including a wide range of crops: cotton, cereals, wine grapes, oil seed, legumes and tree crops such as olives, nuts and cherries. However, flows in the Macquarie River are highly variable with evidence of prolonged periods of below average flow. For example, during the Federation drought, storages were at 4% of full supply volume, causing suspension of the water sharing plan and significant water restrictions to townships such as Dubbo.

The New South Wales Department of Industry has developed a risk-based method to assess impacts of water scarcity to the regional economy and ecosystem assets of the Macquarie Valley. The method is based on hydrological and economic modelling, where the IQQM water resources model (Integrated Quantity and Quality Model) will undertake daily water balance simulations over a long-term climatic period.

To facilitate daily water balance modelling, stochastic inputs are required that account for variability and potential projected future changes to rainfall and evaporation at multiple sites. To simulate key hydrological features of interest it is necessary for the stochastic inputs to reproduce variability and gradients in the rainfall and evaporation across all sites within the region and multiple timescales: daily, monthly, annual, and multi-annual scales.

1.1 Project Scope

The project scope is to deliver stochastically generated rainfall and evaporation at multiple sites within the Macquarie Valley and surrounding region. The list of sites is provided in Appendix A, comprising 100 rainfall sites and 45 evaporation sites (the latter made up of 31 'Morton Wet', 7 'IQQM' and 7 'reference crop' sites). There are 145 timeseries to be generated but only 100 unique locations, since the 45 evaporation 'sites' are co-located. Of the 100 locations, 69 are rainfall only, 24 are rainfall and Morton Wet evaporation, and the remaining 7 sites are rainfall with all three variants of evaporation. A 129 year common period (1890-2018) is used to calibrate and evaluate the rainfall/evaporation model.

A single replicate of length 10,000 years is required for a number of climatic cases (Table 2). In each case the climate represents long-term stationary assumptions.

- 'Model A' calibrates to daily and seasonal variability from the observed record, but does not account for inter-annual sources of variability available from climate indices.
- 'Model B' calibrates separate parameters to positive and negative phases of the Interdecadal Pacific Oscillation (IPO) to account for inter-annual variability, using IPO data extracted over the instrumental record (i.e. from 1890-2018).
- 'Model C' uses paleoclimate information of the IPO to inform the distribution of possible dwell times in each phase of the IPO. Given that 'Model C' uses the most complete available information on long-term climate variability by blending both historical and paleoclimate information, it is intended as the primary characterisation of historical variability, whereas 'Model A' and B are mostly intended for comparison.
- 'Model D' to 'Model G' represent rescaled versions of 'Model C' that account for projected changes for RCP4.5 from the CSIRO Climate Futures Tool. The four separate models correspond to climatic conditions for time slices centred on the years 2030, 2050, 2070 and 2090. RCP4.5 was identified as the most appropriate projection to use, since the project requirements are for the indicative effects of climate change rather than for exploring the full range of RCPs and projection uncertainty.

The generated timeseries for Models A-C are intended to characterise statistical features of the historical rainfall, including inter-annual and multi-decadal variability, with a particular view to replicating the climatic drivers of drought. The output is generated as a single timeseries (e.g. 10,000 years) as it provides

maximum flexibility in terms of being used as a single extended timeseries or broken up into shorter replicates to suit modelling requirements (e.g. 100 x 100 year replicates instead of a single 10,000 year replicate). To statistically evaluate the performance of the model, the 10,000 year simulations are partitioned according to 77 replicates of 129 years to match the length of the historical record for direct comparison of statistical quantities. The evaluated statistics include the proportion of wet days, mean and standard deviation of monthly and annual totals of rainfall, variability in multi-annual totals (2-, 5- and 10-year totals) and an analysis of 1-day, 2-day and 3-day annual maximums.

Table 3 Cases of simulated data outputs. 'Model C' (*) is intended as the primary output for evaluation of historical climate conditions

Model	Case Description
A	Base case: no climate partitioning
B	Instrumental IPO: Conditioned on the Interdecadal Pacific Oscillation, instrumental record only
C*	Paleo IPO: Conditioned on the IPO using paleo proxies to inform climate states
D	Future climate 2030: As for case C, but rescaled to match climate conditions of 2030
E	Future climate 2050: As for case C, but rescaled to match climate conditions of 2050
F	Future climate 2070: As for case C, but rescaled to match climate conditions of 2070
G	Future climate 2090: As for case C, but rescaled to match climate conditions of 2090

1.2 Background

The Macquarie River forms part of the Barwon-Darling basin, located in central western New South Wales. The catchment headwaters are in the Great Dividing Range near Bathurst at an elevation of 650 mAHD (Figure 1), but with some catchment peaks approaching 1400 mAHD (Mount Canobolas) with annual average rainfall greater than 1200 mm. The river flows northwest for 960 km toward the Barwon River near Brewarrina, with elevations less than 100 mAHD. Rainfall over most of the lower catchment averages 300-500 mm/year with higher totals in summer. Annual average evaporation ranges from 1100 mm to 1800 mm across the catchment.

The Macquarie River has highly variable flows; for example at Dubbo, the annual flows have historically ranged from 24,100 ML to 10,113,000 ML (NSW Department of Primary Industries, 2016), with annual average flow 1,175,000 ML. The low flows typically occur during extended (i.e. multi-year) drought periods (e.g. 1935-42, 2001-2009). As the result of decreasing channel capacity, irrigation and the presence of numerous effluent channels, annual average flow reduces from Dubbo to less than 330,000 ML above the Macquarie marshes and less than 150,000 ML below the marshes (NSW Department of Primary Industries, 2016). The catchment is hydrologically complex, with numerous anabranches in the lower reaches and surface-water/groundwater interactions in the upper Macquarie (NSW Department of Industry, 2018).

There are two significant dams in the headwaters, Windamere Dam (368,000 ML on the Cudgegong River, built in 1984) and Burrendong Dam (1,678,000 ML on the Macquarie River, built in 1967). The dams provide water for irrigators, stock, domestic use and town supply as well as flood storage capacity. The catchment population is less than 200,000 people, concentrated in the town centres of Bathurst, Dubbo, Mudgee, Orange and Wellington. The towns have higher priority access to water above irrigation licenses. Over 80 percent of the land is used for agriculture to support sheep and cattle grazing as well as a range of broadacre and orchard/higher value horticulture (e.g. cotton, cereals, wine grapes, oil seed, legumes and tree crops such as olives, nuts and cherries). The river also supports an array of recreational activities including fishing, water sports, bushwalking and camping.

The quantity and quality of water is equally significant for the biodiversity of the Macquarie River ecosystem. The Macquarie marshes are listed under the Ramsar convention and are one of the largest inland semi-permanent wetlands in the Murray-Darling Basin. The marshes cover a diverse range of habitat and vegetation types, hosting numerous endangered and threatened species of native birds and fish. There are numerous additional ecosystem assets including lakes, billabongs, wetlands and flood-dependent forests.

Given the high degree of variability in the climatic system there are significant challenges in managing the provision of water for irrigation and ecosystem functions. Future climate change poses additional risks to the region, and though uncertain, it is expected that surface water availability is more likely to decrease than increase across the basin (Van Dijk et al, 2016). In particular, there are significant consequences if future droughts occur with similar or greater magnitude than historical droughts. If the water security reaches critically low levels there is the potential for high water restrictions, loss of ecosystem assets, biodiversity stress, no water allocated for agricultural activity, reduced mining activity and significant indirect impacts on local townships and the regional economy.

An IQQM water balance model has been developed based on the Macquarie Water Sharing Plan which takes into account contemporary infrastructure, water access entitlements and water sharing rules. The Macquarie IQQM model will be used as the basis of risk-based assessment, with critical outputs including estimates of water availability and allocation for various scenarios of economic and environmental impact. This project exists to provide stochastic data of climatic forcings as a necessary input for water balance modelling.

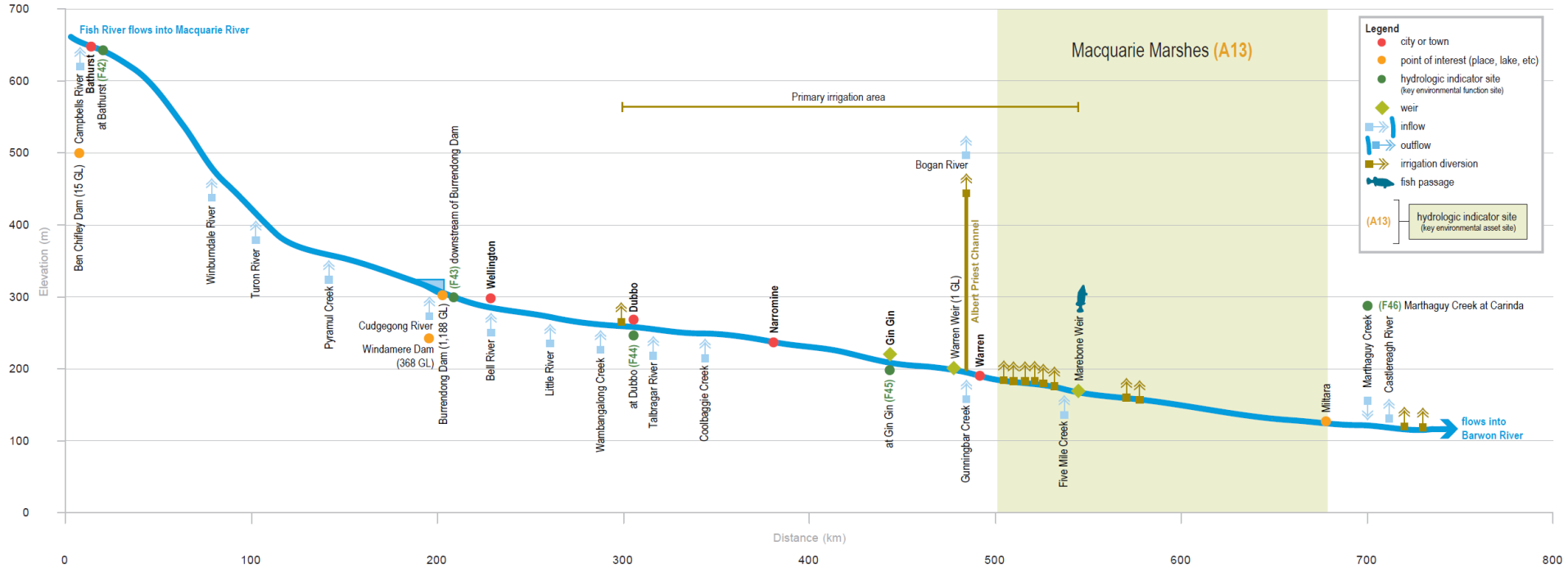

Figure 1 Elevation Profile of the Macquarie River (MDB, 2018)

2 Methodology

2.1 Observation Data

2.1.1 Rainfall data

Figure 2 shows the locations of rainfall data, which were provided at 100 locations (see Appendix A for complete list). The data were originally sourced from the SILO database, therefore there were no missing values and all sites had considerable length due to infilling methods from SILO. The start dates are either 1/1/1890 or 1/1/1889 and the end dates are 11/09/2018. For calibration all available data from 1890 onwards was used. For evaluation, the last portion of 2018 was padded with data from 2017 to give an indicative total for 2018 rather than to discard 9 months of data within the evaluation. This means all evaluation replicates had an identical length of 129 years.

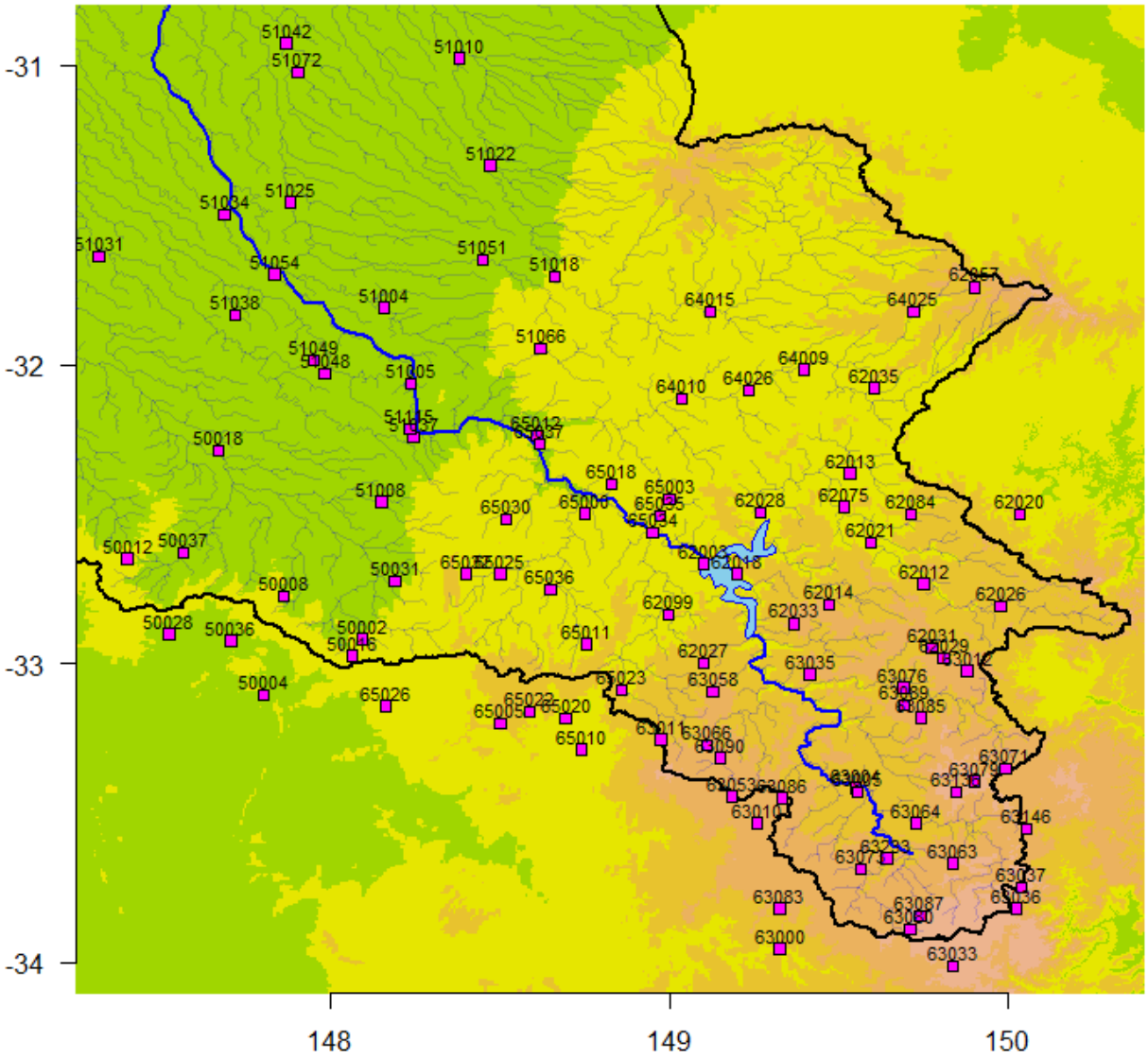

Figure 2 Location of Rainfall Sites (See Appendix A for Site Details)

Analysis of the observed data shows that the highest rainfalls are concentrated in the southeast mountainous corner of the catchment (Figure 3, left). There is a significant gradient over the catchment with a majority of the lower catchment receiving less than 500 mm rainfall on average. The seasonal distribution (Figure 3, right) shows that there is considerable variability across the sites. The highest rainfalls are in summer, autumn rainfall is less than summer and winter is more variable than other seasons.

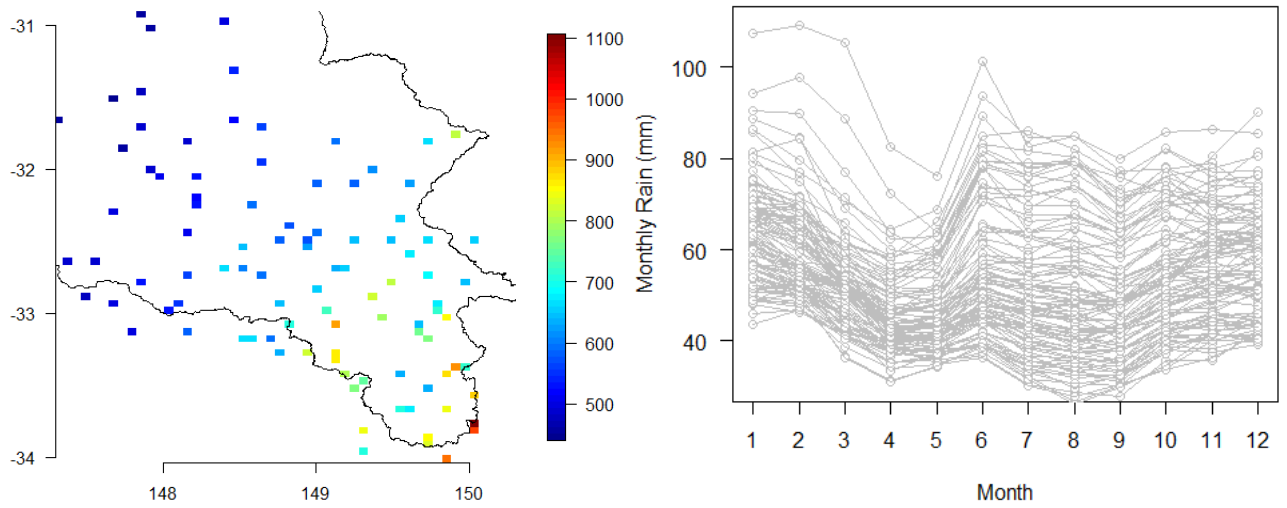

Figure 3 Distribution of average rainfall at 100 rainfall sites (left) spatial gradient of annual totals (right) variation in monthly totals throughout the year

2.1.2 Evaporation data

Data were provided for 31 Morton Wet sites, 7 'IQQM' evaporation sites and 7 FAO56 reference crop sites (the term evaporation is used throughout to mean evapotranspiration). There are 45 separate evaporation timeseries, but only 31 unique locations since the 7 'IQQM' and 7 FAO56 timeseries were co-located at Morton Wet locations. The sites are listed in Appendix A and shown in Figure 4. The Morton Wet and FAO56 reference crop data were obtained from the SILO database, therefore there were no missing values and the data cover the period 1/1/1889 to 11/09/2018. The IQQM estimates span the period 1/1/1890 to 28/8/2017. All available data was used in the model calibration.

The evaporation ranges from 1100 mm in the southeast mountainous corner (Figure 5, top row) to 1800 mm inland. There is a strong seasonal cycle with highest evaporation in summer and lowest evaporation in winter (middle and bottom rows at monthly and daily timescales respectively). The three columns in Figure 5 show differences between the 'Morton Wet' (left) 'IQQM' (middle) and FAO56 (right) evaporation variants. The Morton Wet and FAO56 variants have similar features, with a gradient from east to west and similar magnitudes. The IQQM variant is noticeably different from the other versions:

- the magnitude is significantly higher and with a different spatial pattern (middle column top row)
- the magnitude and the variability is higher (middle column middle row)
- the daily distribution is 'blocky' at the monthly scale with stippling showing persistence of the same value for many days within the month (middle column bottom row)

The provenance of the IQQM 'data' is an Excel based model and there was evidence of error flags in the timeseries (denoted by instances of #VALUE! in 62021_17-evg.csv, years 1871 and 1875). Distinct features of the modelled data are evident in the daily timeseries (Figure 6), where it is likely that the model correlates evaporation with rainfall depending on the condition of either a 'wet' or 'dry' day. It can be seen that a single evaporation value persists for all days within the month except for some random shifts to a different value (inferred here as the wet days). The values for a given month vary each year on record to achieve the overall distribution of monthly evaporation.

Despite these criticisms of the IQQM evaporation data (i.e., those made in relation to Figure 6), the data are reasonable in so far as they are assumed to preserve the monthly distribution of evaporation, the seasonal cycle and known correlation with rainfall. The daily persistence of evaporation values within each month is assumed here to be spurious; the implication is that subsequent models based on this 'data' will have an anomalously high correlation at the daily scale. Also, although the mean of monthly evaporation

totals is preserved, the variability of monthly totals is likely to be spuriously high. The interpretation for hydrological modelling is that while the distribution of evaporation is preserved across multiple years, within any given year it could be biased due to persistence in daily evaporation (especially for blocks of dry days). Although this effect is noticeable in the evaporation data, it is not clear whether this is of practical significance to subsequent modelled flows.

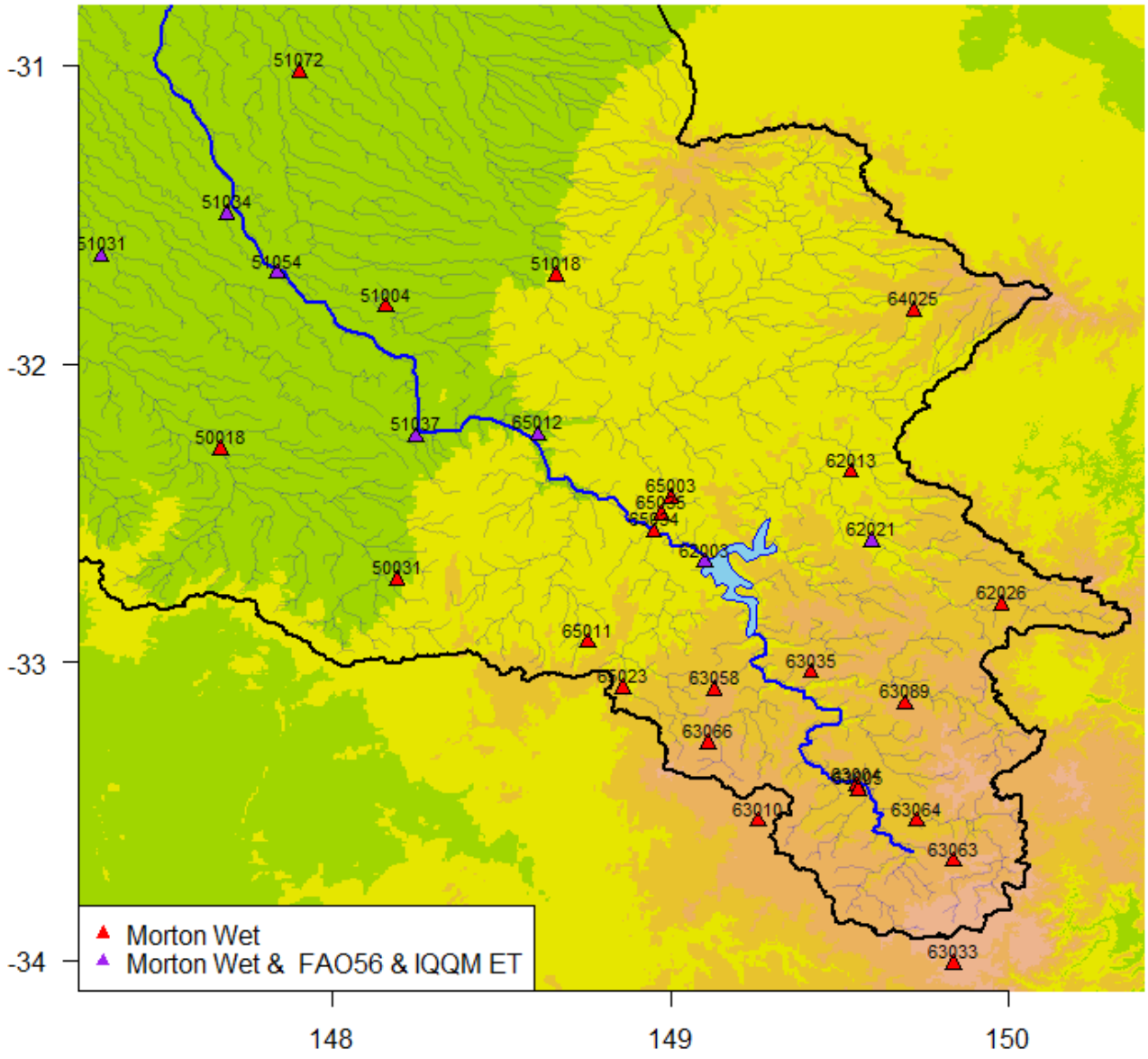

Figure 4 Location of Evaporation Sites (See Appendix A for Site Details)

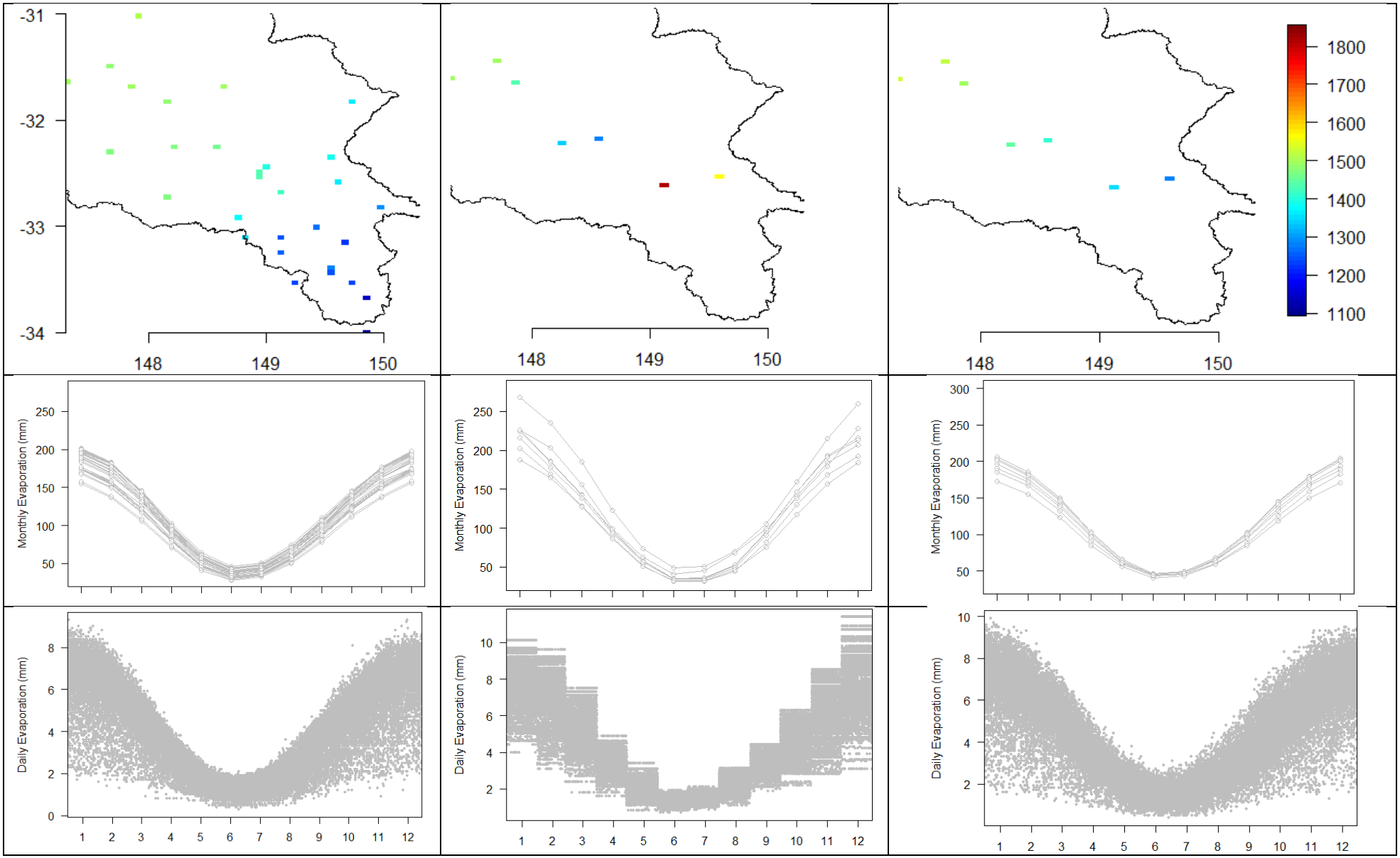

Figure 5 (left) Morton Wet evaporation (middle) IQQM evaporation and (right) FAO56 evaporation. Top row shows the spatial distribution, middle row shows monthly averages for each year on record, bottom row shows distribution of daily evaporation for representative site. IQQM data has a different spatial distribution, higher seasonal variation and 'blocky' daily distribution.

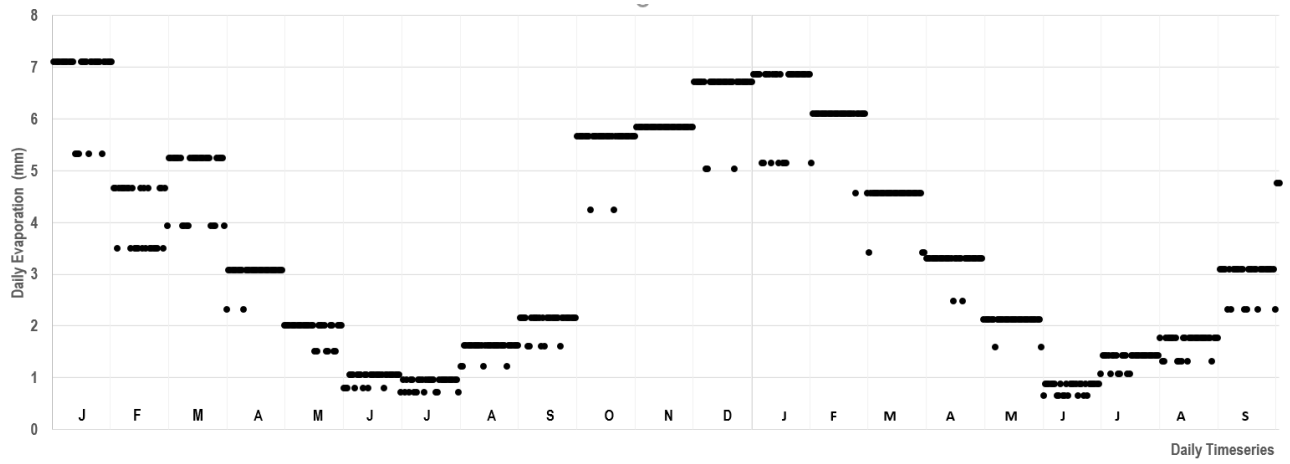

Figure 6 Representative sample of 'IQQM' evaporation data for site E32. It appears the data has been generated from a model which assumes the same value for almost all days within a given month but a different value for each repeated month (e.g. compare January to January). There are random shifts for some days, which are likely due to a model which correlates evaporation to wet days (assumed inference).

2.1.3 Instrumental records of low-frequency climatic variability

Data for the Interdecadal Pacific Oscillation was obtained from Henley et al. (2015) for the period 1854-2018. The Hadley SST version of the IPO was used, and is plotted in Figure 7, showing periods where the IPO is in a positive and negative state respectively. Because the IPO is constructed as a low-pass filter, estimates are not available in the first/last 5 years of the record. Since the IPO estimates end in 2012, the current state from 2012 was assumed for the period out to 2018 rather than excluding this period from the calibration. The IPO was used to partition data and calibrate the model separately to each partition. The partition years were:

- Positive phase: 1877-1888, 1896-1907, 1912-1942, 1978-1997
- Negative phase: 1889-1895, 1908-1911, 1943-1977, 1998-2012 (+ 2013-2018 assumed)

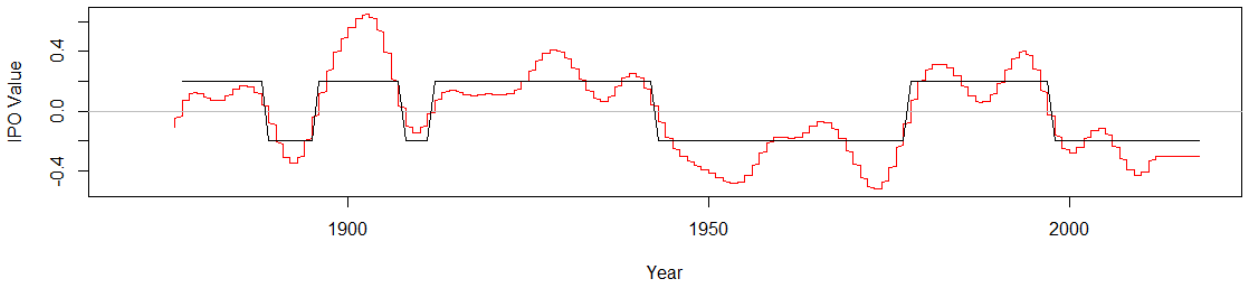

Figure 7 Timseries of Interdecadal Pacific Oscillation (red) showing positive and negative states (black)

2.1.4 Paleo records of low-frequency climatic variability

Henley et al. (2011) developed a weighted average of seven paleoclimatic timeseries, including tree rings and coral from about the Pacific Ocean, to produce a combined paleo IPO signal (referred to as the CPIPO index). Figure 8 compares the instrumental IPO timeseries with the CPIPO timeseries, which shows a favourable comparison (Nash Sutcliffe efficiency, 0.75, and comparable distributions of run-lengths). The distribution of run lengths was analysed to identify the gamma distribution as the most appropriate model to represent the dwell time in each IPO phase (Henley et al., 2011). Figure 9 compares the distribution of dwell times from the instrumental and the paleo record. The paleoclimatic IPO distribution has a lower mean, but higher variance. Whereas the longest dwell time from the instrumental record was 35 years (Figure 7, 1943-1977, IPO negative), both distributions show that it is possible to achieve dwell times of much greater duration (upper tail of Figure 9).

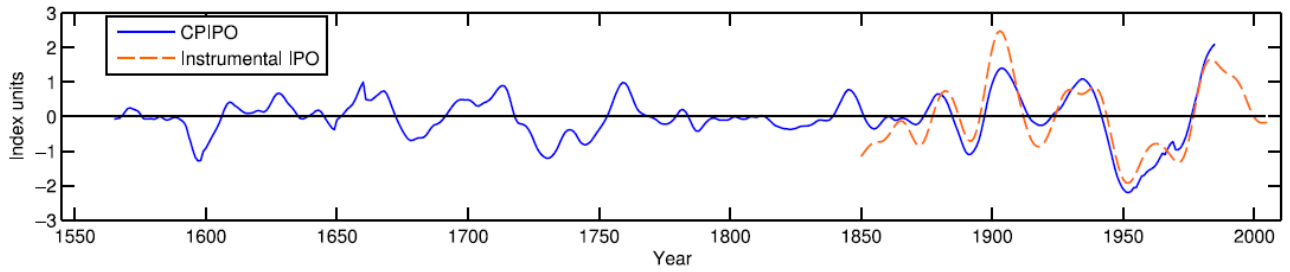

Figure 8 Comparison of the instrumental IPO timeseries to the combined paleo IPO timeseries, Figure 1 from Henley et al. (2011)

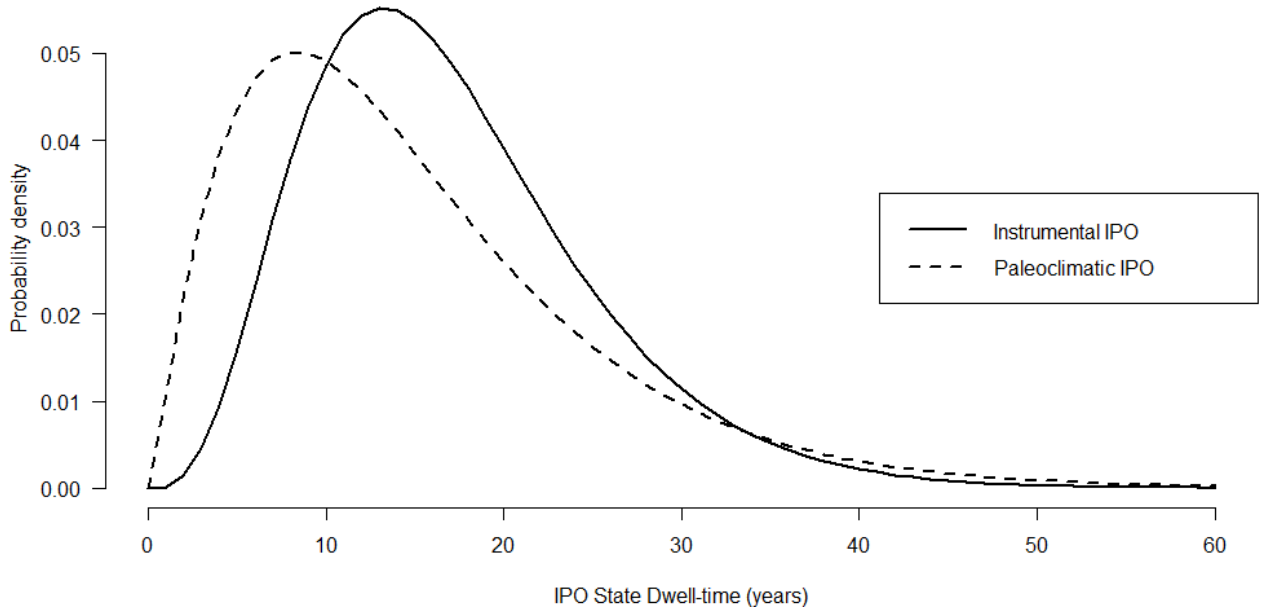

Figure 9 Distribution of dwell-times for phases of the IPO, solid lines represent the estimated distribution from the instrumental IPO record, dashed lines represent the estimated distribution from paleoclimatic IPO reconstructions (from Henley et al, 2011)

2.1.5 Analysis of IPO partitioned rainfall data

Partitioning the rainfall timeseries by the IPO (time periods listed in Section 2.2.3) demonstrates a systematic shift in amounts between the two climate states. Figure 10 shows that on average the difference between the IPO positive and negative states is 90 mm and that the phenomenon is consistent across all sites.

Figure 11 shows the timeseries of annual total rainfall for each year on record. The top panel shows the annual rainfall for each site (wettest on average shown at the top to driest at the bottom) along with black lines which mark transitions in the IPO state. The bottom panel shows the average across all sites. A number of features of the rainfall are evident:

- There is a strong rainfall gradient. Within a single year, annual totals can range from less than 300 mm to more than 1800 mm.
- There is significant variation from year to year. The annual total can shift substantially and does not necessarily persist with similar values for multiple years.
- In addition to the overall variation in annual totals, there is the possibility for significantly above/below average periods to persist for multiple years (e.g. 1890-1895 above average, 1879-1982 below average).
- The effect of spatial correlation is varied, but overall very strong. The wettest years tend to have all sites with significantly increased rainfall (e.g. 2010), whereas other 'wet' years have only a small

number of very wet sites (e.g. 1890s). To see this, consider the spread of yellow and red pixels which represent the wettest sites: some years are very striped showing that all sites have high rainfall while other years show only a cluster of high rainfall sites at the top of the top panel plot.

- While the IPO partitions yield a 90 mm difference for each site (Figure 10) the distribution of annual totals shows that there is significant variability within the IPO state. For example, the period 1997-2018 is an IPO negative phase (nominally the 'wet' phase) but has a similar average to the preceding IPO positive period 1978-1997.

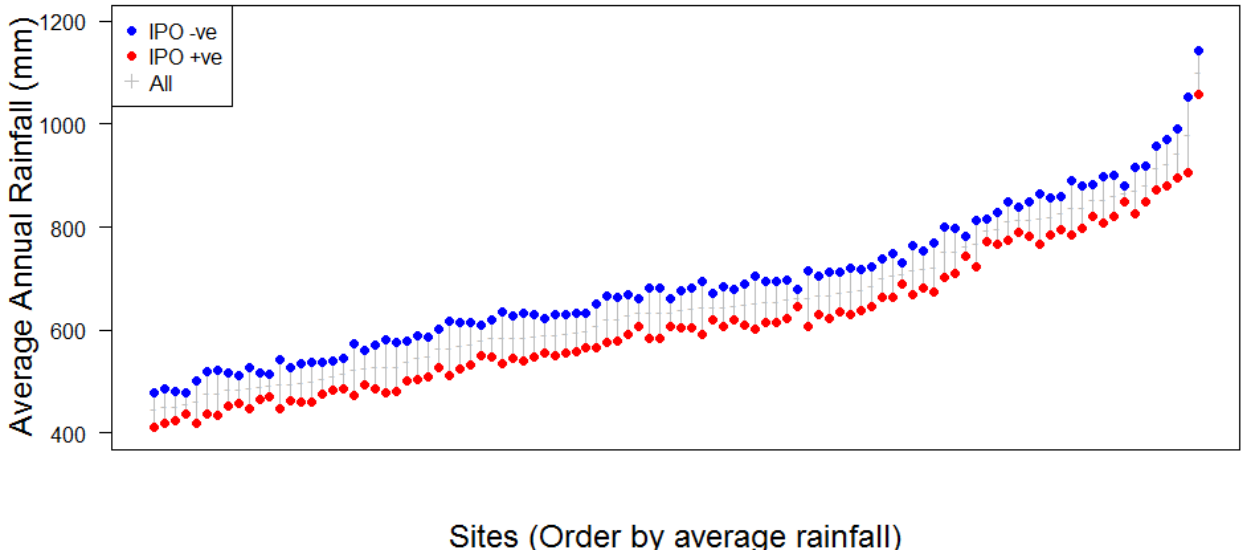

Figure 10 Annual rainfall totals at 100 sites sorted in ascending order. Each vertical bar represents 1 site. The IPO negative state (blue symbols) receives ~90 mm more rainfall than the IPO positive state (red symbols).

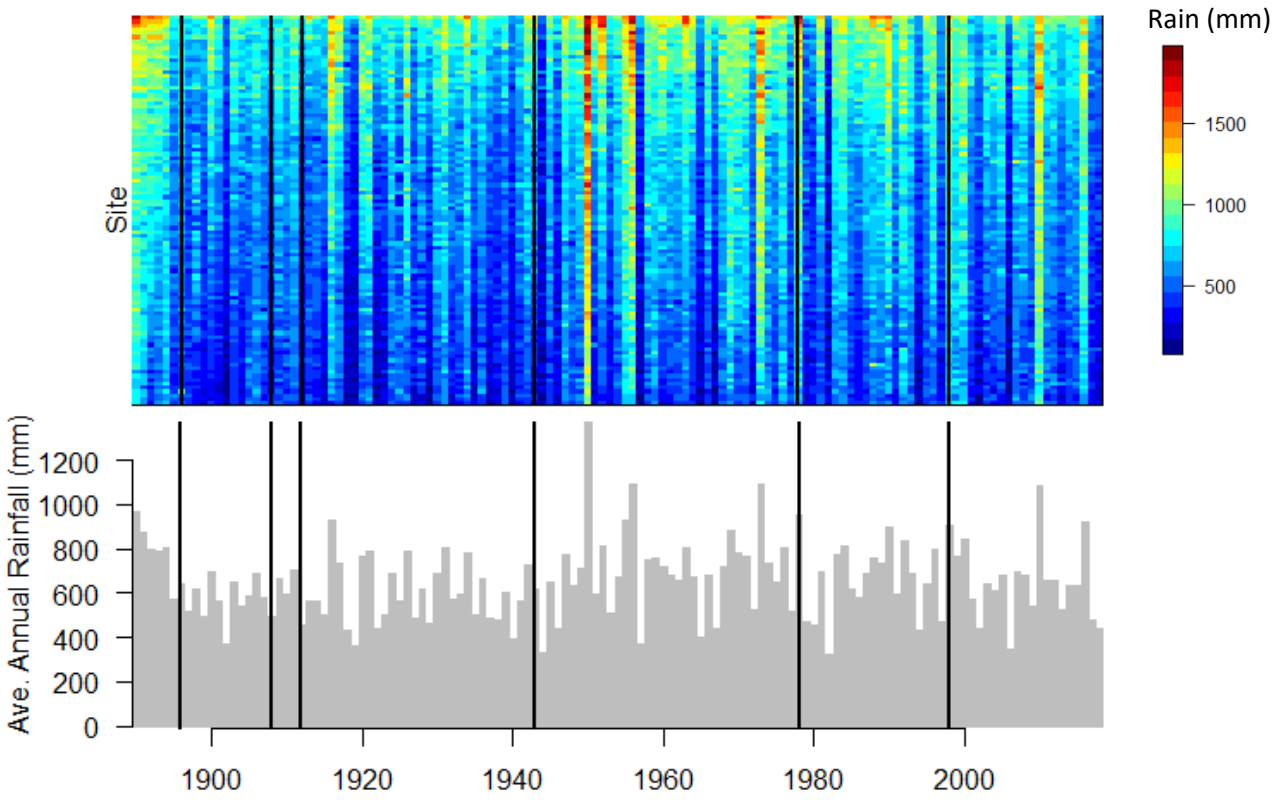

Figure 11 Yearly timeseries of annual total rainfall. Black lines show years corresponding to changes in the IPO state. (top) the annual rainfall is shown for each site where the sites have been sorted by their long-term average so that the wettest site appears at the top of the figure and the driest site appears at the bottom. (bottom) barplot of the arithmetic average across all sites.

2.1.6 Analysis of IPO partitioned evaporation data

Figure 12 shows that the effect of partitioning evaporation by the IPO is less pronounced than for rainfall. There is a 17 mm difference in evaporation between the positive and negative states. Figure 13 shows the timeseries of annual total evaporation for each year on record. The top panel shows the annual evaporation for each site (highest average evaporation shown at the top) along with black lines which mark transitions in the IPO state. As with the rainfall, there is significant variation from year to year, a pronounced gradient and spatial correlation leading to years where the majority of sites have above/below average evaporation.

Figure 14 shows a scatterplot of annual rainfall with annual evaporation. There is a clear negative relationship between the two. The plot shows years stratified by IPO phases, but there is significant overlap of the two, with the exception of the very high rainfall years.

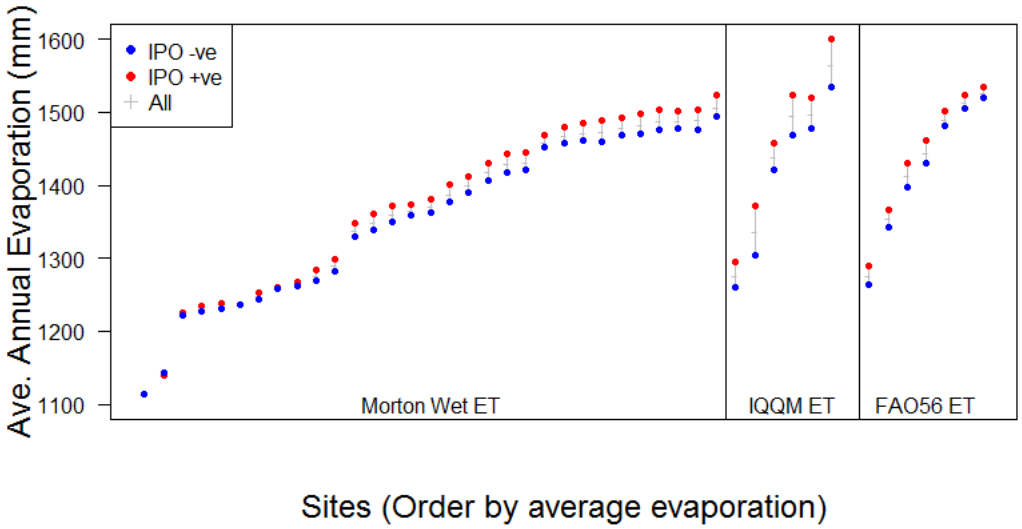

Figure 12 Annual evaporation totals at 45 sites, separated by evaporation type and each group sorted in ascending order. Each vertical bar represents 1 site. The IPO negative state (blue symbols) receives marginally less evaporation, approximately 17 mm less than the IPO positive state.

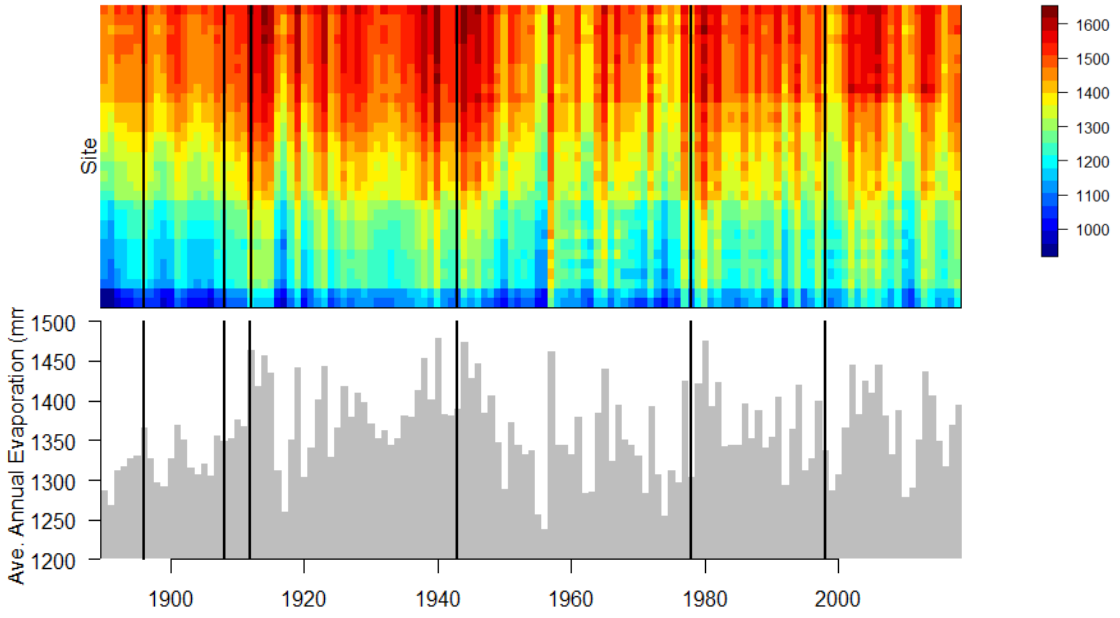

Figure 13 Yearly timeseries of annual total evaporation (Morton Wet sites only). Black lines show changes in the IPO state. (top) the annual evaporation is shown for each site where the sites have been sorted by their long-term average so that the most evaporative site appears at the top. (bottom) barplot of the arithmetic average across all sites.

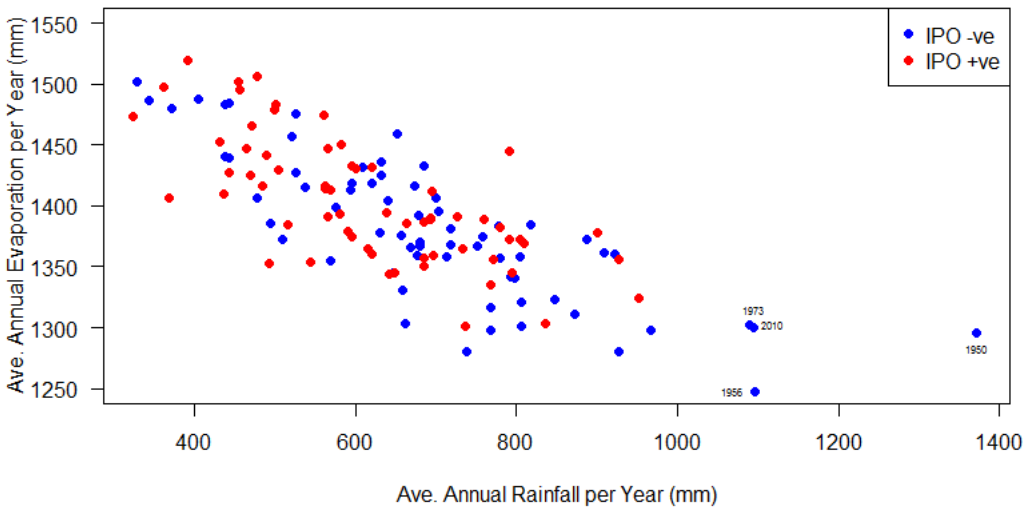

Figure 14 Scatterplot of annual average rainfall and evaporation for 45 sites. The totals are stratified by the IPO.

2.1.7 Future climate

The Climate Change in Australia website (CSIRO and Bureau of Meteorology, 2015) provides sets of scaling factors for the natural resource management regions of Australia based on projections of up to 40 different global climate models. Data are expressed as anomalies with respect to a reference climate of 1986-2005 and available for four different time slices (2020-39, 2040-2059, 2060-2079, 2080-2099), three representative concentration pathways (RCP2.6, RCP4.5 and RCP8.5) and four seasons. Note that the baseline variability from this project is 1890-2018 was assumed to be similar to the 1986-2005 baseline used to generate the climate factors.

Figure 15 and Figure 16 show the variability in model simulations for rainfall and evaporation respectively. The middle line is the median value of the model simulations, the bars show the range of model simulations of 20-year average climate and the whiskers show the projected range of individual years by also taking into account year-to-year variability (10^{th} and 90^{th} percentiles).

It was identified in the scope of this project that an indicative timeseries of future conditions was required and that subsequent hydrological modelling was not intended to compare multiple RCP scenarios. For this reason only RCP4.5 is used for generating outputs of future climate conditions. Figure 15 shows that the expected value of rainfall decreases into the future (up to 10% in spring for RCP4.5). Figure 16 shows that the expected value of evaporation will increase into the future (up to 8% in autumn/winter for RCP4.5)

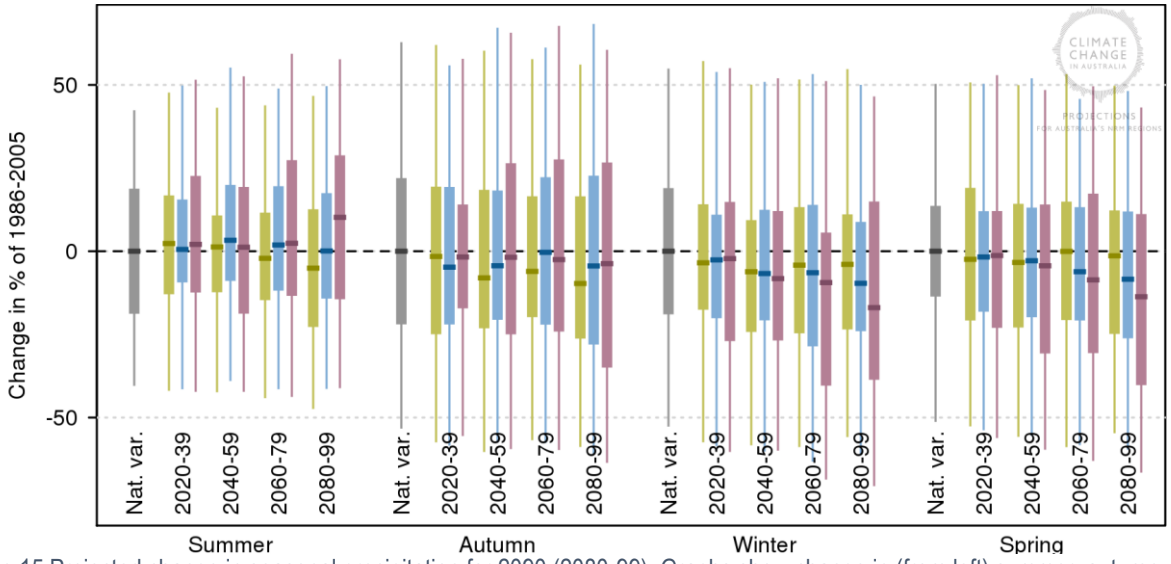

Figure 15 Projected change in seasonal precipitation for 2090 (2080-99). Graphs show change in (from left) summer, autumn, winter and spring. Anomalies are given in % relative to 1995 (1986-2005) under RCP2.6 (Green), RCP4.5 (blue) and RCP8.5 (purple).

Natural climate variability is represented by the grey bar. Plot reproduced from Climate Change in Australia website (CSIRO and Bureau of Meteorology, 2015)

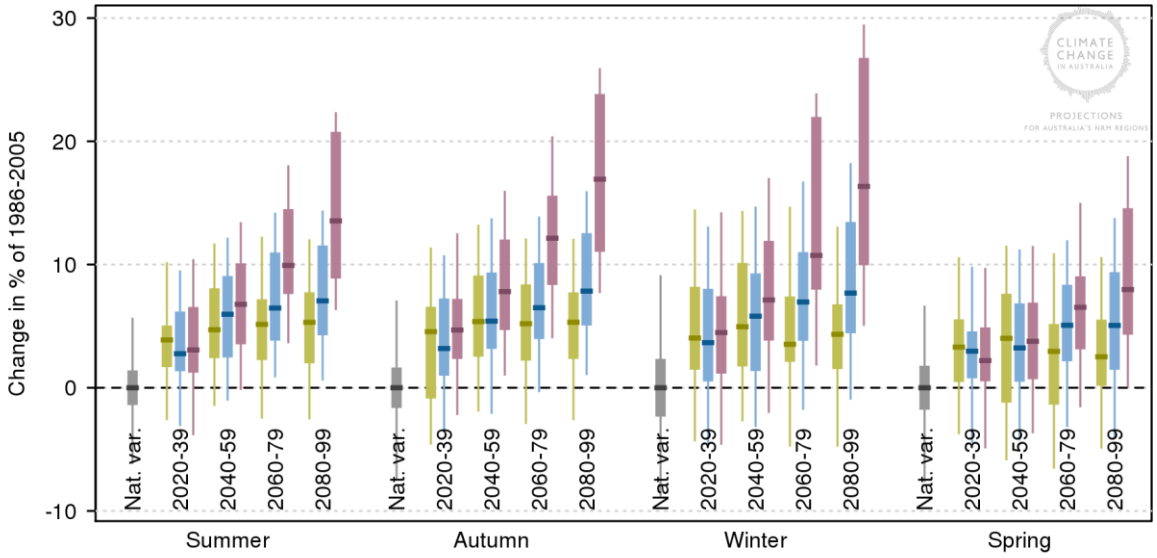

Figure 16 Projected change in seasonal evapotranspiration for 2090 (2080-99). Graphs show change in (from left) summer, autumn, winter and spring. Anomalies are given in % relative to 1995 (1986-2005) under RCP2.6 (Green), RCP4.5 (blue) and RCP8.5 (purple). Natural climate variability is represented by the grey bar. Plot reproduced from Climate Change in Australia website (CSIRO and Bureau of Meteorology, 2015)

2.2 Model Specification – Base model

To simulate daily rainfall and evaporation at multiple sites it is important to have a model that can reproduce the marginal distribution at each site as well as the correlations between all sites. The model requirements are different for rainfall and evaporation.

Rainfall: At the daily scale there is a large percentage of dry values and the magnitudes on rainy days follow a skewed distribution. There is temporal correlation in both the pattern of wet and dry values as well as the magnitudes. It is important to preserve this correlation since hydrological response can depend on the successive wetting and drying of a catchment. The correlation of wet values is also important for rainfall extremes, since many larger rural catchments have a flood response in the order of one or more days. Monthly variation in rainfall is important to replicate, as well as the variability from year to year, so that the distribution of annual totals has appropriate variability from year to year. Lastly, it is possible for rainfall anomalies (above/below average periods) to persist for multiple years (or even decades), which is an essential consideration for drought studies. Spatially, it is important for a model to be flexible enough to permit differences at each site (e.g. to represent trends across the catchment) as well as account for the correlation between sites (to reproduce catchment totals).

Evaporation: Unlike rainfall, evaporation is always positive, which makes it easier to fit distributions. Nonetheless, at the daily scale evaporation can follow a non-symmetric distribution and has a complicated correlation structure: there is a known negative relationship with rainfall, but also considerable persistence over many days. The seasonal cycle of evaporation is well defined, with smooth variation and large differences between the mean and variability. As with rainfall, annual and multi-annual totals are important for modelling drought. Spatially, evaporation varies smoothly (compared to rainfall which can be patchy).

One popular approach for generating daily rainfall is a two-step method that simulates the wet-dry occurrences and then the conditional rainfall amounts (Kleiber et al., 2012; Wilks, 2009). A challenge with this approach is to parsimoniously condition the amounts (whether rainfall or evaporation) on the wet-dry pattern, which can be challenging at multiple sites given the many wet/dry combinations. An alternative

approach is to use a transformed latent (i.e. hidden) variable that maps the wet and dry occurrences to a single distribution: dry values stem from the lower truncated portion and the amounts stem from the upper portion (Baxevani and Lennartsson, 2015). A multi-site version of this model was introduced by Rasmussen (2013), which has a convenient calibration structure to simplify the identification of parameters (the at-site means and standard deviation can be fitted separately from the autocorrelation and spatial correlation).

The following sections provide a description of the model used in this study. A full technical explanation of the rainfall model can be found in Bennett et al. (2018), so the following sections provide a brief conceptual explanation when explaining the rainfall component. A more detailed explanation is provided for the evaporation and evaporation-rainfall relationship since this is not covered in Bennett et al. (2018). Given the complexities due to evaporation data having three different types (Morton Wet, IQQM, FAO56), details are provided on how the correlation between the types was structured.

2.2.1 At-site rainfall model

The rainfall model uses a latent variable concept, which proceeds by sampling from a normally distributed 'hidden' variable. This concept is shown in Figure 17, where a latent variable can be transformed to a rainfall value by truncating values below zero and by rescaling values above zero to match the distribution of rainfall observations. The transformation of rainfall is achieved using a power transformation.

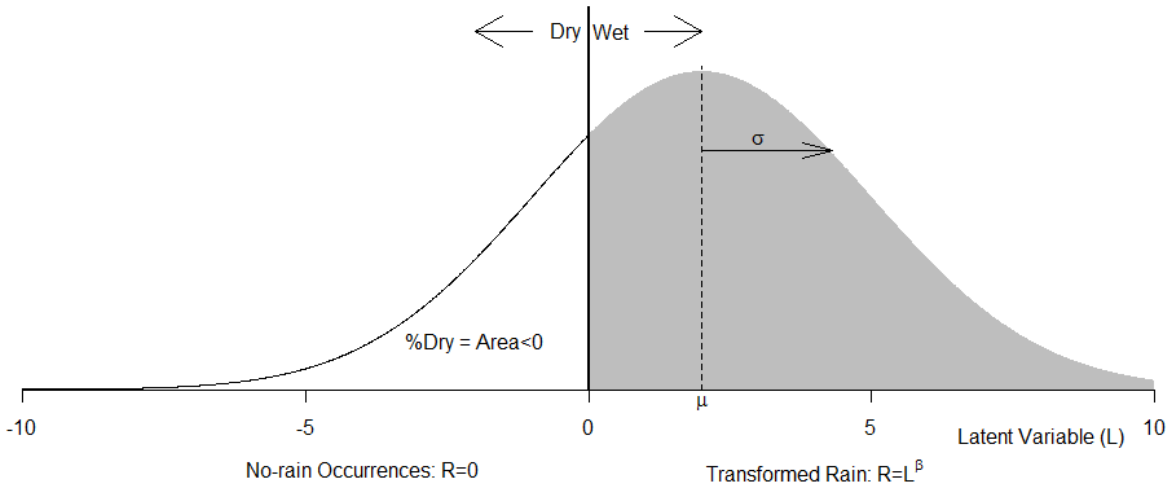

Figure 17 Schematic of latent variable concept

Let r_t^i be the rainfall at site $i = 1, \dots, N$ and $t = 1, \dots, T$. For example, a 100 year simulation would have $T = 365 \times 100$ (ignoring leap years). The rainfall amount can be related to a normally distributed latent variable, l_t^i , via truncation and power transformation,

$$r_t^i = \begin{cases} \left(l_t^i\right)^{\beta_t^i} & l_t^i > 0 \\ 0 & \text{otherwise} \end{cases} \quad \text{where} \quad l_t^i \sim N\left(\mu_{Rt}^i, \sigma_{Rt}^i\right) \qquad (1)$$

where β_t^i is a power transformation parameter. Note that the distribution is specified by two parameters μ_{Rt}^i and σ_{Rt}^i, the mean and standard deviation for each site and timestep. Here, the parameters are varied on a monthly basis, so all timesteps within the same month have identical parameters. Simulating from this distribution reproduces the daily distribution of rainfall for a given time period (e.g. month), including the proportion of zeros. An advantage of the model is that it has parameters to match the mean and variability of daily rainfall. However, the transformation is not always perfect because it needs to match the moments of the rainfall distribution as well as the proportion of zero values.

To model sequences of rainfall values, auto-correlation of the latent variable is considered. Because the variable is Gaussian, it is possible to use a single auto-correlation parameter for a given site to reproduce

sequences of wet and dry values as well as correlation in the amounts of the wet values. The temporal structure at a site is modelled via an AR(1) process.

$$l_t = \mu_t + \varphi_{Rt}(l_{t-1} - \mu_{R_{t-1}}) + \epsilon_t \quad (2)$$

where φ_{R_t} is the autoregressive parameter and the autoregressive error distribution ϵ_t is normally distributed

$$\epsilon_t \sim N\left(0, \sqrt{1-\varphi_{Rt}^2}\,\sigma_{R_t}\right) \quad (3)$$

Figure 18 shows the autoregressive parameter for 100 sites for each month. There is a significant difference in the parameter values within a given month. While it is possible to accommodate these differences when single sites are generated independently, it is difficult to preserve this feature in a multi-site setting (see Rasmussen 2013). For this reason, only the average value is used for each month. The result of this assumption is a loss of variability at the daily timescale, which affects wet-dry patterns and wet/dry spell durations.

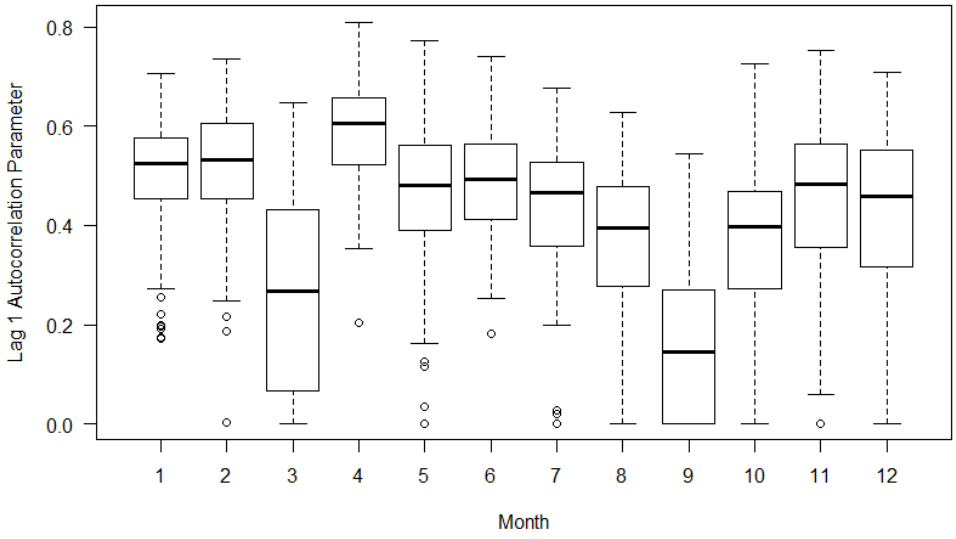

Figure 18 Distribution of lag-1 daily autocorrelation parameter across 100 rainfall sites for each month

A simulation of the single-site daily rainfall model is visualised in Figure 19 for 100 replicates aggregated to monthly totals and compared to the corresponding observations (red symbol). The

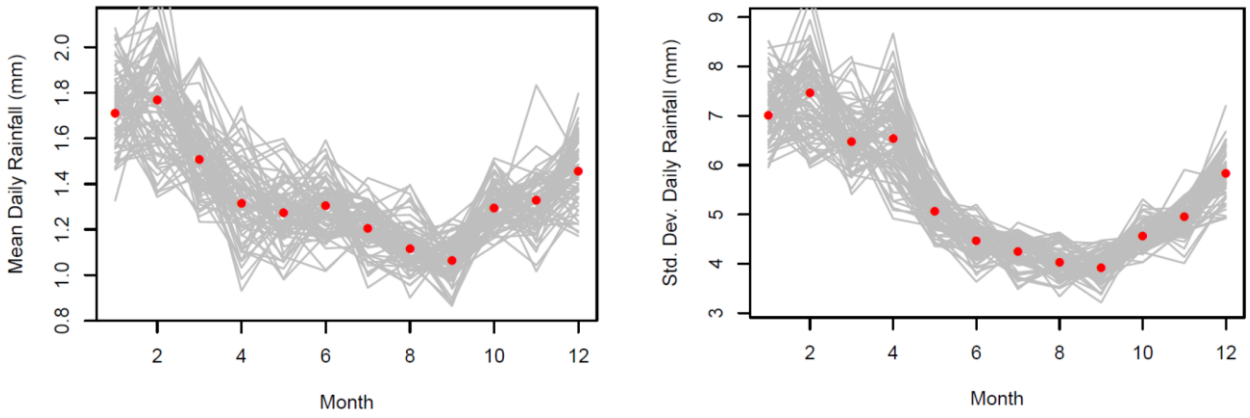

Figure 19 Distribution of rainfall. Observed (red symbol) versus 100 simulated replicates (grey lines) monthly means (left) and monthly standard deviations (right)

2.2.2 At-site evaporation model

Whereas rainfall is highly variable, has a skewed distribution and complex wet-dry pattern, evaporation is a continuous variable (no zeros) and is significantly less skewed. Figure 20 shows a boxplot summary of daily evaporation for each month of a representative site. While the seasonal variation is obvious, a subtle feature of this data is that summer evaporation is skewed (as indicated by the outliers), which is explored in further detail below.

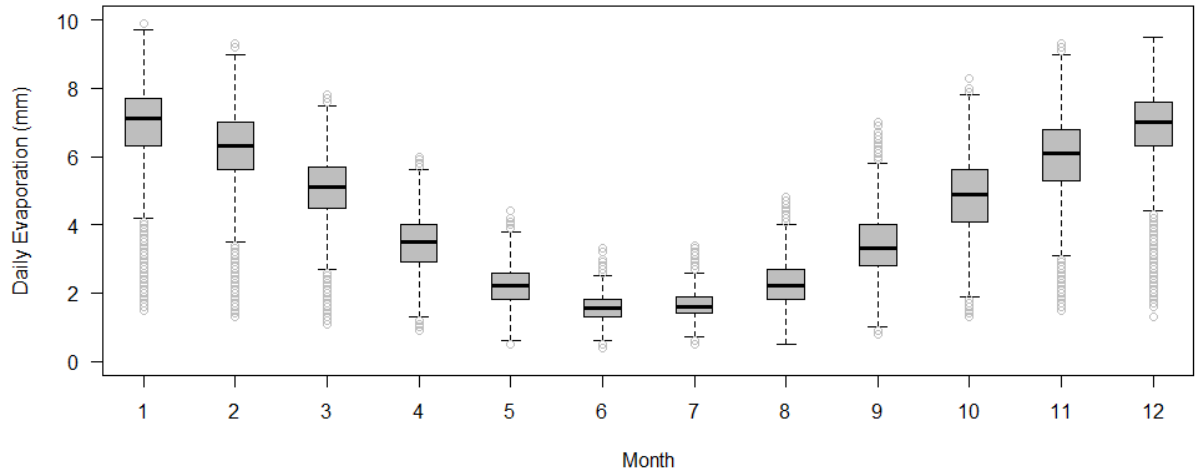

Figure 20 Distribution of daily evaporation for a representative site (which one) for each month

Figure 21 depicts the method used to generate the skewed distribution of daily evaporation, especially for summer months. A split normal distribution is used where the half above the mode has a different standard deviation from the half below the mode.

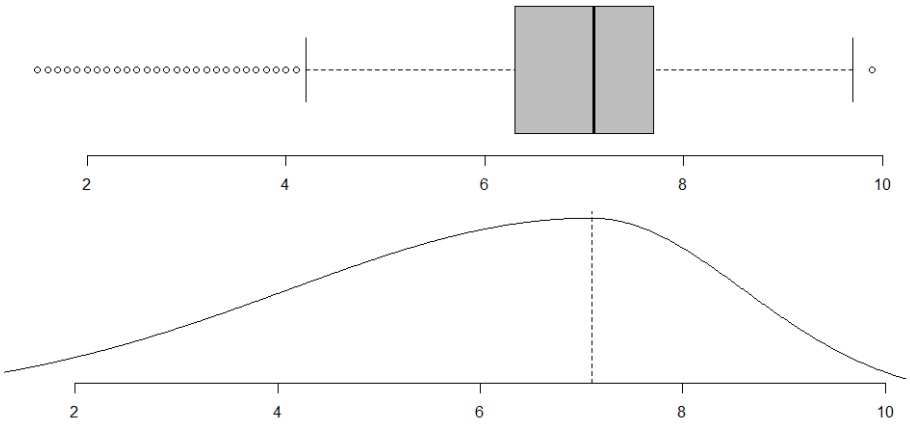

Figure 21 Schematic of method used to reproduce skewness in distribution of daily evaporation

Given the strong seasonal signal and the 'smooth' transition in evaporation between seasons, a sinusoidal method was used to model daily evaporation (whereas the rainfall model has sets of 12 parameters to represent each month). Figure 22 (top) shows the distribution of daily evaporation for all years from a representative site along with a mean sinusoid trend fitted to the data. Subtracting this trend from the data yields residuals with zero mean, but with evidence of seasonality in the variation.

The sinusoidal equations for the mean evaporation $\mu_{E,t}$ on a given day, t, is specified by the linear regression:

$$\mu_{E,t} = \theta_1 + \theta_2 \cos(2\pi t/365.25) + \theta_3 sin(2\pi t/365.25) \quad (4)$$

where θ are the regression coefficients and t is the day. Once the mean model is fitted, the residuals of the evaporation are calculated as:

$$E'_t = E_t - \mu_{E,t} \quad (5)$$

where the fitted mean is subtracted away from the observed evaporation E_t to give the residuals E'_t.

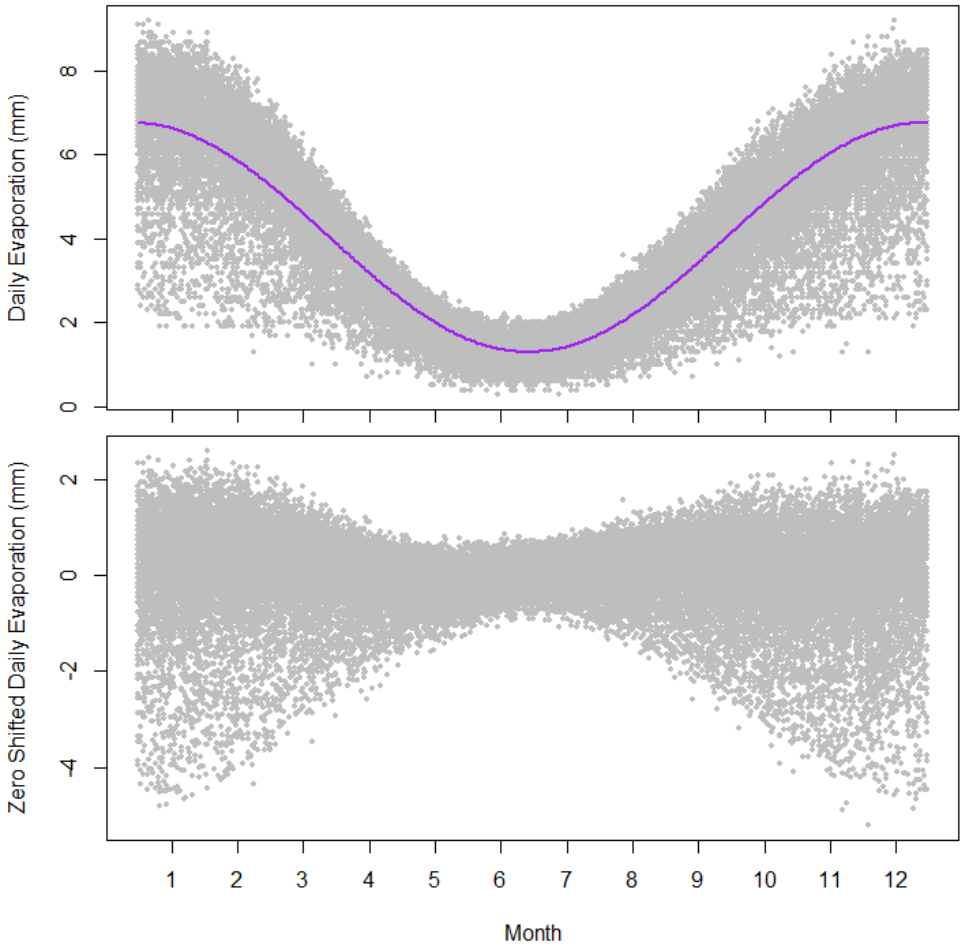

Figure 22 Daily evaporation for a representative site (top) fitted mean trend, (bottom) residuals after removing the mean

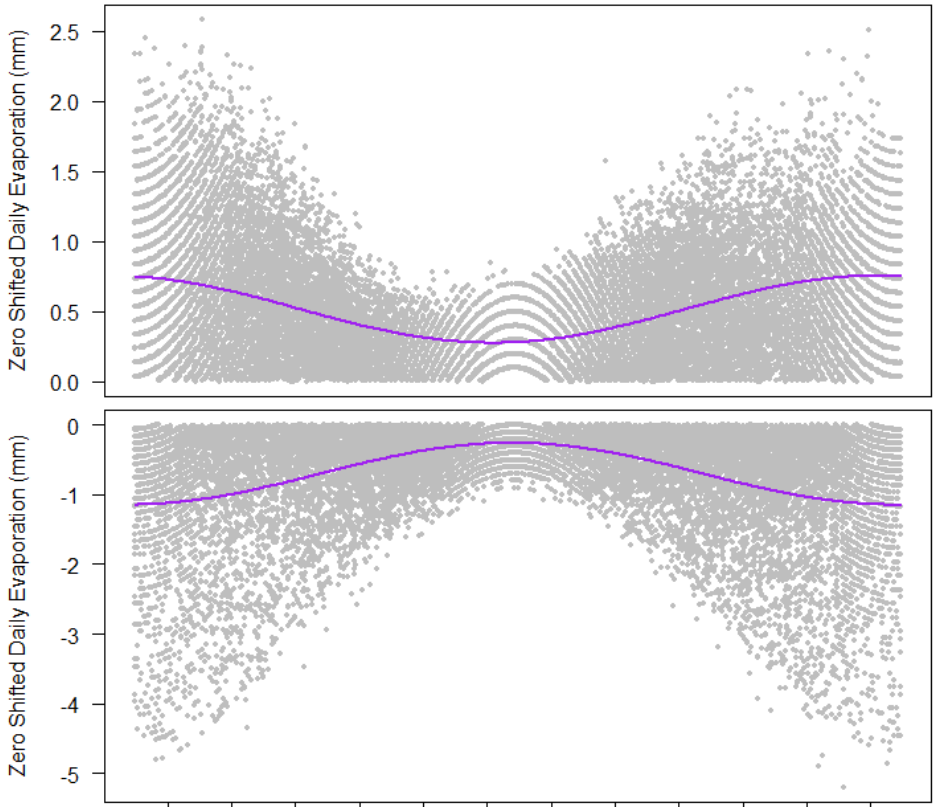

Figure 23 Fitted trends to mean-corrected residuals (top) positive and (bottom) negative

Sinusoidal regression equations for the positive and negative aspects of the residuals are similarly fitted (Figure 23)

$$\sigma_{E,t}^{+} = \theta_4 + \theta_5 \cos(2\pi t/365.25\,) + \theta_6 sin(2\pi t/365.25\,) \quad (6)$$
$$\sigma_{E,t}^{-} = \theta_7 + \theta_8 \cos(2\pi t/365.25\,) + \theta_9 sin(2\pi t/365.25\,) \quad (7)$$

where $\sigma_{E,t}^{+}$ is the standard deviation parameter for a given day of the positive residuals and $\sigma_{E,t}^{-}$ is the counterpart for the negative residuals.

The standardised residuals E_t'' are obtained by dividing the evaporation residuals E_t' by the relevant standard deviation parameter for a given day.

$$E_t'' = \begin{cases} E_t'/\sigma_{E,t}^{+} & \text{where } E_t' > 0 \\ E_t'/\sigma_{E,t}^{-} & \text{where } E_t' \leq 0 \end{cases} \quad (8)$$

An example of the standardised residuals is shown in Figure 24. The overall spread of the distribution is approximately normal, but there are some noticeable artefacts. The distribution is not identically distributed throughout the year, which is because the sinusoid is not a perfect fit for the seasonality. There is a 'fingerprint' stippling effect in the middle of the year, which is also due to (i) the sinusoid transformation (causing the curve) and (ii) the digitized input (only 1 decimal place) along with the small range of values in winter (Figure 22) causing the transformed values to appear quantized. None of these artefacts are significant because the normal distribution is a good approximation to the standardised residuals.

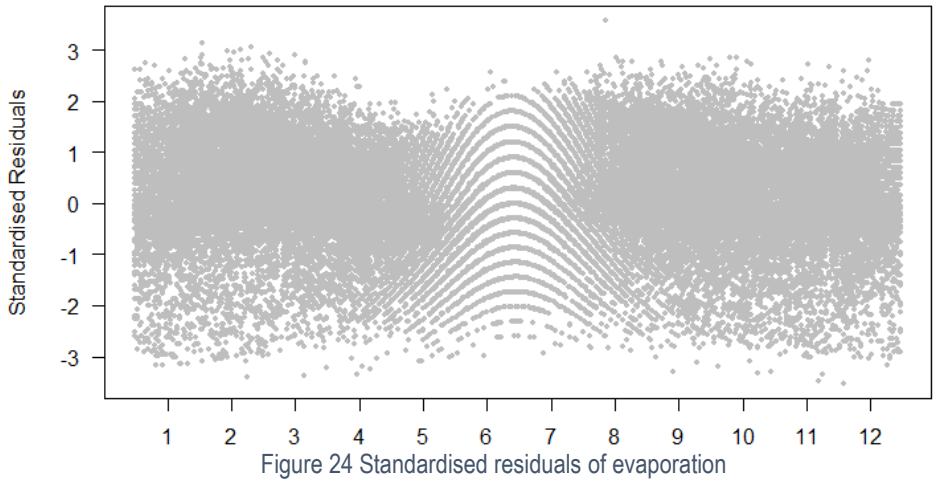

Figure 24 Standardised residuals of evaporation

Once the standardised residuals are obtained, it is necessary to determine the auto-correlation structure of the residuals. Figure 25 shows the autocorrelation for a representative site. An AR(1) autoregressive model is used to represent the temporal correlation structure of evaporation

$$E_t'' = 0 + \varphi_{Et}(E_{t-1}'' - 0) + \epsilon_t \quad (9)$$

where the mean of the residuals is 0, φ_{E_t} is the autoregressive parameter and the autoregressive error distribution ϵ_t is normally distributed

$$\epsilon_t \sim N\left(0, \sqrt{1-\varphi_{Et}^2}\right) \quad (10)$$

The autoregressive model is able to reproduce the main correlations in the first few lags, but it does not reproduce the low levels of correlation present up to lag 40.

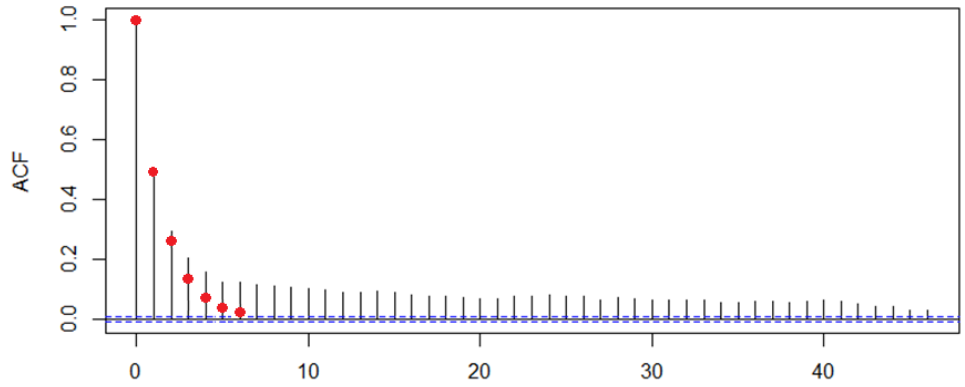

Figure 25 Autocorrelation of standardised residuals for a representative site, x axis represents daily lags

A simulation of 100 replicates of the single site evaporation model is shown in Figure 26 at the daily scale and Figure 27 at the monthly scale (in terms of monthly mean and monthly standard deviation). The dashed lines show the 99.7% confidence interval of the simulations, which agree with the underlying distribution of observations (grey symbols). Even with the split-normal distribution, there is a noticeable discrepancy in the lower tail of the summer months (observed grey values can be seen below the red simulated values). The reason for this is due to a limitation of the sinusoid linear regression: an explanatory variable with a sharper transition than a sinusoid would be required to allow for higher variability in the summer months.

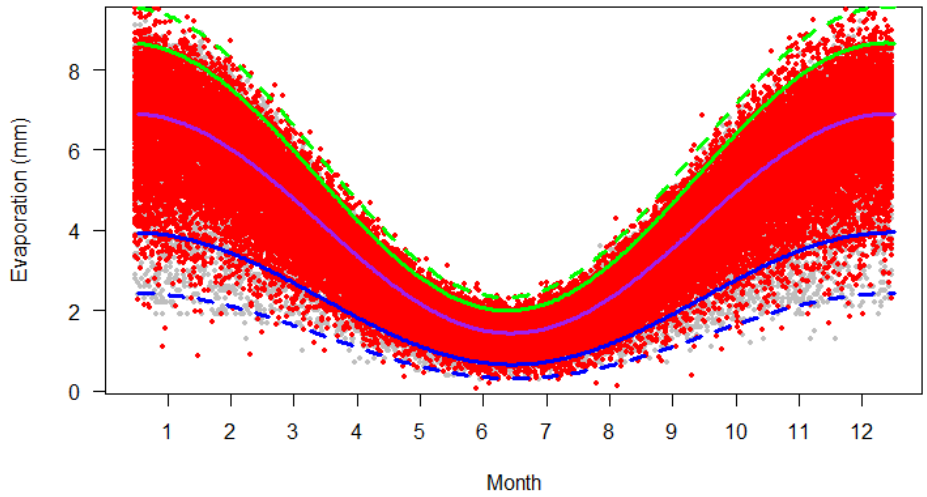

Figure 26 Example simulation from single-site model of evaporation. Grey symbols are observations, red symbols are simulation. Solid purple shows the simulated mean, solid blue/green show the lower/upper 95% interval and dashed blue/green show the lower/upper 99.7% interval

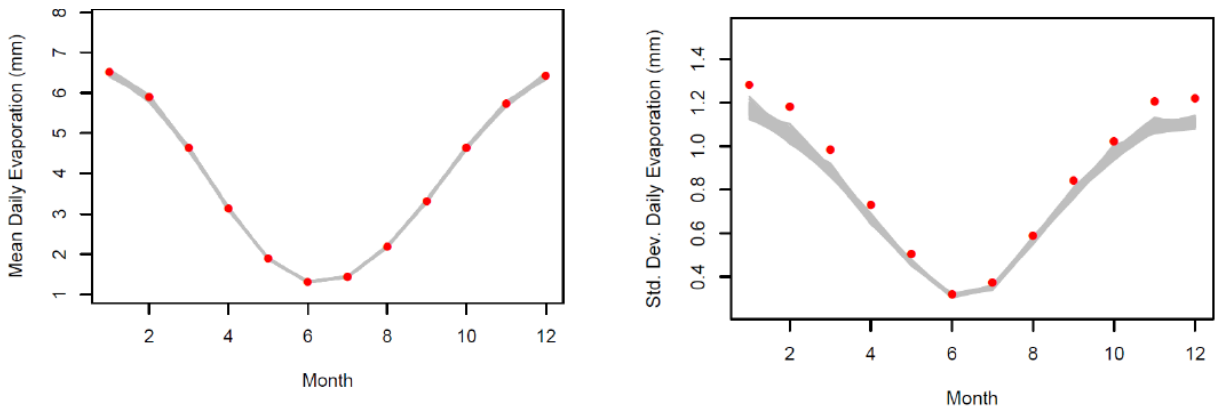

Figure 27 Distribution of rainfall. Observed (red symbol) versus 100 simulated replicates (grey lines) monthly means (left) and monthly standard deviations (right)

2.2.3 Multi-site rainfall model

Developing the multisite model from the single-site model requires the spatial cross-correlation between sites. An example of the correlation with distance is shown for 100 pairs of rainfall sites for a selected month (all the months look similar). There is a noticeable scatter in the data due to variation within the region, but it is nonetheless very high (e.g. after 250 km the correlation is 0.6). Because the model is a multisite model, it is possible to fit the sample correlations exactly. In other words, because it is not required to infill/interpolate between the gauges it is not required to fit a smooth correlation function to the data (which would reduce the variability). Estimating the pairwise correlation for all sites yields the correlation matrix shown in Figure 30. The main point of interest is the blue stripes that persist in a couple of the rows/columns, indicating these sites have a low correlation to the rest of the region (e.g. site R10, R12, R13, and R22). Given there are 100 sites, the lower correlation at these sites is not likely to have a big impact on the overall catchment rainfall.

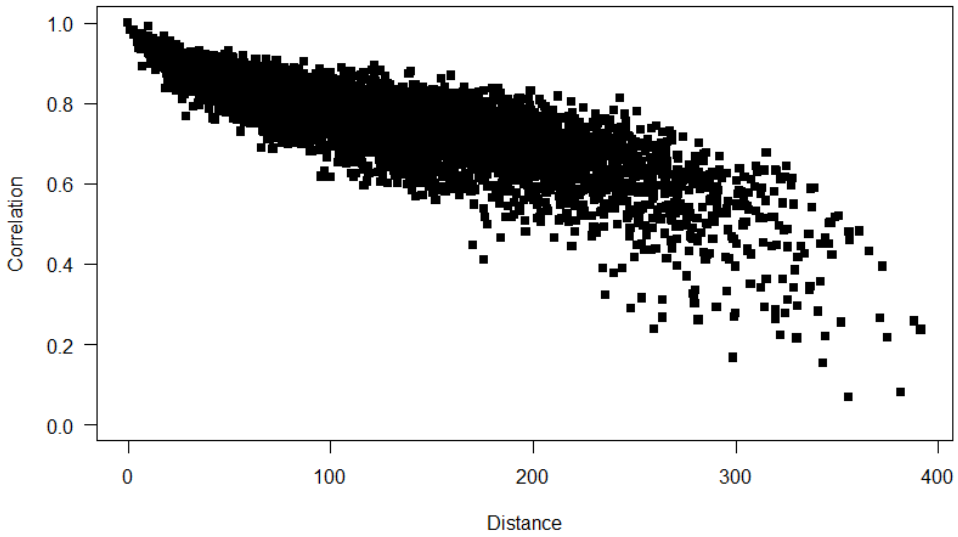

Figure 28 Rainfall sample correlation values with distance for a representative site and month

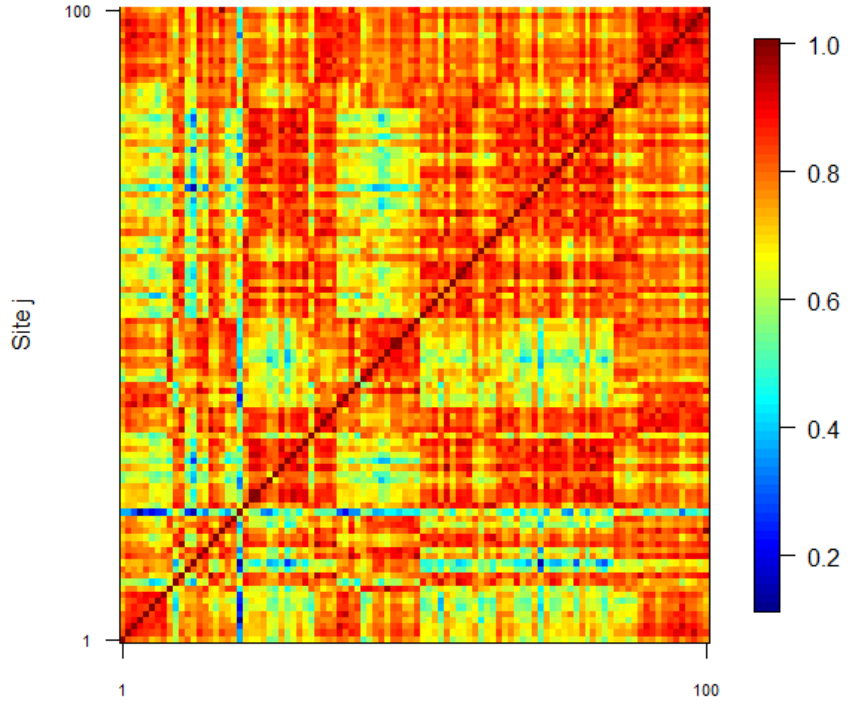

Figure 29 Rain-Rain correlation matrix for 100 sites

2.2.4 Multi-site evaporation model

The correlation structure of the evaporation data is more complicated because of the three different types. As with the rainfall, it is not necessary to fit a smoothed correlation function to the data because a multi-site model is being used (rather than continuous in space). An example of the evaporation correlations is shown in Figure 30. A colour-coded matrix is provided in the right panel of Figure 30 to show the pairings of the various types. As with rainfall there are significant correlations with distance, where the correlation after 250 km is approximately 0.6 when each type (Mwet – black, IQQM – blue, FAO56 – red) is compared to itself. When there is a cross-correlation between two different types of evaporation, the correlation is lower (for example FAO56 with Mwet – magenta). The IQQM evaporations have the lowest correlation to other data (Mwet – orange, FAO56 – green), suggesting this data is not strongly related to the other evaporation data types for the region. This can also be seen in the correlation matrix (Figure 31).

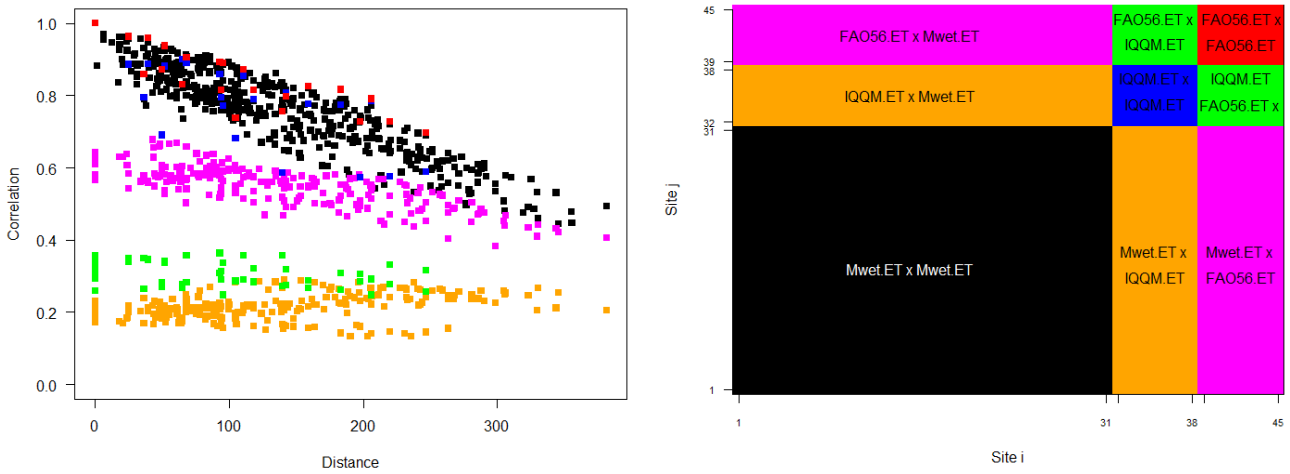

Figure 30 Structure of evaporation correlations (left) shows sample correlation with distance for a representative site. Banding of the correlation is evident due pairing of to the different types of evaporation: Mwet-Mwet (black); Mwet-IQQM (orange); Mwet-FAO56 (magenta); IQQM-IQQM (blue); IQQM-FAO56 (green) and FAO56-FAO56 (red). (right) A key for the different pairings of evaporation type in the structure of the covariance matrix.

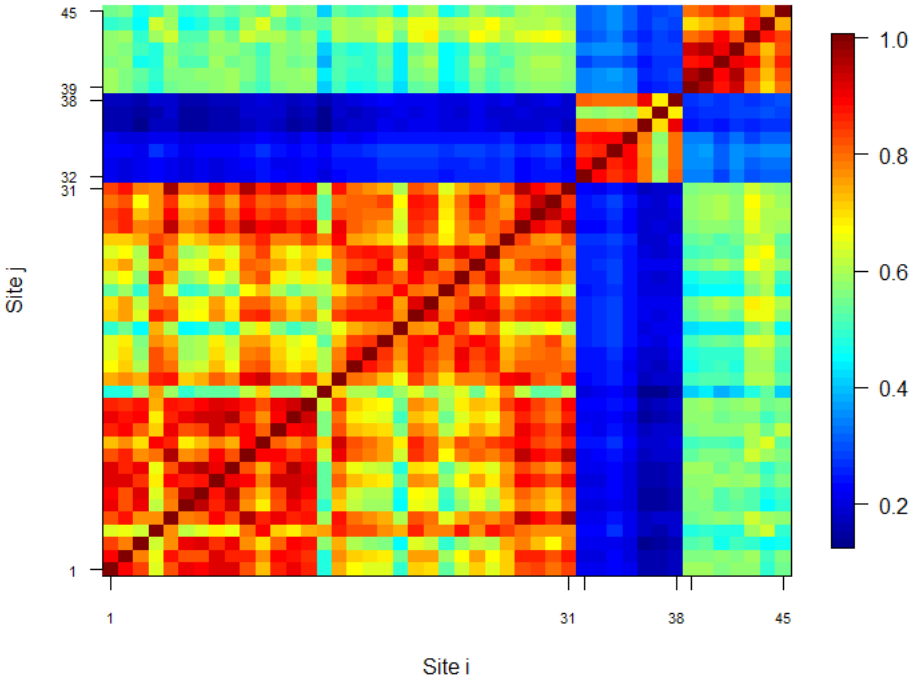

Figure 31 Evap-Evap correlation matrix for 45 sites

2.2.5 Joint simulation of rainfall and evaporation

With the multisite specifications in the prior sections it is possible to simulate multisite rainfall at 100 sites, or multisite evaporation at 45 sites, but not (yet) possible to jointly simulate rainfall and evaporation jointly at 145. To achieve this it is necessary to account for the correlation between rainfall and evaporation. Figure 32 shows a representative analysis of rain-evaporation correlation with distance. The correlation is negative and typically in the range 0.2 – 0.3, even for distances 250 km apart. As with Figure 30, there is a small degree of striping, which is due to the different evaporation types.

An exponential correlation function is fitted (red line) to the rainfall-evaporation cross correlations

$$COR(d) = Cexp(-d/\alpha) \quad (11)$$

where $COR(.)$ is the correlation, d is the distance between a pair of locations, α is the range parameter and C is the scale parameter. A model is fitted to the cross correlations to ensure the robustness of the overall correlation model (when using sample correlations there can be issues with the positive definite structure of the correlation matrix). Using a fitted model introduces some smoothness into this element of the correlations, but it should not be significant because the correlations are relatively low and because they are relatively consistent (between 0.2 – 0.3).

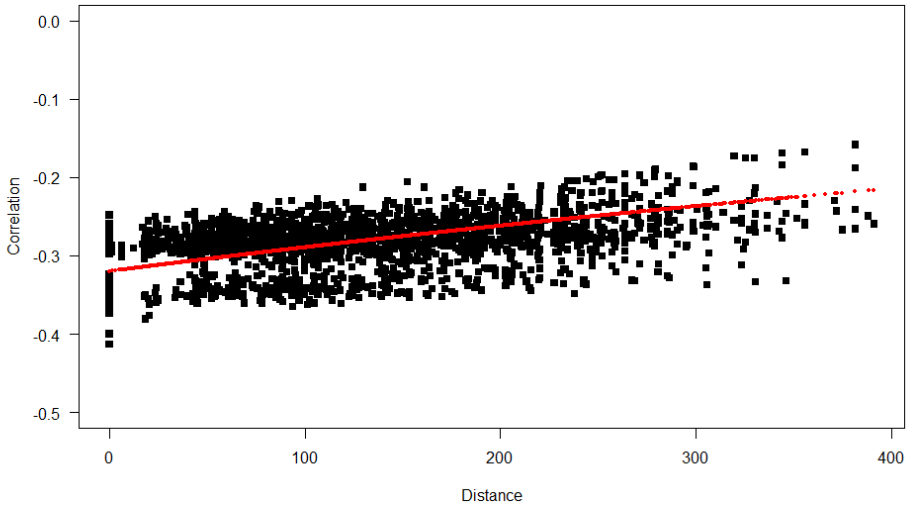

Figure 32 Rainfall-Evaporation sample correlation values with distance for a representative site and month, observations (black) and fitted correlation function (red)

Figure 33 shows a jointly populated rainfall-evaporation correlation matrix, where the diagonal terms reproduce the existing rain-rain (Figure 29) and evap-evap (Figure 31) correlation matrices. The off-diagonals are based on correlations from Figure 32.

Figure 34 shows the extension of the spatial rain-evap correlation model (Figure 32) to include the lag-1 correlation parameter. The diagonal terms give the lag-0 spatial correlations for timesteps t and $t+1$ respectively. The off-diagonal terms give the lag-1 space-time correlations (e.g. site i time t with respect to site j time $t+1$). The space-time correlations are obtained by assuming a contemporaneous model structure (Rasmussen, 2013). This means that the space-time correlation can be decomposed into a spatial correlation multiplied by a single temporal correlation (for that month) which is the same at all sites. The benefit of this assumption is model stability. The limitation of this assumption is that all sites must use the same autocorrelation parameter (as noted in Figure 18, it is variable). The impact of this assumption is a reduction in the flexibility to represent different sites (they will all have the same autocorrelation for the latent variable). This means that statistics strongly associated with autocorrelation at the daily scale may lack variability (e.g. length of daily wet/dry spells). The correlation matrix in Figure 34 represents a full specification of the correlation structure needed to simulate the model across all sites and multiple timesteps for a given calibration period.

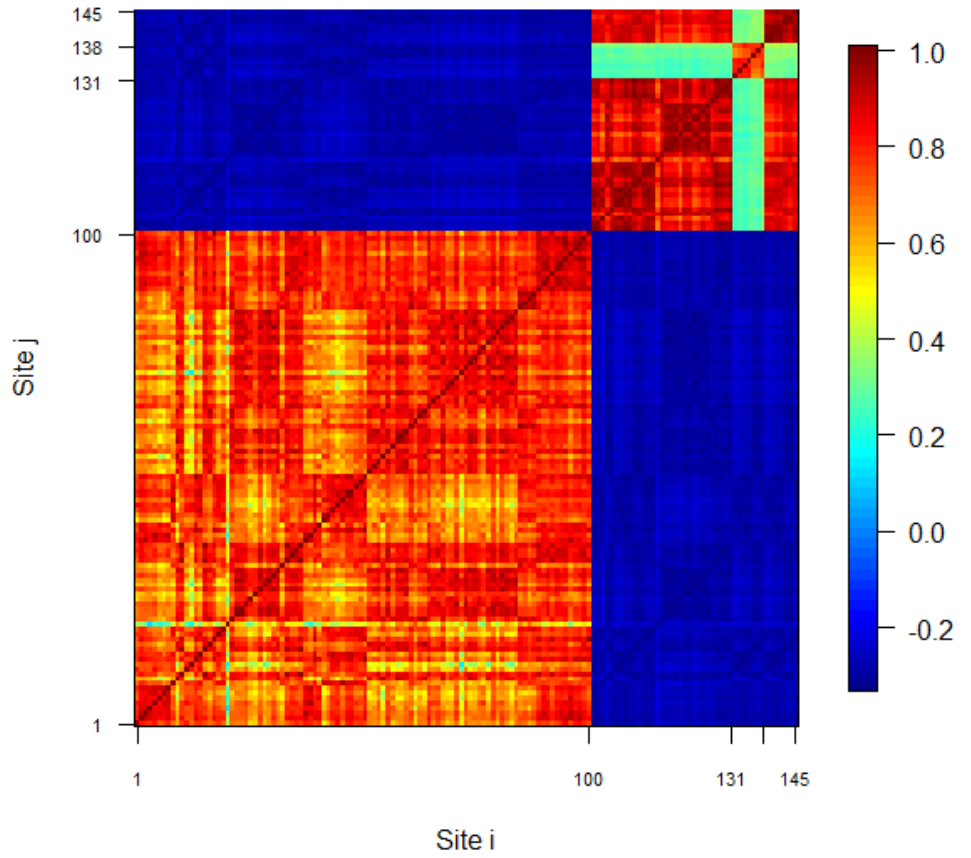

Figure 33 Nested block-correlation matrix joint simulation of 100 rain sites and 45 evaporation sites. Rain-Rain correlation is the bottom left block (Figure 29); Evap-Evap as the top-right block (Figure 31) and the off-diagonal blocks showing negative correlations obtained from the Rain-Evap function (Figure 32).

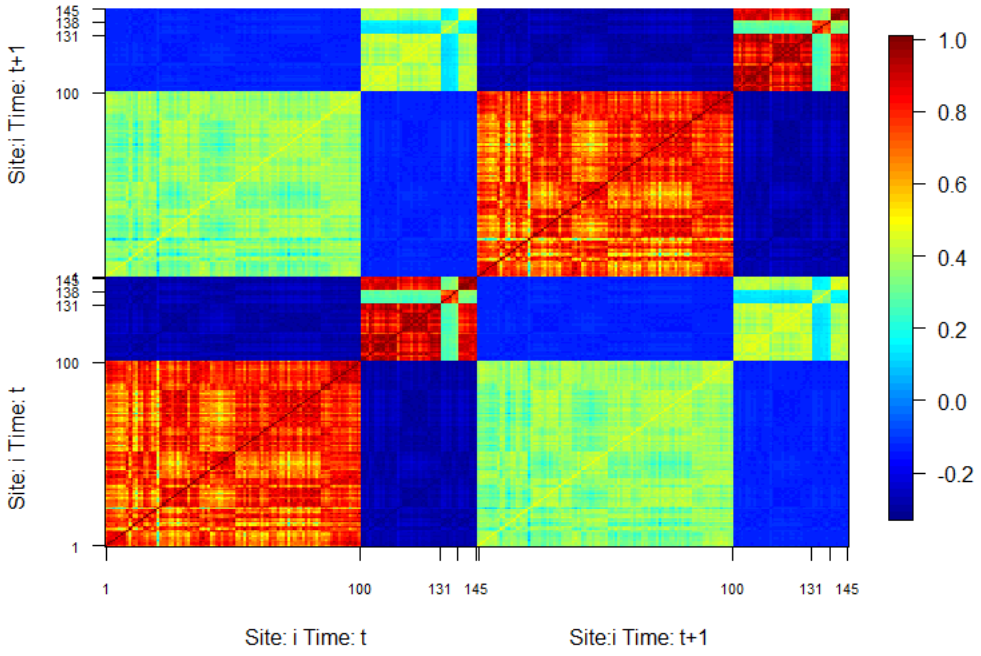

Figure 34 Nested block-correlation matrix joint simulation of 145 sites and two timesteps, lower left block time (t, t) and upper right block (t+1, t+1) are nested matrices from Figure 26 of static spatial correlations, the off-diagonal blocks represent the lag-1 in time (t, t+1) cross-correlations between pairs of sites. The off-diagonals are rescaled from the spatial correlations by a constant autocorrelation parameter across all sites (space-time separable covariance structure).

2.3 Extended Model Specification – Climatic Variability and Future Climate

2.3.1 IPO Dwell-time distribution from instrumental and paleoclimatic record

The IPO is modelled according to two states negative and positive. Let $\boldsymbol{D}^- = (D_1^-, D_2^-, \dots)$ denote the dwelling time in the negative IPO state and $\boldsymbol{D}^+ = (D_1^+, D_2^+, \dots)$ denote the dwelling time in the positive IPO state, in years. The IPO is modelled as an alternating renewal process where the system starts in an arbitrary state, for example the positive state, and persists for a duration D_1^+ before transitioning to the negative state for a period D_1^- and then back for the duration D_2^+ . The oscillation continues for a number of cycles nc, until the total duration spanning the duration equals the length of the simulation $\sum_{j=1}^{nc} D_j^+ + D_j^- = (T/365)$. All dwelling times are considered by be independent and identically distributed, and to come from a gamma distribution (Henley et al., 2011, Figure 4, see also Figure 9 this report), defined as

$$f(x) = \frac{1}{s^a \Gamma(a)} x^{a-1} exp\left(-\frac{x}{s}\right) \quad (12)$$

where a is the shape parameter, s is the scale parameter and $\Gamma(a)$ is the gamma function. For the j^{th} year, the dwelling time, whether in the positive or negative state, is independently sampled from the gamma distribution

$$D_j^{\mp} \sim gamma(a, s) \quad (13)$$

where the parameters are related to the distribution mean, m, and standard deviation, s, as $a = (m/s)^2$ and $s = (m/s)^2/m$.

For the instrumental IPO record, the dwelling time distribution for IPO phases has the properties , $m = 17$ and $s = 8$ (Henley et al., 2011). For the paleoclimatic IPO record, the dwelling time distribution for IPO phases has the properties, $m = 15$ and $s = 10$ (Henley et al., 2011). An example simulation is shown for 1000 years based on parameters from the IPO instrumental record, an example of a state persisting for 58 years can be seen between years 88 to 144.

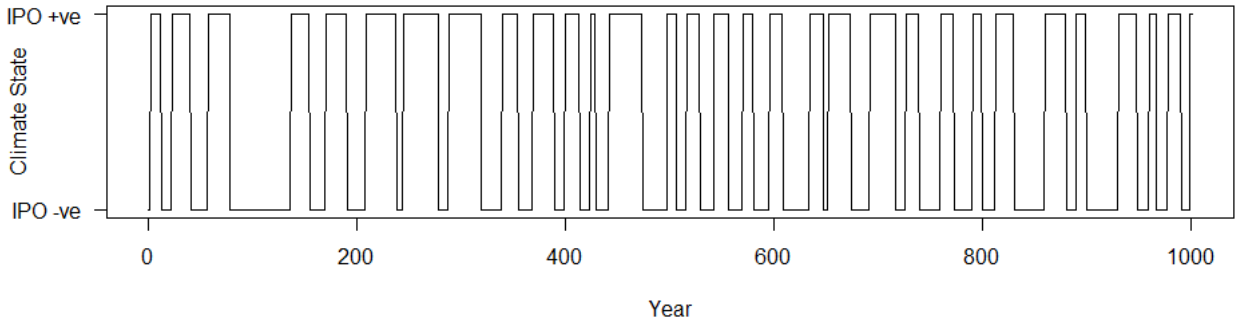

Figure 35 Example simulation of 1000 years IPO states from the alternating renewal model with parameters from the IPO instrumental record.

2.3.2 Future changes as a result of anthropogenic climate change

The Climate Change in Australia website (CSIRO and Bureau of Meteorology, 2015) provides distributions of scaling factors comparing projected rainfall and evaporation to historical variability. Factors from the RCP4.5 scenario are available at a seasonal level and are used to scale simulations to match the conditions of representative 20-year time slices centred on the years 2030, 2050, 2070, 2090. While this methodology is relatively simple, it is intended to provide an indication of plausible future changes that may inform water balance modelling (e.g. decreases in rainfall, increases in evaporation relative to baseline variability).

There are two consequences for the climate scaling due to the output method being a single 10,000 year replicate.

1. The first consequence is that for a single 10,000 year replicate, it is appropriate to use only the mean value for each time slice to scale the timeseries. The model projections also indicate some differences in variability and model uncertainty (respectively differences in the 'whiskers' and the 'box' from Figure 15 and Figure 16 of projections compared to the baseline). This information cannot readily be incorporated into a single 10,000 replicate. To include this variability would require the addition of spurious oscillations/perturbations in the timeseries that could be misinforming about realistic variability (i.e. they emulate model uncertainty but do not reflect an authentic physical feature). By only using the mean value to scale, the simulated data will have some over-precision that would not otherwise be present if rainfall and evaporation were downscaled directly from one or more GCMs.
2. The second consequence is that because there are only four scaling factors per time slice (one for each season), it is useful to interpolate these factors so the timeseries transitions smoothly. This is done to avoid abrupt shifts that might complicate the interpretation of a subsequent water balance assessment. Figure 36 and Figure 37 show the curves of interpolated factors used to scale the timeseries, which were developed using a periodic spline function (so the 31/13 to 01/01 boundary condition matches). Care should be used in subsequent assessments to avoid overly prescriptive interpretations that might arise from using the rescaled data. For example, Figure 36 shows that in autumn (March-April-May) the scaling factor is approximately -5% for the 2030 and 2050 timeslices, then moves to -0.5% for the 2070 timeslice and then back to -5% for the 2090 timeslice. This is not necessarily a physical mechanism, but could readily be an artefact of model averaging that is pronounced when model uncertainty is not considered.

The method of rescaling is a straightforward multiplication of the scaling factors in Figure 36 and Figure 37 for each day of the year. This implies that the entire distribution will be affected, e.g. the mean, the standard deviation and the extremes.

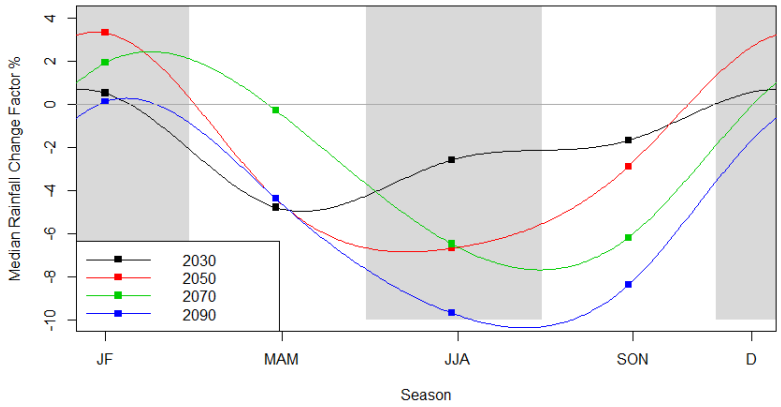

Figure 36 Change factors for projected rainfall RCP4.5 shown for multiple time periods and seasons, CSIRO Climate Futures

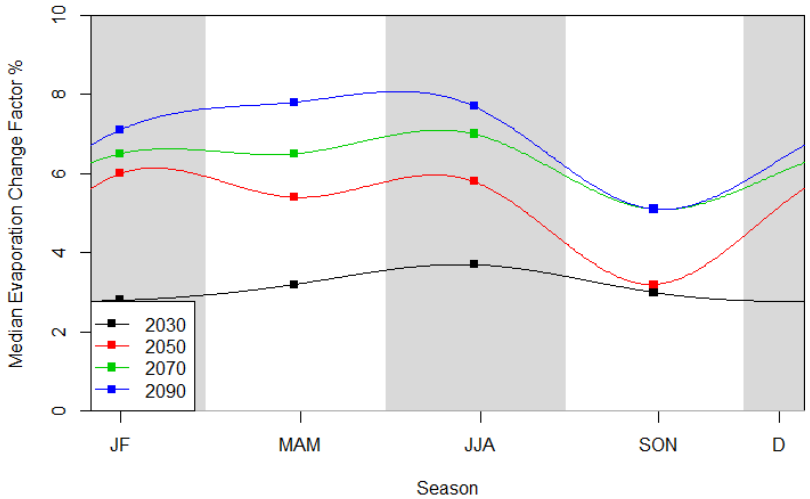

Figure 37 Change factors for projected evaporation RCP4.5 shown for multiple time periods and seasons, CSIRO Climate Futures

2.4 Model Calibration

Details of the calibration procedure are provided in Bennett et al. (2018), therefore only an overview is provided here. At all stages, the method of moments and least squares are used to determine parameters.

2.4.1 Step 1. Rainfall – Single site rainfall distribution

The data for each site are partitioned monthly, where separate parameters are fit for each month on record. The mean and standard deviation of rainfall amounts, as well as the proportion of dry days is calculated. These statistics are matched to the corresponding properties of the truncated power transformed normal distribution from Eq. (1), having parameters $\mu_{Rt}^{i}, \sigma_{Rt}^{i}, \beta$. Thus there are 3 x 12 parameters per site.

2.4.2 Step 2. Rainfall – Single site temporal correlation

The autocorrelation is calculated for each site based on the rain-day periods for a given month. To determine the parameter φ_{R_t}, this statistic is transformed to the equivalent correlation of the underlying latent variable by accounting for the effects of truncation (Bennett et al., 2018). There is one parameter per month per site. However, the contemporaneous multisite autoregressive model requires a common autocorrelation parameter for all sites. The parameter value is averaged across all sites to yield one parameter per month.

2.4.3 Step 3. Rainfall – Spatial correlation

The procedure for estimating spatial correlation is identical to single-site autocorrelation, except that it is calculated for the lag-0 in time cross-correlation for a pair of sites. Because the model is not continuous in space, it is not necessary to fit a correlation function. Instead the sample correlations can be used for each pair of sites to parameterise the correlation matrix. For $n = 100$ sites there are $n(n-1)/2 = 4950$ unique pairs of sites (i.e. 4950 parameters per month).

2.4.4 Step 4. Evaporation – Single site evaporation distribution

The regression function for the mean daily evaporation is fitted first to the daily observations using Eq. (4) and then subtracted from the observations to produce a residual timeseries, Eq. (5). The residuals are split according to positive and negative values, with a separate regression function fitted to each partition, Eq. (6) and Eq. (7). On dividing through by the fitted model, standardised residuals are obtained using Eq. (8). The remaining timeseries is assumed to be normally distributed. There are three sets of regression equations, each having three parameters, giving nine parameters per site.

2.4.5 Step 5. Evaporation – Single site temporal correlation

The lag-1 autocorrelation is calculated of the standardised residual observed timeseries (obtained from Step 4). This parameter φ_{E_t} is set equal to the lag-1 sample autocorrelation. As with the rainfall autocorrelation, this value is averaged across all sites, yielding a contemporaneous version of the evaporation model. Thus there is only one parameter per month.

2.4.6 Step 6. Evaporation – Spatial correlation

The lag-0 cross correlation for all pairs of evaporation sites is calculated. Because the model is not continuous in space, it is not necessary to fit a correlation function. Instead the sample correlations can be used for each pair of sites to parameterise the correlation matrix. For $n = 45$ sites there are $n(n-1)/2 = 990$ unique pairs of sites (i.e. 990 parameters per month). As discussed with respect to Figure 30, the different types of evaporation have different correlation properties, but these are directly represented in the correlation matrix because each pair of sites has its own sample correlation.

2.4.7 Step 7. Rainfall-Evaporation – Spatial correlation

The lag0 in time cross-correlation is calculated between each of the 100 rainfall sites and the 45 evaporation sites. The parameters of the correlation function (range α and scale C in Eq. (11)) are fitted to the cross-correlations using least squares. There are two parameters fitted per month. The correlation function is used instead of sample correlations for improved model stability.

2.4.8 Step 8. Space-time correlation

There are no extra steps required to fit the space-time correlations, that is, the lag-1 in time cross correlation between sites. These correlations are assumed to follow a space-time separable structure. In other words the lag-1 cross correlation is obtained from the lag-1 autocorrelation (Steps 2 and 5) multiplied with the lag-0 cross correlation (Steps 3, 6 and 7).

2.4.9 Step 9. IPO calibration

Steps 1 to 8 specify the model calibration requirements for 'Model A' – the base model. To calibrate the model for model B, the timeseries are partitioned into the IPO positive and negative states indicated in Section 2.1.3. A separate set of parameters is fitted to each partition. The parameters for the dwelling time in each IPO phase are obtained from Henley et al. (2011).

2.4.10 Step 10. Future Climate

The seasonal climate factors for the future climate conditions, RCP4.5 were obtained from the Climate Change in Australia website (CSIRO and Bureau of Meteorology, 2015). The median values for each season of a given time slice were interpolated using a periodic spline to provide smooth transitions between the seasons.

2.5 Model Evaluation

Evaluation of stochastically generated weather can involve many different aspects including a range of timescales, locations and statistics of relevance. Many evaluation methods rely on visual inspection and qualitative assessment. Bennett et al. (2018) demonstrated the benefit of using a systematic quantitative assessment, which provides consistent evaluation and the ability to pool evaluations over a larger grouping.

The general approach of Bennett et al. (2018) is used here having three categories 'Good', 'Fair' and 'Poor'. A variation has been made to the performance criterion for the 'Fair' category, which had limited utility in Bennett et al. (2018) as a 'borderline' category. The following sections outline the rules of the specific tests. It is not important for the tests to represent a statistical hypothesis test, only that they can reliably differentiate between classes of performance as a relative measure. Performance plots of all the relevant statistics are also provided in Annexes to this report for each location, therefore enabling visual inspection of the results in conjunction with the formal model evaluation approach. Regardless of the method, interpreting the evaluation requires consideration for the relevance of the statistic to the application of interest.

2.5.1 Evaluation of distribution quantiles

A common case to evaluate is how well the quantiles of a distribution are matched between observations and simulations. Figure 38 provides a schematic illustration of two tests used to evaluate 'goodness of fit' of distribution quantiles and classify the fit of the entire distribution to a relevant category. The two tests are:

TEST 1: Are more than 90% of the observations within the 90% confidence intervals of the simulation?

- If the first test is passed, a classification of 'Good' is applied. This is shown in Example A (Figure 38), where some quantiles may be outside the interval, but there are not many.

- If the first test is not passed, a second follow-up test is required. This is shown in Example B, where many quantiles are outside the interval.

TEST 2: Comparing the simulated 90% confidence intervals to the 90% range of sampling variability for each statistic, are more than 90% of the intervals overlapping?

- This test is more lenient test than Test 1. A bootstrap method can be used to calculate the sample variability of the observed statistic. If most quantiles overlap then a classification of 'Fair' is applied (see Example C).
- If both tests are failed a classification of 'Poor' is applied (see Example D).

2.5.2 Evaluation of distribution of monthly totals

Another common case is to evaluate the distribution of monthly totals, since the model uses monthly parameters for some aspects and because of the significance of the seasonal cycle. The evaluation in this report considers the mean and standard deviation of monthly totals from 129 year record lengths. Having multiple simulated replicates (e.g. 77 replicates) produces a distribution of means and a distribution of standard deviations of monthly totals.

The same tests used on the quantiles (Section 2.5.1) are used on the distribution of means and distribution of standard deviation for the 12 months. The same concept of requiring a 90% match is applied, but in the context of monthly distributions there are only 12 data points, so the criteria is rounded so that 11 of the 12 months must be within the confidence interval.

Figure 39 provides a flow chart for this type of statistic, which is near identical to Figure 38. Note that 'Good' and 'Fair' labels can be achieved with the possibility that one month's observed statistic is outside the simulated limits. As with the prior illustration, Test 2 is more lenient because it allows for sample variability in the observation. Based on sampling properties of the normal distribution, the sample variability for the mean monthly total can be calculated analytically for the 90% limits as $X_{\mu}^{90\%} = \hat{\mu} \pm 1.64\hat{\sigma}/\sqrt{n}$ and for the 90% limits of the standard deviation of monthly totals as $X_{\sigma}^{90\%} = \hat{\sigma} \pm 1.64\hat{\sigma}/\sqrt{2n}$, where $\hat{\mu}$ is the estimated mean of observed monthly totals and $\hat{\sigma}$ is the estimated standard deviation of the observed monthly totals and n is the number of observations (here $n = 129$ years)

2.5.3 Pooling performance over multiple sites

Table 4 shows the rules used to pool multiple sites and determine an overall summary classification for that statistic. When more than 50% of the individual sites are labelled 'Good', a classification of 'Overall Good' is applied to that statistic. A similar rule is applied to determine the classifications 'Overall Fair' and 'Overall Poor'. Where there is no single category with more than 50% the labels of 'Overall Fair-Good', 'Overall Fair-Poor' and 'Overall Variable' are used according to the rules outlined in Table 4.

Table 4 Aggregate performance categorisation criteria from Bennett et al. (2018)

Overall Performance Categorisation	Test	Example
'Overall Good'	'good' > 50 %	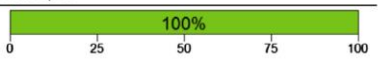
'Overall Fair'	'fair' > 50 %	
'Overall Poor'	'poor'> 50%	
'Overall Fair – Good'	'fair' & 'good' > 'poor'	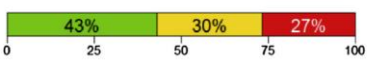
'Overall Fair – Poor'	'fair' & 'poor'> 'good'	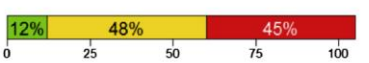
'Overall Variable'	'good' & 'poor' > 'fair'	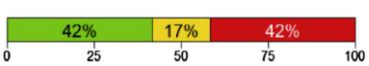

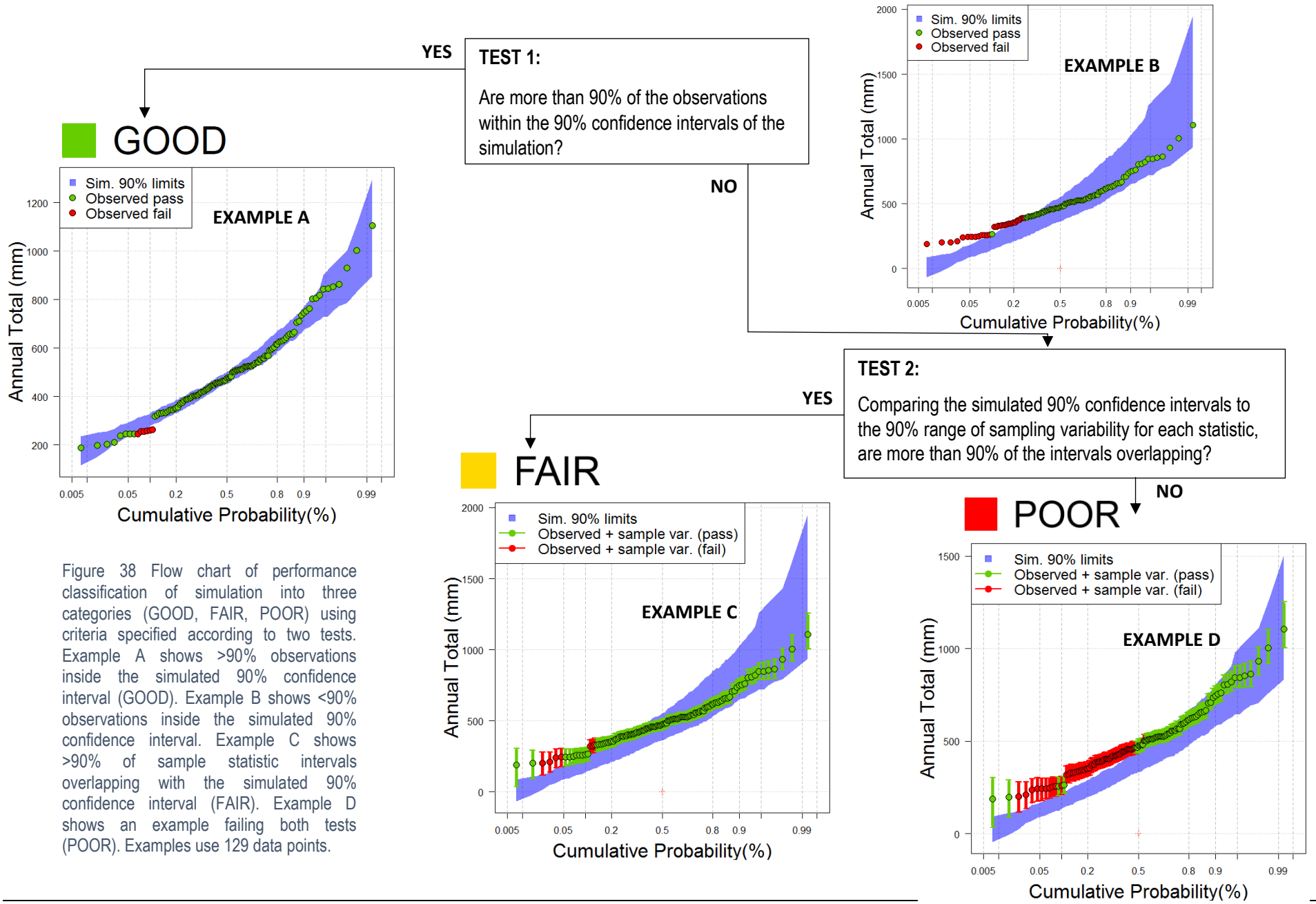

Figure 38 Flow chart of performance classification of simulation into three categories (GOOD, FAIR, POOR) using criteria specified according to two tests. Example A shows >90% observations inside the simulated 90% confidence interval (GOOD). Example B shows <90% observations inside the simulated 90% confidence interval. Example C shows >90% of sample statistic intervals overlapping with the simulated 90% confidence interval (FAIR). Example D shows an example failing both tests (POOR). Examples use 129 data points.

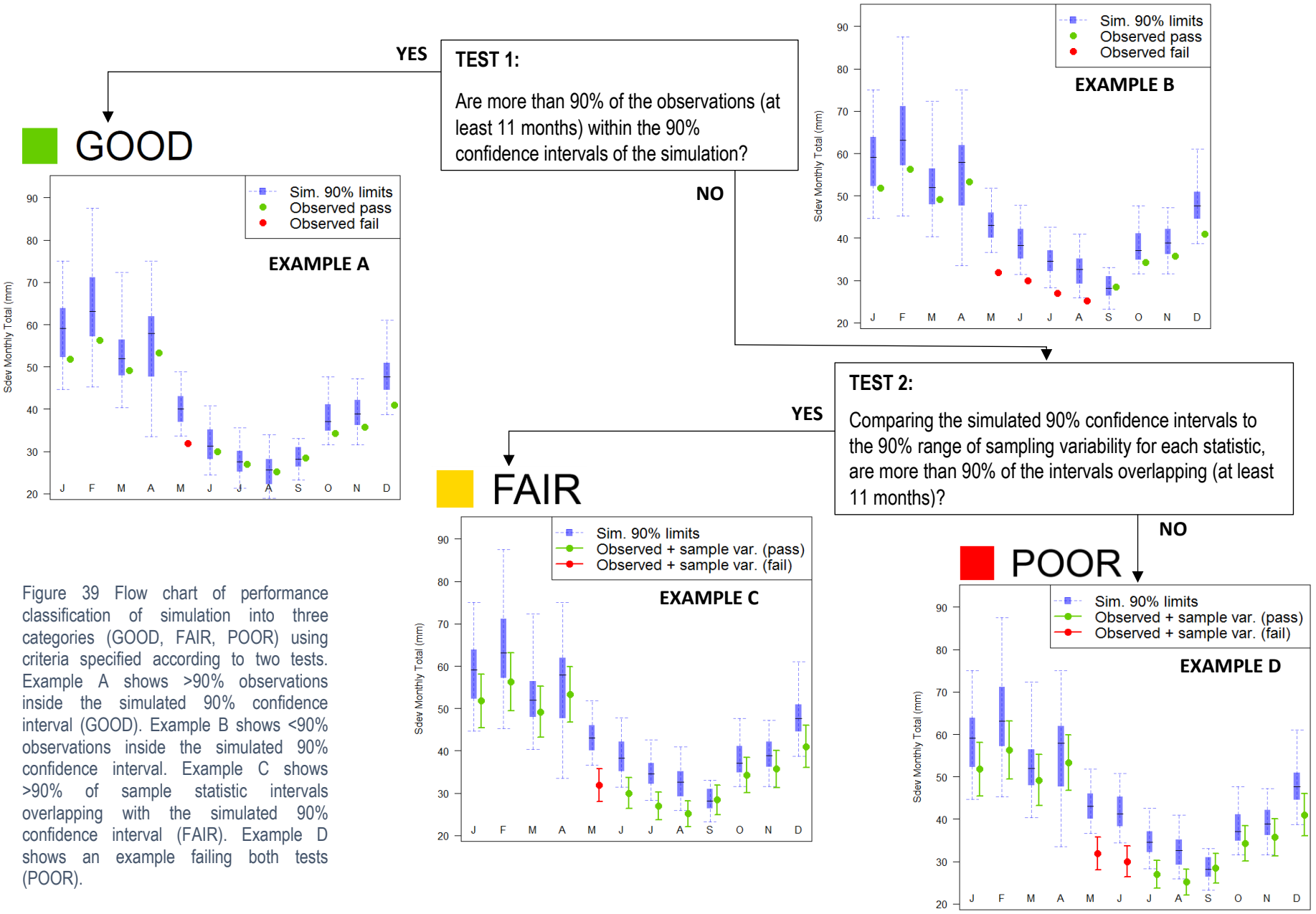

Figure 39 Flow chart of performance classification of simulation into three categories (GOOD, FAIR, POOR) using criteria specified according to two tests. Example A shows >90% observations inside the simulated 90% confidence interval (GOOD). Example B shows <90% observations inside the simulated 90% confidence interval. Example C shows >90% of sample statistic intervals overlapping with the simulated 90% confidence interval (FAIR). Example D shows an example failing both tests (POOR).

3 Results

3.1 Model Evaluation Summary

This performance evaluation in this section focuses on Model C, which is the most informative simulation from the historical record because it includes information based on the paleoclimate IPO. Because 'Model C' is intended as the primary output for representing the historical record, it is evaluated in detail in this section, with discussion of performance at representative sites and reference to Annex documentation for assessment of all sites.

The performance summary of 'Model A' (base model) and 'Model B' (instrumental IPO) is provided in Appendix B, but Annex documentation for site-by-site analyses of these model variants has been omitted, but can be provided on request if needed. The comparison shows that the overall performance across the model variants is similar. Models D-G are based on future projections and so performance evaluation based on the historical climate is not available for these outputs

Table 5 summarises the performance of the rainfall across the 100 sites.

- The strength of the model can be seen in its ability to reproduce totals at monthly, annual, inter-annual and decadal scales. The 1-, 2-, 5- and 10-year totals are 'Overall Good', with only 8 sites out of 100 receiving an evaluation of 'Fair' at one or more of these scales.
- The mean of monthly totals is matched perfectly at all sites, but the standard deviation of monthly totals is 'Overall Fair', where the simulations are typically more variable at the monthly scale.
- The distribution of the proportion of wet days at the annual scale is shown to be 'Overall Poor'. This is a known limitation of the model (Bennett et al., 2018), and is due to simplifying assumptions in the temporal correlation structure. The characteristics of the performance are discussed in detail in Section 3.2.3. The succinct explanation is that the model outputs are less variable than the observations. This can be seen in Table 5 by inspecting the mean of the monthly proportion of wet days, which is 'Overall Good' (i.e. the process is unbiased at most sites), but that the standard deviation in the monthly proportion of wet days is 'Overall Fair'.
- The annual maximums are 'Overall Good' for 1-day maximums and 'Overall Fair' for multi-day accumulations. Section 3.2.5 will demonstrate that despite the 'Fair' performance at the majority of sites, the simulations do not deviate far from the observations. The 'Overall Fair' performance is a consequence of simplifications in the temporal correlation structure of the model (Section 2.2.1).

Table 5 Rainfall evaluation summary of performance, 'Model C' Paleoclimatic IPO model variant, 100 rainfall sites 129 years length, 77 replicates. Traffic light criterion specified by systematic evaluation method (Section 2.5). The x-axis shows the percentage of sites in each category of 'Good' (green), 'Fair' (yellow) or 'Poor' (red). Detailed plots for each site in Annex documentation.

Statistic	Evaluation of Model Performance	Overall label	Detailed Statistics
Distribution of Annual Total Rainfall	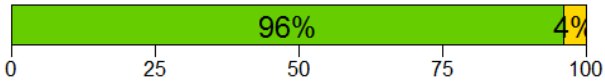	OVERALL GOOD	Annex A
Distribution of 2-year Rainfall Totals	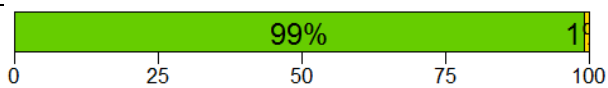	OVERALL GOOD	Annex A
Distribution of 5-year Rainfall Totals	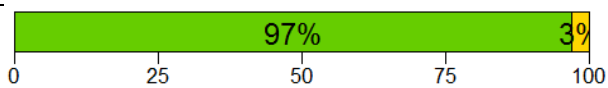	OVERALL GOOD	Annex A
Distribution of 10-year Rainfall Totals	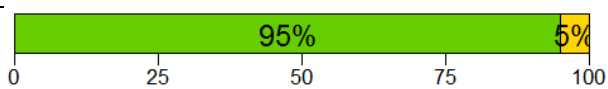	OVERALL GOOD	Annex A
Mean of Monthly Rainfall Totals	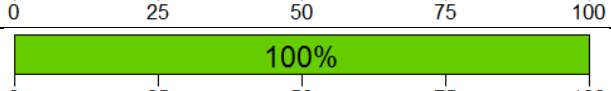	OVERALL GOOD	Annex B

Standard Deviation Monthly Rain Totals	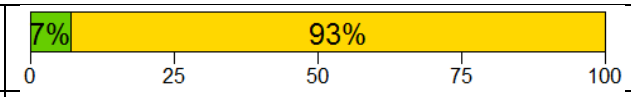	OVERALL FAIR	Annex B
Distribution of Annual Proportion Wet Days	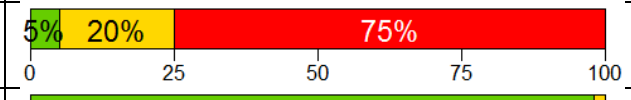	OVERALL POOR	Annex C
Mean of Monthly Proportion Wet Days	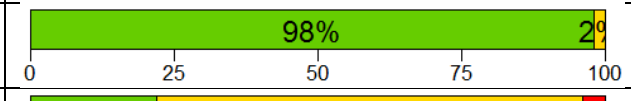	OVERALL GOOD	Annex D
Std. Dev. Monthly Prop. Wet Days	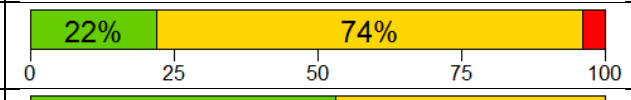	OVERALL FAIR	Annex D
Annual 1-day Rainfall Maximum Distrib.	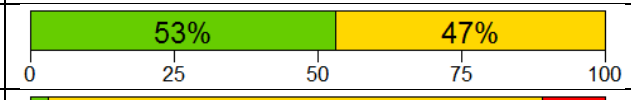	OVERALL GOOD	Annex E
Annual 2-day Rainfall Maximum Distrib.	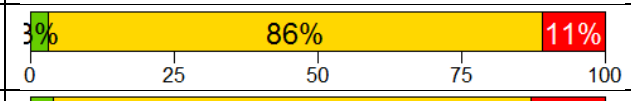	OVERALL FAIR	Annex E
Annual 3-day Rainfall Maximum Distrib.	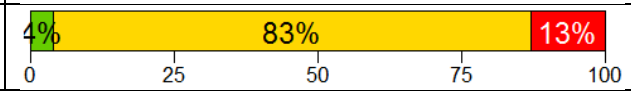	OVERALL FAIR	Annex E

Table 6 provides the performance summary for the evaporation simulations, which is based on 45 sites. Similar to the rainfall evaluation, the performance is 'Overall Good' for the totals at the annual and inter-annual scales. At the monthly scale, the characteristics of the model are similar to the rainfall, that the mean of monthly evaporation totals is 'Overall Good' but the standard deviation of monthly totals is 'Overall Fair'. The sites with 'Poor' performance in the standard deviation of monthly totals are the IQQM evaporation, where the mismatch in performance occurs due to an artefact of the observed data (discussed further in Section 3.2.7).

Table 6 Evaporation evaluation summary of performance, 'Model C' Paleoclimatic IPO model variant, 45 evaporation sites 129 years length, 77 replicates. Traffic light criterion specified by systematic evaluation method (Section 2.6). The x-axis shows the percentage of sites in each category of 'Good' (green), 'Fair' (yellow) or 'Poor' (red). Detailed plots for each site in Annex documentation.

Statistic	Evaluation of Model Performance	Overall label	Detailed Statistics
Distribution of Annual Total Evaporation	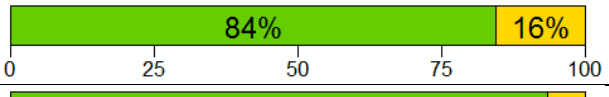	OVERALL GOOD	Annex F
Distribution of 2-year Evaporation Totals	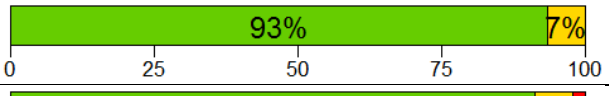	OVERALL GOOD	Annex F
Distribution of 5-year Evaporation Totals	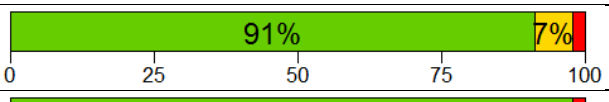	OVERALL GOOD	Annex F
Distribution of 10-year Evaporation Totals	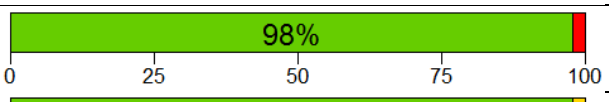	OVERALL GOOD	Annex F
Mean of Monthly Evaporation Totals	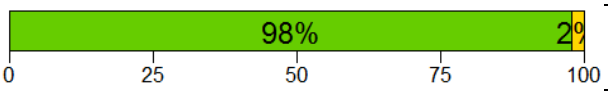	OVERALL GOOD	Annex G
Standard Deviation Monthly Evap Totals	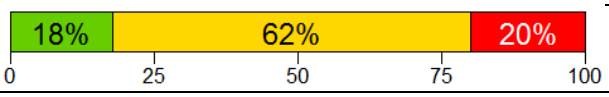	OVERALL FAIR	Annex G

3.2 Detailed Evaluation of Distributions

3.2.1 Multi-Year Annual Rainfall Totals (1-, 2-, 5-, and 10-years)

From Table 5 annual rainfall totals at one or more years is 'Overall Good', with almost all sites having 'Good' performance. Statistics at the annual, multi-year and decadal scales are critical to reproduce for drought risk assessment. The 'Overall Good' performance of these statistics indicates that the seasonal component and climatic components of the model are functioning with appropriate levels of variability.

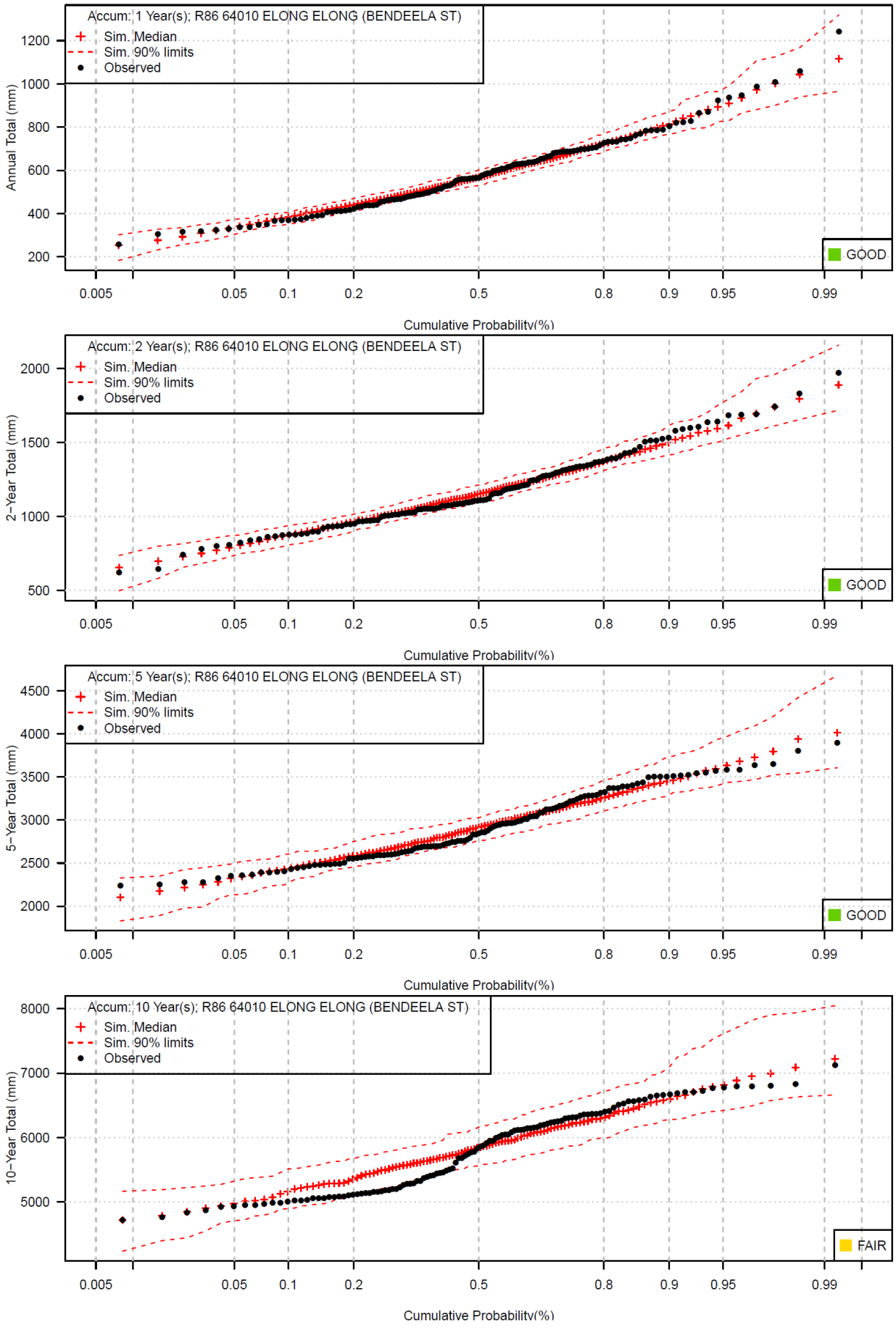

Figure 40 Distribution of annual rainfall totals for 1-, 2-, 5- and 10-year totals for a representative location simulation shows 90% confidence interval, performance tag GOOD (see Section 2.5)

Figure 40 shows an example using site R86, selected because it has an evaluation of both 'Good' (at the 1-, 2- and 10-year scales) and 'Fair' (at the 5-year scale). The 'Good' evaluation is typical of the performance of this statistic showing that the mean and variability of the simulations match the observations well. Assessing the 'Fair' performance it is clear that the mean and variability of the simulations is acceptable, with the simulations not deviating far from the observations. From Figure 40, by comparing the lowest total in each panel to the lower 90% limit, it is clear that the simulations are able to generate rainfall totals below the lowest values in the observation record.

3.2.2 Mean and Standard Deviation of Monthly Rainfall Totals

From Table 5 mean of the monthly totals is 'Overall Good' and the standard deviation of the monthly totals is 'Overall Fair'. Figure 41 provides an example for site R1, which is typical for the majority of sites. No sites exhibit 'Poor' performance. The model reproduces mean values well, which is an expected feature from the model parameterisation (since each site has its own mean parameter). While each site has a standard deviation parameter, the standard deviation of monthly totals is also a function of the auto-correlation process at daily and monthly scales.

Figure 41 (left panel) shows that the mean of the monthly totals are 'Good'. Regarding the standard deviation, Figure 41 shows that the 90% interval from the simulations is higher than the observations for the months May to August (leading to the classification 'Fair'). To help with interpreting this difference, Figure 42 provides the full distribution of monthly totals for one replicate at this site. The interquartile range of the boxes is very similar for all months, but the upper tail of the distribution (the whisker and outliers) is typically heavier in the simulation (grey boxes). A practical interpretation is that the simulation has occasional very wet months which are wetter than the observational support. Because the distribution of monthly totals is skewed, standard deviations in Figure 41 are sensitive to the behaviour of the tail.

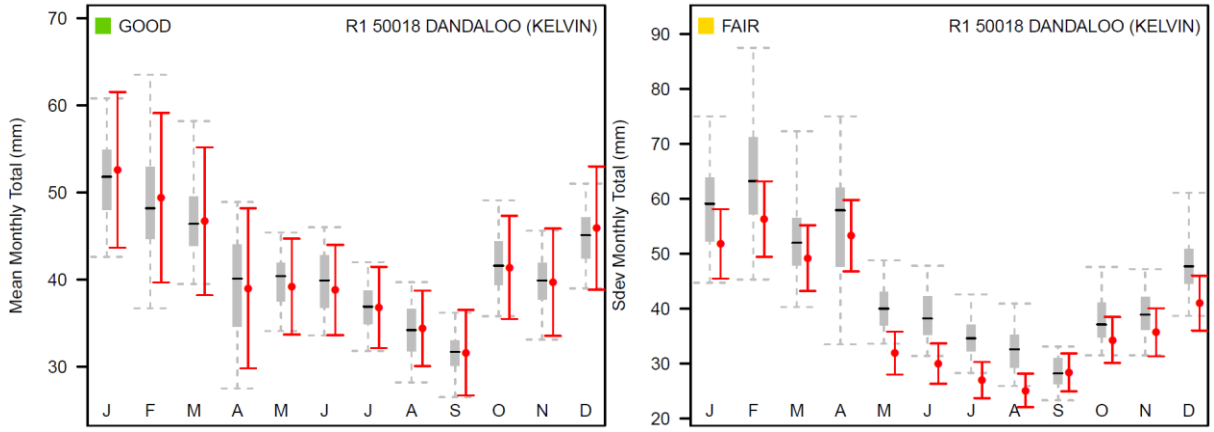

Figure 41 Distribution of (left) means of monthly totals; (right) standard deviations of monthly totals. Whiskers of grey box plot extend to the 90% interval. Red shows the observed mean/standard deviation along with error bars showing the standard error of each observed statistic. Performance tag GOOD for the means; performance tag FAIR for the standard deviations

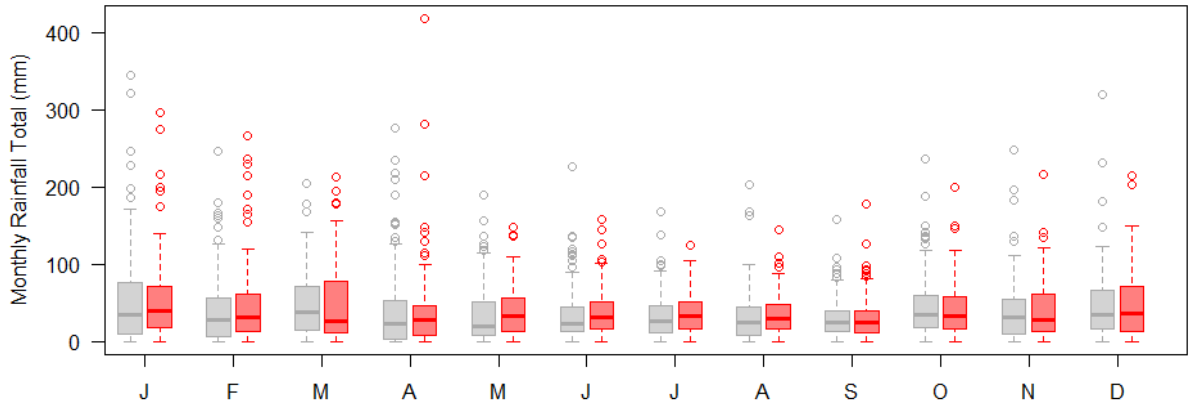

Figure 42 Paired comparison of full distribution of monthly totals for one representative site R1 50018 and one replicate. Grey monthly boxplot has 129 years of simulated data from one replicate and red monthly boxplot has 129 years of observations.

3.2.3 Annual Wet Day Proportion

From Table 5, the distribution of the proportion of wet days at the annual scale is 'Overall Poor'. Figure 43 provides example for four representative sites: R1, R2, R3 and R4. In all examples, the distributions are unbiased, but the variability of the simulations is typically less than the observations.

To explore the practical understanding of this performance, Table 7 compares the observed number of wet days for the driest year on record to the equivalent value from simulated replicates. This comparison corresponds to the lowest observation in each plot from Figure 43 relative to the simulated values at that quantile (where the number of wet days is obtained from the proportion by multiplication of 365.25). Interpreting Table 7, for the driest year, the observed number of wet days at the 'Poor' sites R3 and R4 is respectively 11 and 10 less wet days than from the median simulations. Taking the 90% limits of the simulations as representative of the spread of the model, the observed statistic is not inside this range at the 'Poor' sites.

Table 7 Observed versus simulation comparison for four representative sites. The number of wet days in the driest year (per 129 record length). The simulation is summarised by the median and the 90% limits.

Site	Classification	Observed (wet days)	Simulated (wet days)		
			5%	50%	95%
R1	FAIR	28	26	32	38
R2	GOOD	38	28	37	43
R3	POOR	38	49	59	67
R4	POOR	28	29	38	45

While the overall simulations are unbiased for the median number of wet days per year (seen in Figure 43), for the driest year on record the simulations are slightly wetter at most sites (Table 7 shows approximately 10 days more rain at 'Poor' sites). A similar analysis of the upper tail would show for the wettest year on record the simulations are slightly drier at most sites. Despite the discrepancy in this statistic, it is not necessarily a significant practical concern. The reason is that because of the threshold, a day is classified as 'wet' for even 0.01 mm rain. From comparisons of the annual totals (Figure 40, Annex A) the simulations have 'Good' reproduction of annual totals at nearly all sites and for all portions of the distribution (the driest years, the median year and the wettest years). In other words, although there is a bias in the number of wet days in the driest year, there is not a bias in the rainfall amount (because the process of rainfall amounts compensates). This could be loosely interpreted that the simulations have slightly (e.g. 10 days) more light-rain 'drizzle' in the driest year on record. For the wettest year on record there are less wet days in the simulation.

The discussion in this section is a good example of the strength and weakness of quantitative performance metrics:

- The strengths are that the evaluation is comprehensively applied to all sites, it is consistently applied, and therefore able to highlight differences in performance (e.g. R1- FAIR, R2- GOOD, R3-POOR, R4-POOR).
- The weakness is that the practical significance of an evaluation is not in itself clear. The annual proportion of wet days receives an 'Overall Poor' rating, but it is important to consider the implications of this performance classification for practical applications of the timeseries. Put another way, some statistics are more important to reproduce than others, depending on the application.

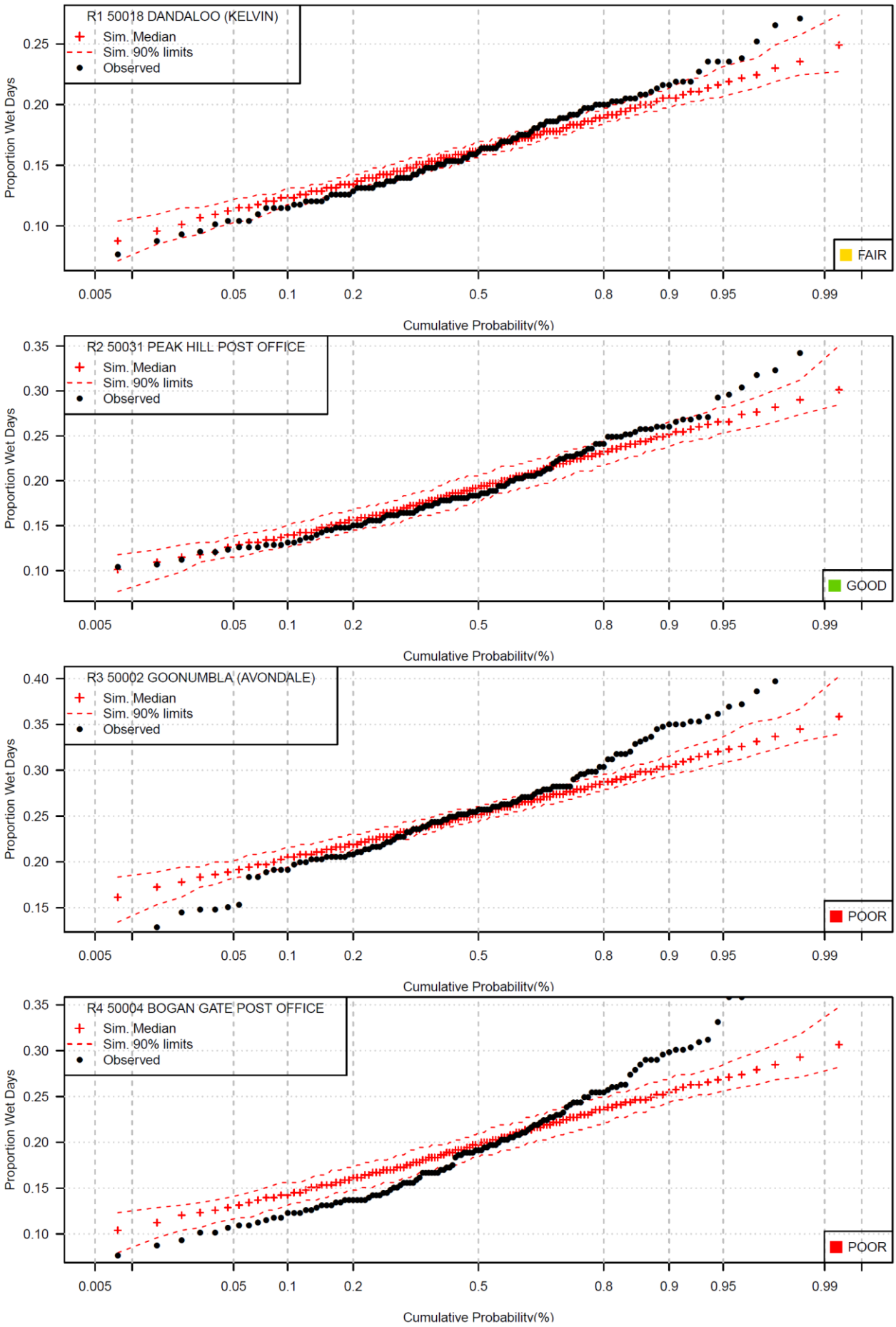

Figure 43 Distribution of the proportion of wet days within a given year. Four representative sites are shown for different performance outcomes, GOOD, FAIR and POOR (see Section 2.5)

3.2.4 Monthly Wet Day Proportion (Mean and Standard Deviation of)

The monthly summary of the proportion of wet days from Table 7 shows that the mean of this statistic is 'Overall Good' and that the standard deviation is 'Overall Fair'. Examples are shown in Figure 44 for three sites R76, R77, R78 and it is clear that the means are consistent in the simulations for each month. The performance of the standard deviation of monthly proportions is 'Fair' across most sites, but some sites can have multiple months that do not match well (e.g. June, July at site 78 in Figure 44). Following the discussion in Section 3.2.3 the lack of variability in the proportion of wet days, while noticeable, is not necessarily a significant practical concern when compared to other statistics such as the mean and variability of monthly totals. Even though the proportion of wet days is less variable in the simulations (Figure 44), comparing back to Figure 41, the monthly total rainfalls are typically more variable in the simulations than observations. This shows that distribution of rainfall amounts compensates for the lack of variability in wet days.

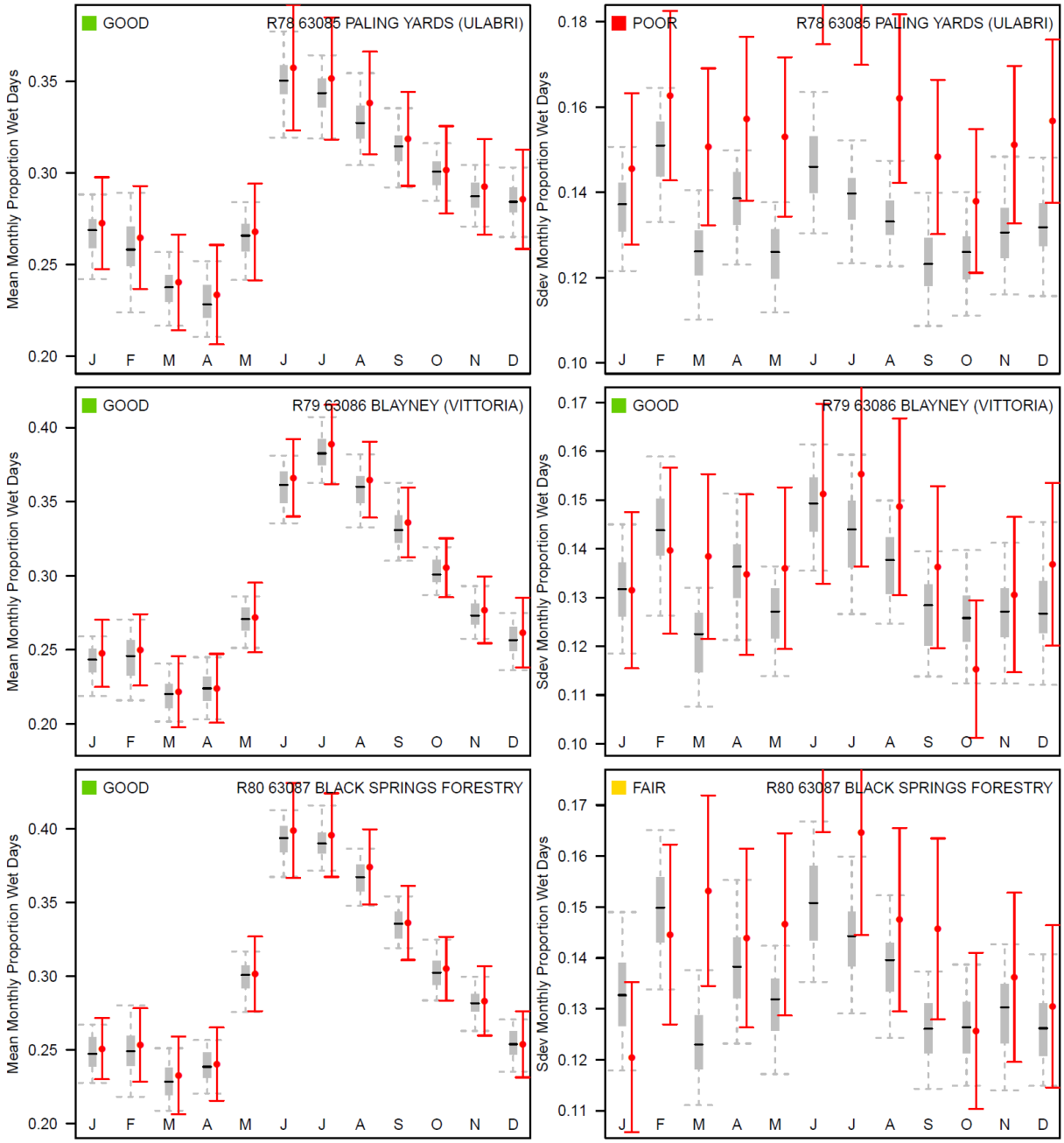

Figure 44 Distribution of (left) means of monthly proportions of wet days (right) standard deviations of monthly proportions of wet days. Whiskers of grey box plot extend to the 90% interval. Red shows the observed mean/standard deviation along with error bars showing the standard error of each observed statistic. Three representative sites are shown R78, R79, R80 for different performance outcomes (see Section 2.5)

3.2.5 Annual Rainfall Maximums (1-, 2-, and 3-day)

From Table 5 the performance of 1-day annual maximums is 'Overall Good' and the performance of 2-day and 3-day maximums is 'Overall Fair'.

Figure 45 provides an example for four representative sites R25, R26, R27, R28, where each row is a different site and the three columns are the three different accumulated 1-, 2- and 3-day maximums. Inspecting this figure shows that for the 'Good' and 'Fair' cases the simulated distribution of annual maximums is similar to the observations. Despite the large number of 'Fair' sites, it is worth noting that it is very difficult for a model to match the extremes because the calibration and parameters are related to moments of the distribution rather than the extremes. Furthermore, multi-day totals are an emergent feature of temporal correlation structure in addition to the daily marginal distribution.

For 2-day maximums there are 11 'Poor' sites and for 3-day maximums there are 13 'Poor' sites. For the example of site R27 in Figure 45, the site is labelled 'Poor' because of a discrepancy in the middle of the distribution but the upper tail has a reasonable match. For site 28, the upper tail does not match well. The limitation at these sites is mostly relevant to flood studies. This may be of concern for studies that are centred on sub-catchments near the 'Poor' performing gauges, especially if those catchments have a response time in the order of several days. If this were the case, it would be possible to post-process the simulated data with quantile mapping to the observed extremes. This would improve the extremes at these sites without significantly affecting other features of the data (e.g. there are only approximately 10% – 15% 'Poor' sites, the annual maximum(s) affects only a small number of data points per year, and only a fraction of the years would require shifting).

3.2.6 Multi-Year Annual Evaporation Totals (1-, 2-, 5-, and 10-years)

Table 6 summarises the performance of the modelled evaporation data. As with the rainfall totals, the 1- , 2-, 5-, and 10-year totals have 'Overall Good' performance. At the annual scale there are 15 sites with 'Fair' performance and at the 5- and 10-year scale there is one site with 'Poor' performance.

Figure 46 shows a representative site, R31, which has 'Fair' performance at the annual scale and 'Good' performance at the multi-year scale. As with the rainfall totals, where a year is labelled 'Fair' the distribution of the simulations remains reasonably close to the observations (i.e. there are no large departures of the distribution). Figure 47 shows performance at R32, which is the sole site having poor reproduction of the annual evaporation totals. Notably, this site is one of the IQQM evaporation sites, and where artefacts of the record have been commented on at the daily and monthly timescale (Section 2.1.2). Figure 47 shows that the distribution is not biased at all timescales, that it has 'Good' performance at the annual scale, but that it is too variable at the 5- and 10-year timescales. If this is a significant practical concern it could be amended with post-processing.

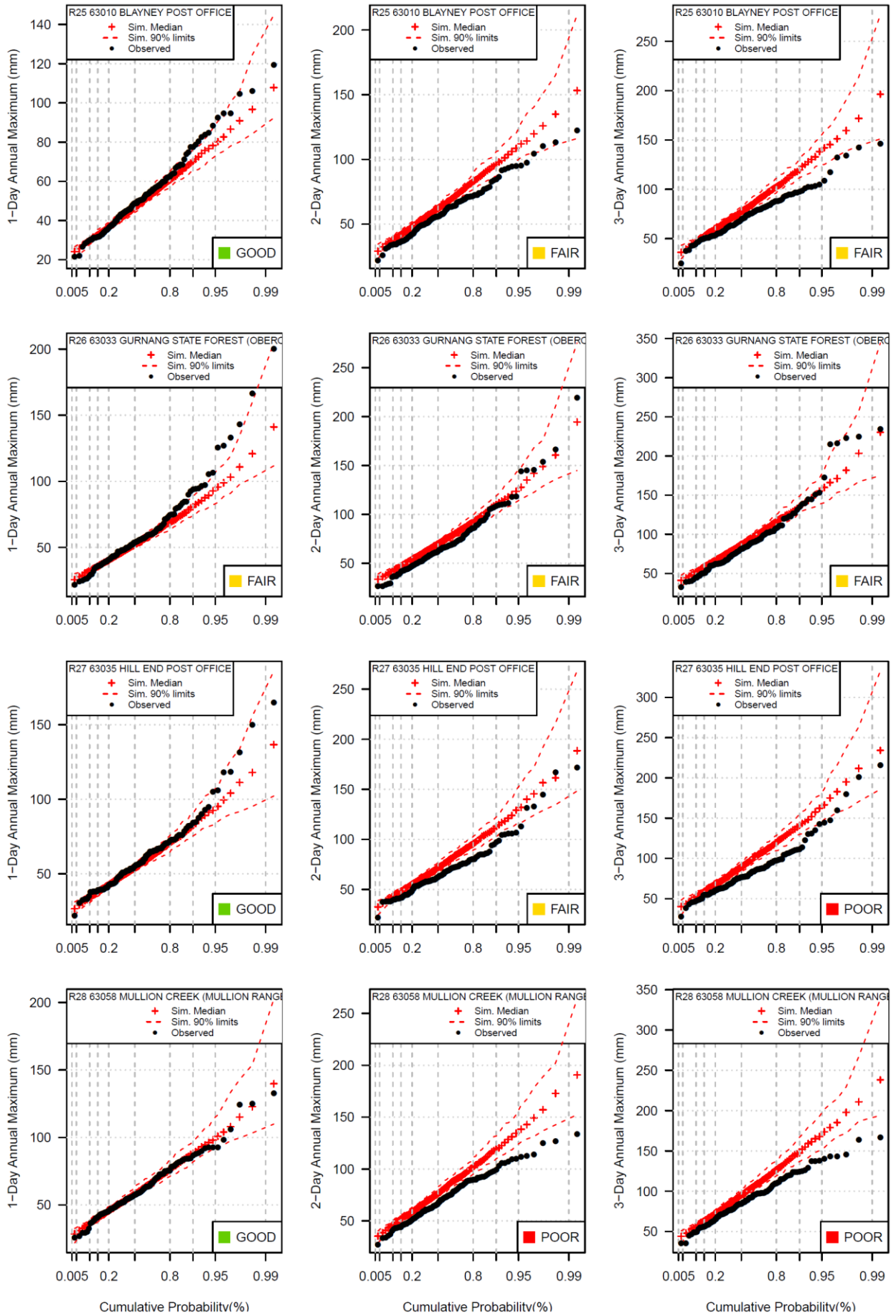

Figure 45 Frequency analysis of extremes (left) annual maximum daily rainfall (middle) annual maximum 2-day rainfall (right) annual maximum 3-day rainfall. Four representative sites R25-R28 are shown for different performance outcomes (see Section 2.5)

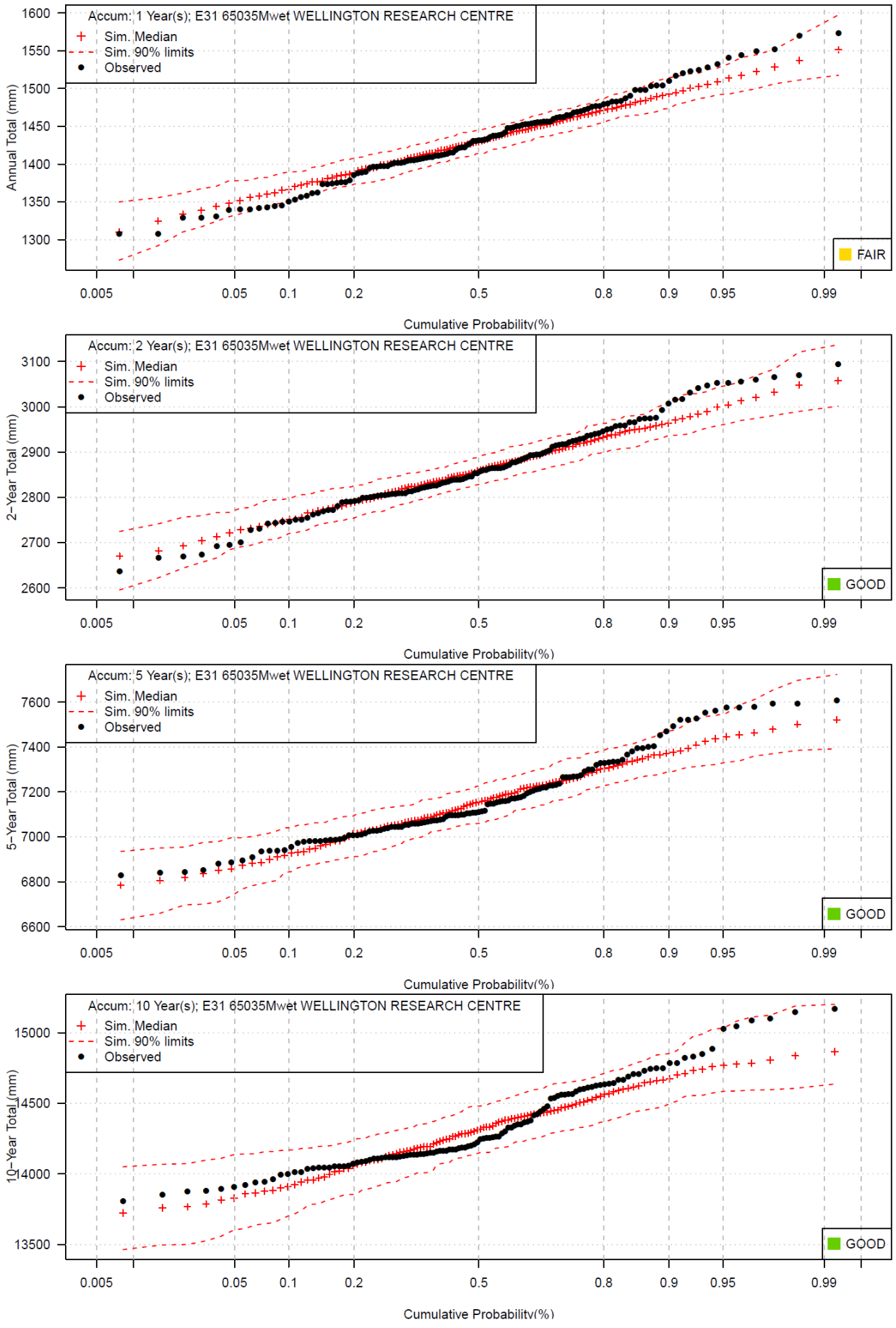

Figure 46 Distribution of annual evaporation totals for 1-, 2-, 5- and 10-year totals for a representative location with 'FAIR' / 'GOOD' performance (see Section 2.5), simulation shows 90% confidence interval

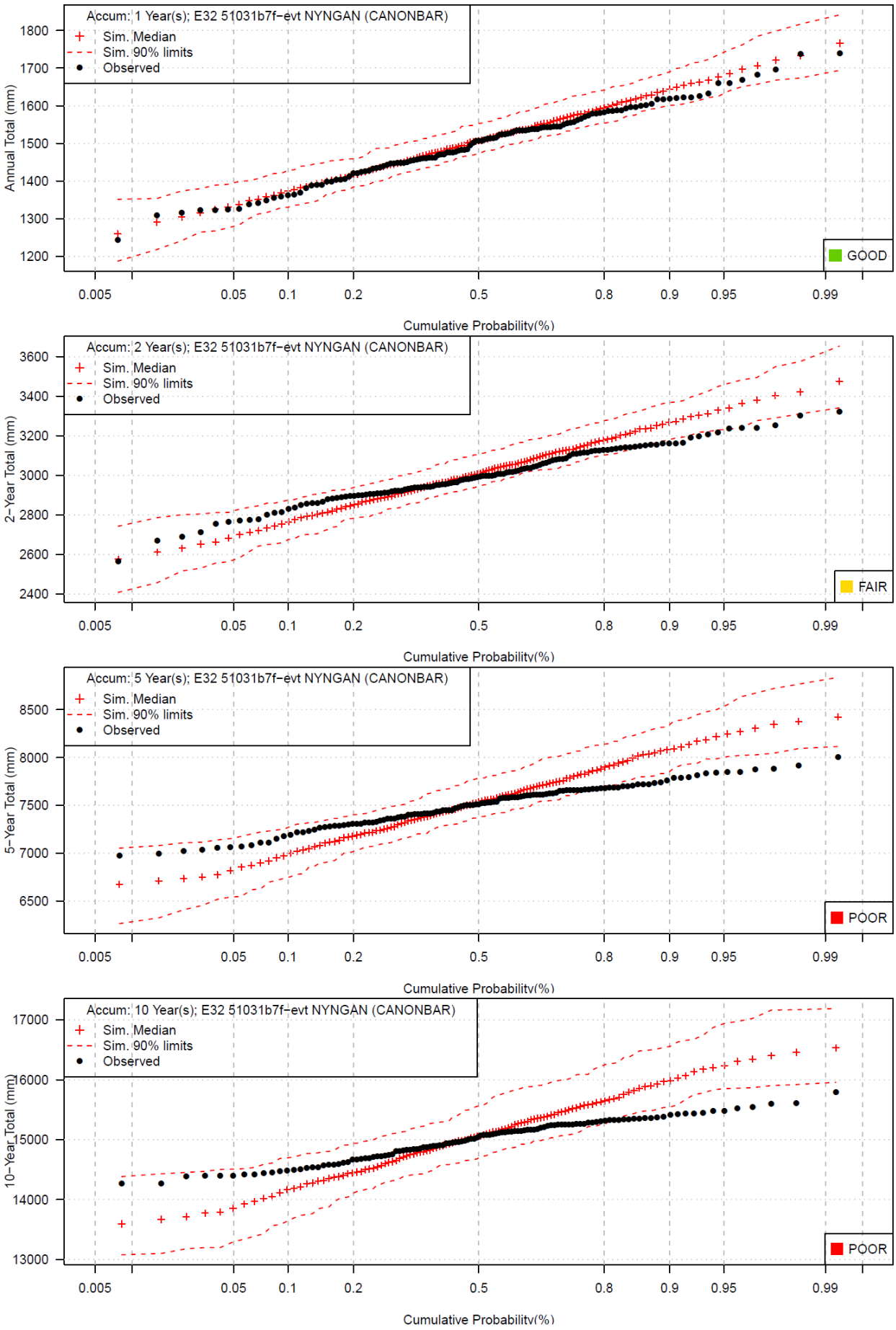

Figure 47 Distribution of annual rainfall totals for 1-, 2-, 5- and 10-year totals for a representative location with 'POOR' performance (see Section 2.5), simulation shows 90% confidence interval

3.2.7 Mean and Standard Deviation of Monthly Evaporation Totals

From Table 6, the performance of the monthly evaporation totals for the distribution mean is 'Overall Good' and for the standard deviation is 'Overall Fair'. Figure 48 shows the performance for two representative sites, E31 and E32. A total of 28 sites have 'Fair' performance and 9 sites have 'Poor' performance for the standard deviation of monthly evaporation totals.

The 'Fair' performance occurs because the variability of the observations about the mean do not follow a sinusoidal function (see for example December observations are lower than November at E31). The sinusoids are fitted to the entire year and therefore smooth out the relationship between months. The implication is that it is possible for one or two months to have a discrepancy in the standard deviation, for example, the standard deviation of evaporation in September is 2 mm lower than the observations. Whereas the observations range from 85 mm to 115 mm (90% interval) the simulations range from 88 mm to 112 mm.

Of the sites with 'Poor' performance seven of these are the IQQM data. Section 2.1.2 showed that this data was simulated to have the same evaporation value each month within a given year, unless there was a rainy day, in which case a different value was used for all rainy days. This assumption causes an artefact that the daily data appear to be more correlated than in reality. The simulation model does not match this temporal correlation structure because the autocorrelation parameter is averaged across all sites (necessary for a contemporaneous model). Without further appreciation of the data which the IQQM evaporation were derived from it is difficult to conclude how reasonable the simulated data is for this metric at these sites. The other two sites with 'Poor' performance are sites E43 and E44. These sites have discrepancies of 1-2 mm lower in the standard deviation for a number of months. Similarly to the 'Fair' sites, the range of simulated monthly total evaporation at these two 'Poor' sites is less than the observations in the order of several millimetres.

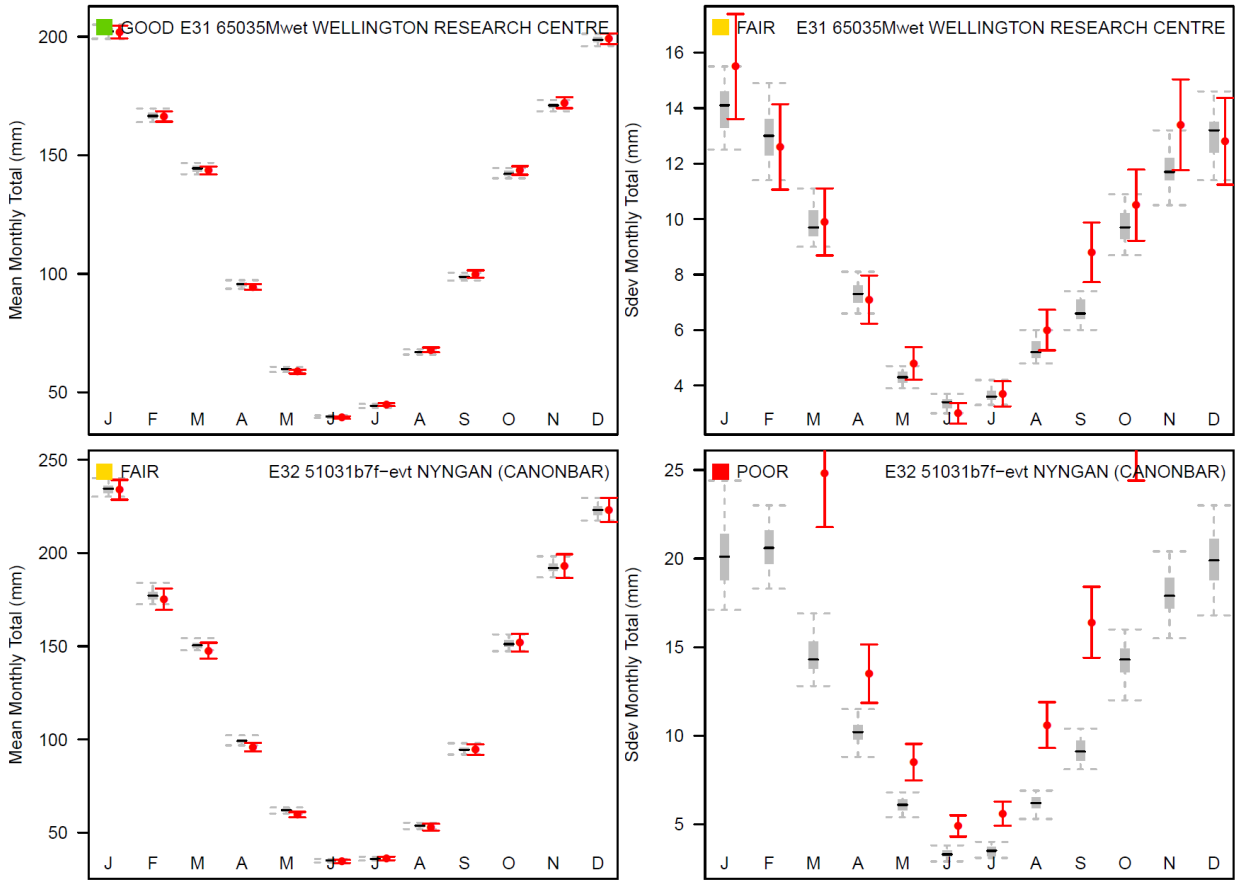

Figure 48 Distribution of monthly evaporation totals (left) means of monthly totals (right) standard deviations of monthly totals. Whiskers of grey box plot extend to the 90% interval. Red shows the observed mean/standard deviation along with error bars showing the standard error of each observed statistic. Two representative sites are shown (see Section 2.5)

4 Discussion and Recommendations

4.1 Model Summary

A significant amount of data has been stochastically generated for use in hydrological modelling of the Macquarie River catchment. Each model variant has 145 timeseries, representing rainfall and evaporation data co-located at 100 unique sites: 69 are rainfall only, 24 are rainfall and Morton Wet evaporation and the remaining 7 sites are rainfall with all 3 variants of evaporation (Morton Wet, IQQM and FAO56). Each timeseries has been output for 10,000 years in a two column (date, value) format, including leap years.

Three of the model variants represent historically equivalent simulations, where 'Model C' was used for the main output and model evaluation, since it incorporates paleoclimatic information of the IPO. The inclusion of IPO states identified that IPO negative years have 90 mm extra rainfall and 17 mm less evaporation, on average. This information has been built into the simulated data. While the longest IPO phase in the instrumental record is 34 years, simulations of 10,000 years can generate much longer IPO phases (instrumental calibrated gives 66 years on average for the longest period, paleoclimate calibrated gives 86 years, based on simulations of Figure 9). It should be noted that there is significant variability within each state (see Figure 11 and Figure 13).

Analysis of the observed data identified numerous features of importance to reproduce in the simulated data, including spatial gradients in the amounts, seasonal variability, inter-annual variability and negative correlation between the rainfall and evaporation. Some artefacts were noted in Section 2.2.3 regarding the IQQM evaporation. The data is generated from a model with a relatively coarse resolution and assumes high persistence in daily evaporation with the exception of rainfall days.

The model is carefully structured to account for spatial and temporal correlations. The spatial correlations (rain-rain and evap-evap) are able to be preserved at each site without any smoothing assumptions (i.e. the 100x100 and 45x45 sample spatial correlations are used directly in the model simulations). There is a negative correlation between daily evaporation and rainfall, of approximately –0.3. This correlation is built into the model using a parametric correlation function to ensure stability. The IQQM data have low correlation to other evaporation estimates – even though they were simulated jointly with other evaporation, there is little benefit from so doing. A contemporaneous assumption is employed in the model which requires the same autocorrelation parameter at all sites. This assumption provides stability to the correlation structure (needed for simulation), but which can lead to a relatively simplified temporal structure which can make the model inflexible for some attributes of the daily rainfall intermittency and properties such as multi-day extremes.

4.2 Summary of Model Evaluation

Model evaluation was based on a systematic method of comparison, where two developed tests were specified and applied to all relevant statistics. The tests rely on having replicates of equivalent length to the observations, therefore the 10,000 years of simulated data were reshaped as 77 replicates of length 129 years. Confidence intervals for observed statistics were estimated from standard errors for means and variances and from a bootstrap method for distribution quantiles. All evaluations require repeated tests across a collection of statistics, such as all months of the year or all quantiles in a distribution. Applying the developed classification rules:

- A label of 'GOOD' is applied when more than 90% of the observations are within the 90% confidence intervals of the simulation. If this criteria is not met, a follow-up tests is applied to determine the classification.

- A label of 'FAIR' is applied by comparing the simulated 90% confidence interval to the 90% range of observed sampling variability and determining that the intervals overlap in at least 90% of the instances. This is a more lenient test than for the 'Good' classification.
- A label of 'POOR' is established if neither the above criteria are met.

A traffic light summary was produced by respectively pooling the classifications across the 100 rainfall sites (Table 5) and 45 evaporation sites (Table 6). An overall classification was applied to a given statistic:

- if more than 50% of the sites have 'Good' performance the statistic is summarised as 'Overall Good';
- if more than 50% of the sites have 'Fair' performance the statistic is summarised as 'Overall Fair'; and
- if more than 50% of the sites have 'Good' performance the statistic is summarised as 'Overall Poor'.

Multi-year totals: Given the importance of drought assessment for the Macquarie Valley, the most important statistics of interest are the distribution of annual totals across multiple years. Rainfall and evaporation totals were considered for accumulation periods of 1-, 2-, 5- and 10-years and showed 'Overall Good' performance.

Monthly totals: For the distribution of monthly totals—for both the rainfall and evaporation respectively—the means were classified as 'Overall Good' and the standard deviation of the distribution was classified 'Overall Fair'. The reasons for the 'Fair' classification are different for the rainfall and evaporation. For rainfall, a practical interpretation of the 'Fair' classification is that the simulated data has occasional very wet months which are wetter than the observational support. Because the distribution of monthly totals is skewed, the standard deviations are sensitive to the behaviour of the tail. For evaporation, the model uses a sinusoid to match the monthly variability, but the observed data are not perfectly sinusoidal in their variability. Based on a representative site, an example of the implication is that for a given month the standard deviation of evaporation was 2 mm lower in the simulation. That is, whereas the observations range from 85 mm to 115 mm (90% interval) the simulations range from 88 mm to 112 mm. This issue arises for only some months due to the smoothing of the sinusoid.

Proportion of wet days: the annual distribution of this statistic was classified as 'Overall Poor'. Visual inspection shows the distribution is unbiased (so the average number of wet days matches), but that the simulations are less variable than the observations. Discussion of representative 'Poor' sites (Table 7) showed that for the driest year on record, the simulations had approximately 10 additional wet days than the observations. It could be loosely interpreted that the simulations have slightly more (e.g. 10 days) 'drizzle' rain in the driest/wettest year on record. This is not necessarily a significant practical issue because the overall number of wet days is unbiased and the annual totals show 'Good' performance, including in the tail regions due to compensation by the process of rainfall amounts.

Multi-day annual maximums: while the daily maximums were classified as 'Overall Good', the 2-day and 3-day maximums were classified as 'Overall Fair'. Extremes are an emergent feature of the model and are not calibrated, so they can be difficult to match. Where there were discrepancies, the observed maximums were typically not far outside the 90% limits of the simulated maximums. At a small number of 'Poor' sites, the maximums showed a discrepancy in the upper tail, which could be post-processed using quantile mapping if necessary. The present study is focussed on drought conditions rather than floods, so this discrepancy is of lower concern. It might be relevant if the data were used for a flood study in a nearby catchment with a response time in the order of several days.

4.3 Summary of Future Climate Outputs

Having established the performance of Model C, it was used as the basis of four model variants that account for future climates from the RCP4.5 scenario. The intention of these model variants is to account for indicative effects of a drying climate bundled with historical variability.

The future climate simulations were developed corresponding to 20-year time slices centred on 2030, 2050, 2070 and 2090. Seasonal scaling factors were taken from the of the Climate Change in Australia website (CSIRO and Bureau of Meteorology, 2015), accounting for up to a 10% rainfall decline (2090 winter) and up to an 8% evaporation increase (2090 autumn, winter). Because the outputs were provided as long timeseries rather than as replicates, only the median change factors were used. This means that additional variability from the projections (above and beyond the baseline climate) was not introduced into the climate scaling – including uncertainty from climate models. When interpreting results from the generated data for future climates it is important to appreciate that these additional sources of variability/uncertainty have not been incorporated. The change factor approach involves multiplication with the base timeseries, which translates means and standard deviations under the assumption of a constant coefficient of variation. This is a reasonable first-order assumption but possible changes to other statistics are not accounted for, including wet-dry patterns, correlation structures and wet proportions.

4.4 Recommendations

A set of output data has been jointly simulated for 100 rainfall sites and 45 evaporation sites, having 10,000 concurrent years at each site. The simulated data is fit for application for drought assessment and has 'Overall Good' reproduction of multi-year rainfall and evaporation totals.

- Of the three historical model variants, 'Model C' is recommended as the best model variant for studying the water balance of the Macquarie River catchment. Models variants A and B are available for comparison if needed. Because all sites were simulated jointly, it is reasonable to use any subset of sites for modelling purposes providing the years are concurrent (i.e. the correlations are preserved). Given the strong gradients in the catchment, care should be taken when selecting sites to ensure they are representative.
- A set of four model variants was developed for studying possible effects of future climate based on RCP4.5. Models D – G each represent a 20-year timeslice into the future and have translated expected amounts using the median value from projections. The generated outputs are as a single continuous timeseries and do not account for uncertainty from climate models, which should be kept in mind when interpreting outputs.
- Subsequent hydrological simulations should consider any impact of the IQQM evaporation data. It appears to be qualitatively and quantitatively different from the other types of evaporation data (a different spatial pattern, higher totals, monthly blocks and high daily persistence).

All model variants reproduce a wide range of features including the distributions of amounts from days to multiples of years, key elements of variability such as the seasonal cycle and climatic oscillations, spatial correlations (by using sample estimates), rainfall-evaporation correlations and projected median changes from a selected climate scenario. The generated output timeseries are fit for the purpose of daily water balance modelling in the Macquarie Valley to facilitate risk assessments related to hydrological functions.

5 References

Baxevani, A. and Lennartsson, J., 2015. A spatiotemporal precipitation generator based on a censored latent Gaussian field. Water Resources Research, 51(6), pp.4338-4358.

Bennett, B., Thyer, M., Leonard, M., Lambert, M., & Bates, B. (2018). A comprehensive and systematic evaluation framework for a parsimonious daily rainfall field model. Journal of Hydrology, 556, 1123-1138.

CSIRO and Bureau of Meteorology (2015), Climate Change in Australia website, accessed 11/2018, http://www.climatechangeinaustralia.gov.au/

Henley, B. J., Thyer, M. A., Kuczera, G., & Franks, S. W. (2011). Climate-informed stochastic hydrological modeling: Incorporating decadal-scale variability using paleo data. Water Resources Research, 47(11)

Henley, B.J., Gergis, J., Karoly, D.J., Power, S.B., Kennedy, J., & Folland, C.K. (2015). A Tripole Index for the Interdecadal Pacific Oscillation. Climate Dynamics, 45(11-12), 3077-3090. doi:10.1007/s00382-015-2525-1

Hutchinson, M. F. (1995). Stochastic space-time weather models from ground-based data. Agricultural and Forest Meteorology, 73(3), 237-264

Kleiber, W., Katz, R.W., Rajagopalan, B., 2012. Daily spatiotemporal precipitation simulation using latent and transformed Gaussian processes. Water Resour. Res. 48, 17

MDB (2018) Macquarie River longitudinal profile, Murray Darling Basin Commission, accessed 21/12/2018, https://www.mdba.gov.au/sites/default/files/pubs/Macquarie_LP.pdf

NSW Department of Industry (2018) Risk Assessment for the Macquarie-Castlereagh water resource plan Area (SW11), Part 1, Schedule D, INT18/162302, pp. 1-253

NSW Department of Primary Industries (2016) Macquarie-Castlereagh water resource plan (surface water), status and issues paper, pp. 1-33

Rasmussen, P. F. (2013). Multisite precipitation generation using a latent autoregressive model. Water Resources Research, 49(4), 1845-1857

Srikanthan, R., & McMahon, T. A. (2001). Stochastic generation of annual, monthly and daily climate data: A review. Hydrology and Earth System Sciences Discussions, 5(4), 653-670.

Van Dijk, A., Evans, Hairsine, P., Khan, S., Nathan, R., Paydar, A., Winey, N., and Zhang (2006). Risks to the Shared Water Resources of the Murray–Darling Basin. Murray–Darling Basin Commission, Canberra, ACT

Wilks, D. S. (1998). Multisite generalization of a daily stochastic precipitation generation model. Journal of Hydrology, 210(1-4), 178-191

6 Appendix A – Finalised list of sites

Table 8 List of 100 rainfall sites used in the study

Internal ID	Station ID	Station Location
R1	50018	DANDALOO (KELVIN)
R2	50031	PEAK HILL POST OFFICE
R3	50002	GOONUMBLA (AVONDALE)
R4	50004	BOGAN GATE POST OFFICE
R5	50012	BURRA BURRA
R6	50016	GOONUMBLA (CORADGERY)
R7	50028	TRUNDLE (MURRUMBOGIE)
R8	50036	TRUNDLE (BROOKVIEW ST)
R9	51072	QUAMBONE (CARWELL)
R10	62026	RYLSTONE (ILFORD RD)
R11	65034	WELLINGTON (AGROWPLOW)
R12	51031	NYNGAN (CANONBAR)
R13	51034	WARREN (MUMBLEBONE)
R14	51037	NARROMINE (ALAGALAH ST)
R15	51054	WARREN (FRAWLEY ST)
R16	62003	MUMBIL (BURRENDONG DAM)
R17	62021	MUDGEE (GEORGE STREET)
R18	65012	DUBBO (DARLING STREET)
R19	51004	TRANGIE (OLD BUNDEMAR)
R20	51018	GILGANDRA (CHELMSFORD AVE)
R21	55041	NUNDLE POST OFFICE
R22	62013	GULGONG POST OFFICE
R23	63004	BATHURST GAOL
R24	63005	BATHURST AGRICULTURAL STATION
R25	63010	BLAYNEY POST OFFICE
R26	63033	GURNANG STATE FOREST (OBERON YA)
R27	63035	HILL END POST OFFICE
R28	63058	MULLION CREEK (MULLION RANGE FRST)
R29	63063	OBERON (SPRINGBANK)
R30	63064	O'CONNELL (STRATFORD)
R31	63066	ORANGE (MCLAUGHLIN ST)
R32	63089	WATTLE FLAT GENERAL STORE
R33	64025	COOLAH (BINNIA ST)
R34	65003	BODANGORA POST OFFICE
R35	65011	CUMNOCK (WILLOW PARK)
R36	65023	MOLONG (HILL ST)
R37	65035	WELLINGTON RESEARCH CENTRE
R38	50008	PEAK HILL (BRUIE PLAINS)
R39	50037	TULLAMORE (OLD POST OFFICE)
R40	51005	NARROMINE (MUMBLE PEG)
R41	51008	WYANGA (BARCOO)
R42	51010	COONAMBLE COMPARISON
R43	51022	GULARGAMBONE (YALCOGRIN ST)
R44	51025	WARREN (HADDON RIG)
R45	51038	NEVERTIRE (CLYDE ST)
R46	51042	QUAMBONE STATION
R47	51048	TRANGIE POST OFFICE
R48	51049	TRANGIE RESEARCH STATION AWS
R49	51051	GILGANDRA (BERIDA)
R50	51066	EUMUNGERIE POST OFFICE
R51	51115	NARROMINE AIRPORT
R52	62012	CUDGEGONG (KIORA)
R53	62014	HARGRAVES (GENERAL STORE)
R54	62018	KATELLA
R55	62020	BYLONG (MONTORO)
R56	62027	SHEPHERDS CREEK
R57	62028	GOOLMA (BROOKLYN)
R58	62029	ILFORD (TARA)
R59	62031	ILFORD (WARRANGUNYAH)
R60	62033	HARGRAVES (WEEROONA)
R61	62035	LEADVILLE (MORETON BAY)
R62	62057	COOLAH (COOLAH CREEK)
R63	62075	GALAMBINE (GOOREE PARK)
R64	62084	BUDGEE BUDGEE (BOTOBOLAR VNYRD)
R65	62099	STUART TOWN (CANOBLA)
R66	63000	ABERCROMBIE (ABERCROMBIE BRIDGE)
R67	63011	BORENORE STORE
R68	63012	RUNNING STREAM (BROOKLYN)
R69	63036	OBERON (JENOLAN CAVES)
R70	63037	OBERON (JENOLAN STATE FOREST)
R71	63053	MILLTHORPE (INALA)
R72	63071	PORTLAND (JAMIESON ST)
R73	63073	ROCKLEY POST OFFICE
R74	63076	SOFALA OLD POST OFFICE
R75	63079	SUNNY CORNER (SNOW LINE)
R76	63080	BLACK SPRINGS (SWATCHFIELD)
R77	63083	TRUNKEY CREEK BLACK STUMP HTL STN
R78	63085	PALING YARDS (ULABRI)
R79	63086	BLAYNEY (VITTORIA)
R80	63087	BLACK SPRINGS FORESTRY
R81	63090	WELLWOOD
R82	63136	YETHOLME (KURRAWONG)
R83	63146	CHEETHAM FLATS (JUNDAS)
R84	63233	ROCKLEY (CLEVELANDS)
R85	64009	DUNEDOO POST OFFICE
R86	64010	ELONG ELONG (BENDEELA ST)
R87	64015	MENDOORAN POST OFFICE
R88	64026	COBBORA (ELLISMAYNE)
R89	65000	ARTHURVILLE (CRAMOND)
R90	65005	BUMBERRY
R91	65010	CUDAL POST OFFICE
R92	65018	GEURIE POST OFFICE
R93	65020	MANILDRA (GEORGE ST)
R94	65022	MANILDRA (HAZELDALE)
R95	65025	OBLEY
R96	65026	PARKES (MACARTHUR STREET)
R97	65030	DUBBO (MENTONE)
R98	65032	WANDOO WANDONG
R99	65036	YEOVAL POST OFFICE
R100	65037	DUBBO STATE FOREST

Table 9 List of 45 evaporation sites used in the study (31 unique locations since E32-E45 are co-located). The Mwet label indicates data following the Morton Wet equation, -evt/evg labels indicate the IQQM evaporation data and FAO56 indicates the sites using reference crop data

Internal ID	Station ID	Station Location
E1	50018Mwet	DANDALOO (KELVIN)
E2	50031Mwet	PEAK HILL POST OFFICE
E3	51072Mwet	QUAMBONE (CARWELL)
E4	62026Mwet	RYLSTONE (ILFORD RD)
E5	65034Mwet	WELLINGTON (AGROWPLOW)
E6	51031Mwet	NYNGAN (CANONBAR)
E7	51034Mwet	WARREN (MUMBLEBONE)
E8	51037Mwet	NARROMINE (ALAGALAH ST)
E9	51054Mwet	WARREN (FRAWLEY ST)
E10	62003Mwet	MUMBIL (BURRENDONG DAM)
E11	62021Mwet	MUDGEE (GEORGE STREET)
E12	65012Mwet	DUBBO (DARLING STREET)
E13	51004Mwet	TRANGIE (OLD BUNDEMAR)
E14	51018Mwet	GILGANDRA (CHELMSFORD AVE)
E15	55041Mwet	NUNDLE POST OFFICE
E16	62013Mwet	GULGONG POST OFFICE
E17	63004Mwet	BATHURST GAOL
E18	63005Mwet	BATHURST AGRICULTURAL STATION
E19	63010Mwet	BLAYNEY POST OFFICE
E20	63033Mwet	GURNANG STATE FOREST (OBERON YA)
E21	63035Mwet	HILL END POST OFFICE
E22	63058Mwet	MULLION CREEK (MULLION RANGE FRST)
E23	63063Mwet	OBERON (SPRINGBANK)
E24	63064Mwet	O'CONNELL (STRATFORD)
E25	63066Mwet	ORANGE (MCLAUGHLIN ST)
E26	63089Mwet	WATTLE FLAT GENERAL STORE
E27	64025Mwet	COOLAH (BINNIA ST)
E28	65003Mwet	BODANGORA POST OFFICE
E29	65011Mwet	CUMNOCK (WILLOW PARK)
E30	65023Mwet	MOLONG (HILL ST)
E31	65035Mwet	WELLINGTON RESEARCH CENTRE
E32	51031b7f-evt	NYNGAN (CANONBAR)
E33	51034b7f-evt	WARREN (MUMBLEBONE)
E34	51037b7f-evt	NARROMINE (ALAGALAH ST)
E35	51054b7f-evt	WARREN (FRAWLEY ST)
E36	62003b17-evg	MUMBIL (BURRENDONG DAM)
E37	62021_17-evg	MUDGEE (GEORGE STREET)
E38	65012b7f-evt	DUBBO (DARLING STREET)
E39	51031_FAO56	NYNGAN (CANONBAR)
E40	51034_FAO56	WARREN (MUMBLEBONE)
E41	51037_FAO56	NARROMINE (ALAGALAH ST)
E42	51054_FAO56	WARREN (FRAWLEY ST)
E43	62003_FAO56	MUMBIL (BURRENDONG DAM)
E44	62021_FAO56	MUDGEE (GEORGE STREET)
E45	65012_FAO56	DUBBO (DARLING STREET)

7 Appendix B – Traffic Light Comparison for 'Model A' (base), 'Model B' (instrumental IPO) and 'Model C' (paleoclimatic IPO)

Table 10 Rainfall evaluation summary of performance for 3 different model variants.

Statistic	Model A: Base	Model B: IPO Instrumental	Model C: IPO Paleoclimatic
Annual Total Rainfall nYr=1	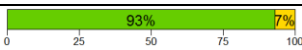	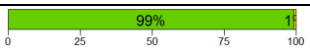	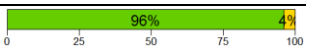
Annual Total Rainfall nYr=2	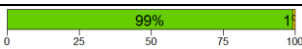	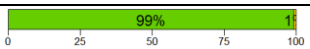	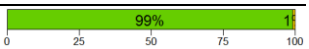
Annual Total Rainfall nYr=5	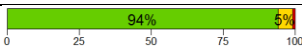	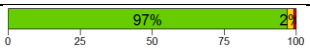	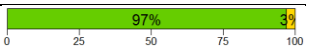
Annual Total Rainfall nYr=10	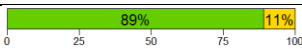	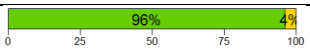	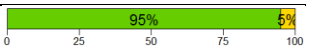
Mean of Monthly Rainfall Totals	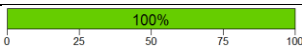	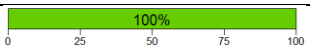	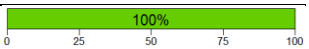
Sdev of Monthly Rainfall Totals	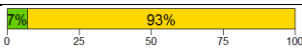	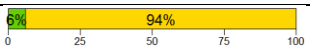	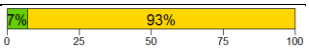
Distribution Prop. Wet Days	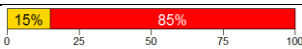	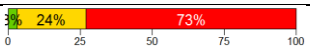	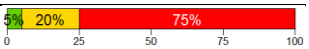
Mean of Monthly Prop. Wet Days	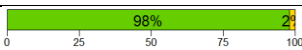	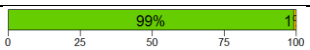	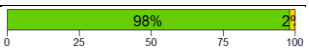
Sdev of Monthly Prop. Wet Days	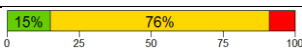	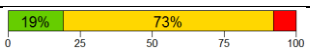	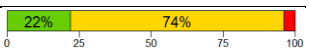
Annual 1-day Rainfall Max.	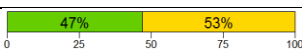	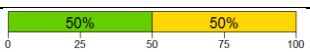	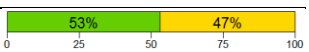
Annual 2-day Rainfall Max.	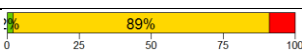	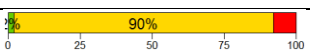	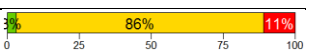
Annual 3-day Rainfall Max.	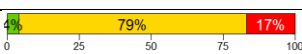	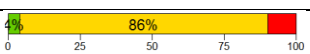	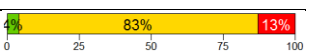

Table 11 Evaporation evaluation summary of performance for 3 different model variants.

Statistic	Model A: Base	Model B: IPO Instrumental	Model C: IPO Paleoclimatic
Annual Total Evap. nYr=1	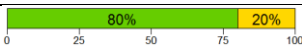	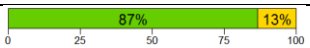	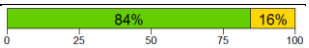
Annual Total Evap. nYr=2	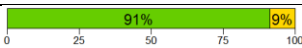	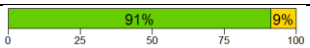	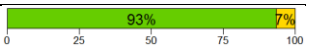
Annual Total Evap. nYr=5	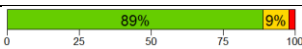	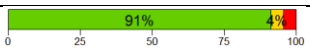	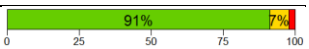
Annual Total Evap. nYr=10	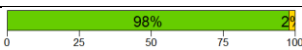	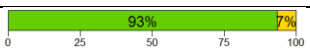	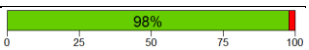
Mean of Monthly Evap. Totals	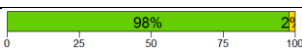	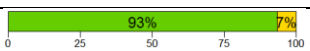	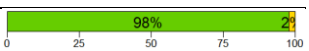
Sdev of Monthly Evap. Totals	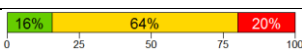	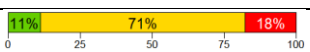	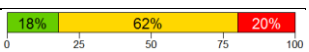

APPENDIX 4: LACHLAN REGION PAPER

Development of multi-site rainfall and evaporation data for the Lachlan Regional Water Strategy by Danielle Verdon-Kidd

Development of multi-site rainfall and evaporation data for the Lachlan Regional Water Strategy

UNIVERSITY OF NEWCASTLE

Report prepared for the NSW Department of Industry – Water (DoI-W) by the University of Newcastle

18 September 2019

Document information

Author contact details
Enquiries should be addressed to:
Dr. Danielle Verdon-Kidd
School of Environmental and Life Sciences
Faculty of Science
University of Newcastle
Callaghan NSW 2308 Australia
T: +61 2 4921 5749
F: +61 2 4921 6925
Email: danielle.verdon@newcastle.edu.au

Document details

Printed:	18 September 2019
Authors:	Danielle Verdon-Kidd
Name of client:	NSW Department of Industry – Water (DoI-W)
Name of project:	Development of multi-site rainfall and evaporation data for the Lachlan Regional Water Strategy
Name of document:	Final Report

Copyright and limitations
This report has been prepared on behalf of and for the exclusive use of the DoI-W, and is subject to and issued in connection with the provisions of the agreement between the University of Newcastle (UoN) and the DoI-W. UoN accepts no liability or responsibility whatsoever for or in respect of any use of or reliance upon this report by any third party.

Table of Contents

1 INTRODUCTION 4

2 DATA AND METHODS 6

2.1 RAINFALL AND EVAPORATION DATA 6

2.2 PALAEOCLIMATE DATA 7

2.3 STOCHASTIC DATA GENERATION 7

2.3.1 MULTI-SITE STOCHASTIC RAINFALL MODEL 8

2.3.2 IPO FORCING OF THE STOCHASTIC MODEL 9

2.3.3 MULTI-SITE EVAPORATION MODEL 9

3 RESULTS 10

3.1 UPDATE OF IPO PERSISTENCE MODEL 10

3.2 STRATIFICATION OF INSTRUMENTAL RAINFALL DATA BY THE IPO 11

3.3 STOCHASTIC DATA GENERATION 12

3.3.1 STATISTICS FOR RAINFALL (NO IPO FORCING) 12

3.3.2 POST PROCESSING OF AUTUMN RAINFALL 14

3.3.3 STATISTICS RAINFALL (IPO FORCING) 16

3.3.4 STOCHASTIC EVAPORATION DATA 18

4 CONCLUSIONS AND RECOMMENDATIONS 20

5 REFERENCES 22

List of Figures

Figure 1 correlation between a) IPO index and global SSTs, b) Condobolin rainfall and global SSTs during the peak IPO impact period (June-February) 4

Figure 2: Allocation levels for each IPO state (coupled with the phase of the El Nino/Southern Oscillation) at the start of the water year and 6 months thereafter (from Verdon-Kidd 2006) 5

Figure 3: Location of rainfall (top panel) and evaporation/evapotranspiration stations (bottom panel). 6

Figure 4: Duration and timing of step changes in the Composite IPO Index between 1662 and 1998 (Verdon and Franks 2006) 7

Figure 5: Comparison of a) Western Pacific PDO, b) Fiji-Tonga IPO and MacDonald and Case PDO 10

Figure 6: Updated Composite IPO index 2018 11

Figure 7: Distribution of rainfall data (annual) at each station during IPO positive (top panel) compared to IPO negative (bottom panel) 12

Figure 8: Monthly rainfall for instrumental (solid line) and stochastic (dashed line) 14

Figure 9: Catchment runoff monthly flow showing increase in productive period due to higher autumn rainfall in stochastic rainfall data (graph provided by DoI-W) 15

Figure 10: Monthly rainfall for instrumental (solid line) and stochastic (dashed line) after the post processing step 16

Figure 11: Catchment runoff monthly flow showing improved representation of monthly flow as a result of post processing the stochastic autumn rainfall data (graph provided by DoI-W) 16

Figure 12: 10-year low rainfall sum for a) the instrumental period and mean of stochastic replicates based on b) all data, c) IPO positive and d) negative data 17

Figure 13: Comparison of lowest 10-year rainfall in instrumental with 2.5 percentile 10 -year low rainfall sums for IPO positive stochastic 17

Figure 14: Example station showing slightly higher monthly rainfall during the first half of the year for the IPO forced stochastic dataset (dashed line) compared to the instrumental (solid line) 18

Figure 15: Evaporation/evapotranspiration on wet days (top panel) and dry days (bottom panel) during January for all 40 stations 19

Figure 16: Monthly evaporation for instrumental (solid line) and stochastic (dashed line) 19

1 Introduction

The NSW Department of Industry – Water (DoI-Water) is currently preparing regional water strategies that will inform the planning and management of each catchment's short and long-term water needs. This report focuses on the development of stochastically generated climate data inputs for the Lachlan Regional Water Strategy.

A key input to the modelling being carried out for the Lachlan Regional Water Strategy is long-term time series (beyond the instrument record) data of rainfall and evaporation to better understand the impacts of climate variability on water resource management for the region. The need for stochastic data was identified due to the temporal limitations of the instrumental record. That is, existing data is unlikely to be long enough to properly represent the full range of wet and dry epochs for planning and management of the regions water supply. Previous work carried out by Dr Verdon-Kidd (at the University of Newcastle) in 2007 showed that persistent regime shifts in the hydroclimate of the Lachlan region are driven by multi-decadal oscillations of the Pacific Ocean (i.e. the Pacific Decadal Oscillation (PDO), also known as the Interdecadal Pacific Oscillation (IPO)). To demonstrate, Figure 1a shows the sea surface temperature signature of the IPO, while Figure 1b highlights significant correlations between rainfall at Condobolin (located in the central Lachlan catchment) and global sea surface temperatures (SSTs). The two figures appear remarkably similar, further confirming that the IPO pattern is a primary driver of rainfall for the Lachlan region. Indeed Verdon (2007) showed that the IPO impact on rainfall is magnified for streamflow, dam volumes and water allocations (Figure 2). Given IPO phases operate over extended periods (circa 15 to 40 years), the instrumental period currently used in hydrological modelling (close to 130 years) is too short to adequately represent the range of durations of these epochs. In response, Dr Verdon-Kidd developed a stochastic framework that incorporated long term persistence associated with the phasing of the IPO based on a paleoclimate informed model.

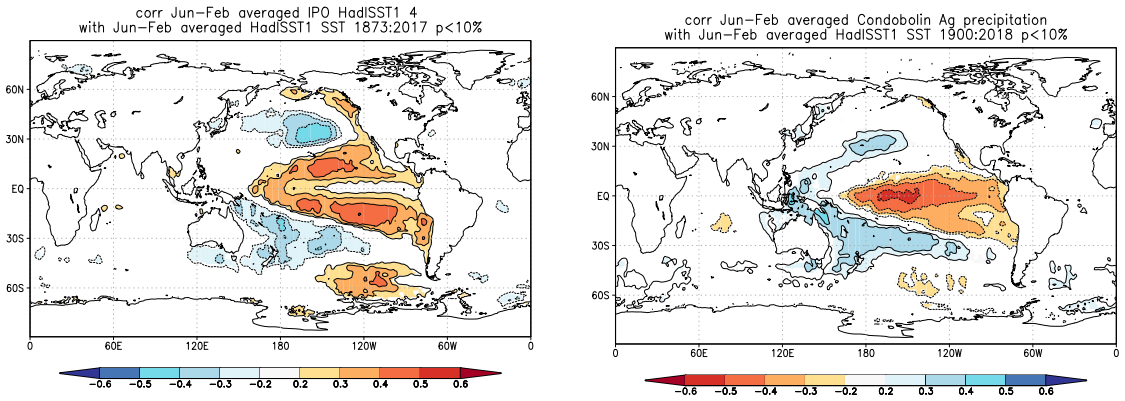

a) b)

Figure 1 correlation between a) IPO index and global SSTs, b) Condobolin rainfall and global SSTs during the peak IPO impact period (June-February)

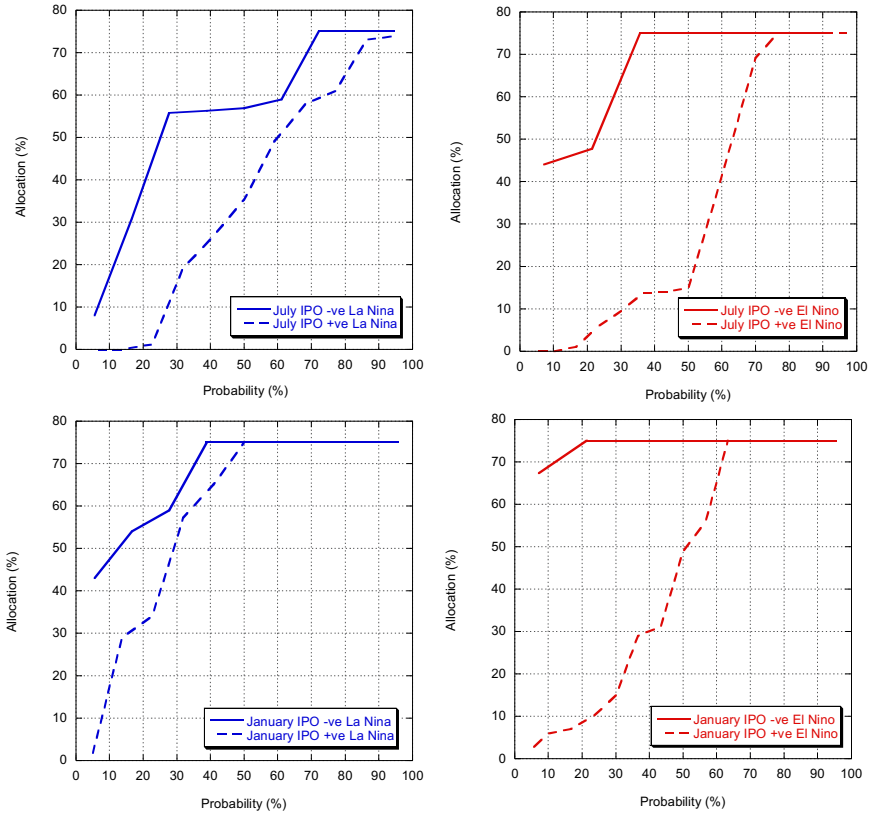

Figure 2: Allocation levels for each IPO state (coupled with the phase of the El Nino/Southern Oscillation) at the start of the water year and 6 months thereafter (from Verdon-Kidd 2006)

In August 2019, the University of Newcastle (UoN) was contracted by the DoI-W to build upon the stochastic framework previously developed by Verdon-Kidd and develop new multi-site stochastic rainfall and evaporation sequences that incorporate the Millennium Drought (the longest and most severe drought on record for the Lachlan) for use in the Lachlan Regional Water Strategy. The terms of reference for the project stipulated the following requirements:

1. Update and extend the IPO persistence model previously developed by Dr Verdon-Kidd using recent IPO reconstructions (not included in the 2007 version);
2. Produce *two sets* of 10 000 year stochastic replicates using the Srikanthan multi-site stochastic model for daily rainfall and matching evaporation sequences for stations provided by the DoI -W. One stochastic data set was to be conditioned on the IPO persistence model, the other with no forcing (traditional stochastic);
3. Allow for testing of stochastic data by DoI-W modelling team and incorporate feedback into final data production;
4. Generate and analyse rainfall and evaporation statistics for both sets of replicates; and
5. Report findings

This report outlines the data and methods (Section 2) used to generate the updated stochastic replicates and summarises the results (Section 3) and conclusions/recommendations (Section 4).

2 Data and methods

2.1 Rainfall and evaporation data

DoI-W initially provided rainfall and evaporation data for the period 1989-2019 for 47 rainfall stations and 32 evaporation/evapotranspiration records. A review of the Lachlan IQQM model, conducted in parallel to this project, resulted in an additional three rainfall and eight evaporation datasets added to the original input data requirements (i.e. a total of 50 rainfall and 40 evaporation stations). The location of the meteorological stations is shown in Figure 3. Note that for some stations there is more than one type of evaporation data required (e.g. IQQM ET, M_wet and FAO56) at the same location

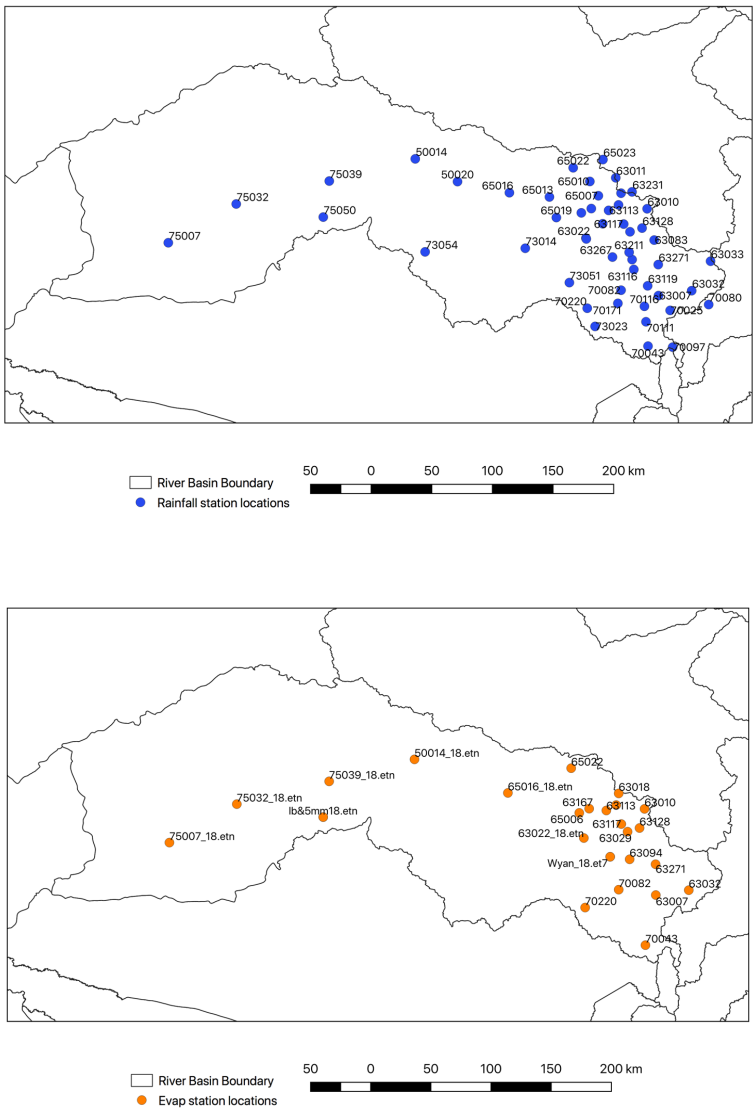

Figure 3: Location of rainfall (top panel) and evaporation/evapotranspiration stations (bottom panel)

2.2 Palaeoclimate data

Verdon and Franks (2006) previously developed a multiproxy IPO/PDO index (termed the "Composite IPO") based on consistent phase changes across five different IPO/PDO reconstructions (individual records included Biondi et al., 2001; D'Arrigo et al., 2001; Gedalof and Smith, 2001; MacDonald and Case, 2005 and Linsley et al., 2000). They found that the probability that this may occur by chance alone was less than 1% confirming that the synchronicity observed between reconstructions was robust. They showed that the shortest IPO epoch (identified using the Composite IPO Index) persisted for just 13 years, while the longest duration was 34 years (Figure 4). Variability in the length of IPO epochs (i.e. residence time) were then explored to determine an appropriate statistical distribution that best describes this, identifying a log-normal distribution fit. By fitting a statistical distribution to the residence times, multiple long-term replicates of the IPO can subsequently be generated by randomly sampling from this distribution, so as to account for a greater degree of climate variability.

Since the original Composite Index, there have been additional IPO/PDO reconstructions developed (e.g. D'Arrigo and Wilson, 2006; Shen et al., 2006; and Linsley et al., 2008). These are all freely accessible at https://www.ncdc.noaa.gov/data-access/paleoclimatology-data/datasets/climate-reconstruction. Therefore, stage one of the current project was to update the IPO model using the new reconstructions and reapply the distribution tests to determine the best fit to the updated IPO data. This ensures the data development is based on the best available science.

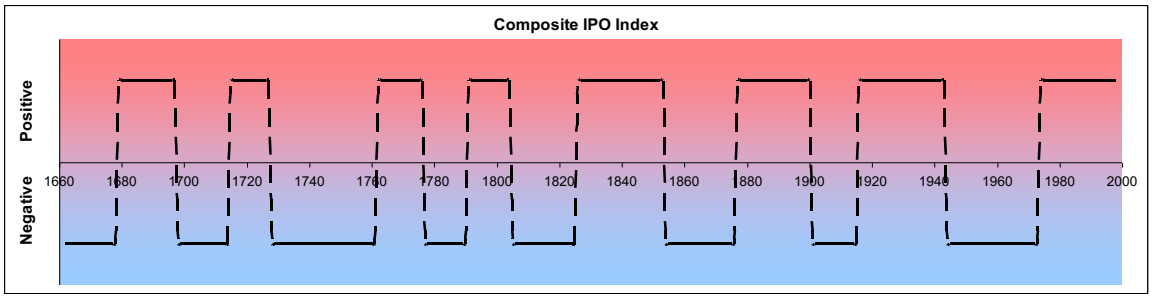

Figure 4: Duration and timing of step changes in the Composite IPO Index between 1662 and 1998 (Verdon and Franks 2006)

2.3 Stochastic data generation

Stages 2 of this project involved generating two sets of stochastic data (rainfall and evapotranspiration) for use in the IQQM modelling. This was achieved using a multi-site weather generator. Stochastic weather generators (SWGs) are statistical models that can simulate plausible random sequences of atmospheric variables such as rainfall (e.g., Wilks and Wilby 1999). There are many SWGs that have been developed and each have their own strengths and weaknesses. Fu et al. (2018) compared four different SWGs using the Gloucester catchment in NSW as a case study. They found that "all four models produced reasonable results in terms of annual, monthly and daily

rainfall occurrence and amount, as well as daily extreme, multi-day extremes and dry/wet spell length", however "every model has its own advantages and disadvantages due to their different theories and principals".

In this study, the Skrikanthan multi-site stochastic model for daily rainfall (Srikanthan et al. 2005) was chosen due to:

a) its use in the previous Verdon 2007 study on which this current project is based, and
b) Fu et al (2018) showed it performed the best in terms of monthly rainfall amount as well as rainfall percentage (monthly rainfall over annual rainfall in percentage term) compared to the other three stochastic models. The ability to reproduce the monthly distribution and intra-annual variability of rainfall is particularly important for hydrological applications.

Two stochastic datasets were developed (10 000 years for 50 rainfall stations):

1. Using the Srikanthan multi-site stochastic model for daily rainfall with the IPO persistence model, and
2. Using the Srikanthan multi-site stochastic model without forced persistence (no IPO).

The following sections describe how these datasets were developed.

2.3.1 Multi-site stochastic rainfall model

The Srikanthan multi-site model is two-part model derived from rainfall occurrence and the rainfall amounts. Details on the theory can be found in (Srikanthan et al. (2005) and is briefly described below.

A first-order two-state Markov chain is first used to determine the occurrence of rainfall. For each site, the Markov chain has the two transition probabilities (the conditional probability of a wet day given that the previous day was dry; the conditional probability of a wet day given that the previous day was wet). Given a network of N locations (in this case 50), there are N(N - 1)/2 pair wise correlations that should be maintained in the generated rainfall occurrences. This is achieved by using correlated uniform random numbers in simulating the occurrence process. The seasonality in daily rainfall occurrence is taken into account by considering each month separately.

The rainfall amounts on wet days are then generated by using a Gamma distribution. Srikanthan (2005) notes that the generated daily rainfall amounts when aggregated into monthly and annual totals will not in general preserve the monthly and annual characteristics. Hence, the daily amount model is nested in a monthly and annual model. This improves the monthly and daily characteristics of the generated rainfall, without effecting the spatial correlation for the monthly and annual rainfall.

The daily rainfall data (1889-2018) from 50 rainfall stations across the Lachlan catchment (Figure 3) were used as input to the stochastic model described above. One hundred daily replicates of 100 years in length were produced for each station. A range of daily, monthly and annual statistics were analysed to assess the performance of the model. Finally, a single 10 000 year daily record was produced for each station by joining the 100 individual series (for ease of running through IQQM). The replicates were also provided to the DoI-W modelling team for testing in the IQQM model and feedback was provided in an iterative approach until a satisfactory outcome was reached.

2.3.2 IPO forcing of the stochastic model

The IPO persistence model was used to condition the stochastic model in order to maintain the long term persistent of wet and dry periods (not necessarily reproduced by traditional SWGs). To achieve this, two sets of rainfall replicates were prepared (using the Srikanthan model); one using rainfall data only from the IPO positive phases and a second using data from only the IPO negative phases. This resulted in two sets of 100 year long daily replicates (one for each IPO phase) for each of the 50 stations. As before the daily, monthly and annual statistics were analysed to assess the performance of the model.

A 10 000 year sequence of the IPO was generated by randomly sampling residence times from the log normal distribution of IPO persistence (Section 2.2). The 10 000 year IPO sequence was then used as a template to construct a single rainfall replicate (for each of the 50 rainfall sites) preserving the persistence of the elevated and suppressed rainfall cycles observed in both the instrumental record and the paleoclimate data.

2.3.3 Multi-site evaporation model

Multi-site evaporation data (40 in total, Figure 3) was produced using a two-state model based on month (given the strongly seasonal nature of ET) and rainfall occurrence (because ET is lower in rainy days). Firstly, monthly distributions were generated from the instrumental data provided at each site (Mwet, Mwet or FAO56 ET depending on site). The monthly distributions were then further split into two states based on the occurrence of rainfall over the catchment on each day. A wet catchment day was defined by at least 50% of the stations having recorded rainfall on that day. This resulted in 24 “groups” of ET data to sample from with spatial correlation maintained. Note that the sensitivity of the criteria used to define a wet day (i.e. 50%) was tested and found to provide the closest match to the instrumental statistics.

A 10 000 year daily evaporation time series was generated for each of the 40 sites by sampling from the two state model (dependent on month and rain day for the simulated rain at the site) using the stochastic rainfall data developed in the previous step to determine the occurrence of rain on each

day. For example, on day 1, if 50% of the stochastic rainfall data (across the 50 stations) produced rainfall, then the ET data was sampled from the January wet day distribution across all 40 ET sites.

3 Results

3.1 Update of IPO persistence model

As noted previously, since the Verdon (2016) Composite IPO Index was developed a number of additional IPO/PDO reconstructions have been published. Of note are two reconstructions focused on the western North Pacific expression of the IPO/PDO using tree rings (D'Arrigo and Wilson, 2006) and historical documents China (Shen, 2006). Further, a Fiji-Tonga IPO reconstruction by Linsley et al. (2008) provides a Central Pacific node. It is also worth noting that a recent trans-Pacific IPO reconstruction was developed (Buckley et al 2019) that is based on a network of tree rings form Indonesia and South Central USA. However, the data is not yet publicly available.

A time series comparison between the two newest IPO/PDO reconstructions representing the western Pacific expression and the original McDonald and Case PDO (used in the Composite Index) is shown in Figure 5a. Similarly, a comparison between the Fiji-Tonga IPO and McDonald and Case is shown in Figure 5b. Correlations between the reconstructions are contained in Table 1.

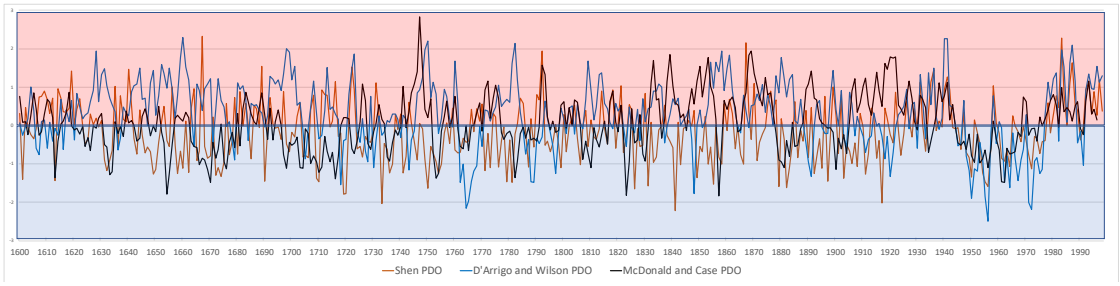

a)

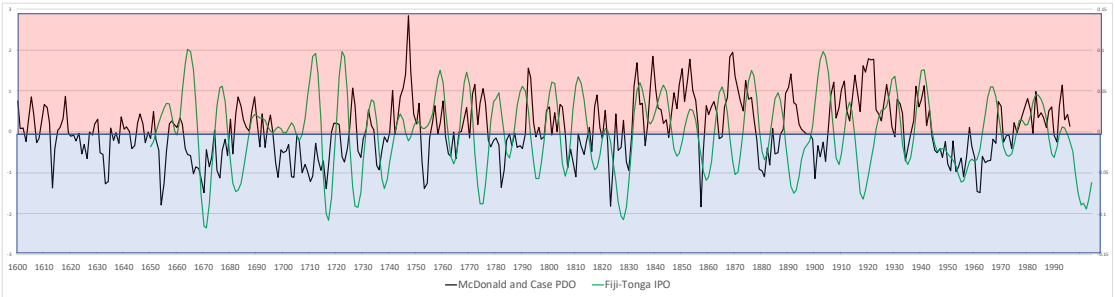

b)

Figure 5: Comparison of a) Western Pacific PDO, b) Fiji-Tonga IPO and MacDonald and Case PDO

Table 1: Correlations between the reconstructions

	D'Arrigo and Wilson PDO	Fiji-Tonga IPO	McDonald and Case PDO
Shen PDO	0.13	0.15	0.05
D'Arrigo and Wilson PDO		0.18	0.01
Fiji-Tonga IPO			-0.01

From Figure 5 and Table 1 we can see that, prior to the calibration period (i.e. circa 1900), the new reconstructions provide little observable or statistical coherence to the original PDO. It is likely that the signal in the western north Pacific is actually a combination of east Asian Monsoon and the PDO/IPO, which likely explains the deviation of the indices. The Fiji-Tonga IPO is also a mixed signal of the Intertropical Convergence Zone (ITCZ) and the IPO (Linsley et al., 2008), again explaining the deviance. Given the Lachlan catchment is not significantly impacted by either the Asian monsoon or the ITCZ, it is important to only use IPO/PDO that are representative of the Pacific dominant influence. Therefore, moving forward these reconstructions are not used to update the Composite Index.

A reconstruction of Murray River flows (which forms the southern portion of the Murray Darling Basin located across the states of New South Wales, Victoria, and South Australia) was developed by Gallant and Gergis (2011). This flow reconstruction (spanning 1783-1998) provides a useful source by which to cross check the validity of the Composite IPO index. The Murray flow reconstruction mostly agrees with Composite IPO Index with exception of the period 1883 to 1896 where the Murray flows were elevated, yet the original Composite IPO suggests this period is predominantly positive (and therefore usually drier). Gallant and Gergis (2011) cite a decoupling of the North and South Pacific Ocean during the late 1800's, early 1900's as a possible reason for discrepancy. A re-analysis of the instrumental IPO using the improved HadSST2 (Rayner et al, 2006) data by Parker et al (2007) provides further support that this period was likely a negative IPO phase.

Based on the above, Figure 6 shows the updated Composite Index which has been extended and revised to cover the period 1631-2018.

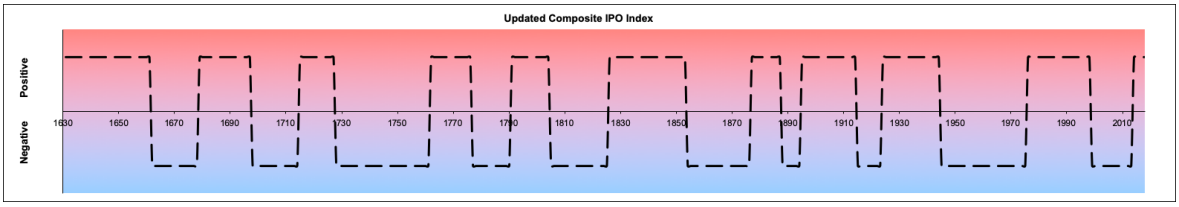

Figure 6: Updated Composite IPO index 2018

The residence times (i.e. persistence of IPO phases) of the updated Composite Index were fitted to a log normal distribution (as per Verdon 2007 framework) so that a randomly generated IPO timeseries of 10 000 years could be generated for use in the stochastic modelling (see Section 2).

3.2 Stratification of instrumental rainfall data by the IPO

The rainfall data from 1889-2018 was stratified into IPO positive and negative phases prior to the stochastic generation step (required for Stage 2 of the project). The distributions were found to be significantly different (i.e. IPO negative phase associated with higher rainfall on average than IPO

positive) as expected due to the strong IPO- rainfall relationship for this catchment. Figure 7 shows a box plot of the rainfall (aggregated to annual totals) within each phase across all 50 stations (Appendix A contains the monthly box plots for each station).

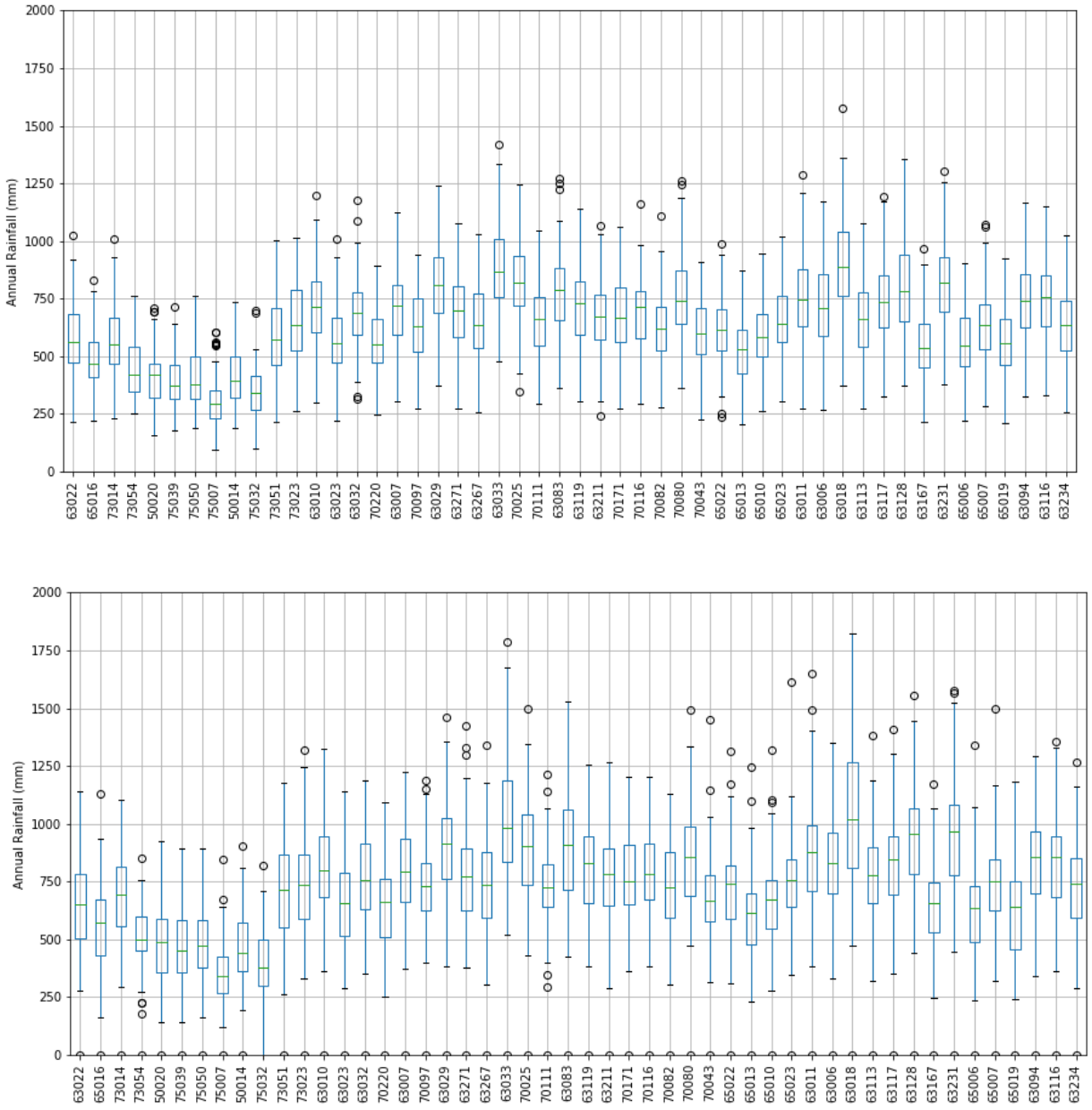

Figure 7: Distribution of rainfall data (annual) at each station during IPO positive (top panel) compared to IPO negative (bottom panel)

3.3 Stochastic data generation

3.3.1 Statistics for rainfall (no IPO forcing)

The mean of various statistics in the stochastic rainfall replicates was compared with the statistic in the instrumental time series data. If the difference between the statistics is within a set tolerance (different for each variable), the stochastic model is considered to have reproduced that statistic

satisfactorily. For each of the 50 stations a total of 13 statistics for annual data, 84 (7 by 12) monthly statistics and 204 (17 by 12) daily statistics are reported. The output from the statistical analysis of the stochastic data is voluminous and as such a separate Appendix (B) containing all daily, monthly and annual statistics is supplied. The reader is referred to Appendix B for all statistics, and a selection of statistics are summarised here.

The **daily statistics** were found to be very well represented by the stochastic data, with 90% of all statistics within tolerance. This is an expected feature of the Strikanthan model as the model is developed foremost on the daily statistics. Importantly, cross correlations of daily rainfall occurrence and rainfall amounts were very well represented and within tolerance, as were the mean number of wet days and mean rainfall of wet days. The primary statistics that were not within tolerance were the maximum wet and dry spell length (mostly underestimated). This is expected given that most WGMs do not preserve persistence and hence the reason or the IPO forcing applied in this project for the second set for stochastic data.

Throughout the project DoI-W expressed an interest in maintaining the **monthly rainfall** characteristics as these are particular important for hydrological modelling. The monthly standard deviation, skew and lag one autocorrelation were all very well reproduced across the 50 rainfall stations (see accompanying Appendix B). The maximum and minimum monthly rainfall of the stochastic data were more extreme in some cases than the instrumental. However, this provides useful plausible extreme scenarios for modelling purposes. The percentage of zero rain days in a month were found to be marginally higher on average for the stochastic replicates compared to the instrumental. While worth noting, this does not seem to affect the monthly rainfall averages.

Overall, the monthly means were well produced across all stations with the following exceptions:

(1) Stochastic data for stations located in the far west of the catchment (see Figure 3) exhibits a marginally higher mean rainfall across most months than the instrumental.

(2) At some stations, Autumn mean rainfall was marginally higher (maximum of 5 mm) for the stochastic data compared to the instrumental.

With respect to (1) a series of tests were carried out and it was determined that the representation of the western stations is biased by the cluster of stations (which have higher rainfalls) in the east of the catchment. That is, the large size (and east-west alignment) of the catchment (and hence distance between stations) has somewhat impacted on the model's ability to maintain statistics across the observed rainfall gradient. This is a limitation of the current approach and future work could involve splitting the catchment into separate zones (however this was outside the scope of the current project). The issue of autumn rainfall (noted in point 2) is discussed below in Section 3.3.2.

With respect to the **Annual statistics** it was observed that for some stations, the annual mean was higher for the stochastic data compared to the instrumental (related to the elevated autumn rainfall, see solution applied in Section 3.3.2). Aside from the mean, the majority of important annual statistics were within tolerance (including the standard deviation, skewness, lag one autocorrelation). The two-year, three-year and five-year low rainfall sums were within tolerance for most cases, however the seven-year and 10-year were underestimated at many stations, along with the annual max and min (as a result of the persistence issue noted above).

3.3.2 Post processing of Autumn rainfall

The first generation of stochastic data provided for testing by the DOI-W modelling team highlighted that the Srikanthan model was simulating marginally higher (maximum of 5 mm) mean monthly rainfall during the autumn months (in particular May) than the instrumental period (shown in Figure 8 for a select station). This in turn resulted in an increase in modelled flow into the reservoirs during the productive winter months (Figure 9).

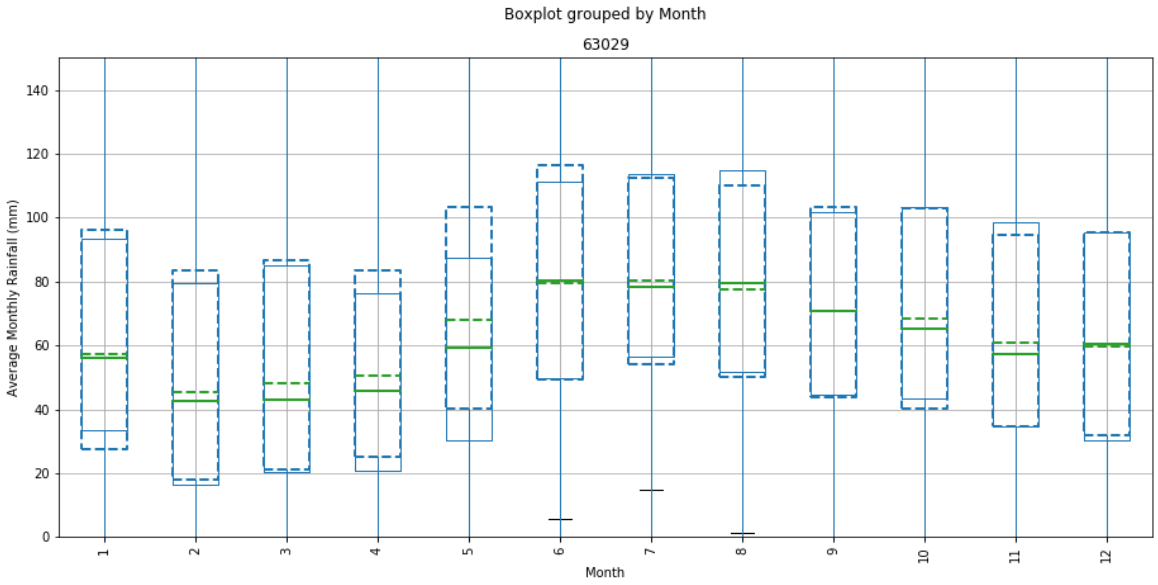

Figure 8: Monthly rainfall for instrumental (solid line) and stochastic (dashed line)

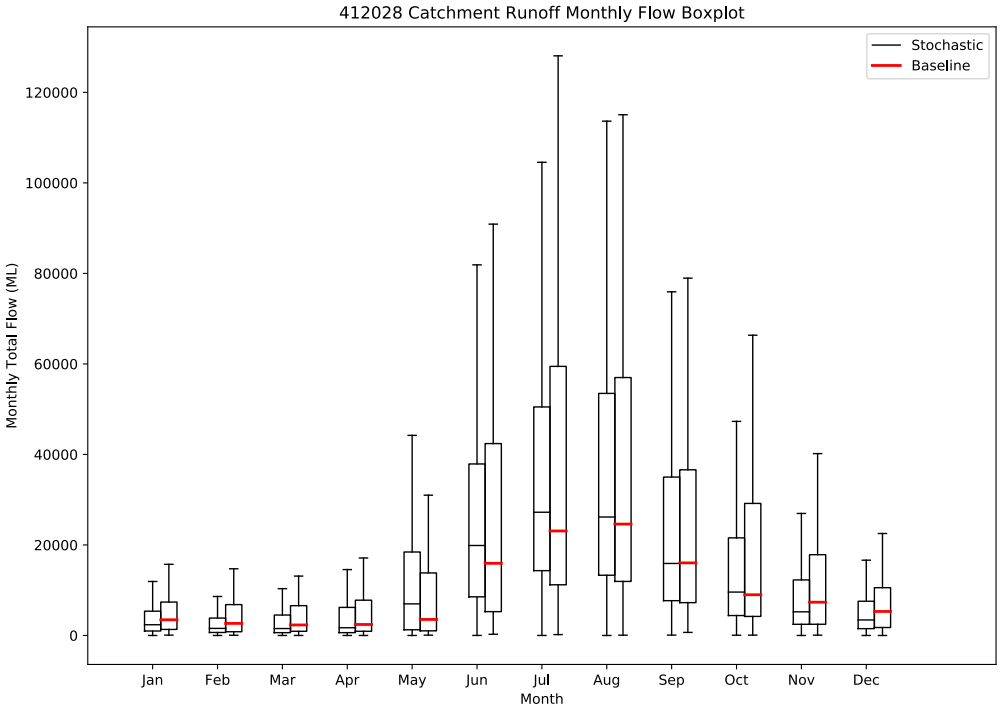

Figure 9: Catchment runoff monthly flow showing increase in productive period due to higher autumn rainfall in stochastic rainfall data (graph provided by DoI-W)

A number of possible reasons for this increase in simulated autumn rain were explored, including a) possible changes in the last ~15 years to autumn rainfall, b) uncertainty in the early rainfall records (prior to 1920) and c) the large spatial extent of the rainfall station network. Simulations were carried out to assess each of these possibilities. It was found that the autumn rainfall monthly averages were higher regardless of the time period on which the stochastic model was trained (i.e. the last 15 years and the first 30 years did not impact on the outcome). However, developing the model on fewer stations (and particular leaving out the western stations) did improve the autumn rainfall representation, confirming the large size of the catchment and number is stations is one causal factor. However, there is a requirement for all datasets to be included in the stochastic model in order to maintain the spatial relationship of rain events across the Lachlan catchment for use in IQQM modelling. Therefore, an option was proposed to DoI-W to apply a post-processing step to adjust the autumn rainfall amounts to better match the instrumental. This method was agreed upon and subsequently applied as a post-processing step to the stochastically generated rainfall. The post-processing step involved calculating the difference between the target mean monthly rainfall (i.e. the instrumental data) and the stochastic mean monthly rainfall for autumn months (for each station) to generate a station specific daily rainfall factor for each autumn month. The daily factor was then applied to the stochastic rainfall (for all rain days) such that the autumn monthly means were sufficiently close to the instrumental. The results of the post processing are shown in Figure 10 and the impact on modelled flows is shown in Figure 11. Note that the flows in

the productive period are better aligned after the post processing of autumn rainfall. Monthly rainfall box plots for all stations with the autumn rainfall post processing step are contained in Appendix C.

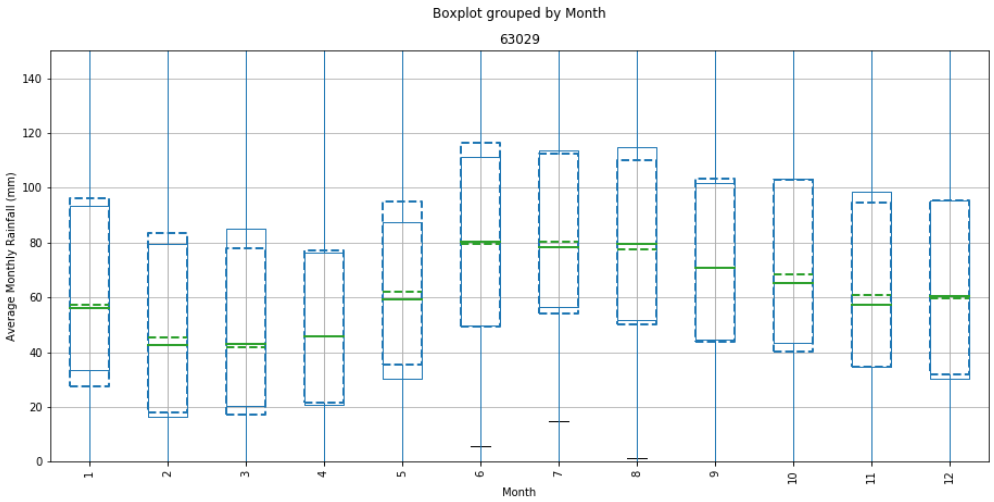

Figure 10: Monthly rainfall for instrumental (solid line) and stochastic (dashed line) after the post processing step

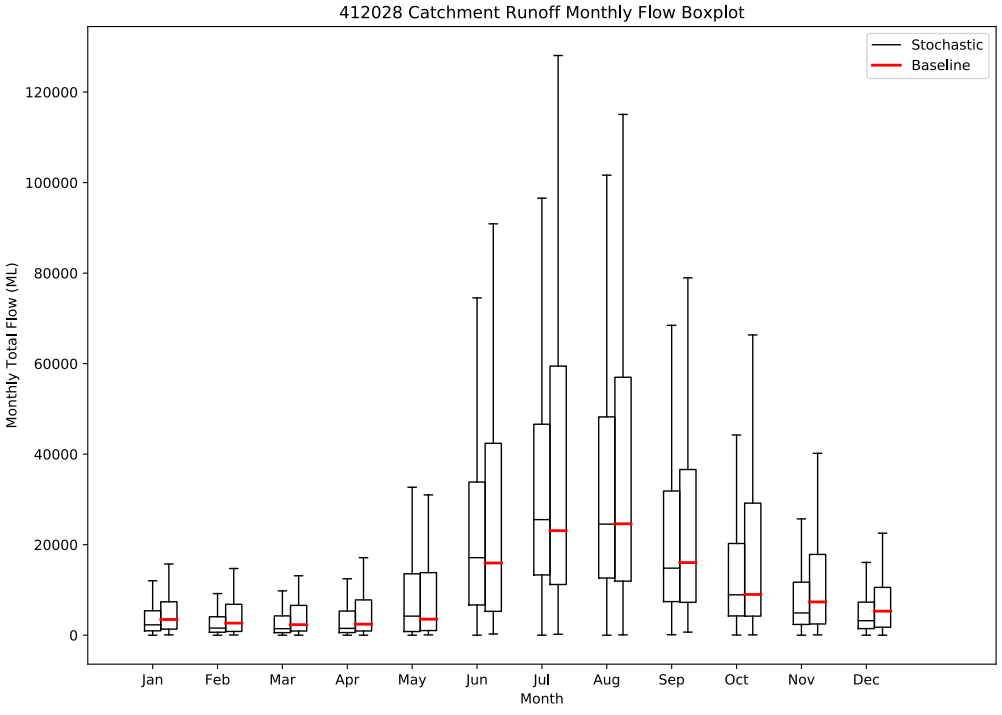

Figure 11: Catchment runoff monthly flow showing improved representation of monthly flow as a result of post processing the stochastic autumn rainfall data (graph provided by DoI-W)

3.3.3 Statistics rainfall (IPO forcing)

As described above the statistics output is voluminous and has been supplied as a separate Appendix D and E which the reader is referred to for details of the daily, monthly and annual statistics.

The primary reason for the IPO forcing model is to improve the representation of long-term variability (persistence) in the replicates which is traditionally not well represented by WGMs including the Srikanthan model. Figure 12 shows the 10 -year low rainfall sums for the instrumental and mean of stochastic and IPO primed datasets for a selection of example stations. While the mean of the traditional stochastic is higher than the instrumental 10 -year, the stochastic data based on the IPO positive period is much closer to the instrumental period. Further, there is a notable difference between the IPO negative and positive 10 year means demonstrating that individually these datasets are preserving the persistent wet (IPO positive) and dry (IPO negative) periods.

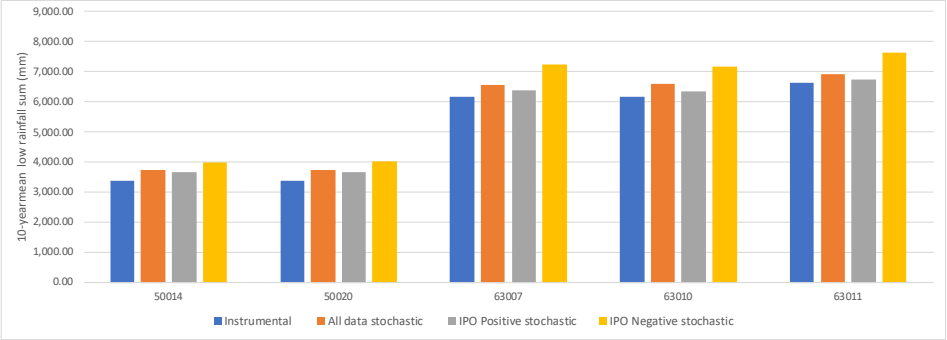

Figure 12: 10-year low rainfall sum for a) the instrumental period and mean of stochastic replicates based on b) all data, c) IPO positive and d) negative data

The original Verdon 2007 study (on which this project is based) looked at worst case dry scenarios by modelling the impacts on flows in the Lachlan. While this particular step is outside the project scope, it is interesting to compare and contrast the “worst case” scenarios generated based on rainfall alone. Figure 13 shows the lowest 2.5 percentile 10-year rainfall sums for the IPO positive stochastic data compared to the lowest 10-year rainfall sum for the instrumental period (for a selection of example stations).

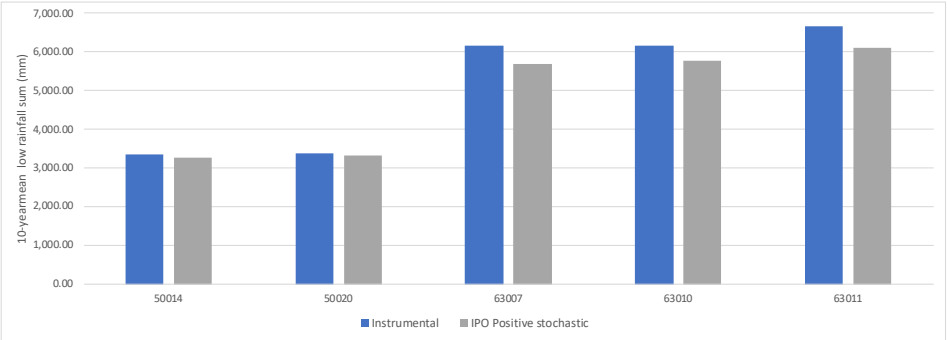

Figure 13: Comparison of lowest 10-year rainfall in instrumental with 2.5 percentile 10 -year low rainfall sums for IPO positive stochastic

The benefit of using a stochastic approach to stress test water supply systems is clearly highlighted in Figure 13. That is, this information can be used to develop statically plausible low flow scenarios to assesses how well the system performs.

The separate IPO based stochastic replicates were combined into a single 10 000 year sequence for each station using the palaeo IPO sampling model as a template (as described in Section 2.3.2. Overall, the combined data resulted in a higher mean monthly rainfall (particularly for the first half of the year) for most stations (Figure 14 shows an example, while all box plots are contained in Appendix F). The reason for this is due to the instrumental period being somewhat biased towards dry, with three extended positive IPO phases between 1890-2018. In contrast there is only one long IPO negative phase (1945-75), while the other two negative phases were much shorter. The 10 000 year sequence maintains a balance of IPO negative and positive phases over a range of durations. Even though the mean is higher, the stochastic data with IPO forcing still contains the persistent dry cycles of the IPO positive input file which as mentioned previously is particularly useful for stress testing the system.

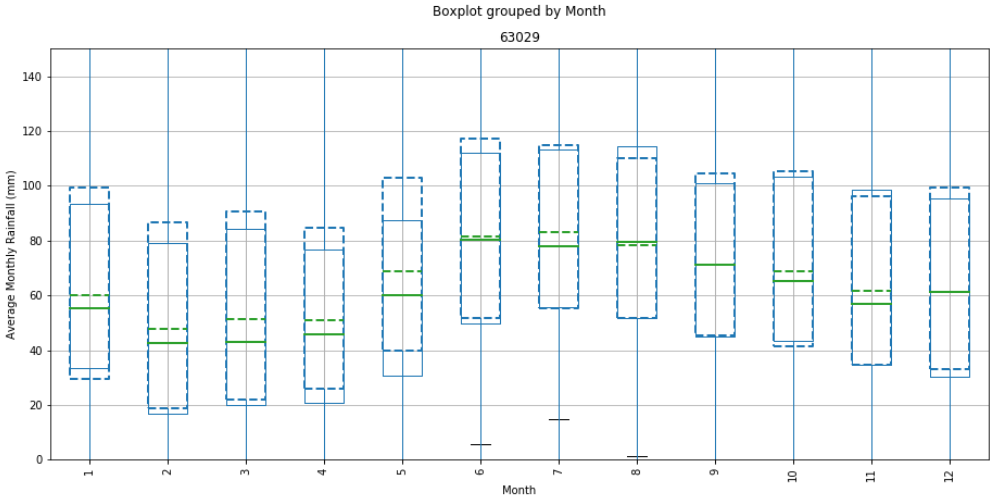

Figure 14: Example station showing slightly higher monthly rainfall during the first half of the year for the IPO forced stochastic dataset (dashed line) compared to the instrumental (solid line)

3.3.4 Stochastic Evaporation data

The two-state resampling evaporation model was developed as per the method outline in Section 2.3.3. Evaporation across the Lachlan catchment was found to have a strong seasonal signal and is lower on average on days where rainfall occurs (Figure 15).

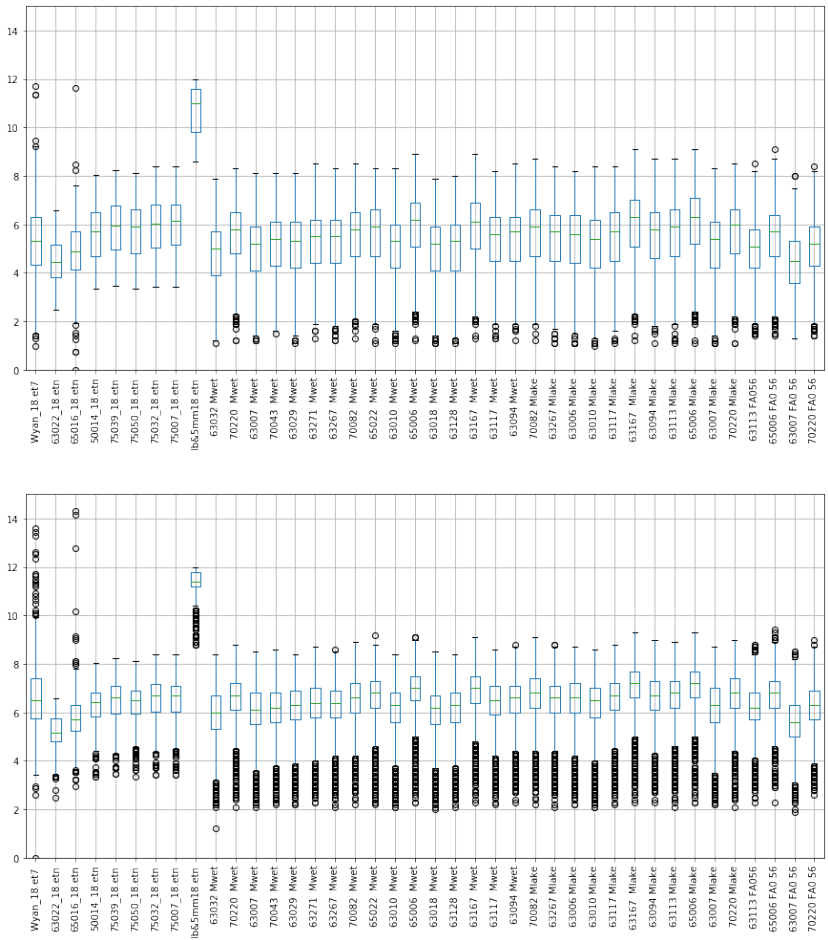

Figure 15: Evaporation/evapotranspiration on wet days (top panel) and dry days (bottom panel) during January for all 40 stations

The resampling model was applied for all 40 evaporation/evapotranspiration datasets requested to develop matching sequences to the stochastically generated rainfall data (10 000 years, two sets). Due to the nature of the resampling procedure used to generate the evaporation data, the statistics of the evaporation data are extremely well preserved. Figure 16 shows the comparison between stochastic monthly evaporation (dashed line) and instrumental (solid line).

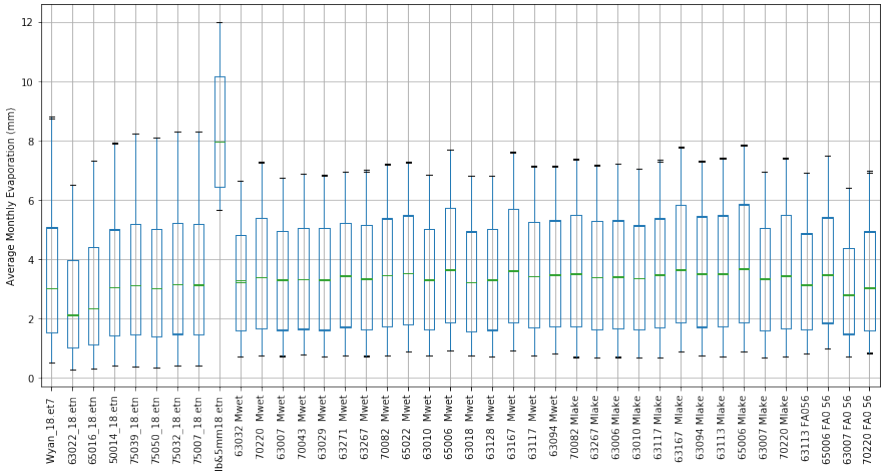

Figure 16: Monthly evaporation for instrumental (solid line) and stochastic (dashed line)

4 Conclusions and recommendations

The aims of this project were achieved including:

1. Update of the IPO persistence model;
2. Development of 10 000 year stochastic datasets for 50 rainfall and 40 evaporation/evapotranspiration stations for the Lachlan (using the Skrikanthan daily model - one set forced with the palaeo IPO model and the second without), and
3. Assessment of stochastic data statistics (incorporating feedback from DoI-W modelling team).

The IPO persistence model of Verdon-Kidd was updated and extended and updated based on cross checks with the Gallant and Gergis (2011) Murray flow reconstruction. Other recent IPO /PDO reconstructions were found to contain mixed signals of the Pacific and other tropical climate phenomena (i.e. ITCZ and Asian Monsoon) and as such, were found to be unsuitable for inclusion in the Composite Index. The updated Composite IPO phase lengths followed a log normal distribution consistent with the original Verdon (2007) study and this distribution was used to develop a synthetic IPO timeseries of 10 000 years for use in the IPO forced stochastic model.

The Srikanthan daily WGM was used to develop stochastic replicates for the rainfall data provided by DoI-W (100 lots of 100 years). This method was chosen because a) it was used in the Verdon (2007) study on which this project is based and b) it tends to preserve the monthly mean better than other WGMs. In this application, it was found that the Srikanthan method produced suitable daily and monthly statistics, however the autumn mean rainfall was marginally higher for the stochastic data compared to the instrumental data. This is most likely the result of catchment size and the large number of datasets. In response, a post-processing step was applied whereby the daily stochastic rainfall in March, April and May were adjusted to provide a closer match to the instrumental record. The additional post-processing step was found to improve the flow representation in the productive period (based on modelling by DoI-W) and a single 10 000 year daily timeseries for each rainfall station was supplied to DoI-W.

The stochastic data based on the Srikanthan model with IPO persistence was found to improve the representation of the long-term statistics (i.e. 10 year low flows). Importantly, the development of the IPO stochastic data allows for stress testing the system using the “worst cases” simulated within the data sets provided. Overall, the stochastic data sets based on this method produced replicates with higher mean monthly rainfall during the first half of the year. This is due to the instrumental period being biased towards dry. A single 10 000 year daily time series for each rainfall station was supplied to DoI-W based on the IPO forced model.

A resampling model was developed during this project to generate matching evaporation sequences to the 10 000 year rainfall sequences (supplied to DoI-W). The model was conditioned

on month and wet/dry days. The benefit of this approach is that the cross correlations are maintained (since samples are taken from all stations on a single day) as well as the other daily, monthly and annual statistics.

Possible future improvements/additions to the work carried out for this project could include:

- Testing of alternative WGMs (e.g. Generalised Linear Model for daily Climate time series (RGLIMCLIM), multi-site precipitation generator (RGENERATRPREC), Multi-site Autoregressive Weather GENerator (RMAWGEN)) to investigate if the autumn rainfall is better represented by these models without the need for the additional post processing step used here. Given that each WGM is different and is better at representing certain statistics than others, developing stochastic datasets based on multiple WGMs would also provide different scenarios on which the IQQM models can be tested.
- Splitting the Lachlan catchment into regional climate zones prior to stochastic data generation and development of a new method to maintain the spatial relationship between zones. This may improve the autumn rainfall and western rainfall representation in particular.
- Testing the sensitivity of the stochastic data generation to the input rainfall data sources (i.e. compare AWAP to SILO). Applying the model to a regularly gridded data set across the catchment may also yield different results as it would remove the bias of the clustered stations located in the east of the catchment.

It is also worth highlighting that the Lachlan River catchment is not the only catchment in eastern Australia with a strong IPO influence. Therefore, the methods developed and applied in this project could feasibly be applied to other neighbouring catchments with similar success.

5 References

Biondi, F., A. Gershunov, D. R. Cayan (2001), North Pacific Decadal Climate Variability since 1661, J. Clim., 14, 5-10.

Buckley, B. M., Ummenhofer, C. C., D'Arrigo, R. D., Hansen, K. G., Truong, L. H., Le, C. N., & Stahle, D. K. (2019). Interdecadal Pacific Oscillation reconstructed from trans-Pacific tree rings: 1350–2004 CE. Climate Dynamics, 1-16.

D'Arrigo, R., R. Villalba, G. Wiles (2001), Tree-ring estimates of Pacific decadal climate variability, Clim. Dyn., 18, 219-224.

D'Arrigo, R., E. Cook, R. Wilson, R. Allan, M. Mann (2005), On the variability of ENSO over the past six centuries, Geophys. Res. Lett., 32, L03711, doi:10.1029/2004GL022055.

D'Arrigo, R., & Wilson, R. (2006). On the Asian expression of the PDO. International Journal of Climatology: A Journal of the Royal Meteorological Society, 26(12), 1607-1617.

Fu, G., Chiew, F. H., & Shi, X. (2018). Generation of multi-site stochastic daily rainfall with four weather generators: a case study of Gloucester catchment in Australia. Theoretical and applied climatology, 134(3-4), 1027-1046.

Gallant, A. J., & Gergis, J. (2011). An experimental streamflow reconstruction for the River Murray, Australia, 1783–1988. Water Resources Research, 47(12).

Gedalof, Z., and D. J. Smith (2001), Interdecadal climate variability and regime-scale shifts in the Pacific North America, Geophys. Res. Lett., 28(8), 1515-1518

Linsley, B. K., G. M. Wellington, D. P. Schrag (2000), Decadal Sea Surface Temperature Variability in the Subtropical Pacific from 1726 to 1997 A.D., Science, 290, 1145-1148.

Linsley, B. K., Zhang, P., Kaplan, A., Howe, S. S., & Wellington, G. M. (2008). Interdecadal-decadal climate variability from multicoral oxygen isotope records in the South Pacific Convergence Zone region since 1650 AD. Paleoceanography, 23(2).

MacDonlad, G. M., and R. A. Case (2005), Variations in the Pacific Decadal Oscillation over the past millennium, Geophys. Res. Lett., 32, L08703, doi:10.1029/2005GL022478.

Shen, C., Wang, W. C., Gong, W., & Hao, Z. (2006). A Pacific Decadal Oscillation record since 1470 AD reconstructed from proxy data of summer rainfall over eastern China. Geophysical Research Letters, 33(3).

Srikanthan, R. (2005). Stochastic generation of daily rainfall data at a number of sites (Vol. 7, p. 66). Tech. Rep. 05.

Verdon DC, Pacific and Indian Ocean Climate Variability ~ Implications for Water Resource Management in Eastern Australia, University of Newcastle, Australia (2007)

Verdon-Kidd DC, Franks SW, 'Long-term behaviour of ENSO: Interactions with the PDO over the past 400 years inferred from paleoclimate records', Geophysical Research Letters, 33 (2006)

Wilks, D. S., & Wilby, R. L. (1999). The weather generation game: a review of stochastic weather models. Progress in physical geography, 23(3), 329-357.

Appendix A –Box Plots of monthly rainfall data for each station stratified by the IPO (IPO negative solid line, IPO positive dashed line)

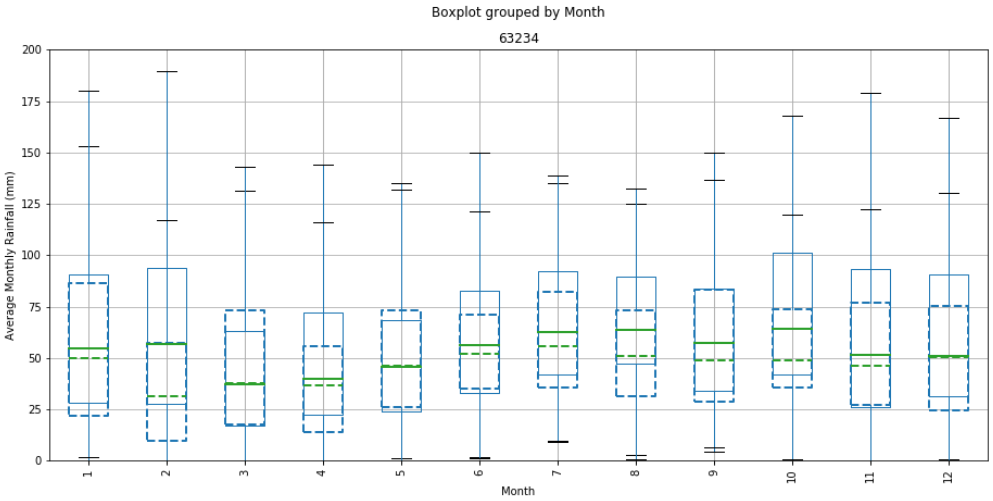

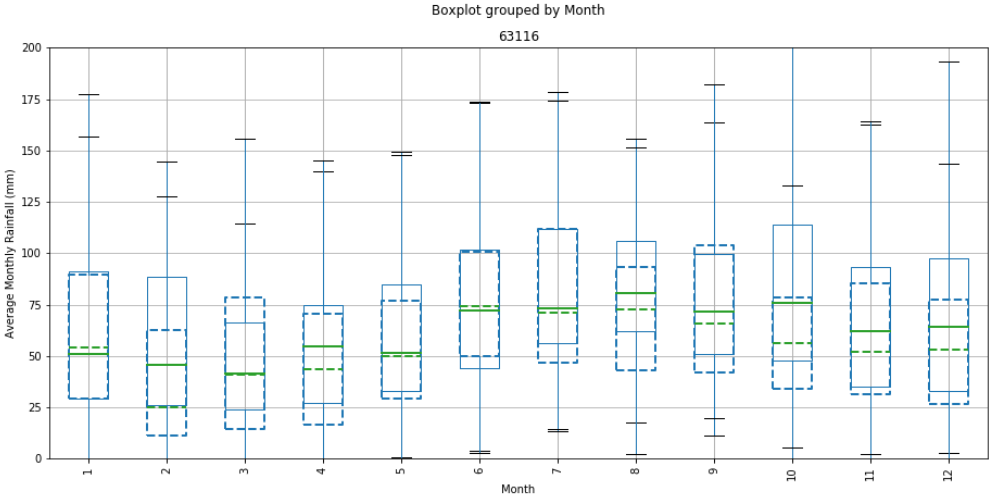

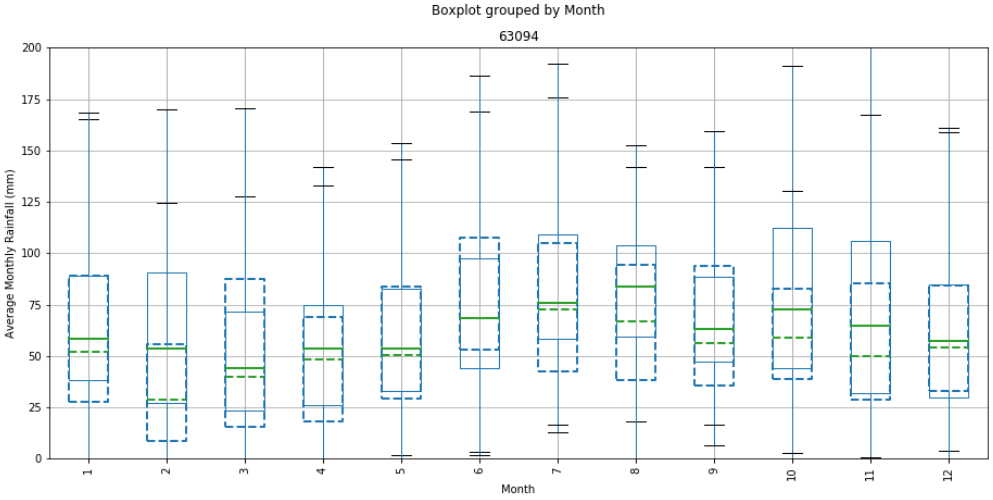

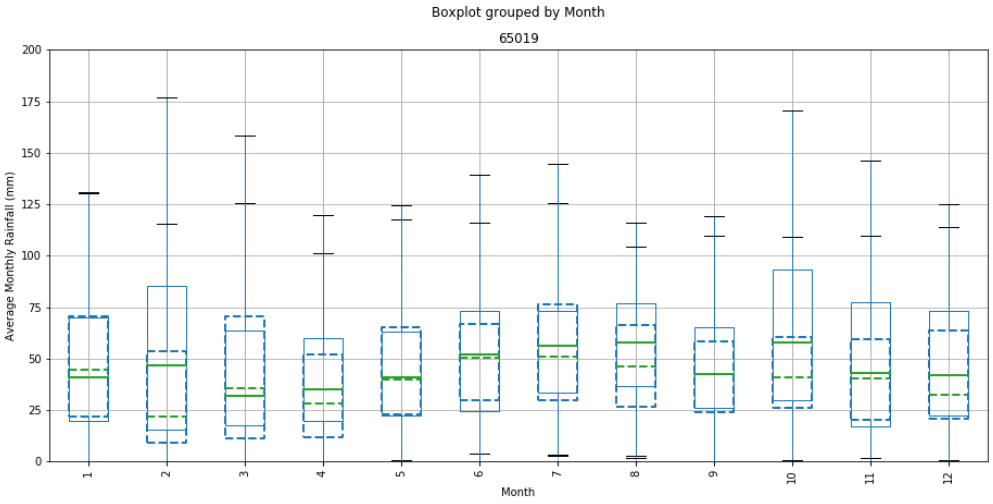
Boxplot grouped by Month
65019
Average Monthly Rainfall (mm)
Month

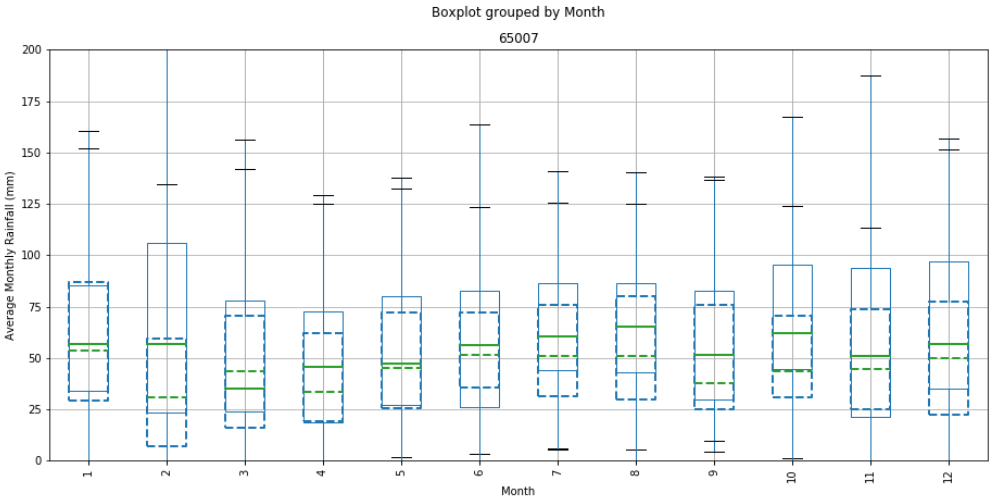
Boxplot grouped by Month
65007
Average Monthly Rainfall (mm)
Month

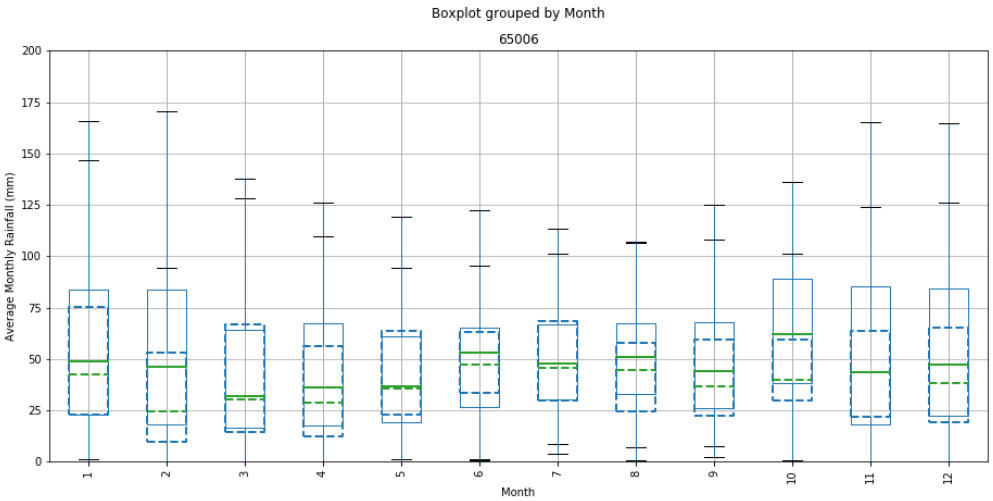
Boxplot grouped by Month
65006
Average Monthly Rainfall (mm)
Month

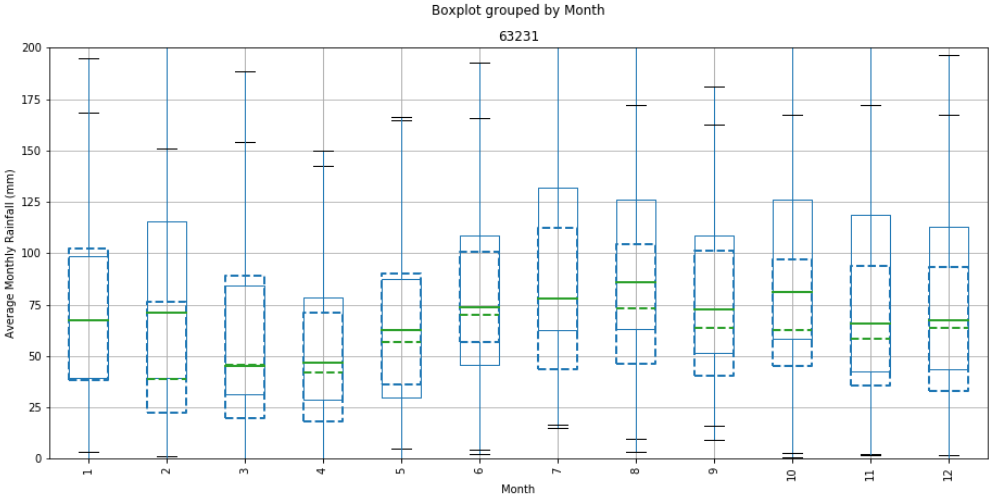
Boxplot grouped by Month
63231
Average Monthly Rainfall (mm)
Month

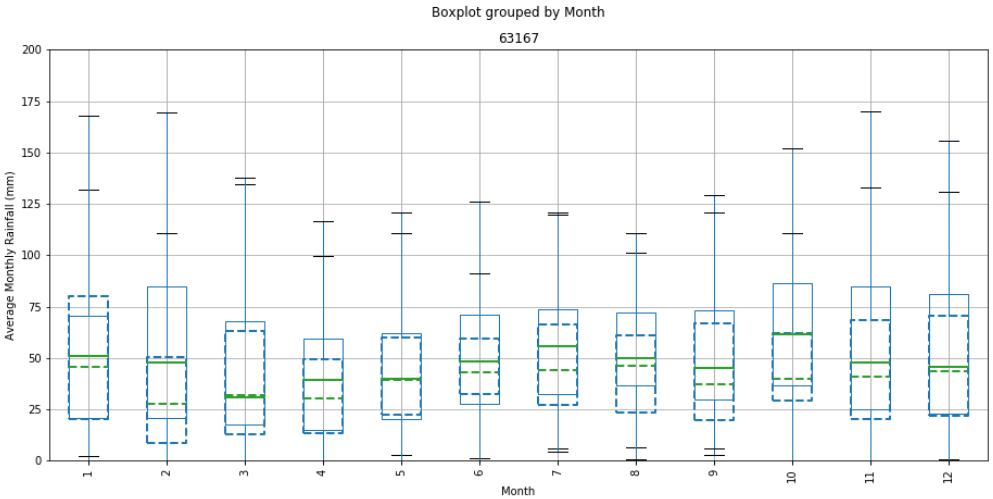
Boxplot grouped by Month
63167
Average Monthly Rainfall (mm)
Month

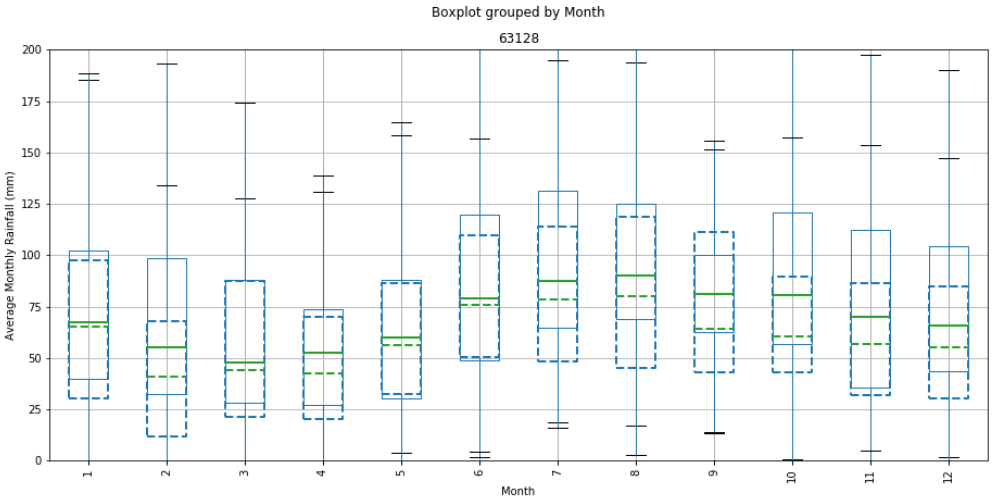
Boxplot grouped by Month
63128
Average Monthly Rainfall (mm)
Month

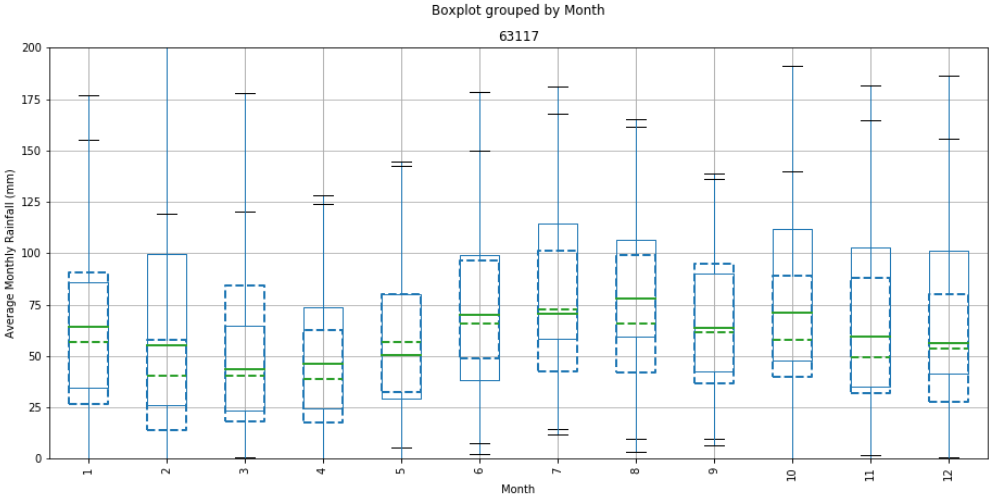
Boxplot grouped by Month
63117
Average Monthly Rainfall (mm)
Month

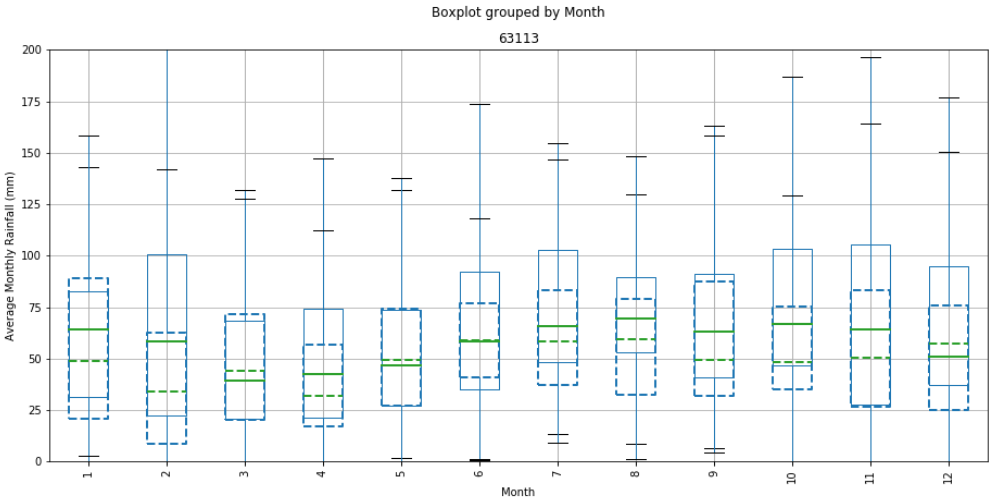
Boxplot grouped by Month
63113
Average Monthly Rainfall (mm)
Month

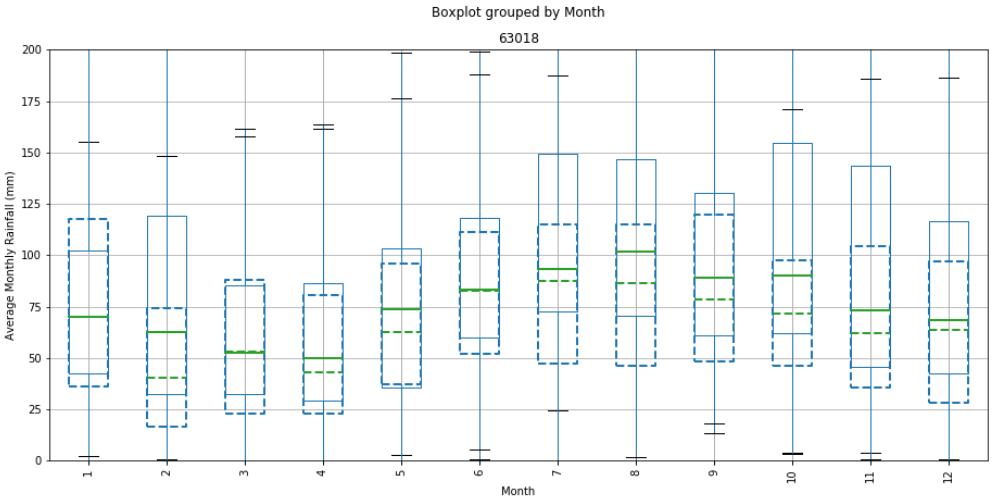
Boxplot grouped by Month
63018
Average Monthly Rainfall (mm)
Month

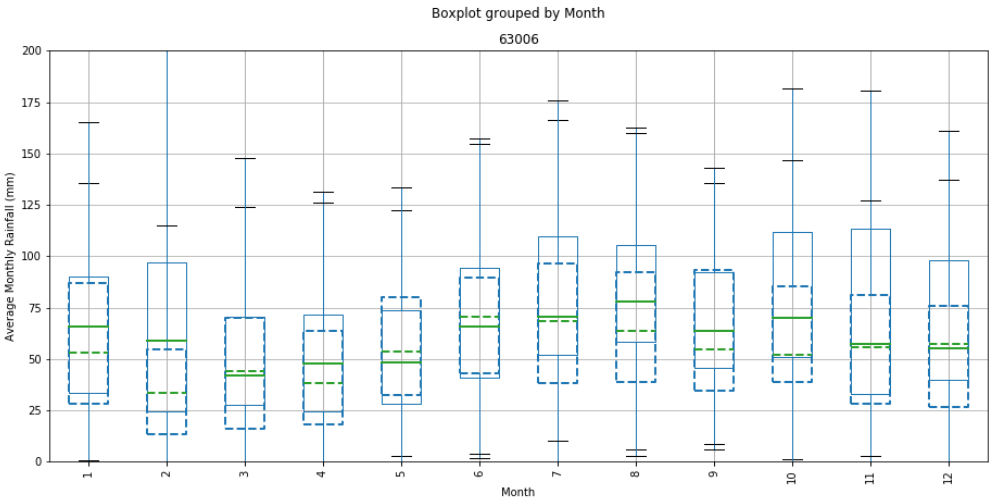
Boxplot grouped by Month
63006
Average Monthly Rainfall (mm)
Month

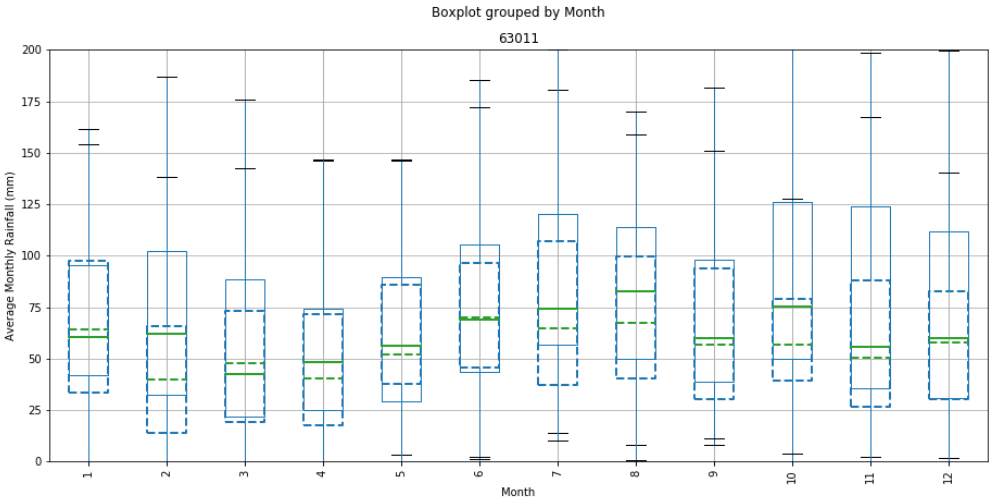
Boxplot grouped by Month
63011
Average Monthly Rainfall (mm)
Month

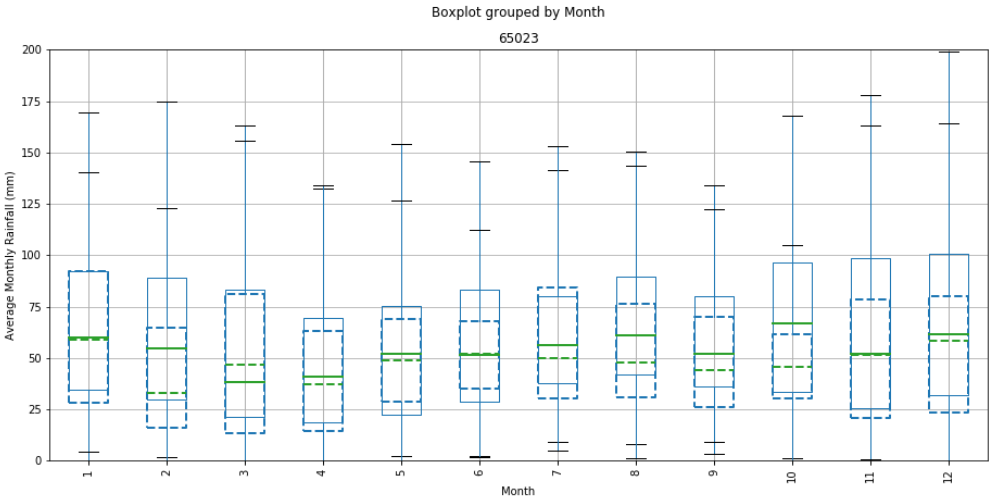
Boxplot grouped by Month
65023
Average Monthly Rainfall (mm)
Month

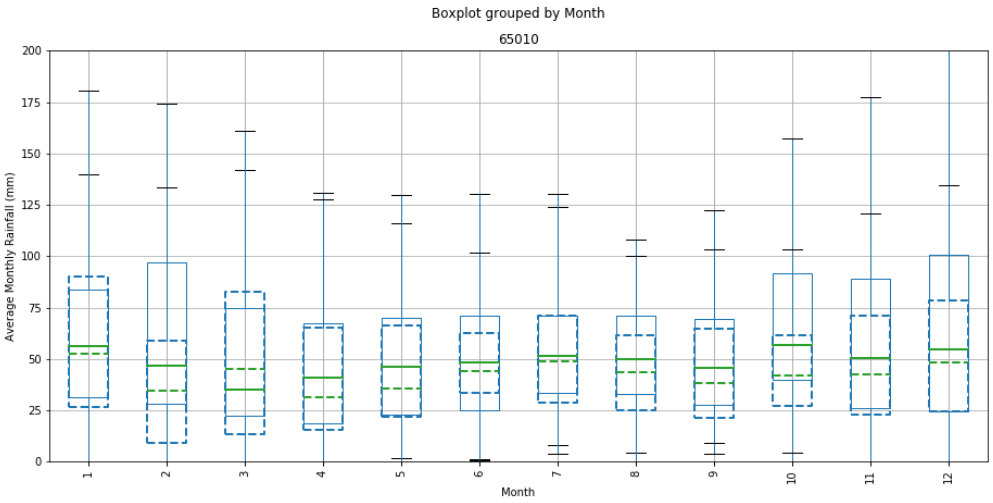
Boxplot grouped by Month
65010
Average Monthly Rainfall (mm)
Month

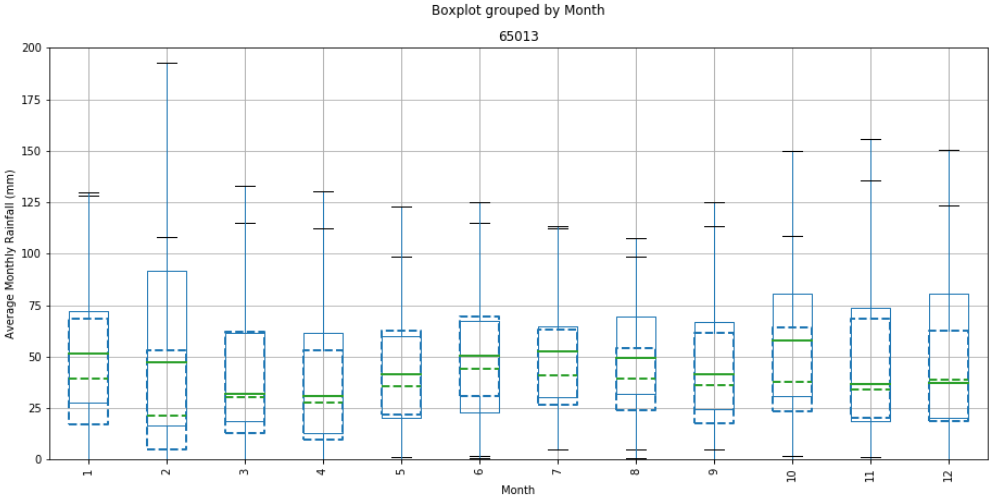
Boxplot grouped by Month
65013
Average Monthly Rainfall (mm)
Month

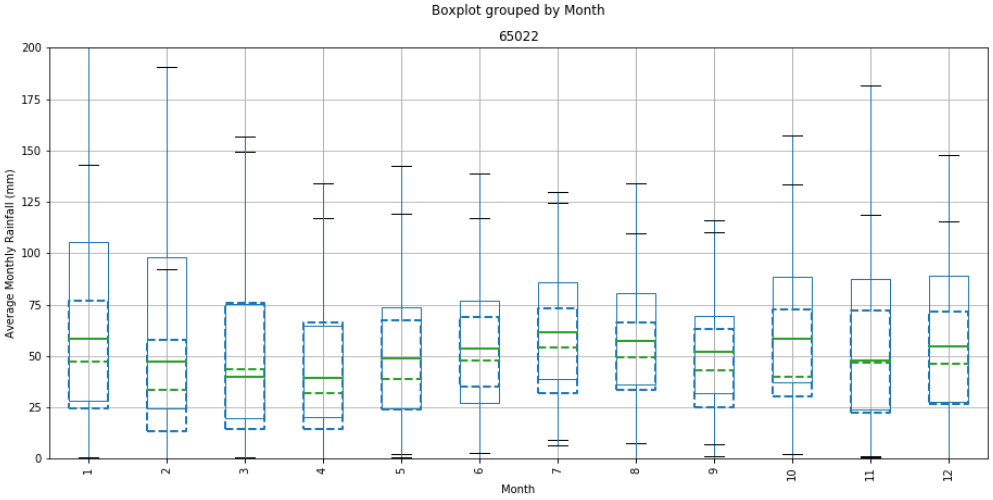
Boxplot grouped by Month
65022
Average Monthly Rainfall (mm)
Month

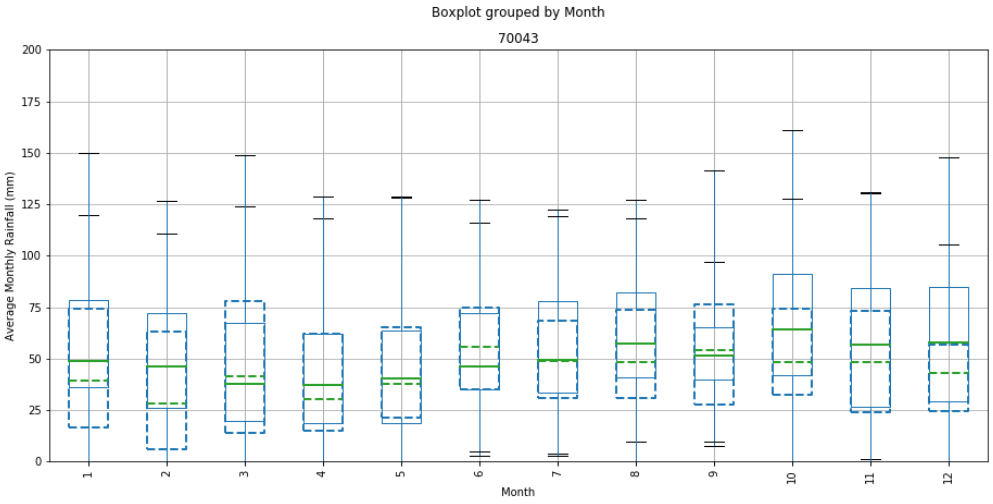
Boxplot grouped by Month
70043
Average Monthly Rainfall (mm)
Month

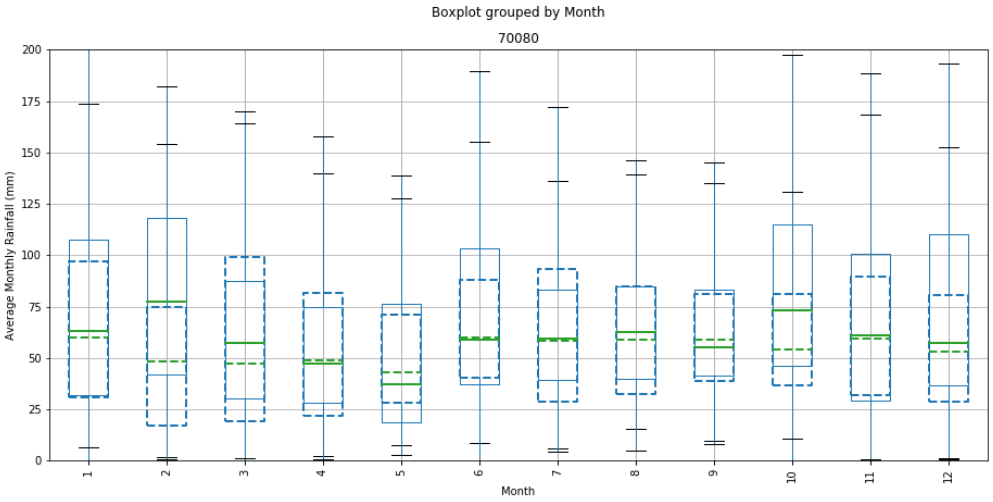
Boxplot grouped by Month
70080
Average Monthly Rainfall (mm)
Month

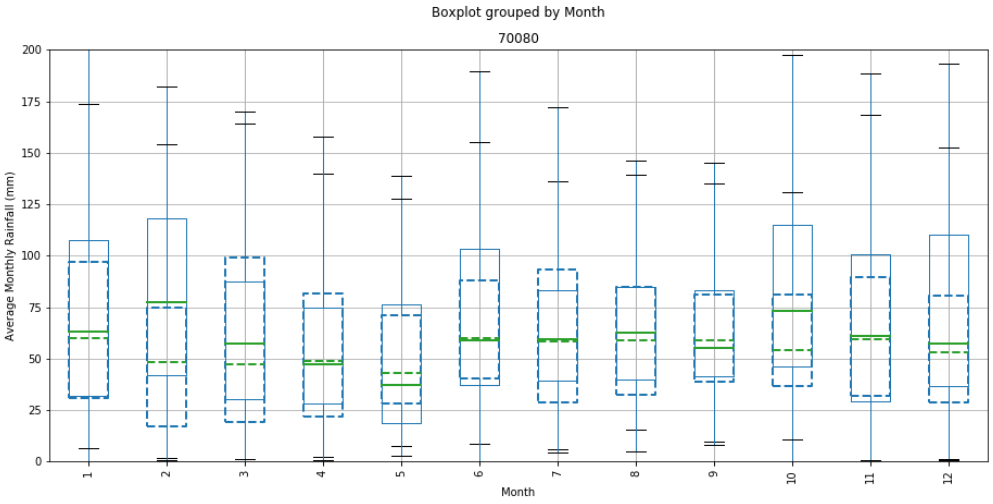
Boxplot grouped by Month
70080
Average Monthly Rainfall (mm)
Month

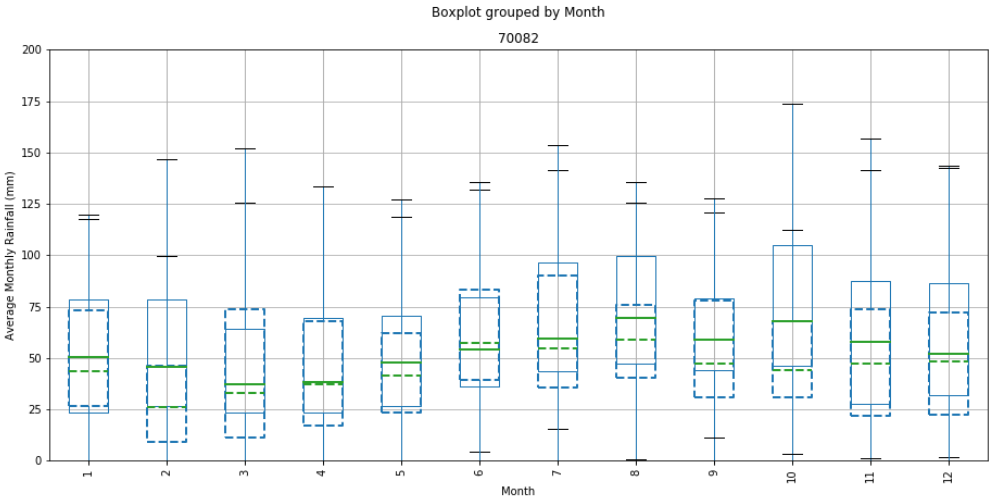
Boxplot grouped by Month
70082
Average Monthly Rainfall (mm)
Month

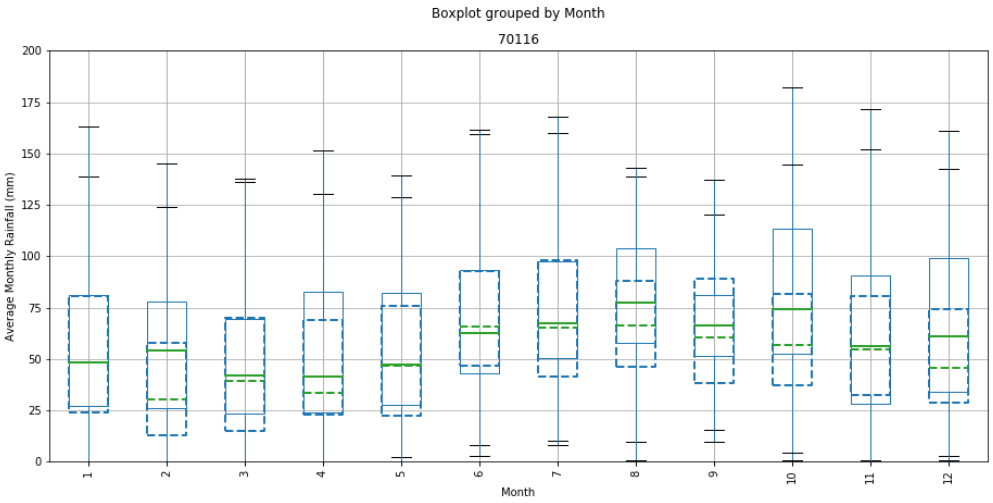
Boxplot grouped by Month
70116
Average Monthly Rainfall (mm)
Month

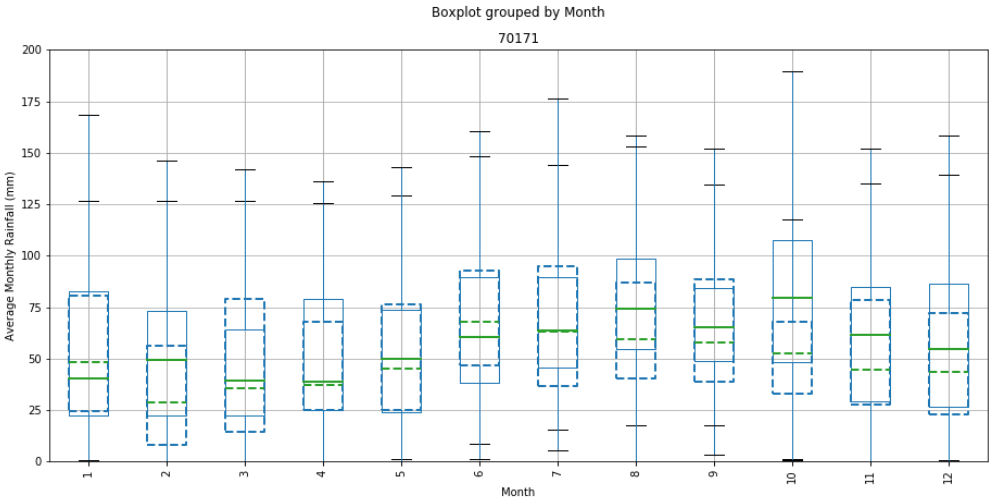
Boxplot grouped by Month
70171
Average Monthly Rainfall (mm)
Month

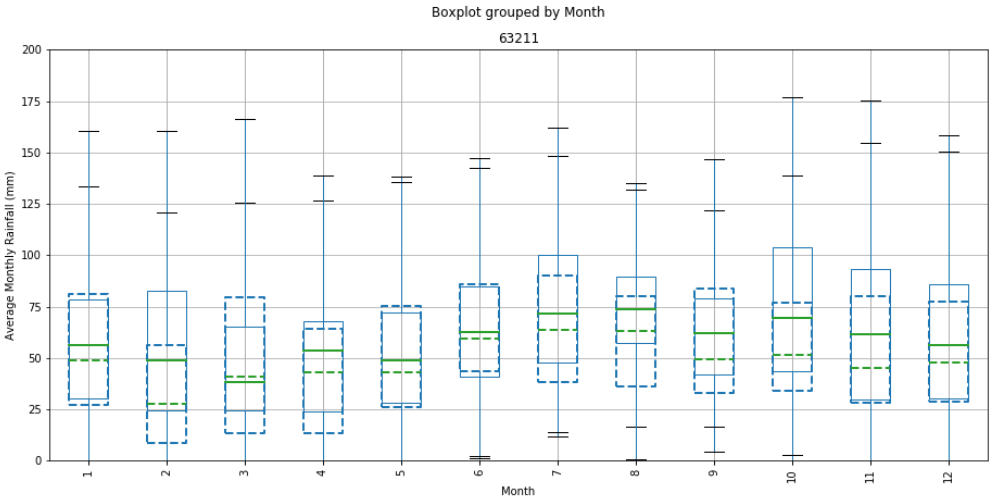
Boxplot grouped by Month
63211
Average Monthly Rainfall (mm)
Month

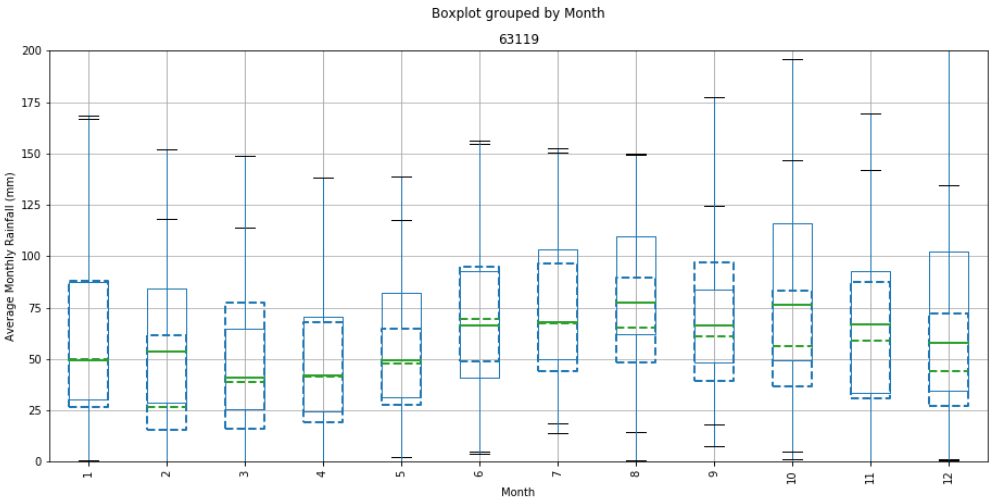
Boxplot grouped by Month
63119
Average Monthly Rainfall (mm)
Month

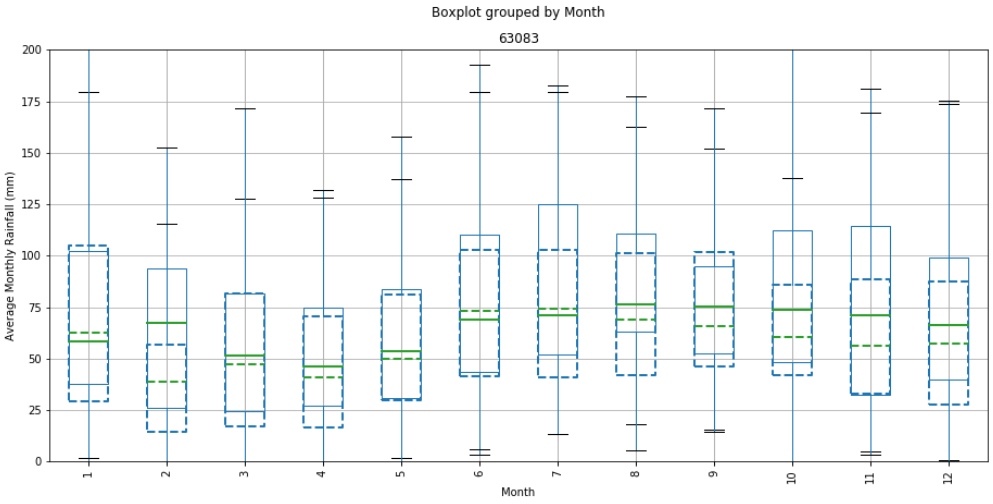
Boxplot grouped by Month
63083
Average Monthly Rainfall (mm)
Month

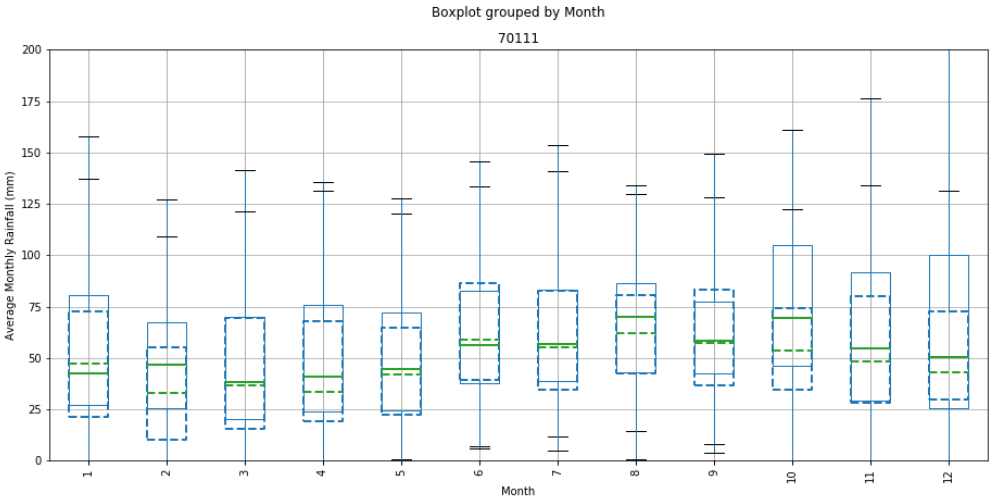
Boxplot grouped by Month
70111
Average Monthly Rainfall (mm)
Month

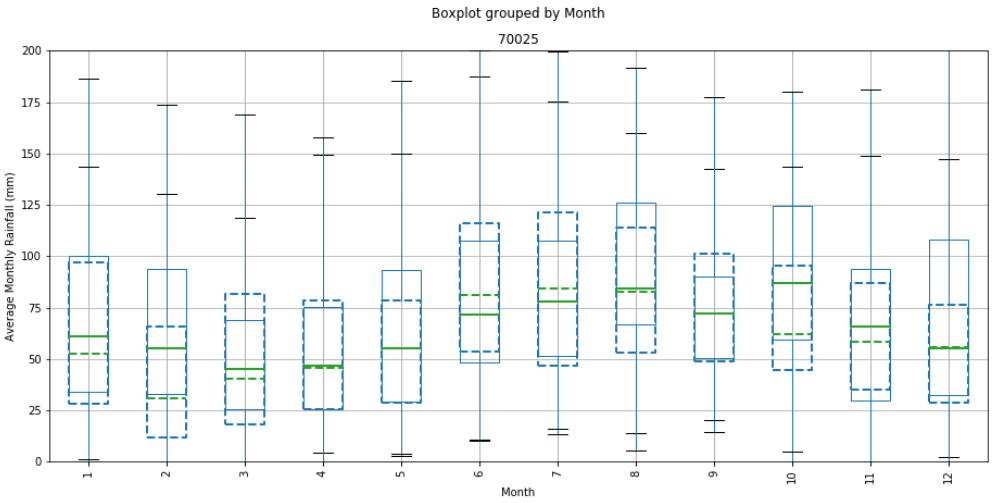
Boxplot grouped by Month
70025
Average Monthly Rainfall (mm)
Month

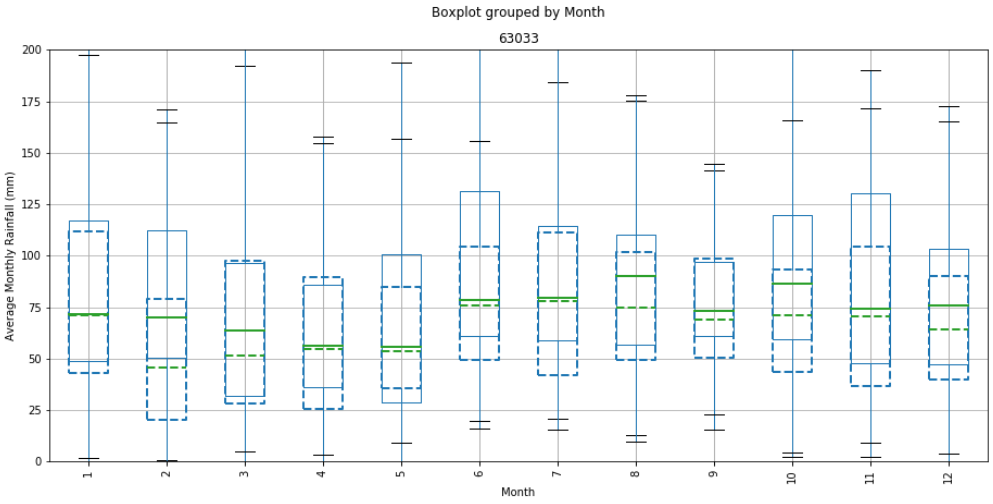
Boxplot grouped by Month
63033
Average Monthly Rainfall (mm)
Month

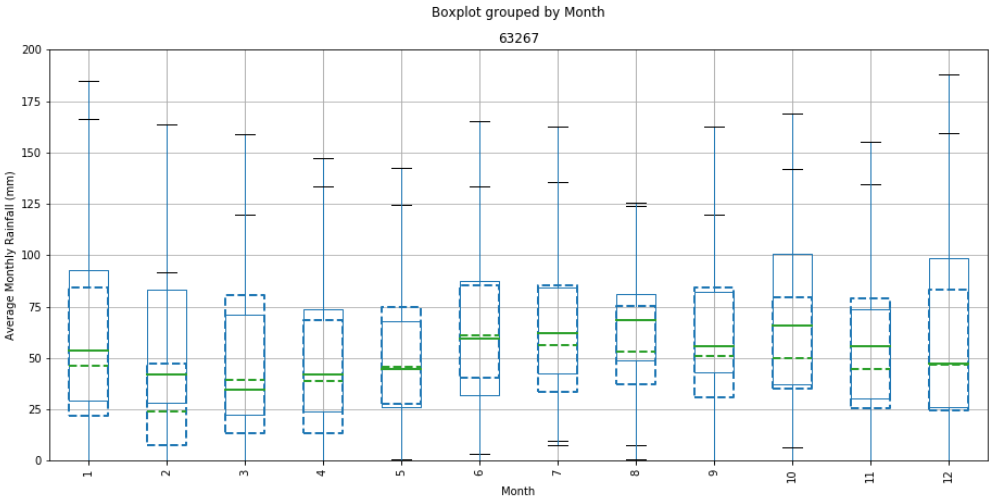
Boxplot grouped by Month
63267
Average Monthly Rainfall (mm)
Month

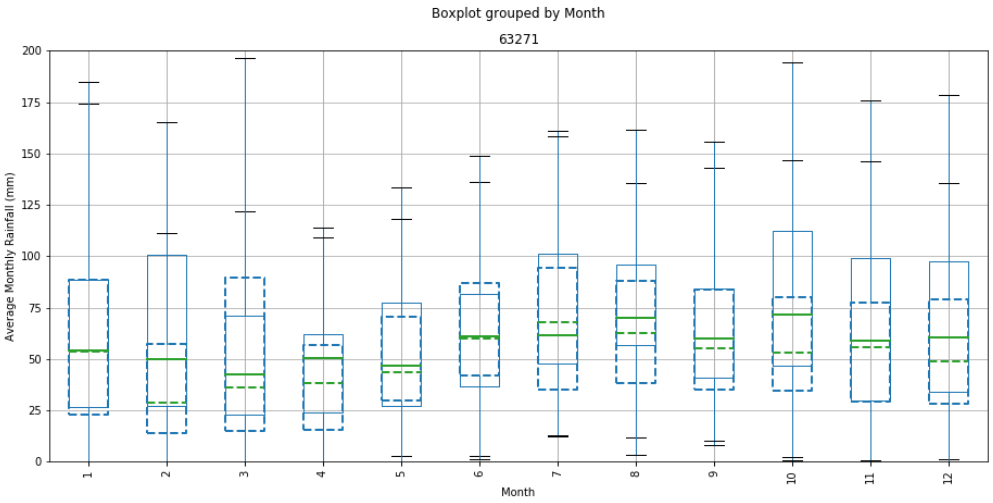
Boxplot grouped by Month
63271
Average Monthly Rainfall (mm)
Month

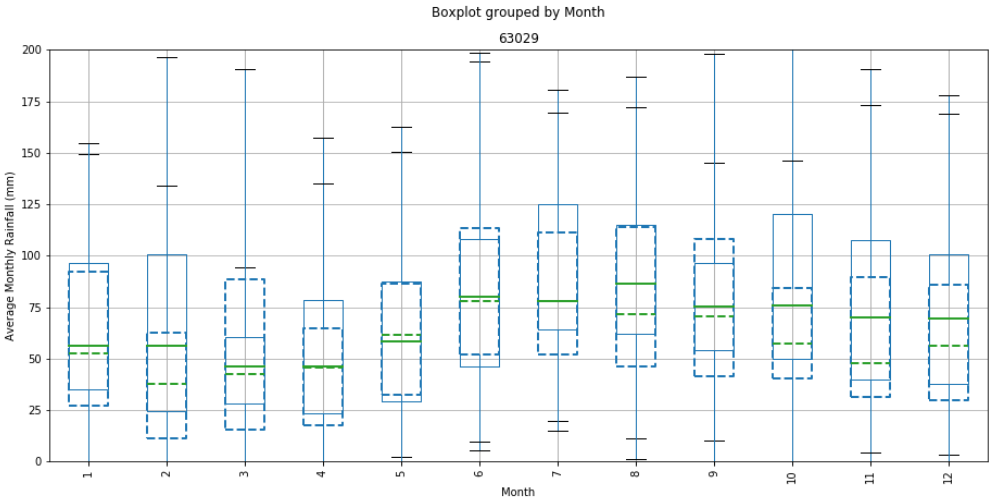
Boxplot grouped by Month
63029
Average Monthly Rainfall (mm)
Month

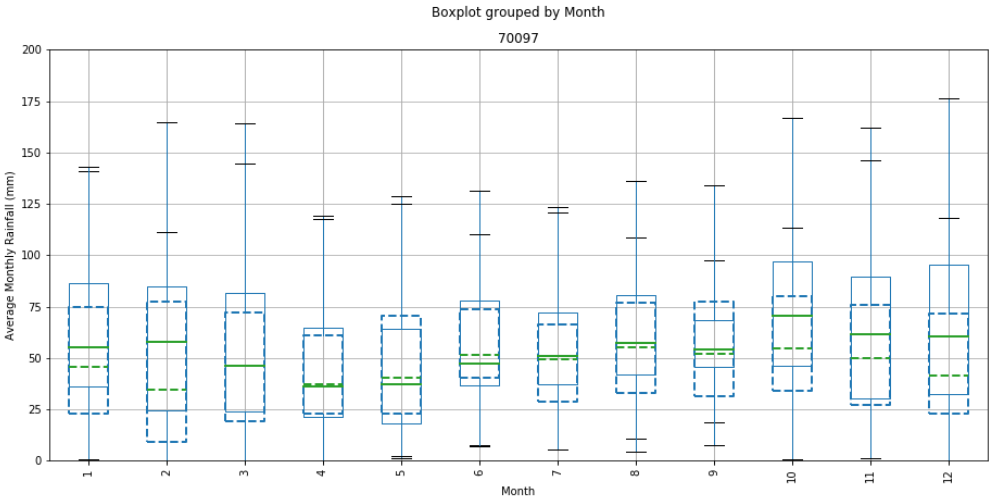
Boxplot grouped by Month
70097
Average Monthly Rainfall (mm)
Month

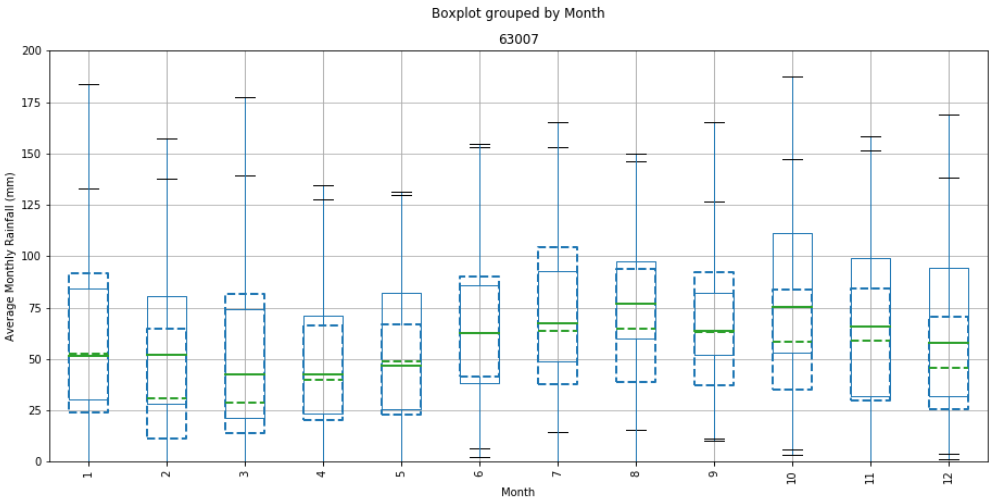
Boxplot grouped by Month
63007
Average Monthly Rainfall (mm)
Month

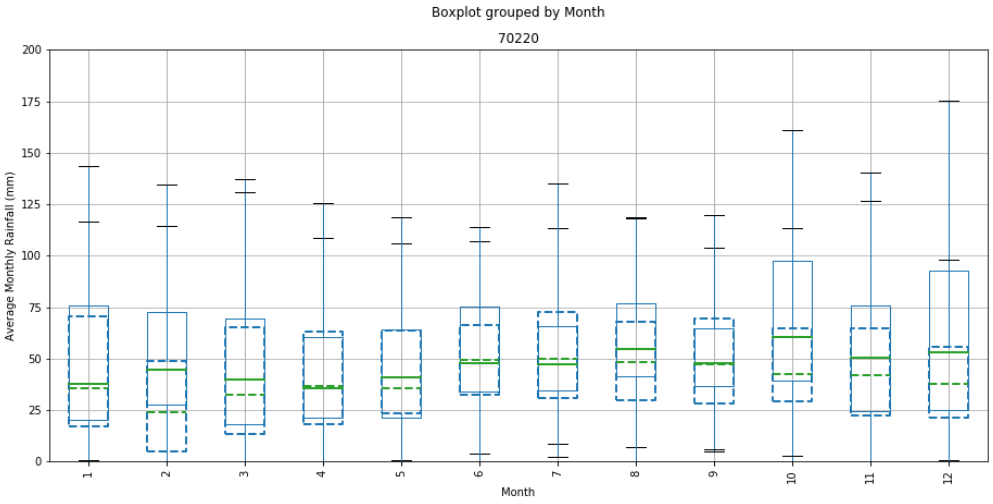
Boxplot grouped by Month
70220
Average Monthly Rainfall (mm)
Month

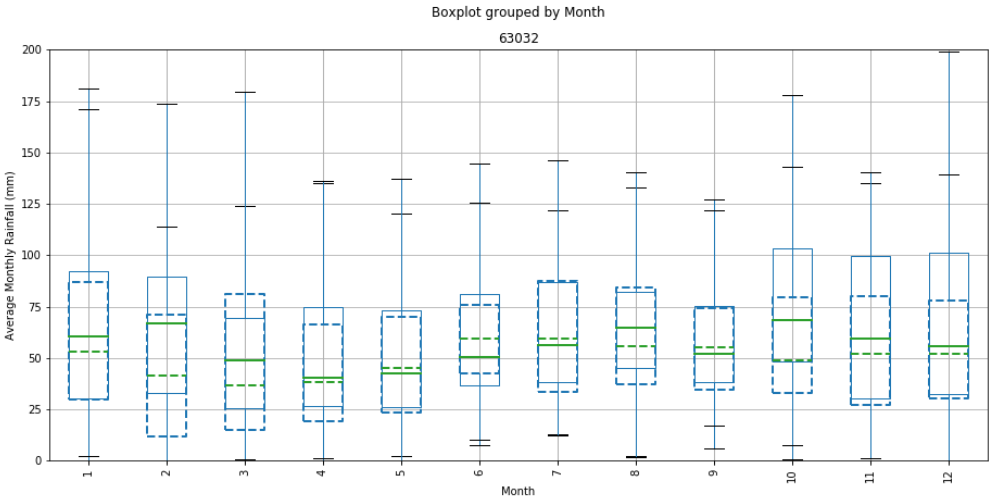
Boxplot grouped by Month
63032
Average Monthly Rainfall (mm)
Month

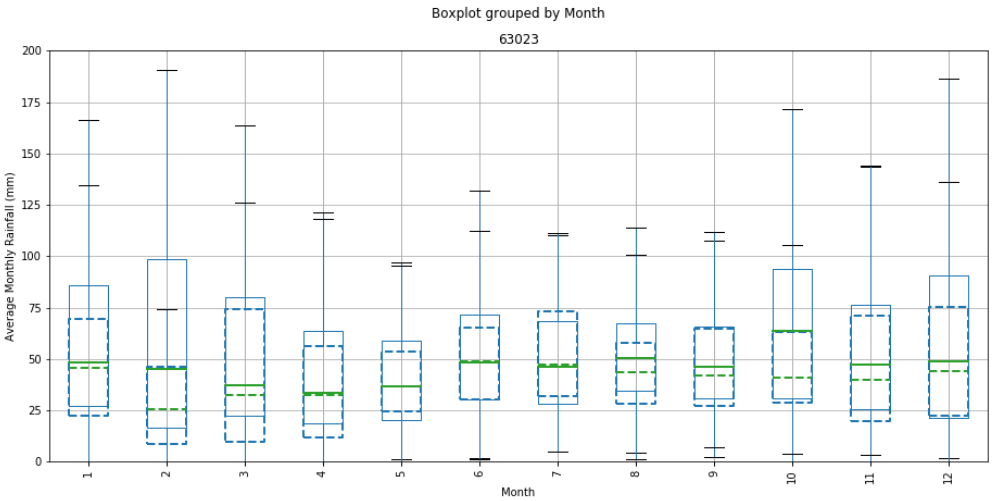
Boxplot grouped by Month
63023
Average Monthly Rainfall (mm)
Month

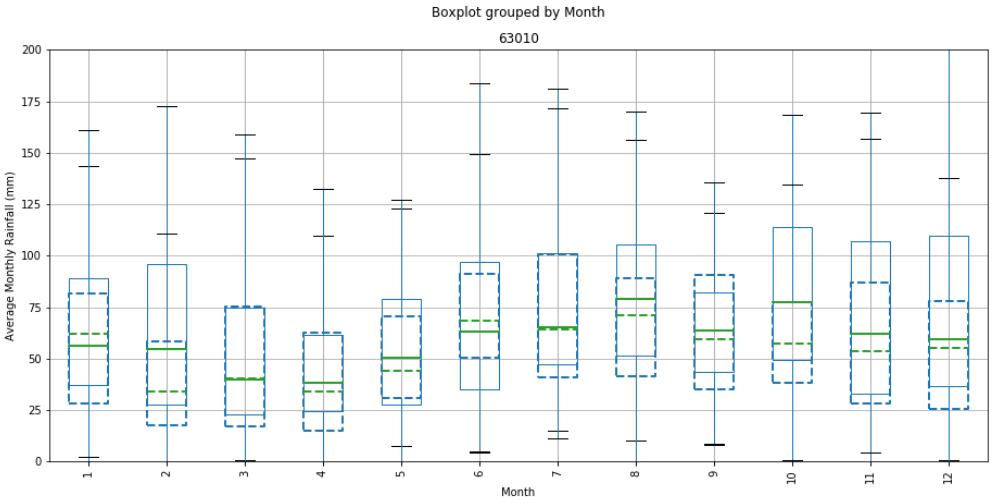
Boxplot grouped by Month
63010
Average Monthly Rainfall (mm)
Month

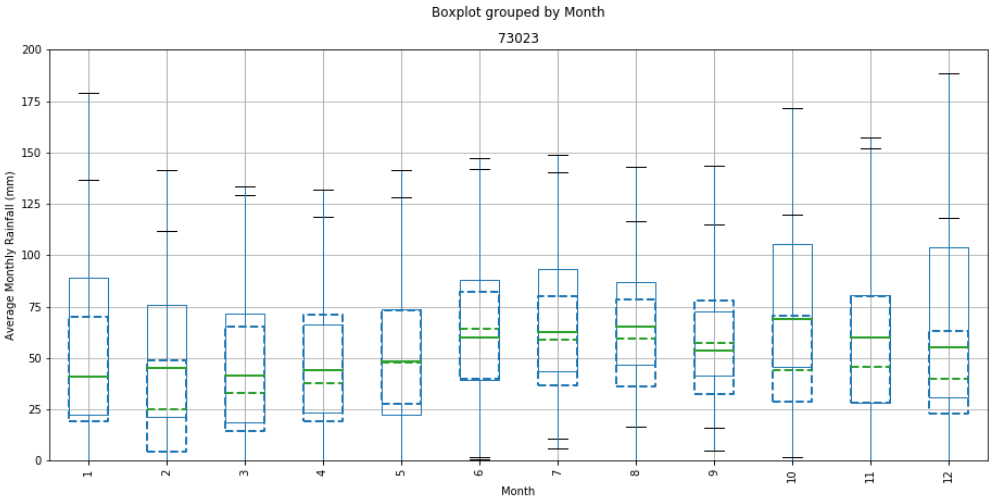
Boxplot grouped by Month
73023
Average Monthly Rainfall (mm)
Month

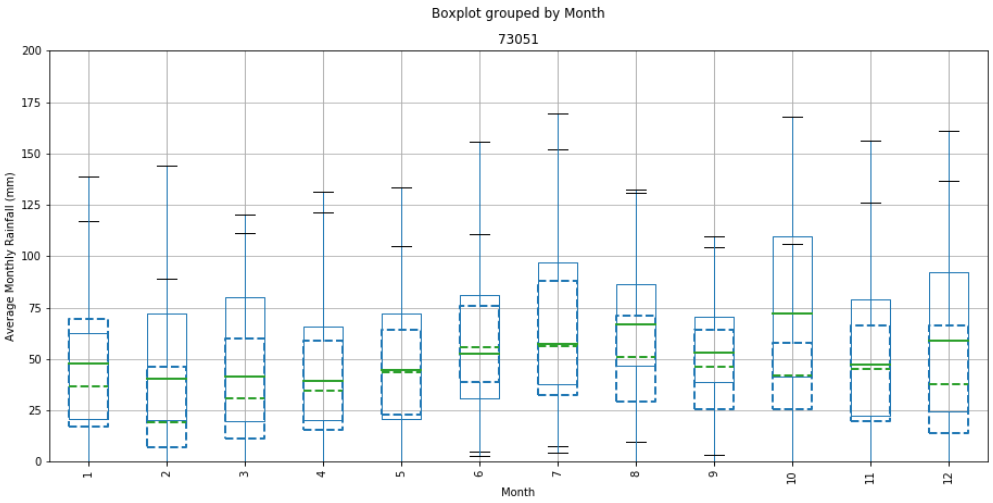
Boxplot grouped by Month
73051
Average Monthly Rainfall (mm)
Month

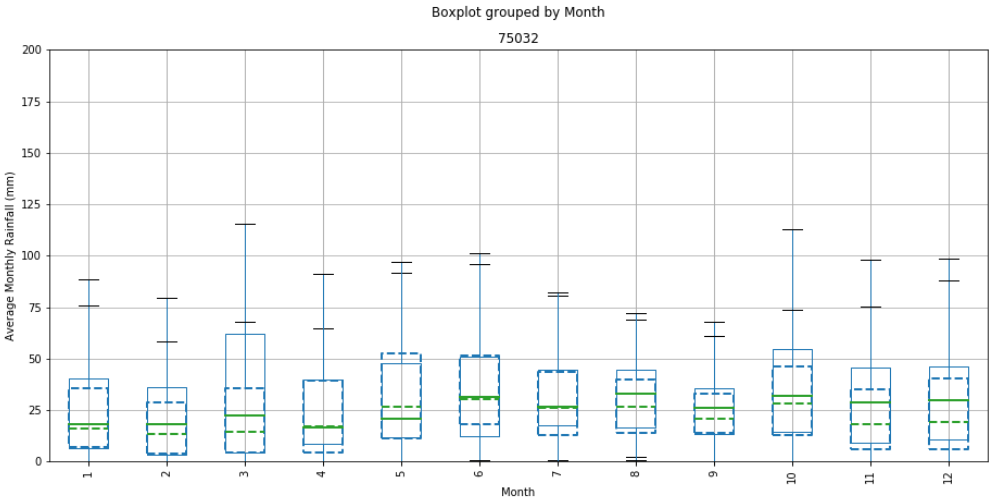
Boxplot grouped by Month
75032
Average Monthly Rainfall (mm)
Month

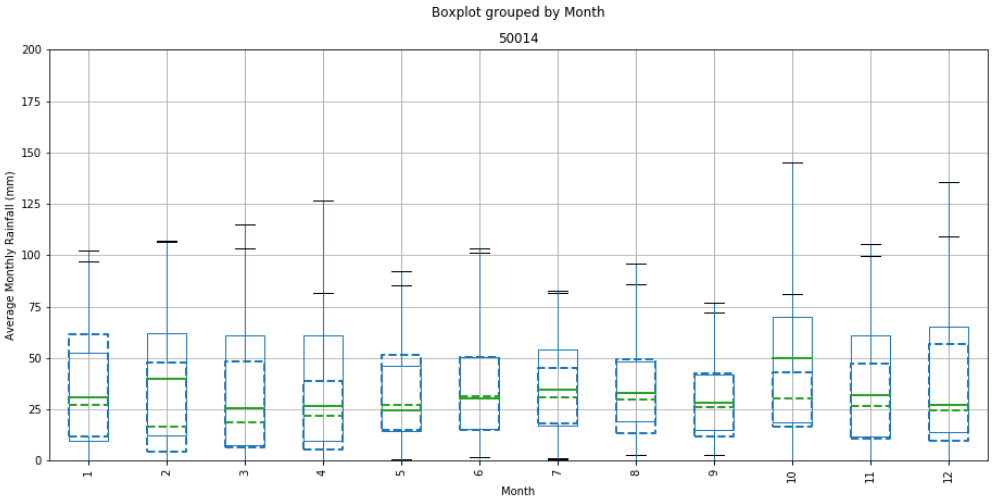
Boxplot grouped by Month
50014
Average Monthly Rainfall (mm)
Month

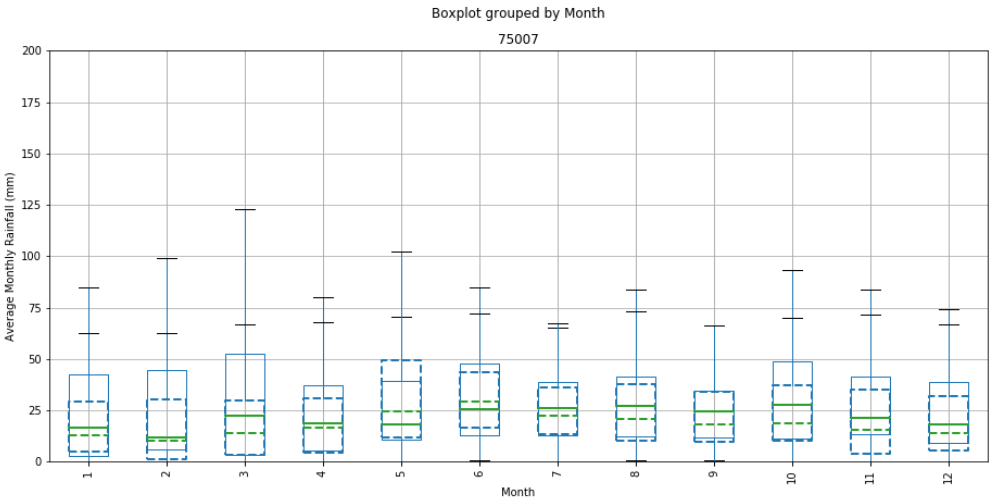
Boxplot grouped by Month
75007
Average Monthly Rainfall (mm)
Month

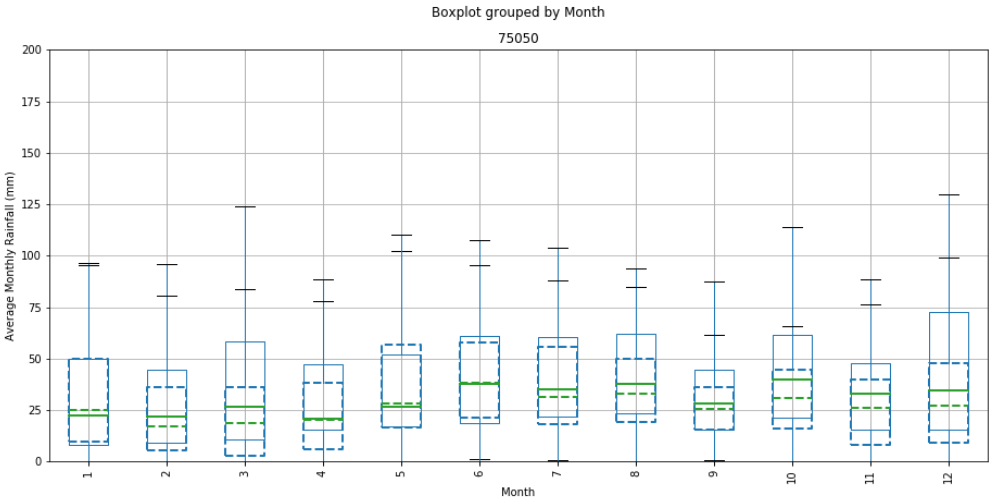
Boxplot grouped by Month
75050
Average Monthly Rainfall (mm)
Month

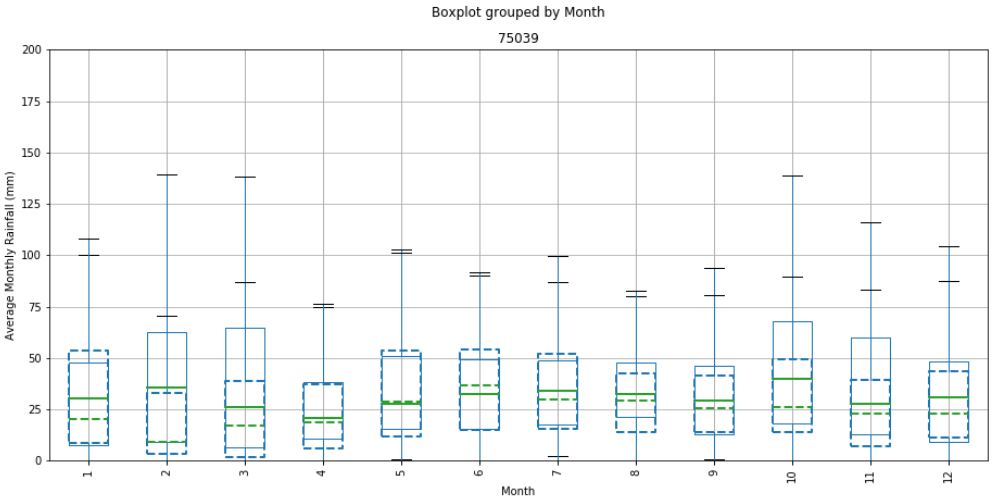
Boxplot grouped by Month
75039
Average Monthly Rainfall (mm)
Month

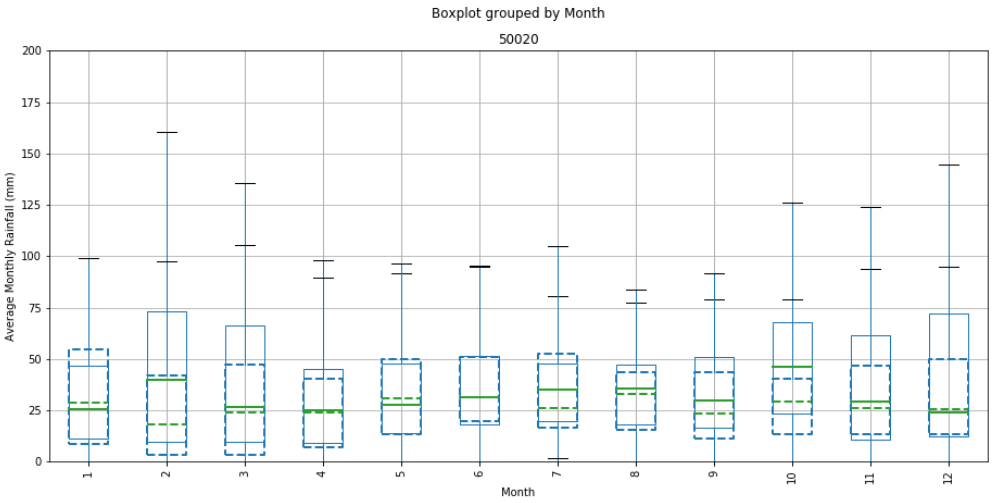
Boxplot grouped by Month
50020
Average Monthly Rainfall (mm)
Month

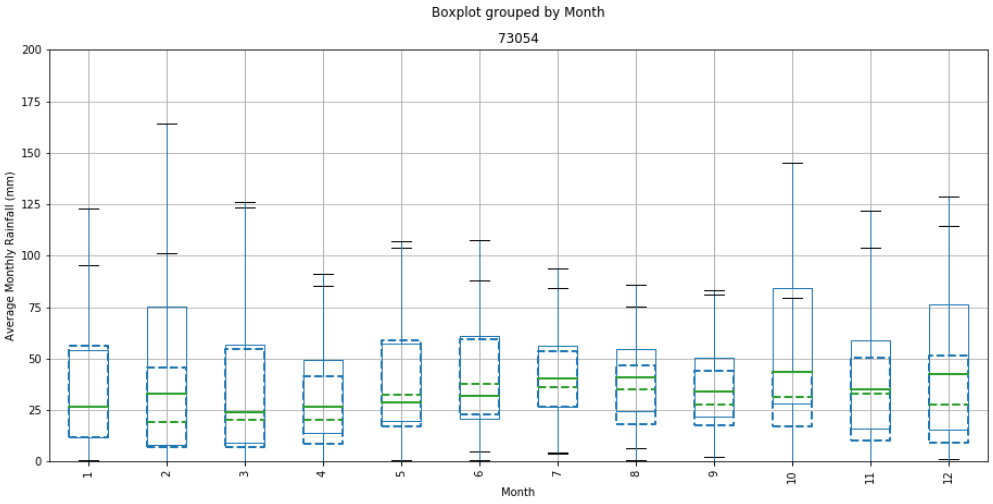
Boxplot grouped by Month
73054
Average Monthly Rainfall (mm)
Month

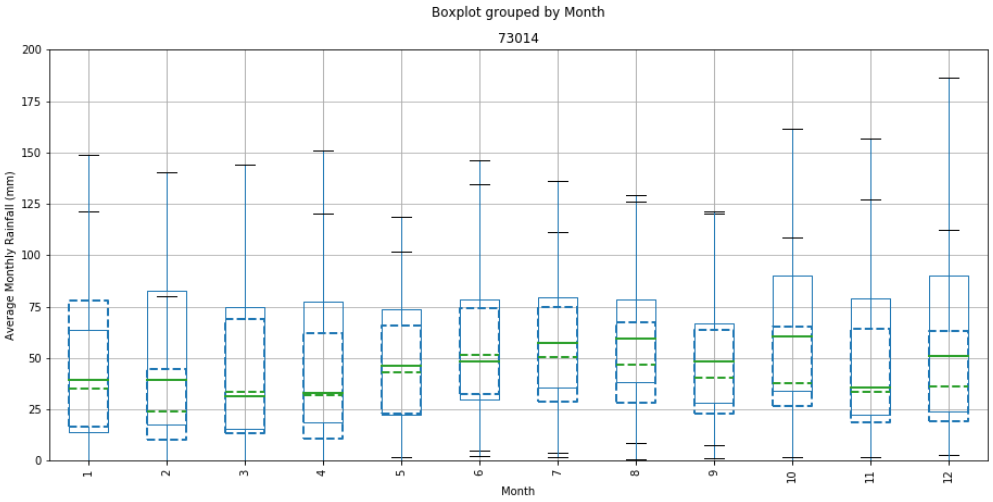
Boxplot grouped by Month
73014
Average Monthly Rainfall (mm)
Month

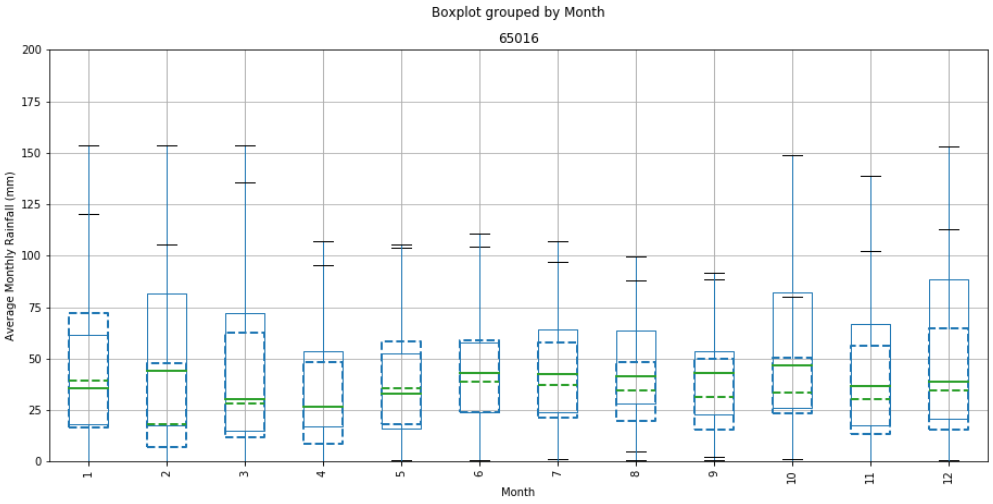
Boxplot grouped by Month
65016
Average Monthly Rainfall (mm)
Month

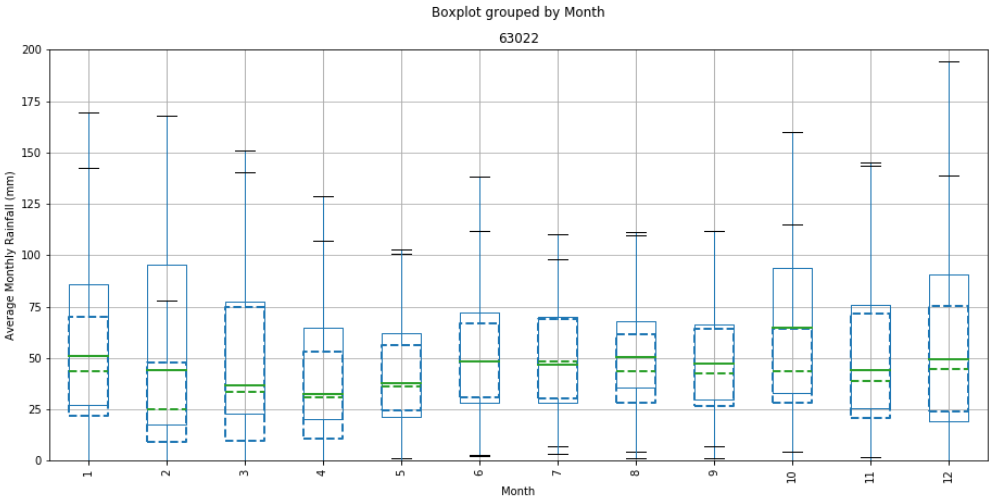
Boxplot grouped by Month
63022
Average Monthly Rainfall (mm)
Month

Appendix C – Box plots of monthly stochastic (dashed) and instrumental (solid) rainfall after post processing the autumn rainfall for all 50 stations

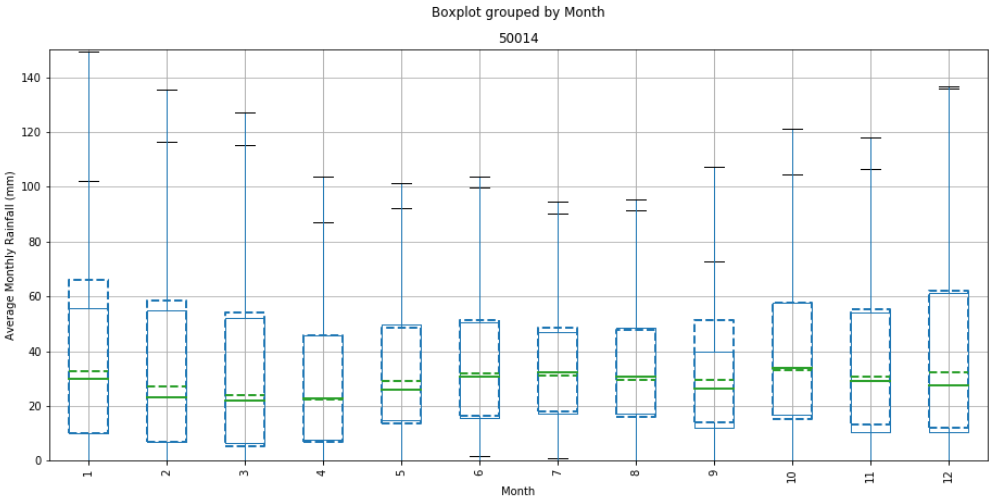

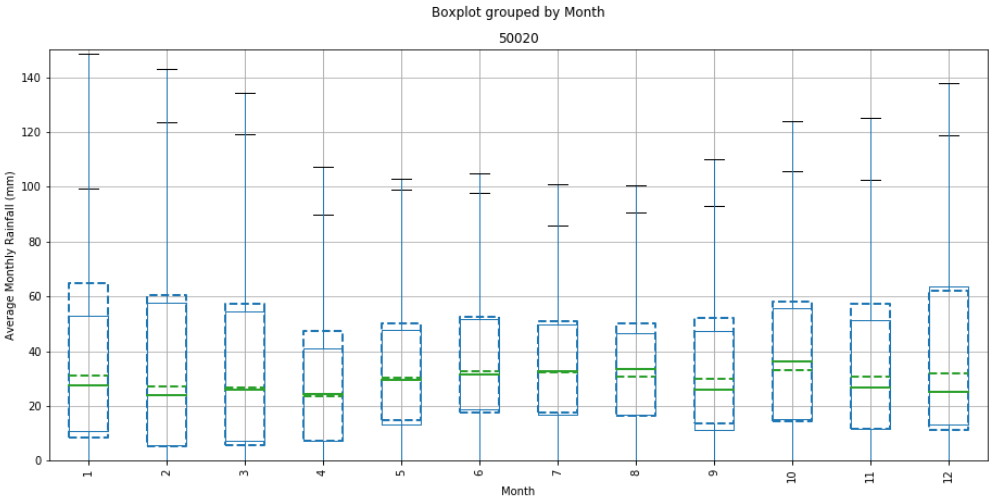

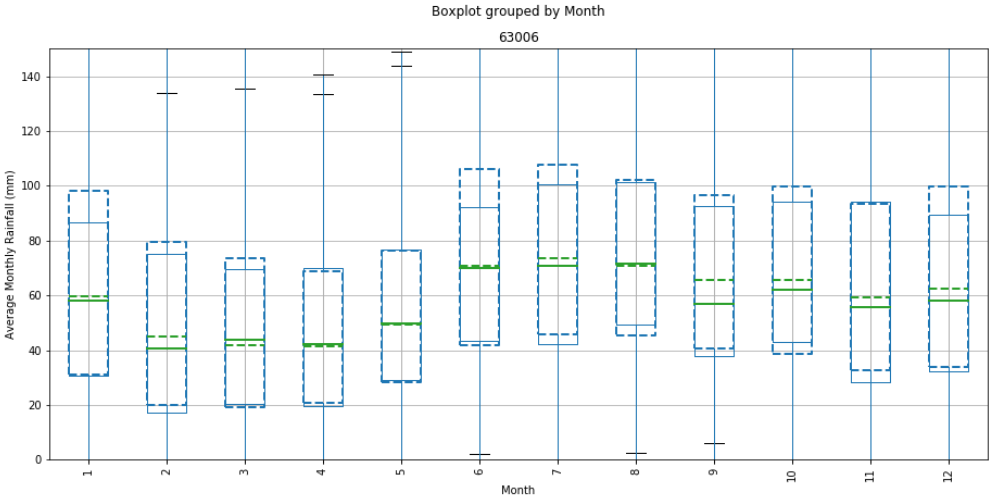

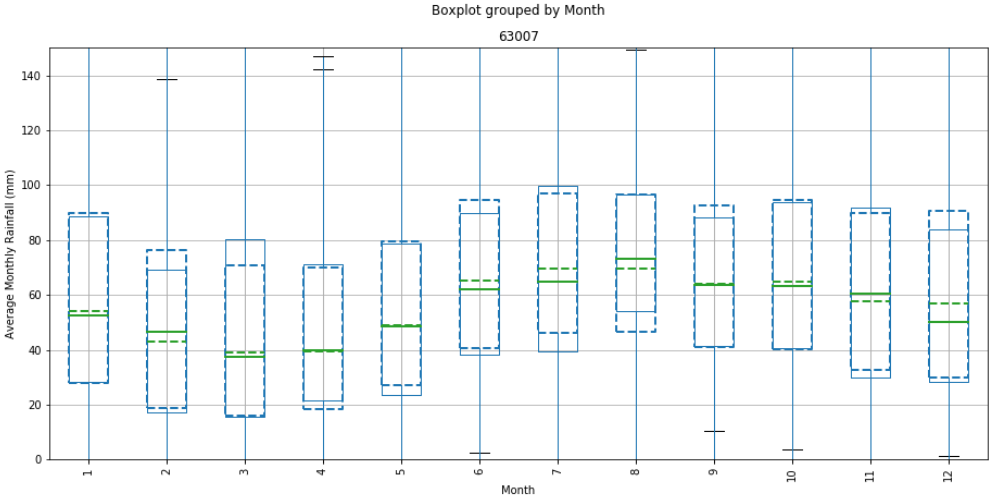
Boxplot grouped by Month
63007
Average Monthly Rainfall (mm)
Month

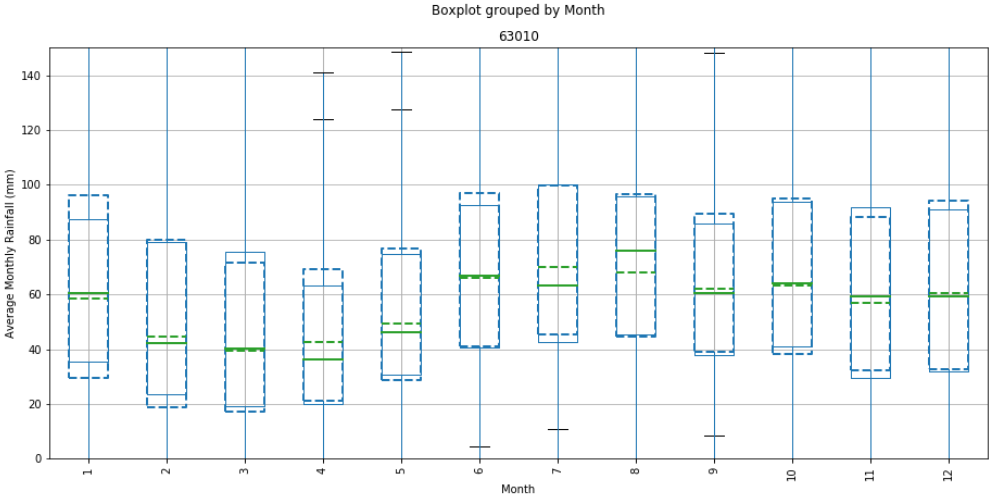
Boxplot grouped by Month
63010
Average Monthly Rainfall (mm)
Month

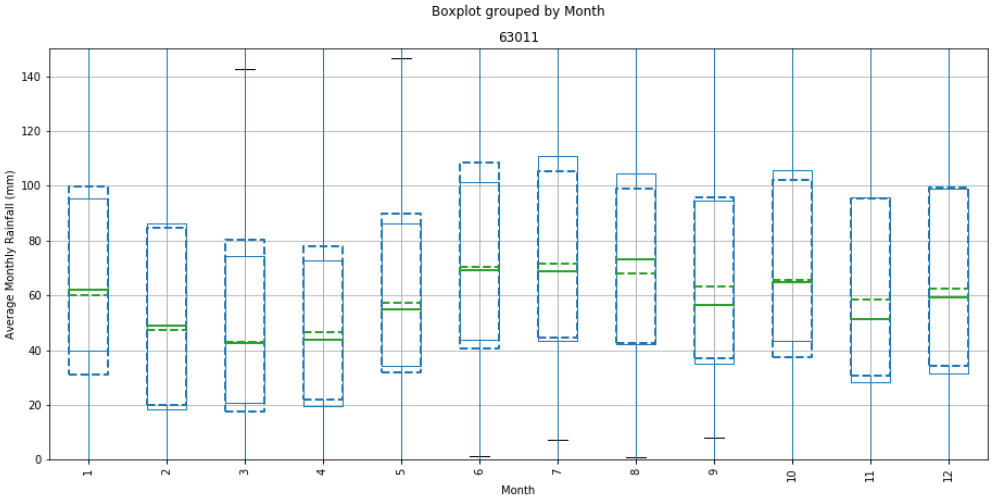
Boxplot grouped by Month
63011
Average Monthly Rainfall (mm)
Month

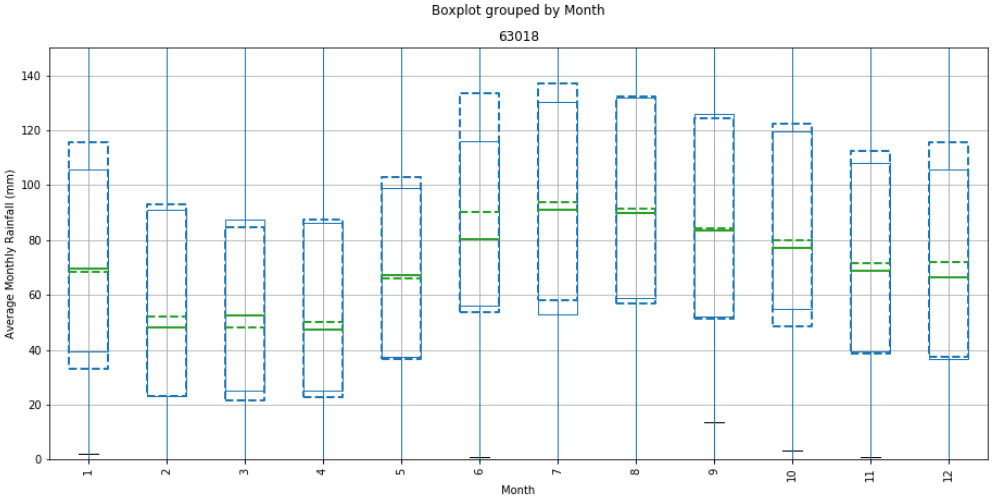
Boxplot grouped by Month
63018
Average Monthly Rainfall (mm)
Month

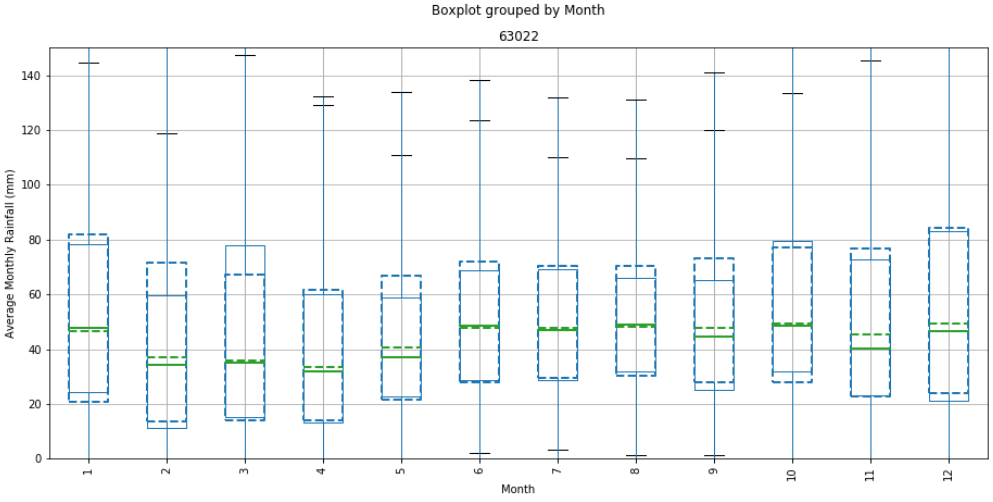
Boxplot grouped by Month
63022
Average Monthly Rainfall (mm)
Month

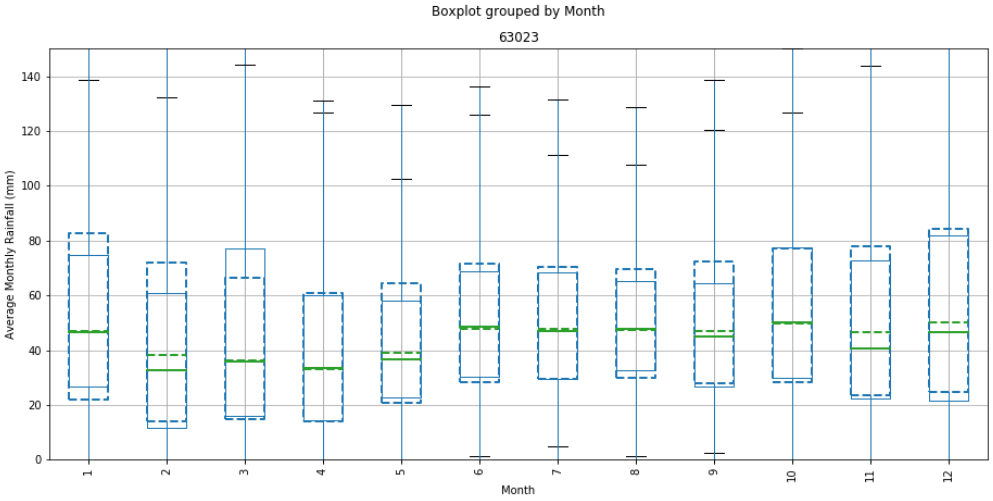
Boxplot grouped by Month
63023
Average Monthly Rainfall (mm)
Month

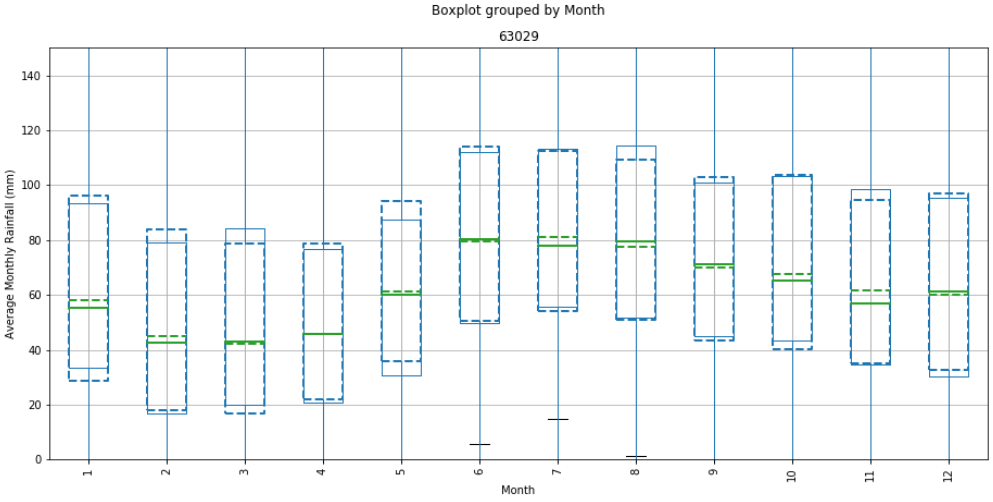
Boxplot grouped by Month
63029
Average Monthly Rainfall (mm)
Month

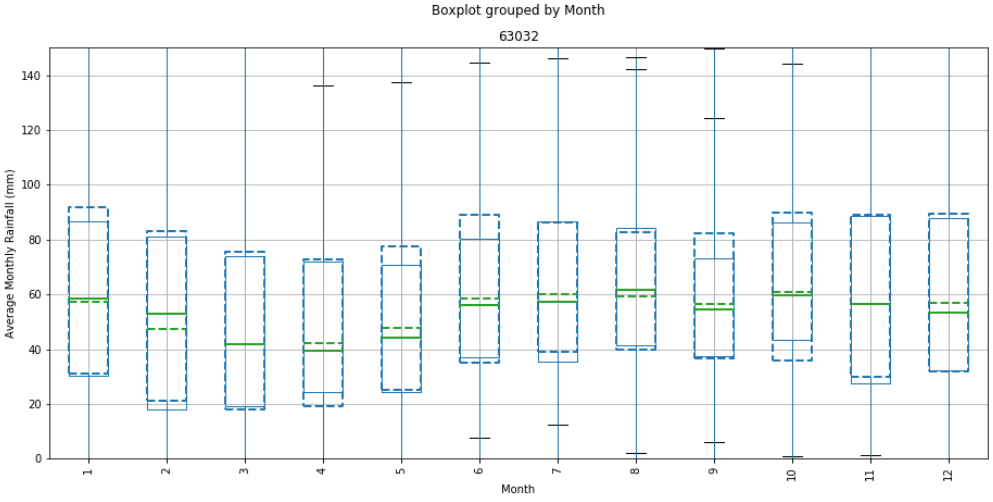
Boxplot grouped by Month
63032
Average Monthly Rainfall (mm)
Month

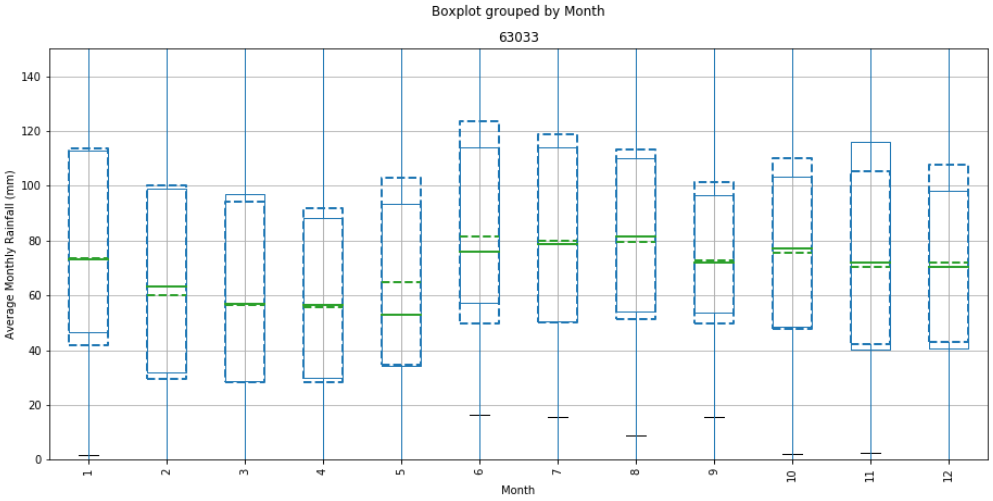
Boxplot grouped by Month
63033
Average Monthly Rainfall (mm)
Month

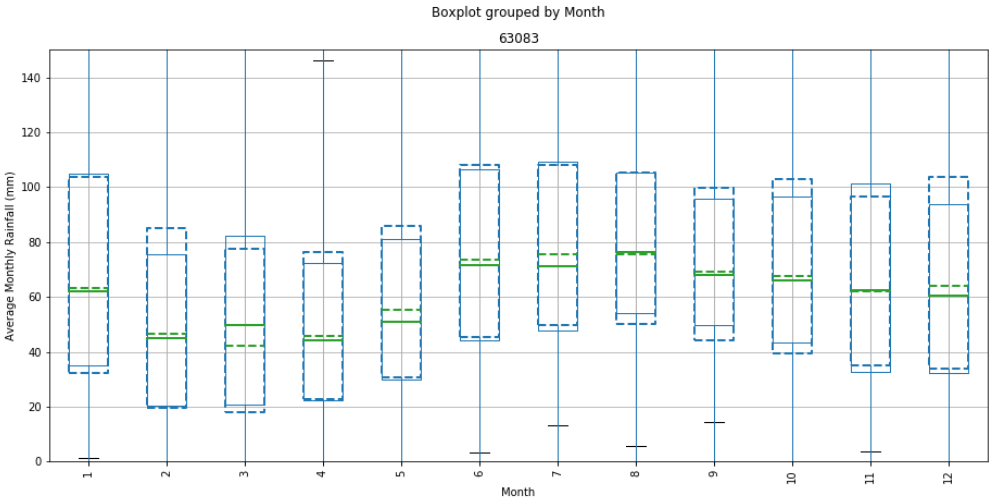
Boxplot grouped by Month
63083
Average Monthly Rainfall (mm)
Month

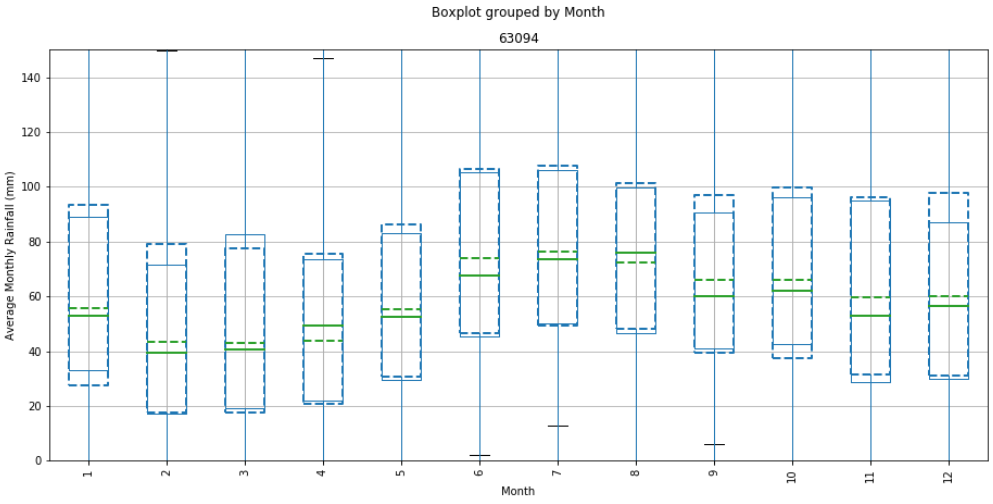
Boxplot grouped by Month
63094
Average Monthly Rainfall (mm)
Month

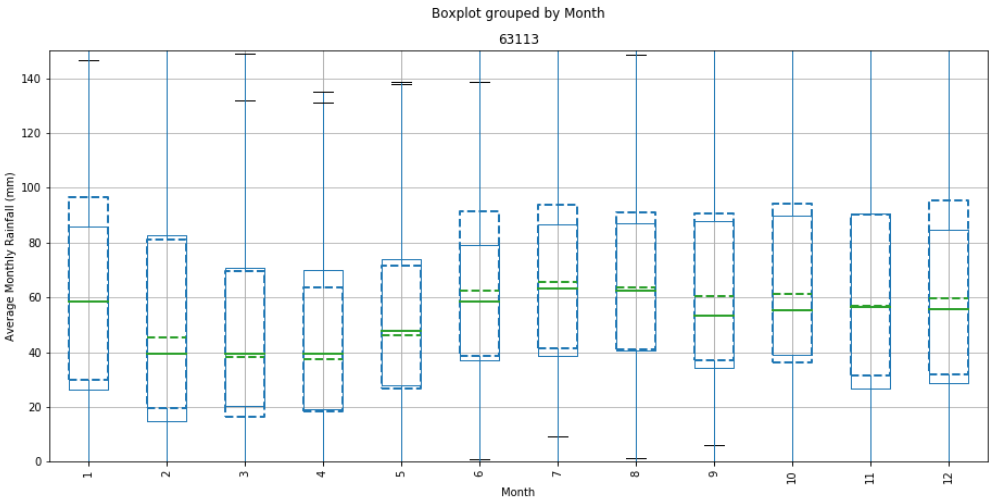
Boxplot grouped by Month
63113
Average Monthly Rainfall (mm)
Month

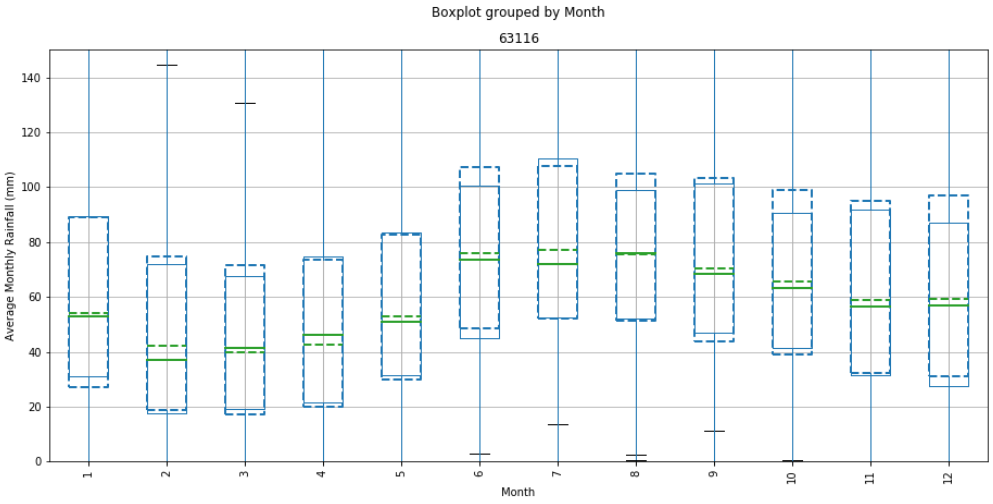
Boxplot grouped by Month
63116
Average Monthly Rainfall (mm)
Month

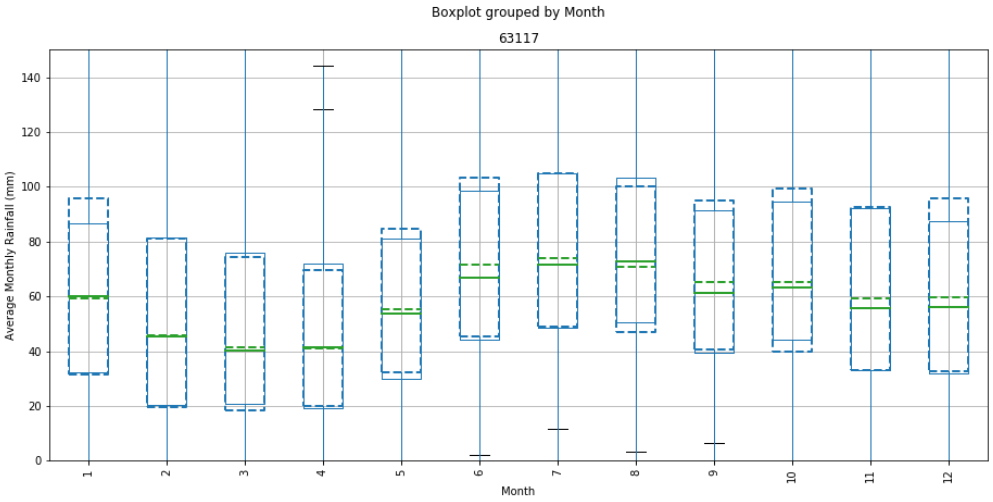
Boxplot grouped by Month
63117
Average Monthly Rainfall (mm)
Month

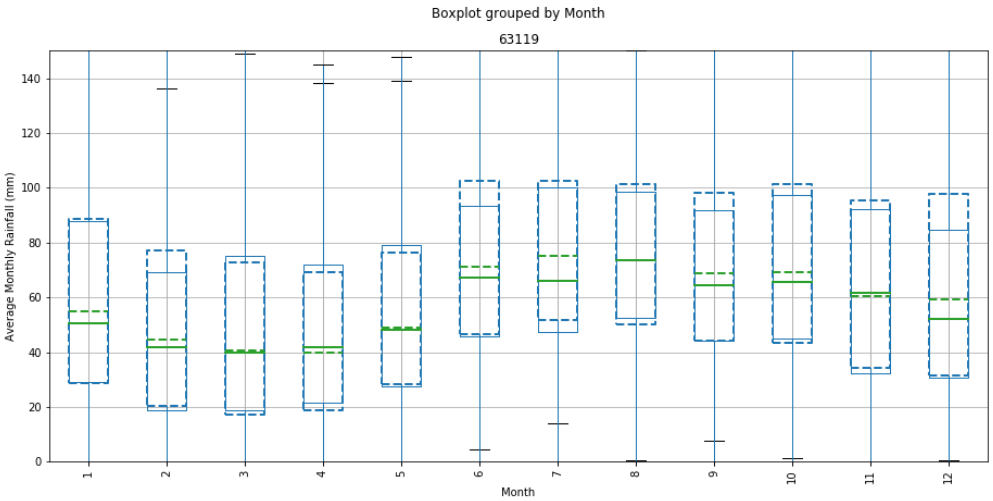
Boxplot grouped by Month
63119
Average Monthly Rainfall (mm)
Month

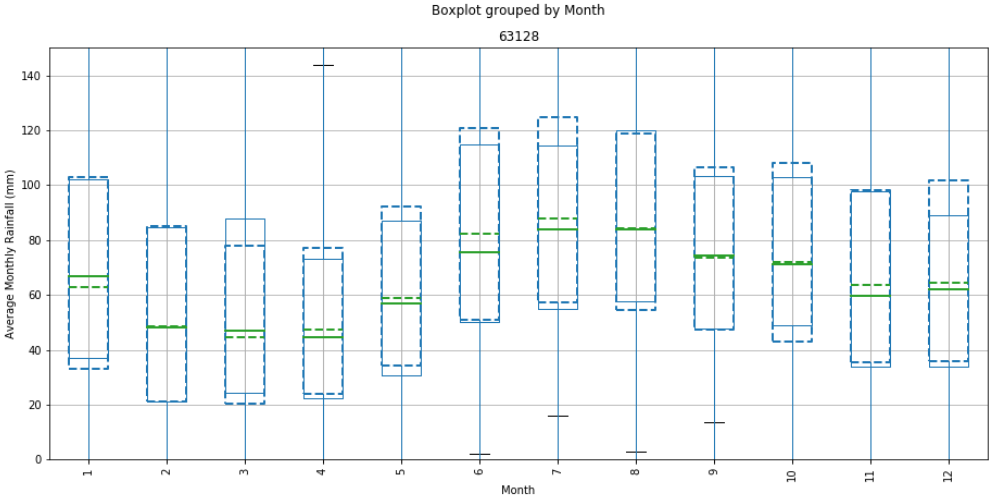
Boxplot grouped by Month
63128
Average Monthly Rainfall (mm)
Month

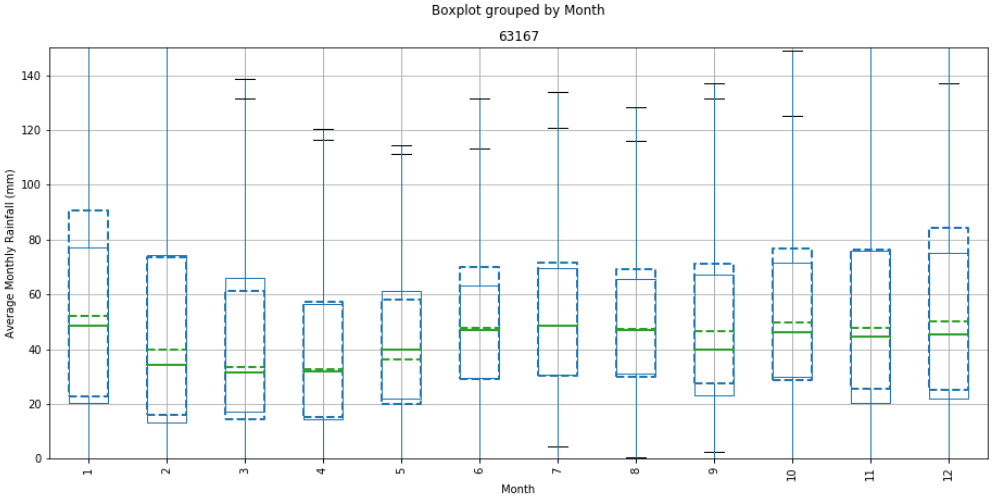
Boxplot grouped by Month
63167
Average Monthly Rainfall (mm)
Month

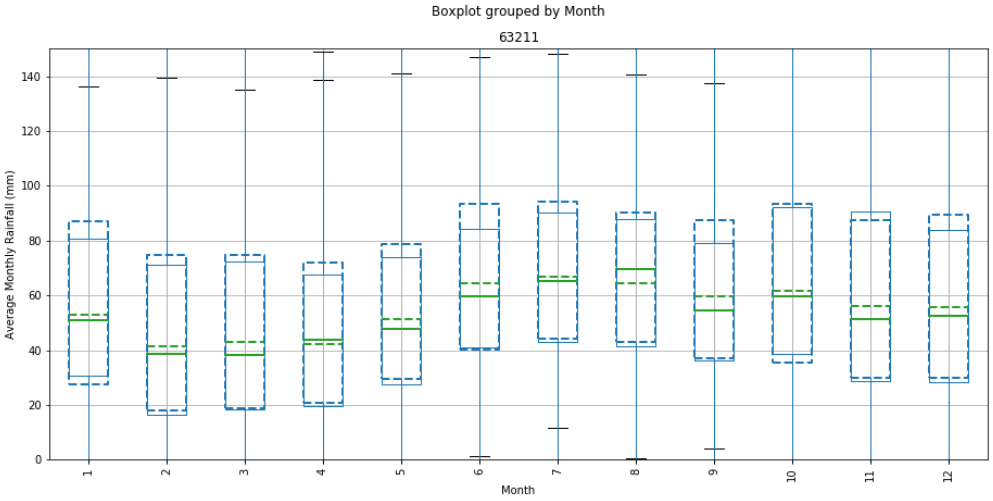
Boxplot grouped by Month
63211
Average Monthly Rainfall (mm)
Month

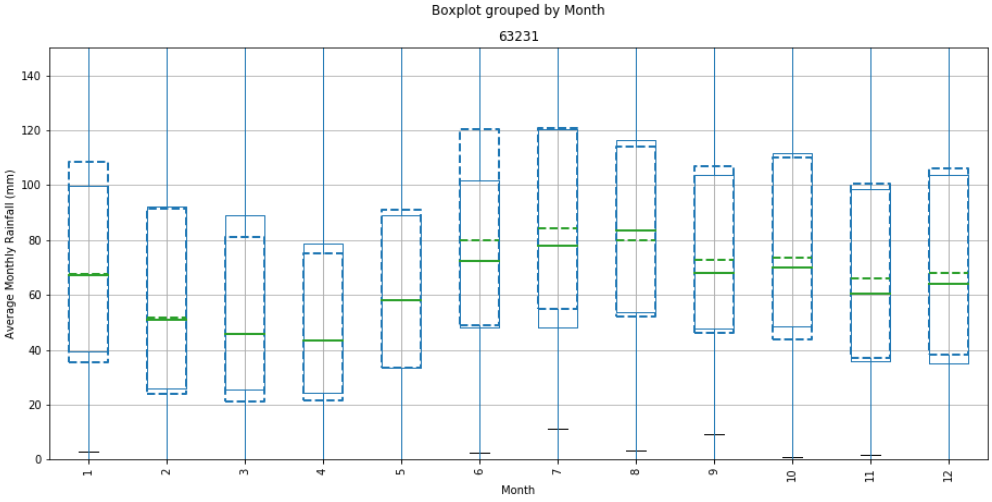
Boxplot grouped by Month
63231
Average Monthly Rainfall (mm)
Month

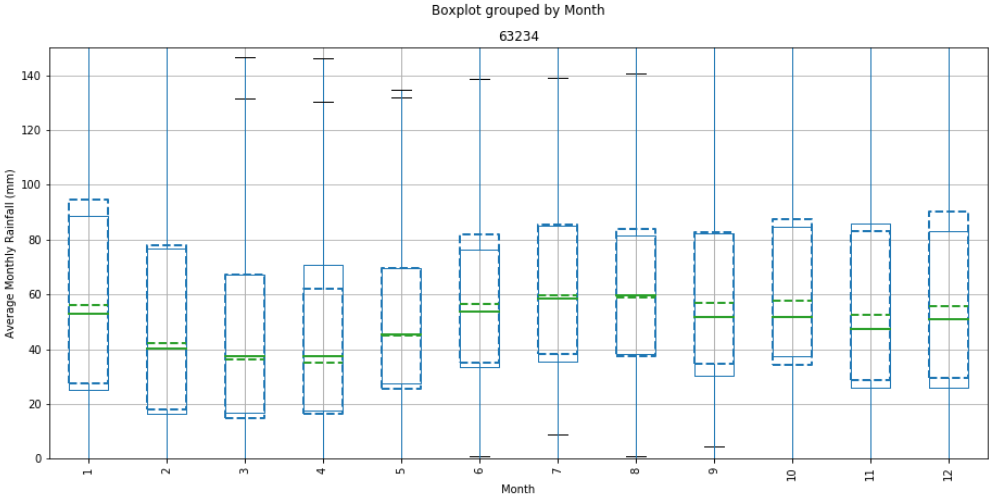
Boxplot grouped by Month
63234
Average Monthly Rainfall (mm)
Month

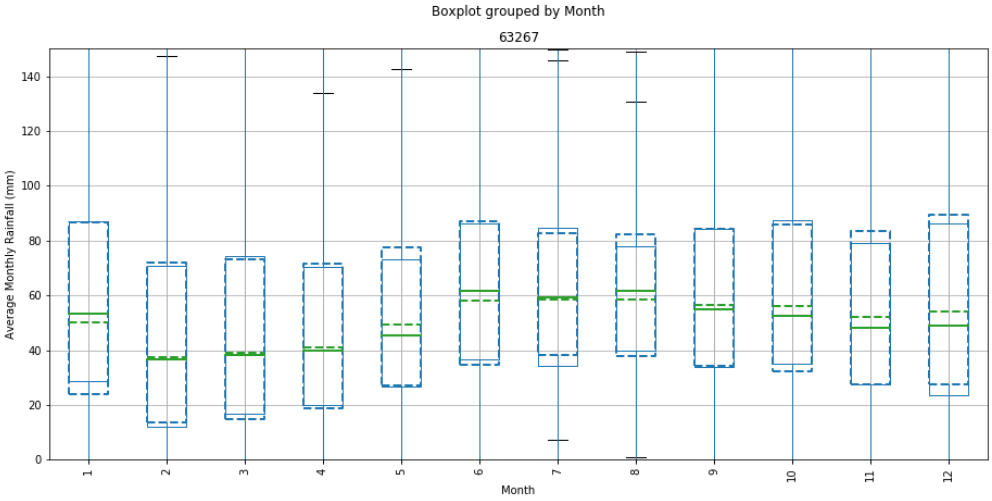
Boxplot grouped by Month
63267
Average Monthly Rainfall (mm)
Month

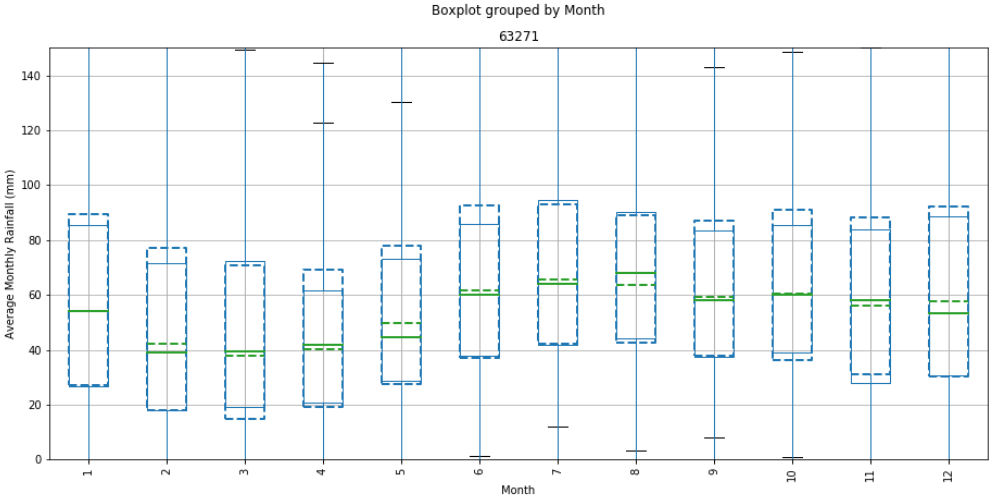
Boxplot grouped by Month
63271
Average Monthly Rainfall (mm)
Month

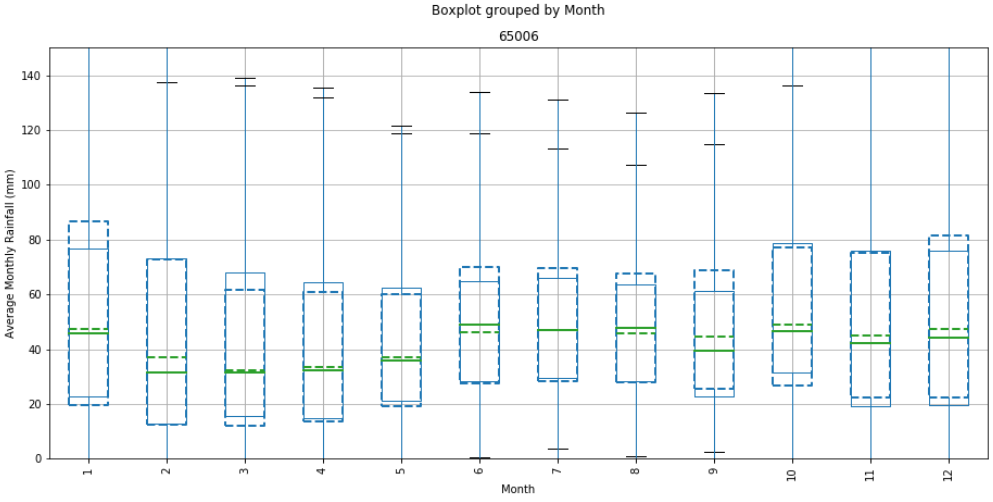
Boxplot grouped by Month
65006
Average Monthly Rainfall (mm)
Month

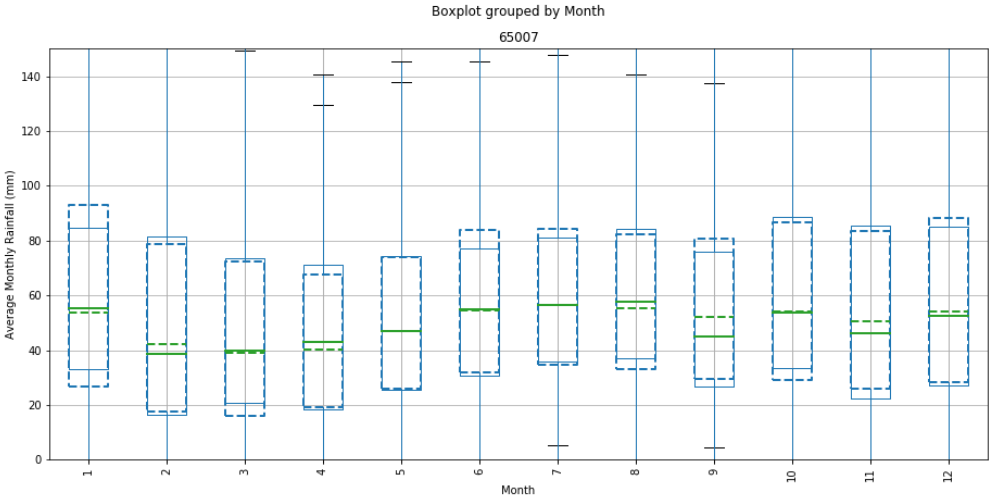
Boxplot grouped by Month
65007
Average Monthly Rainfall (mm)
Month

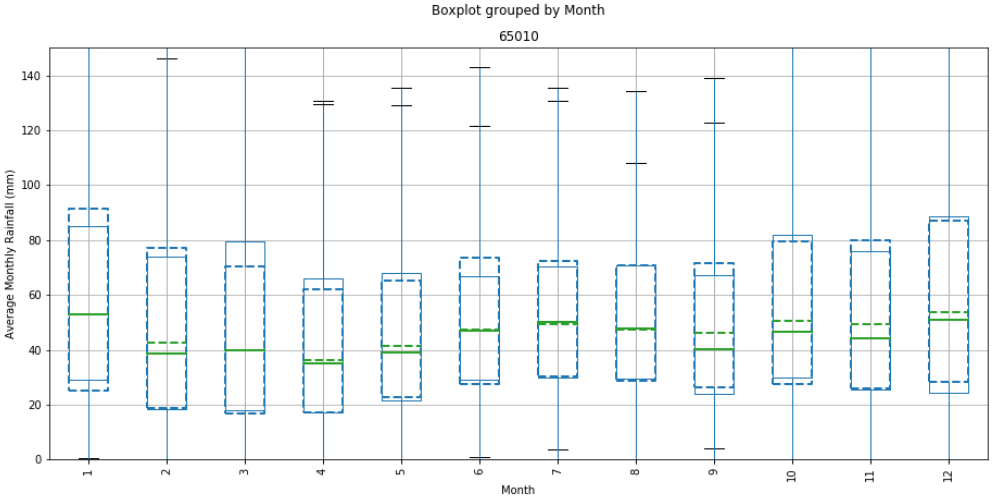
Boxplot grouped by Month
65010
Average Monthly Rainfall (mm)
Month

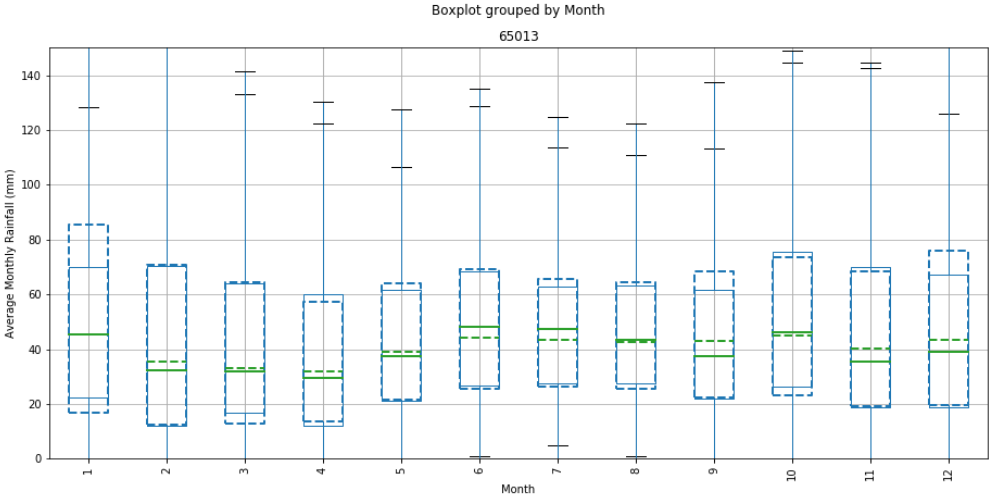
Boxplot grouped by Month
65013
Average Monthly Rainfall (mm)
Month

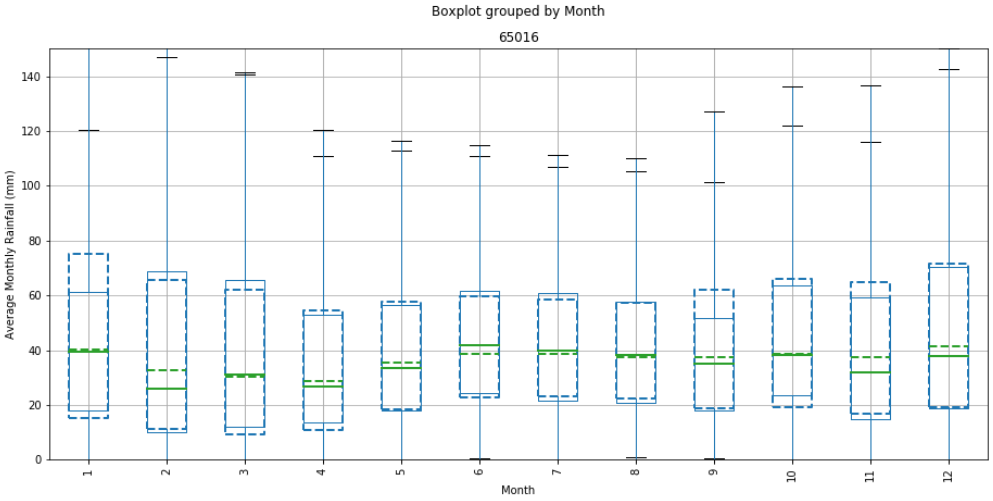
Boxplot grouped by Month
65016
Average Monthly Rainfall (mm)
Month

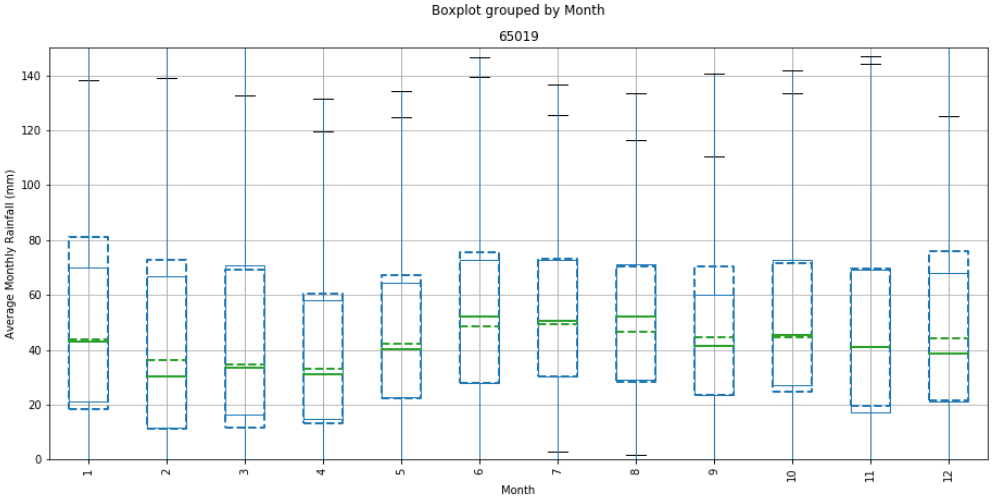
Boxplot grouped by Month
65019
Average Monthly Rainfall (mm)
Month

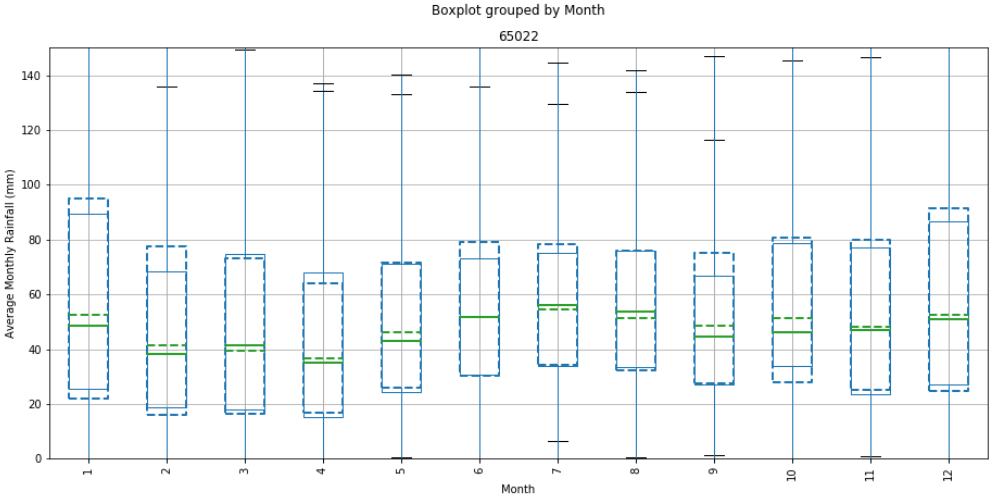
Boxplot grouped by Month
65022
Average Monthly Rainfall (mm)
Month

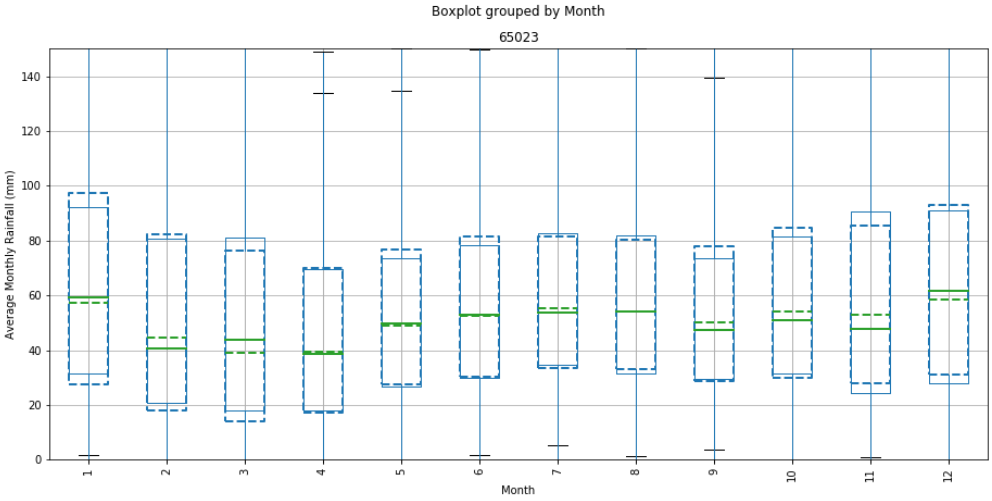
Boxplot grouped by Month
65023
Average Monthly Rainfall (mm)
Month

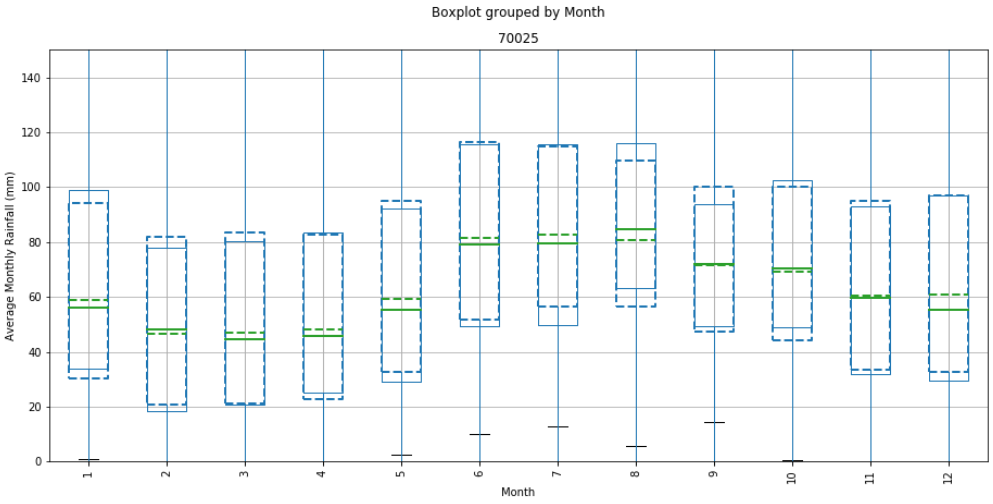
Boxplot grouped by Month
70025
Average Monthly Rainfall (mm)
Month

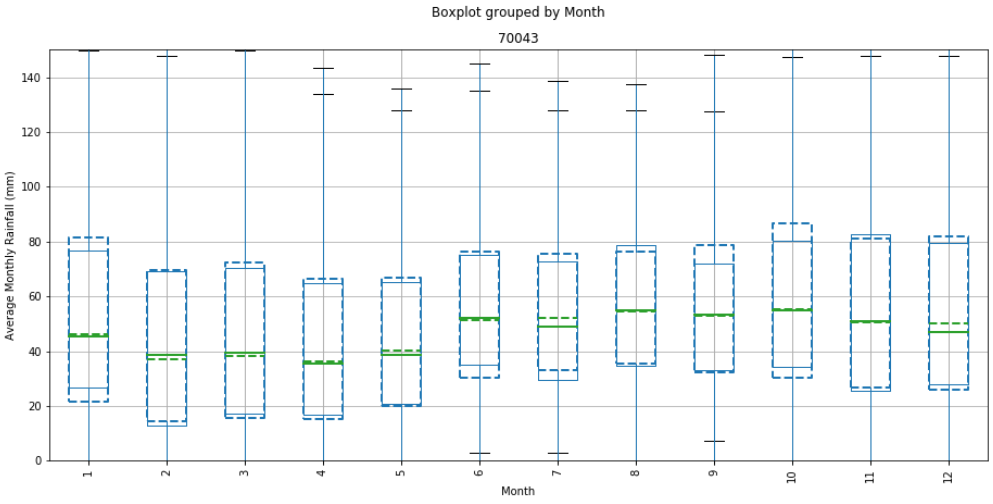
Boxplot grouped by Month
70043
Average Monthly Rainfall (mm)
Month

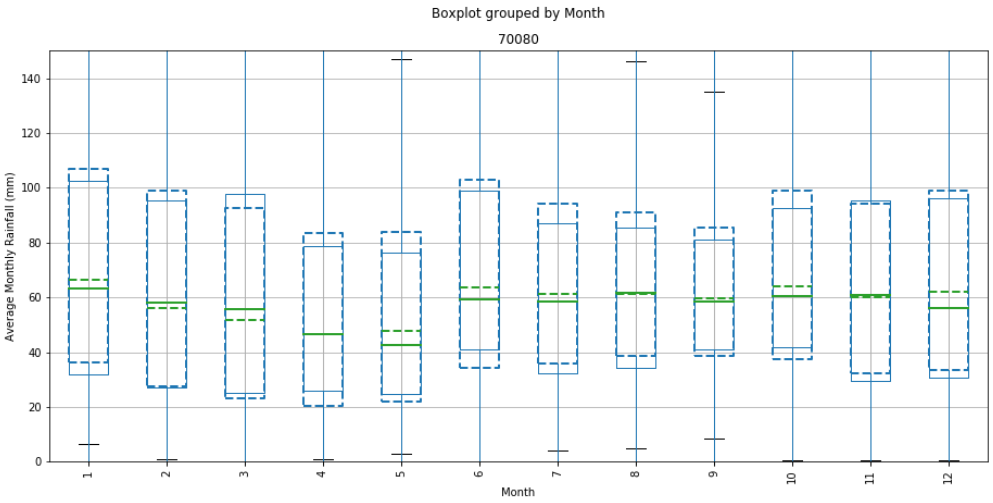
Boxplot grouped by Month
70080
Average Monthly Rainfall (mm)
Month

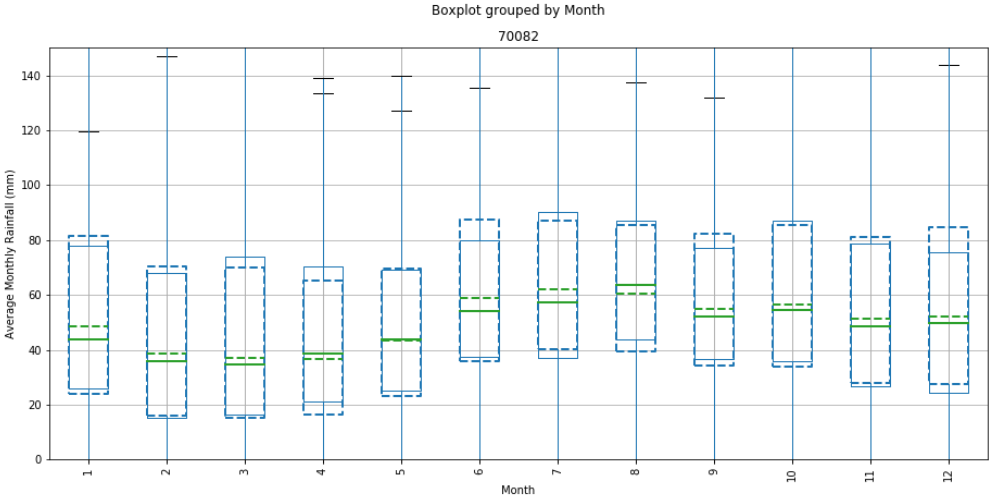
Boxplot grouped by Month
70082
Average Monthly Rainfall (mm)
Month

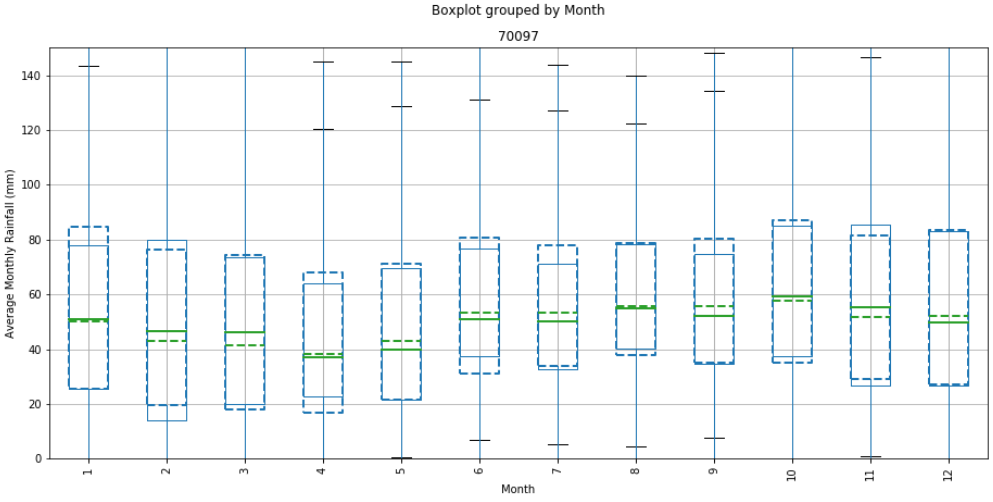
Boxplot grouped by Month
70097
Average Monthly Rainfall (mm)
Month

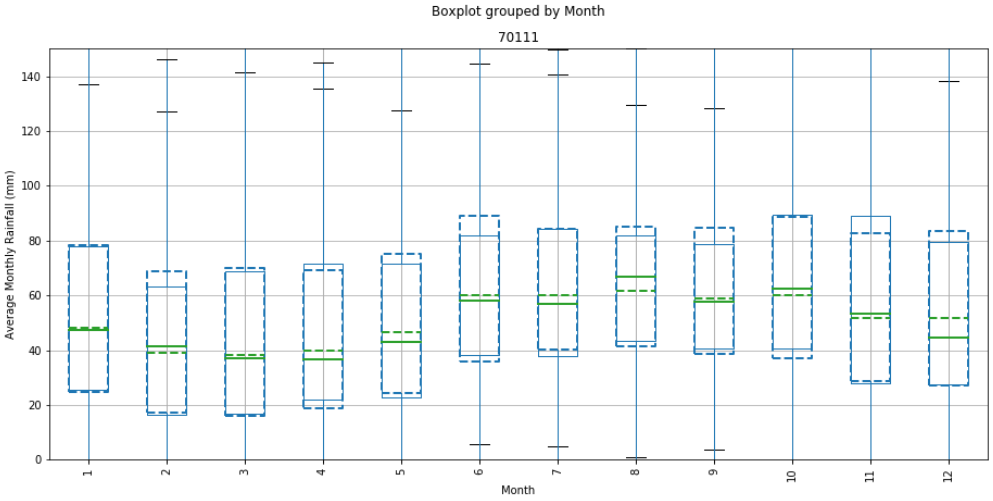
Boxplot grouped by Month
70111
Average Monthly Rainfall (mm)
Month

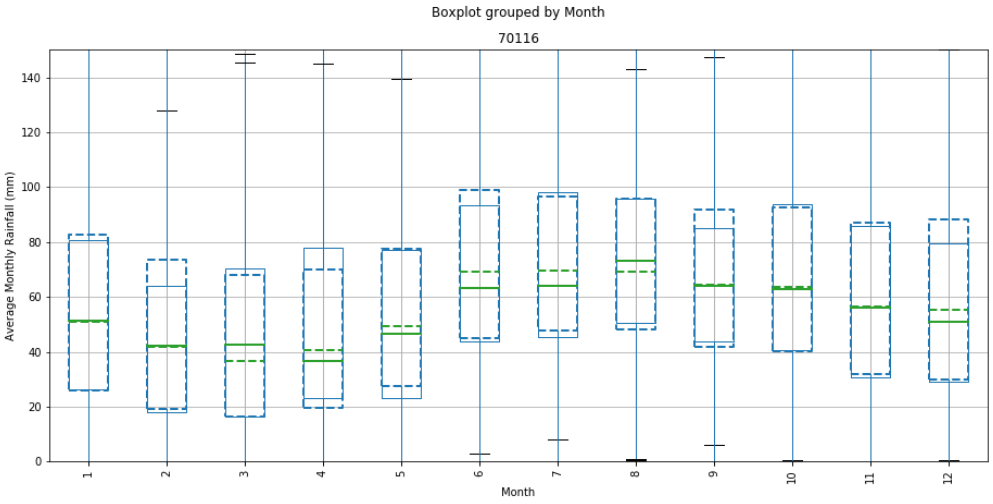
Boxplot grouped by Month
70116
Average Monthly Rainfall (mm)
Month

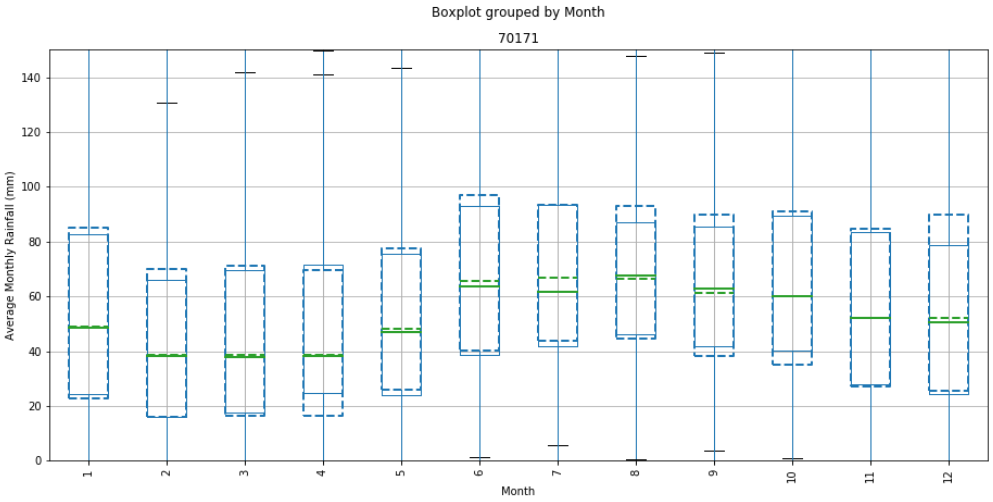
Boxplot grouped by Month
70171
Average Monthly Rainfall (mm)
Month

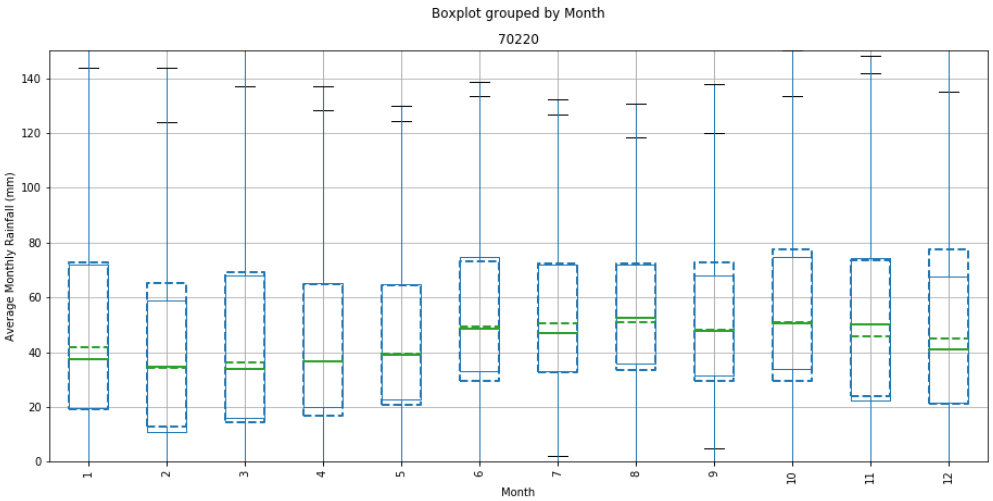
Boxplot grouped by Month
70220
Average Monthly Rainfall (mm)
Month

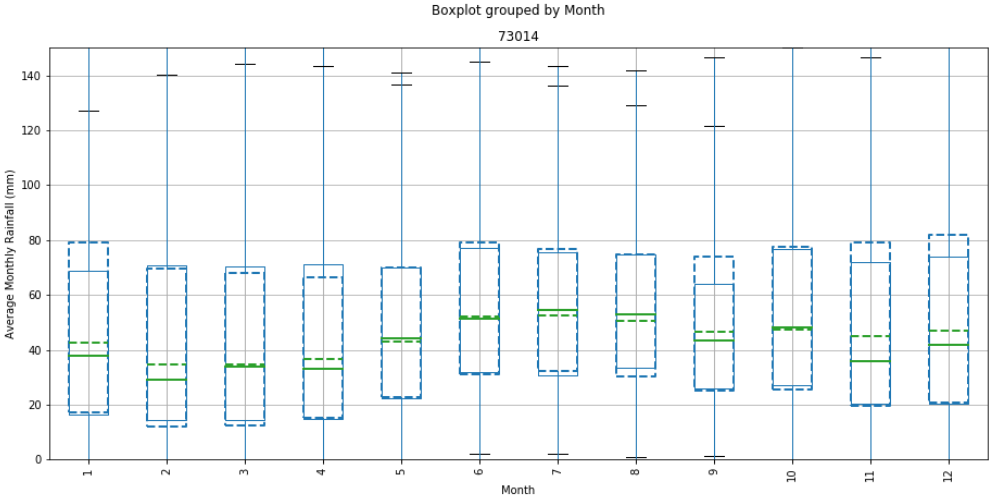
Boxplot grouped by Month
73014
Average Monthly Rainfall (mm)
Month

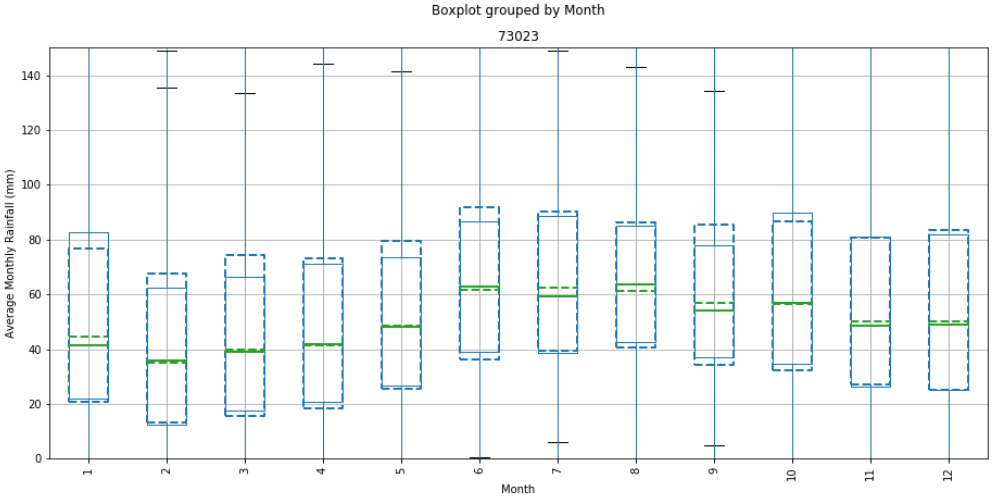
Boxplot grouped by Month
73023
Average Monthly Rainfall (mm)
Month

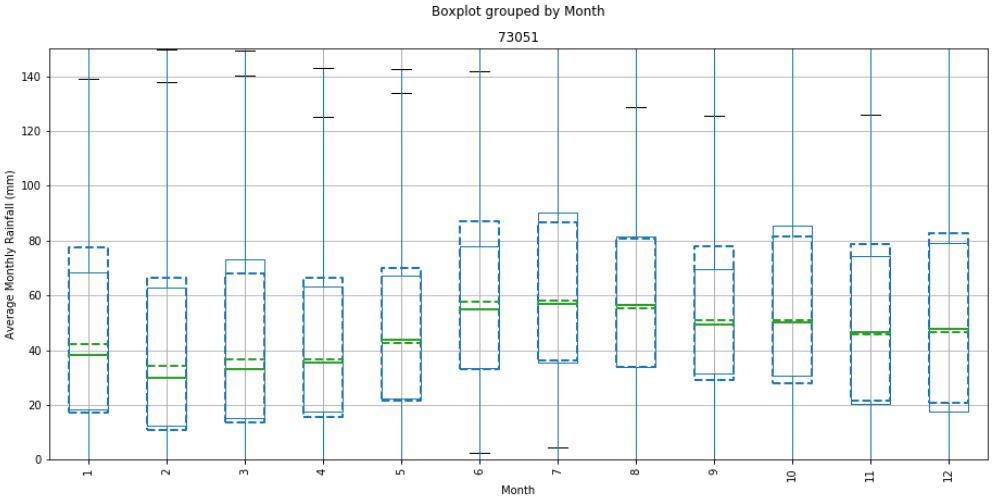
Boxplot grouped by Month
73051
Average Monthly Rainfall (mm)
Month

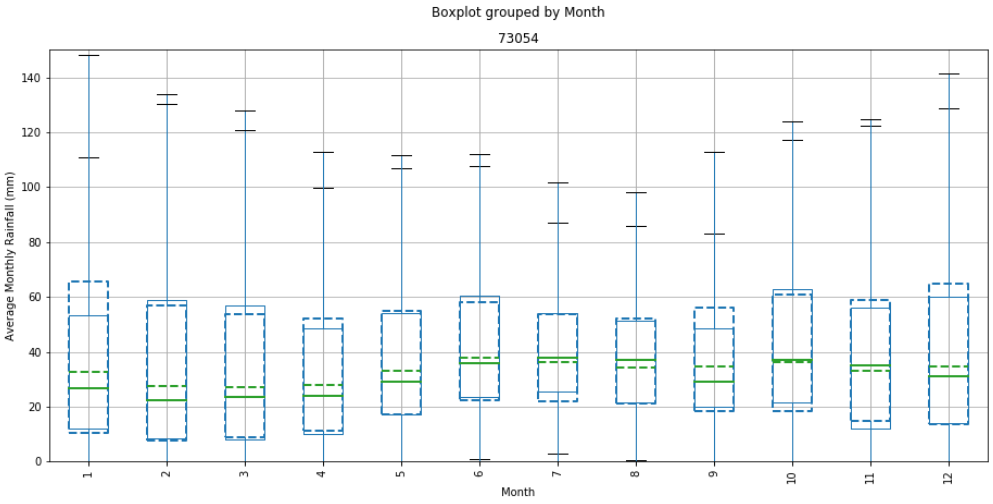
Boxplot grouped by Month
73054
Average Monthly Rainfall (mm)
Month

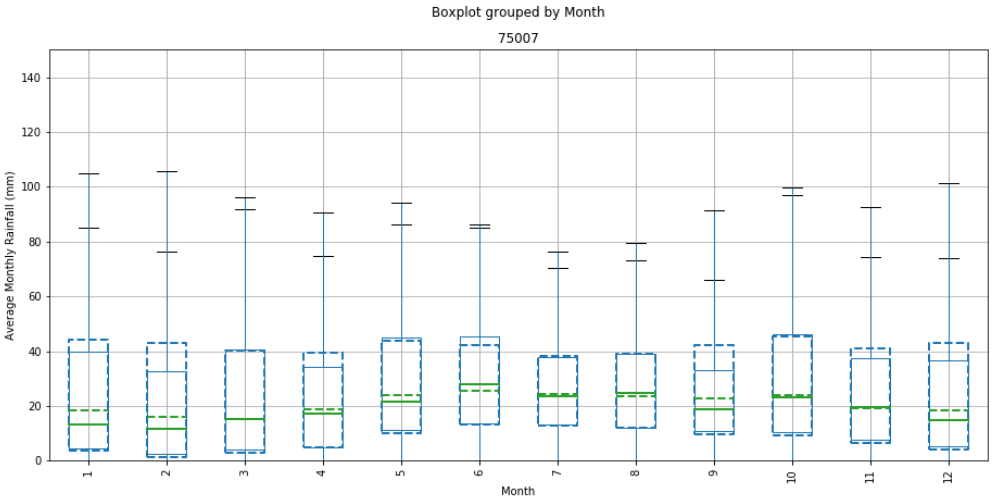
Boxplot grouped by Month
75007
Average Monthly Rainfall (mm)
Month

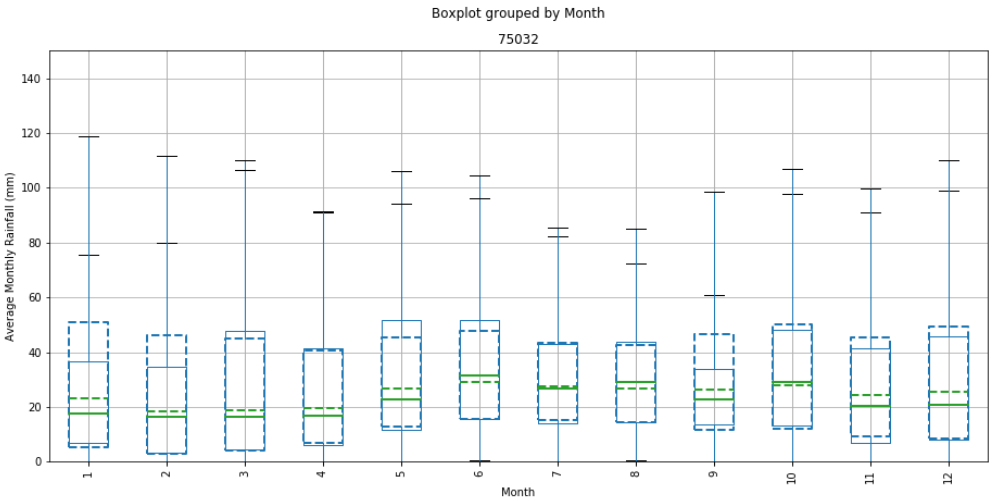
Boxplot grouped by Month
75032
Average Monthly Rainfall (mm)
Month

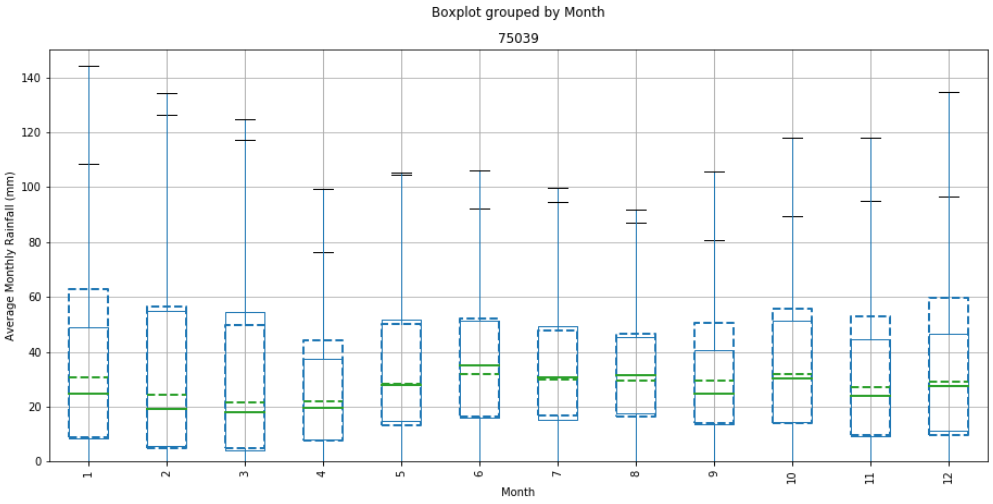
Boxplot grouped by Month
75039
Average Monthly Rainfall (mm)
Month
0
20
40
60
80
100
120
140
1
2
3
4
5
6
7
8
9
10
11
12

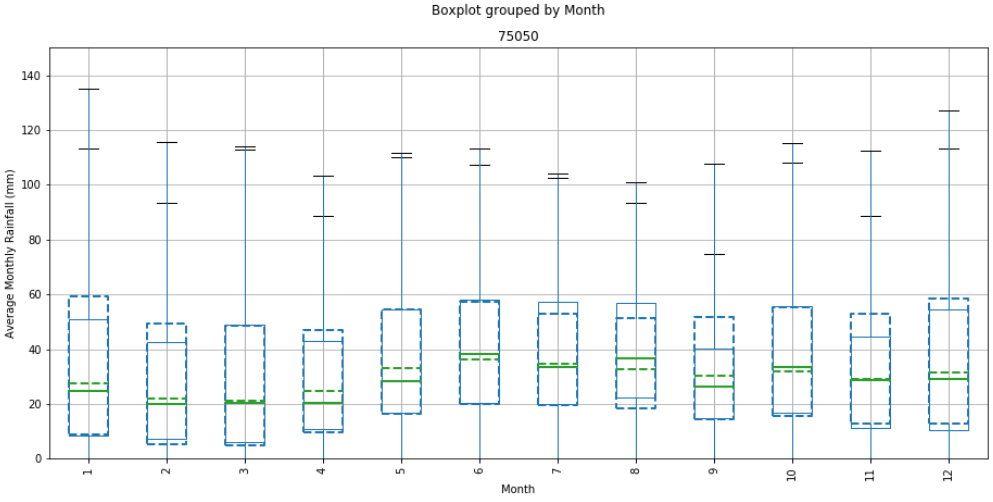
Boxplot grouped by Month
75050
Average Monthly Rainfall (mm)
Month
0
20
40
60
80
100
120
140
1
2
3
4
5
6
7
8
9
10
11
12

Appendix F - Box plots of monthly IPO forced stochastic (dashed) and instrumental (solid) rainfall

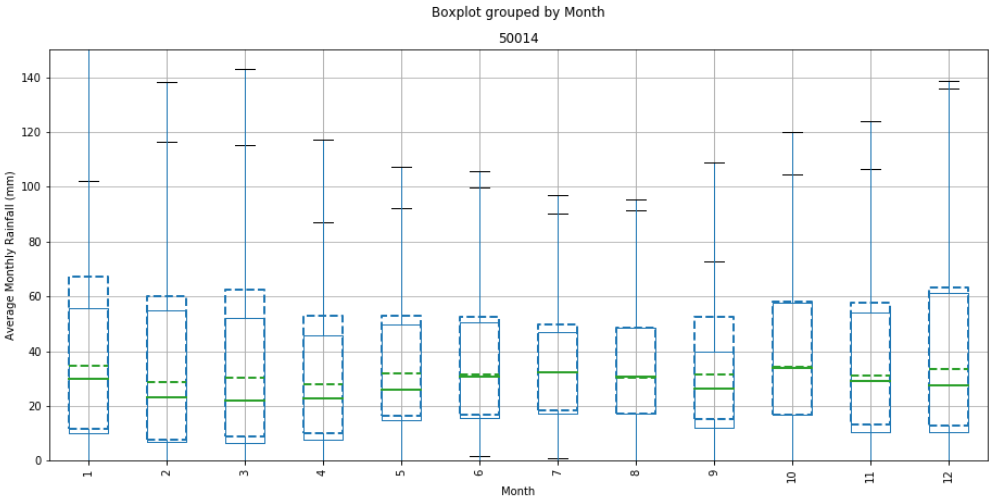

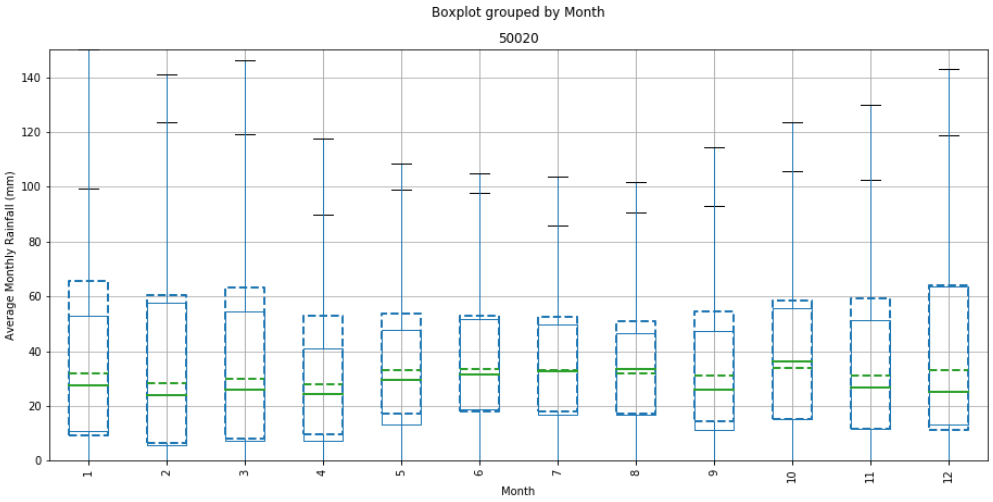

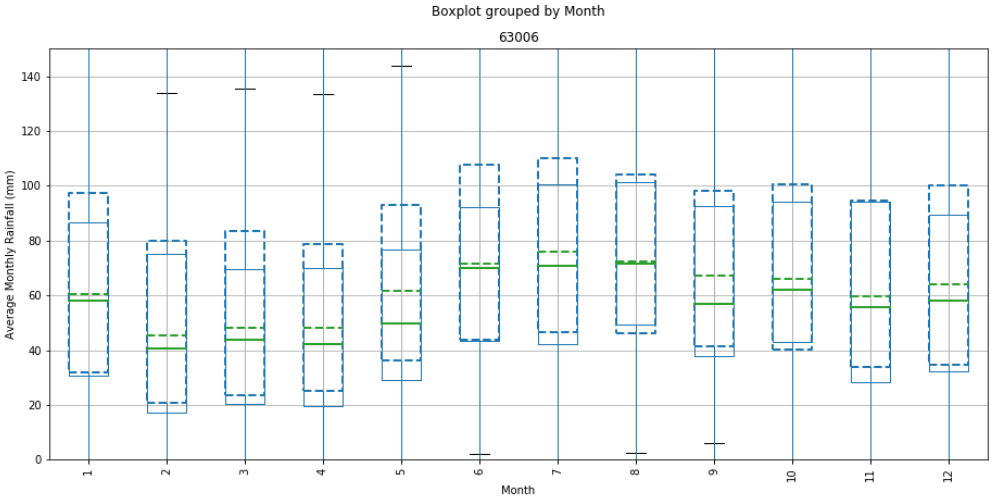

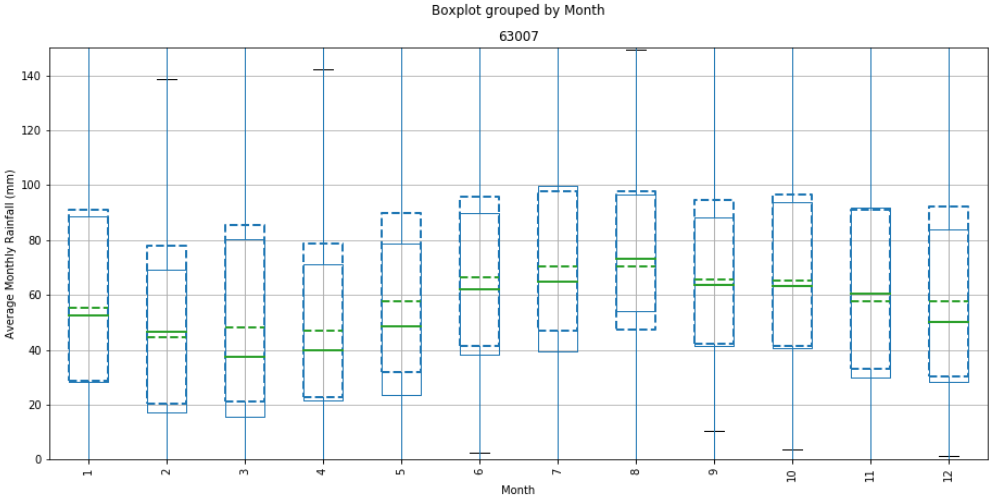
Boxplot grouped by Month
63007
Average Monthly Rainfall (mm)
Month

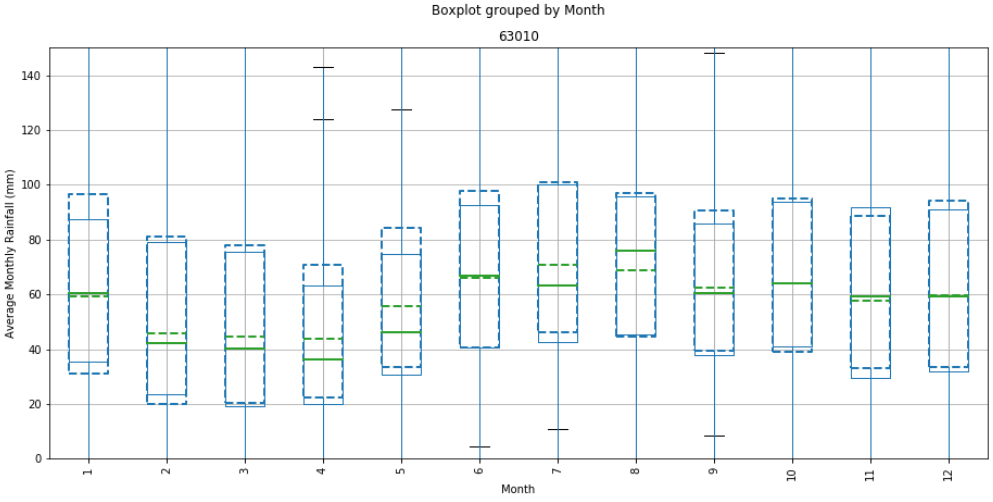
Boxplot grouped by Month
63010
Average Monthly Rainfall (mm)
Month

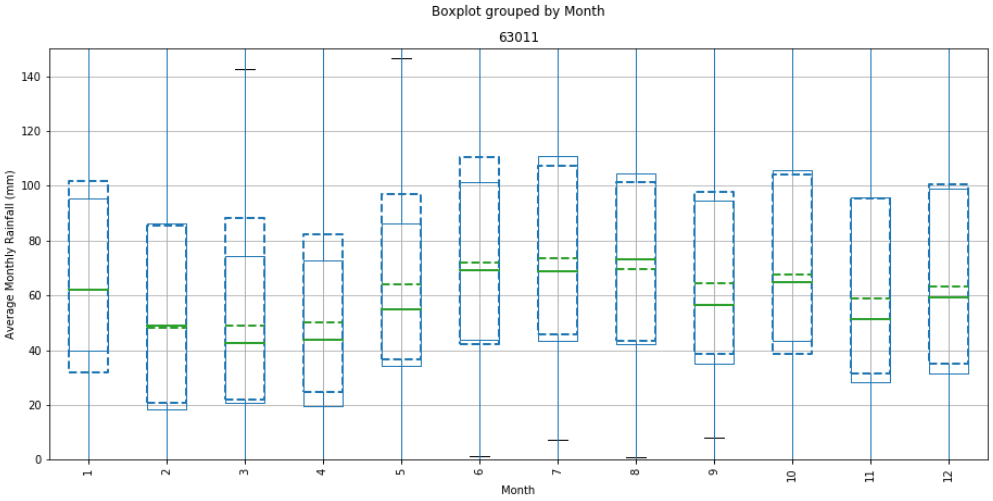
Boxplot grouped by Month
63011
Average Monthly Rainfall (mm)
Month

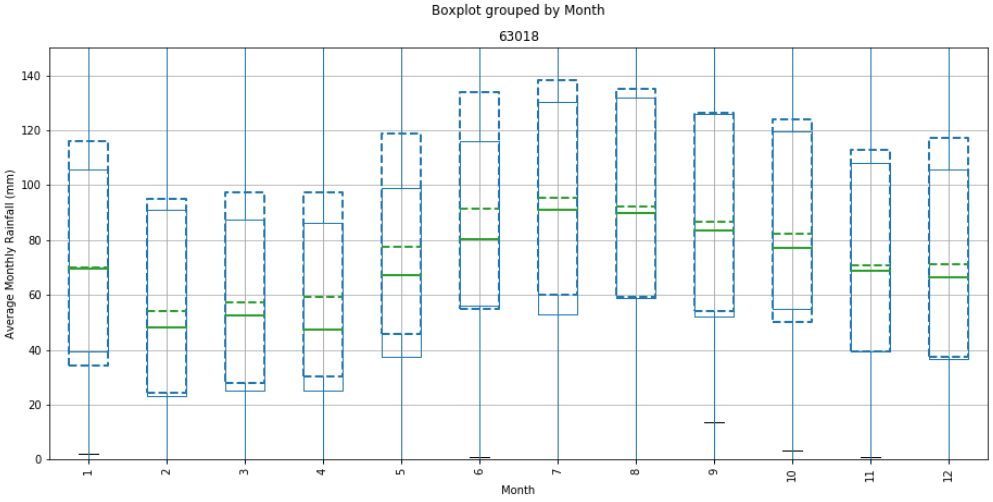
Boxplot grouped by Month
63018
Average Monthly Rainfall (mm)
Month

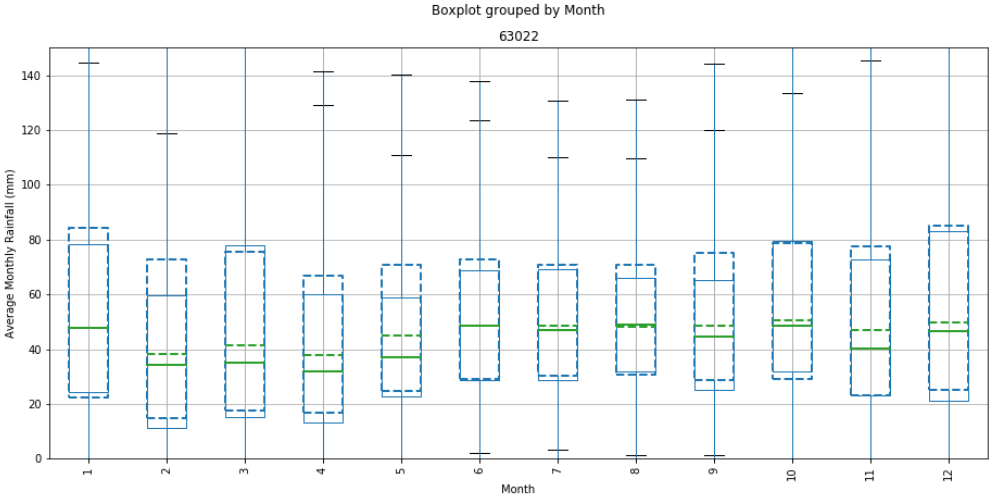
Boxplot grouped by Month
63022
Average Monthly Rainfall (mm)
Month

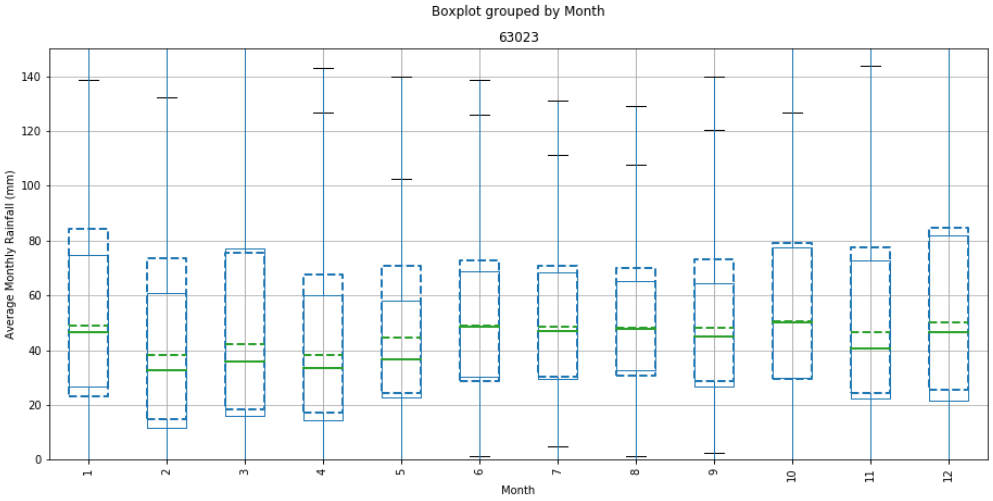
Boxplot grouped by Month
63023
Average Monthly Rainfall (mm)
Month

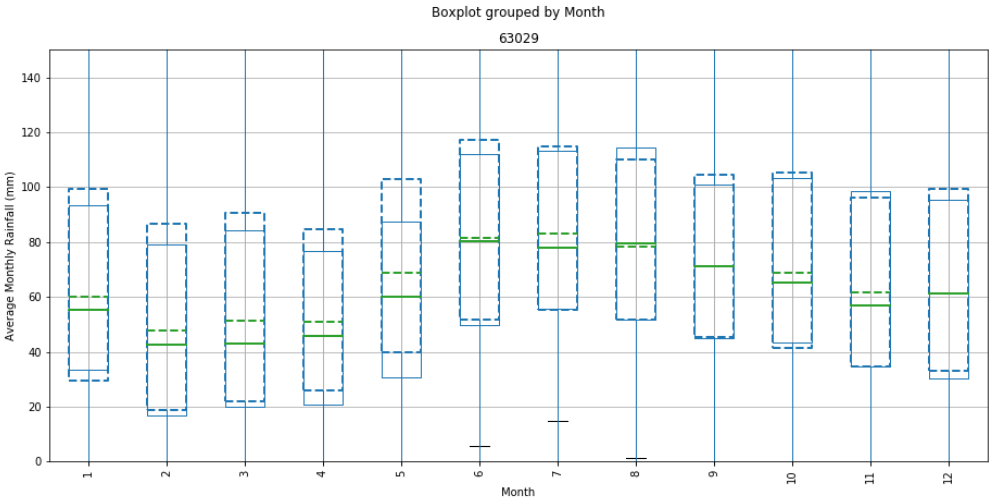
Boxplot grouped by Month
63029
Average Monthly Rainfall (mm)
Month

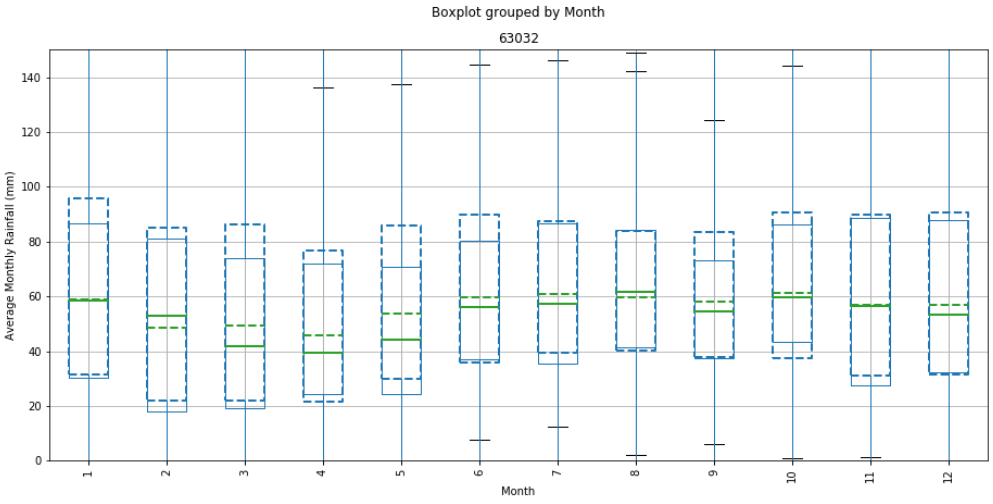
Boxplot grouped by Month
63032
Average Monthly Rainfall (mm)
Month

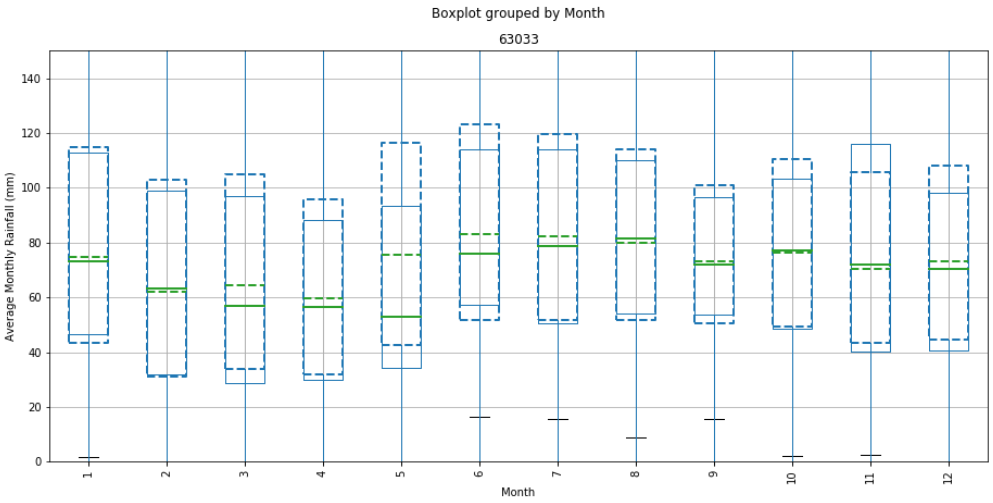
Boxplot grouped by Month
63033
Average Monthly Rainfall (mm)
Month

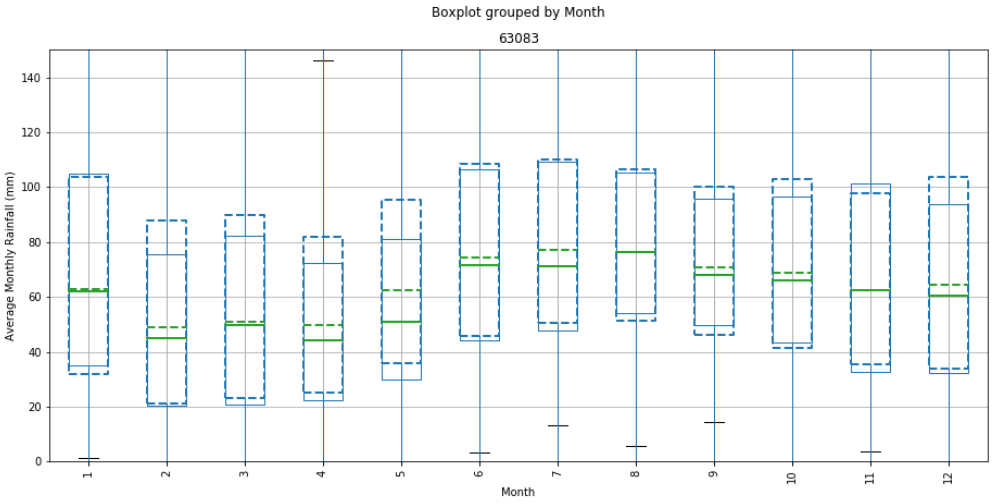
Boxplot grouped by Month
63083
Average Monthly Rainfall (mm)
Month

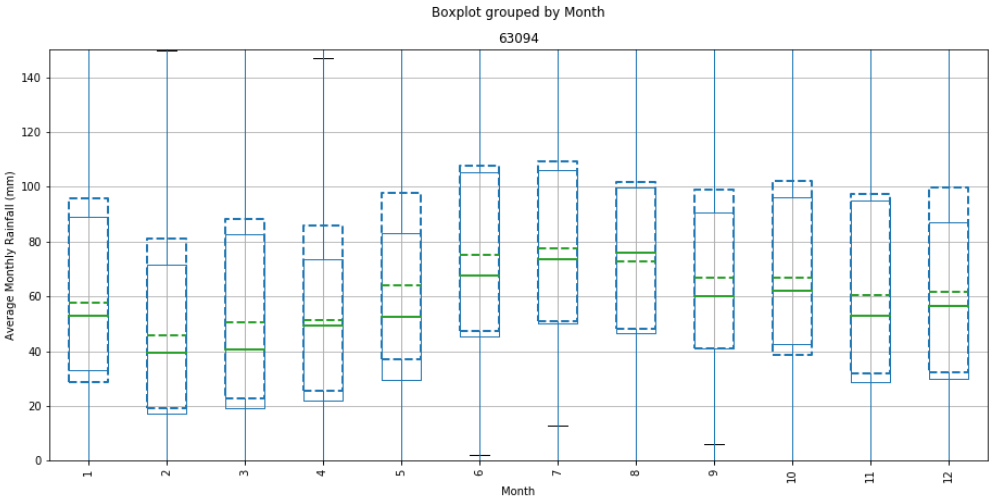
Boxplot grouped by Month
63094
Average Monthly Rainfall (mm)
Month

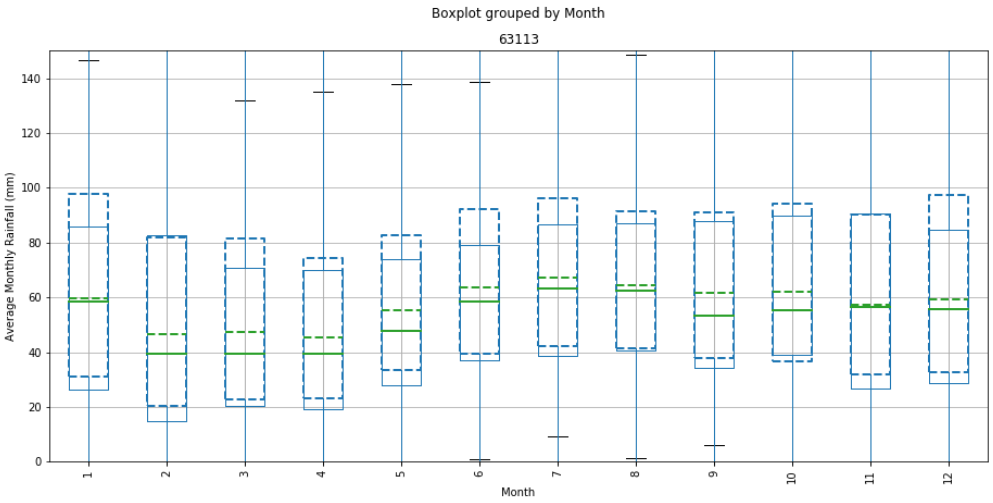
Boxplot grouped by Month
63113
Average Monthly Rainfall (mm)
Month

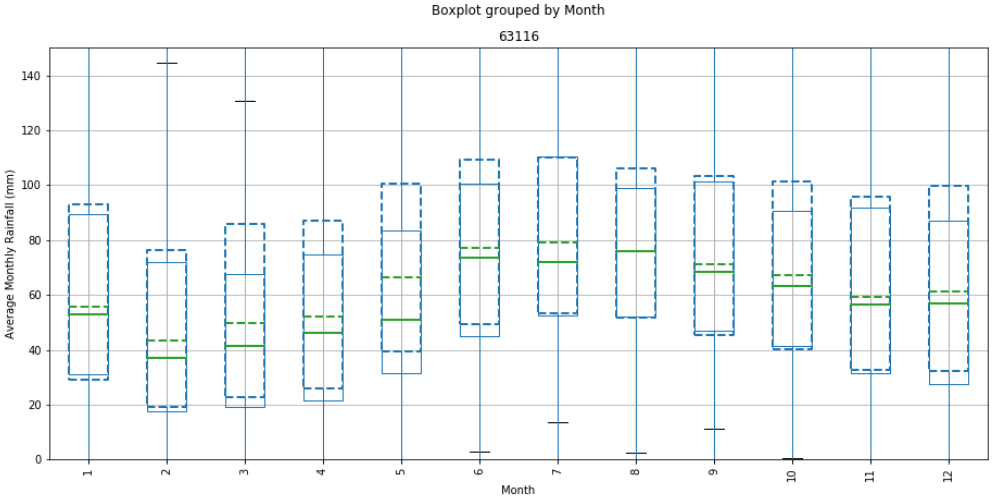
Boxplot grouped by Month
63116
Average Monthly Rainfall (mm)
Month

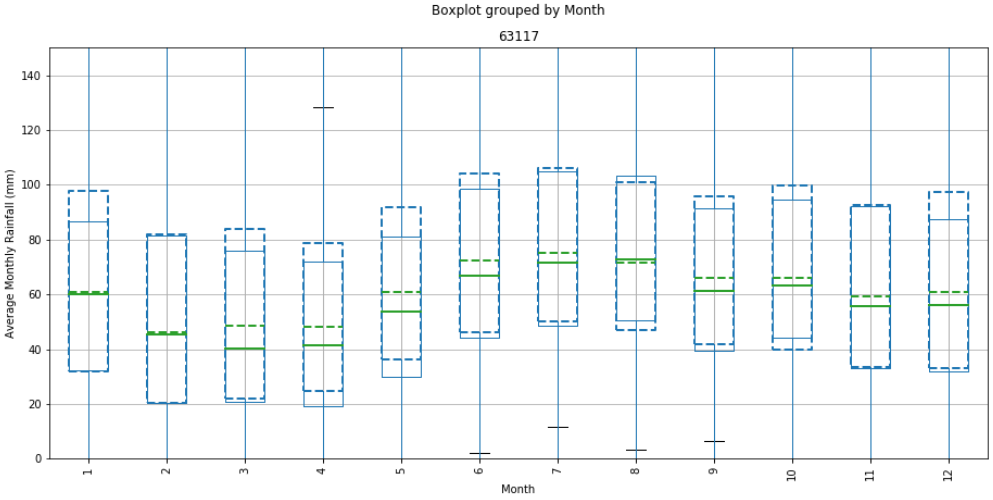
Boxplot grouped by Month
63117
Average Monthly Rainfall (mm)
Month

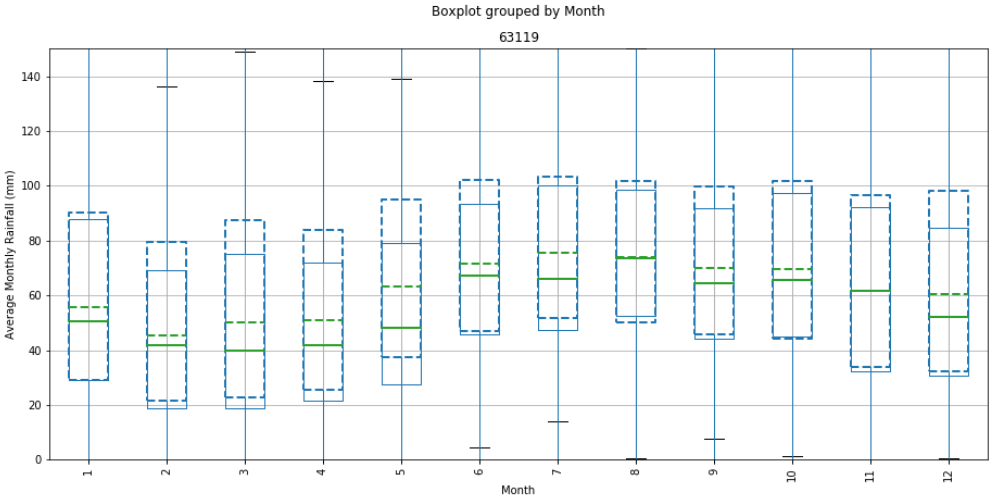
Boxplot grouped by Month
63119
Average Monthly Rainfall (mm)
Month

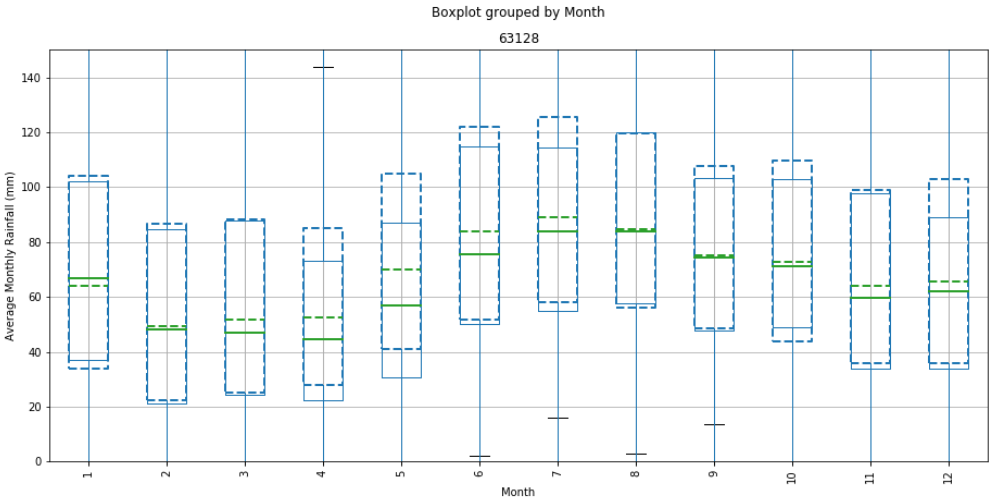
Boxplot grouped by Month
63128
Average Monthly Rainfall (mm)
Month

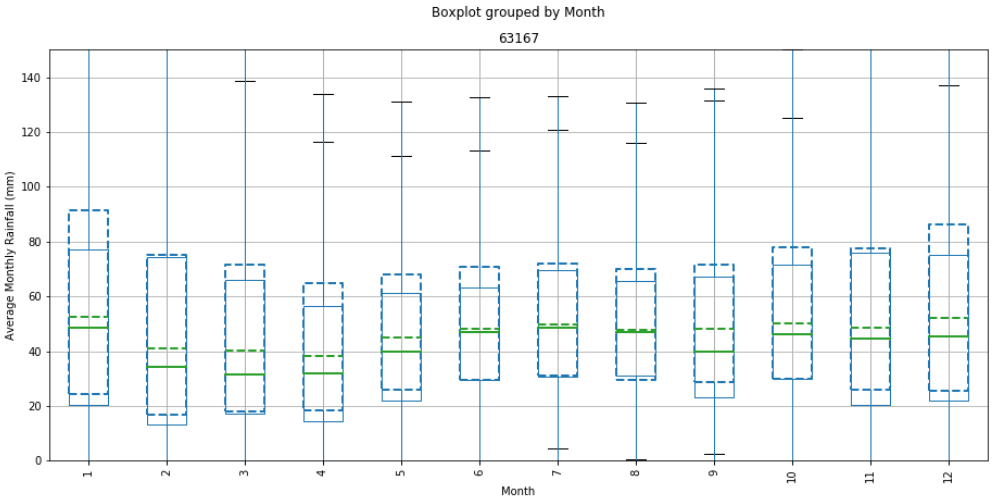
Boxplot grouped by Month
63167
Average Monthly Rainfall (mm)
Month

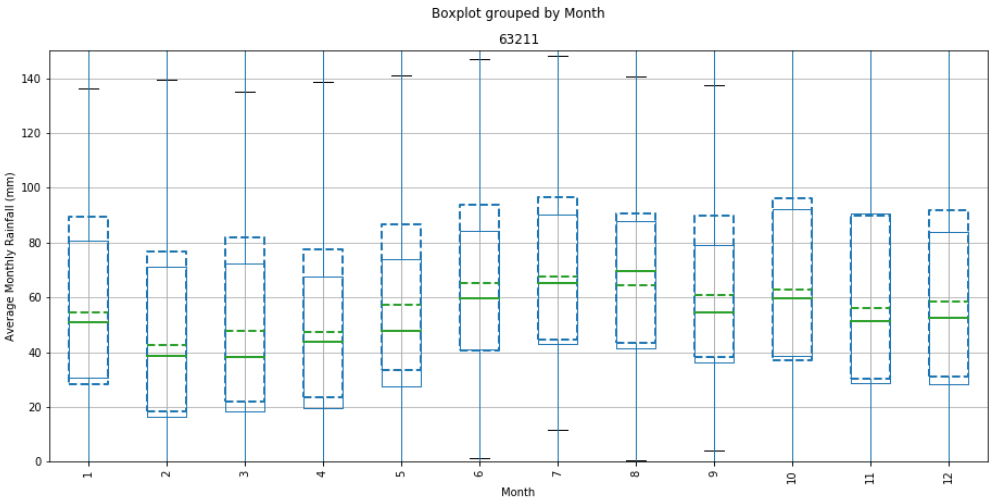
Boxplot grouped by Month
63211
Average Monthly Rainfall (mm)
Month

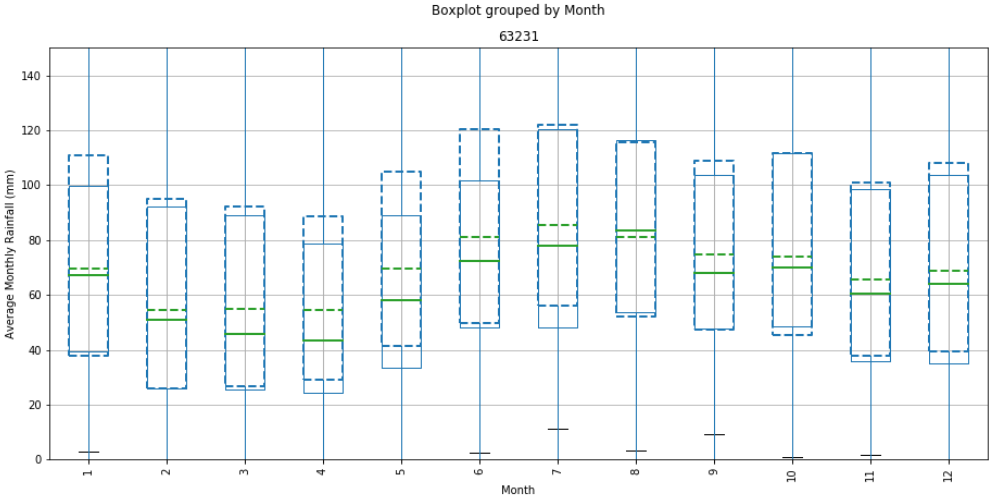
Boxplot grouped by Month
63231
Average Monthly Rainfall (mm)
Month

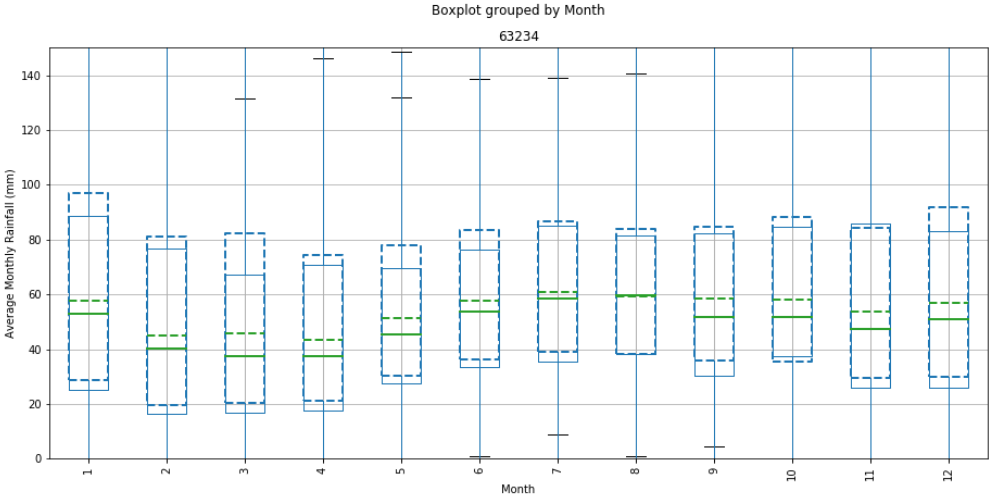
Boxplot grouped by Month
63234
Average Monthly Rainfall (mm)
Month

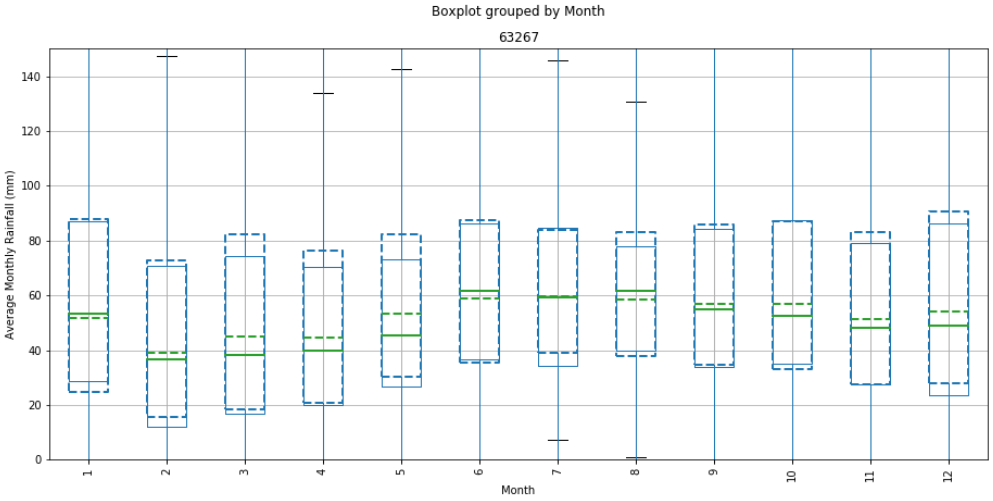
Boxplot grouped by Month
63267
Average Monthly Rainfall (mm)
Month

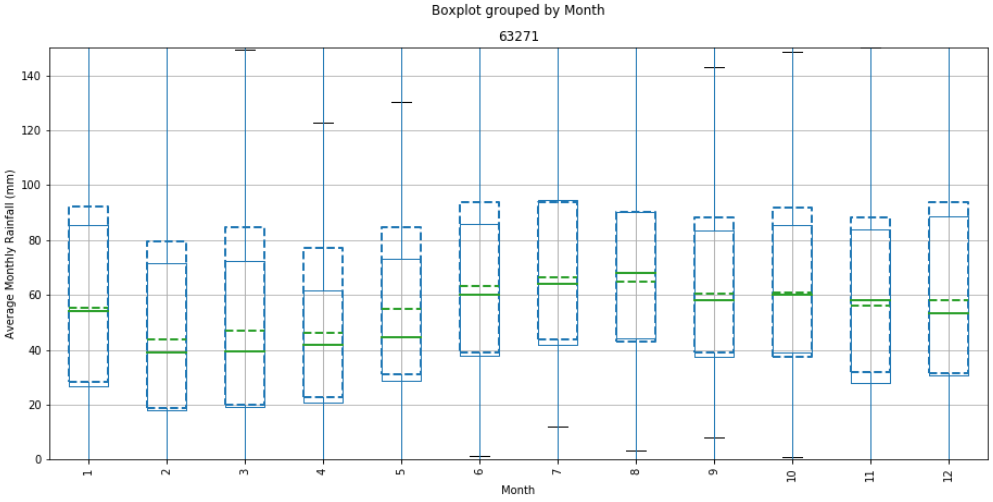
Boxplot grouped by Month
63271
Average Monthly Rainfall (mm)
Month

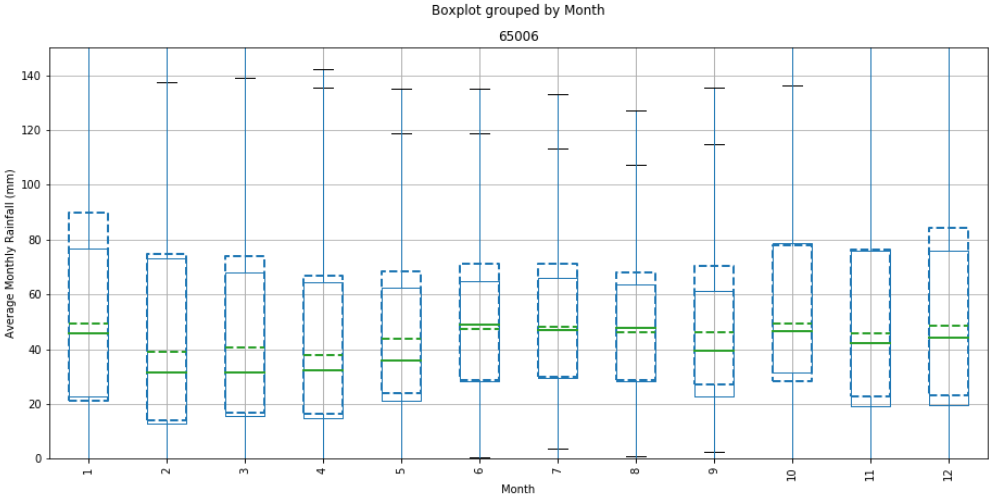
Boxplot grouped by Month
65006
Average Monthly Rainfall (mm)
Month

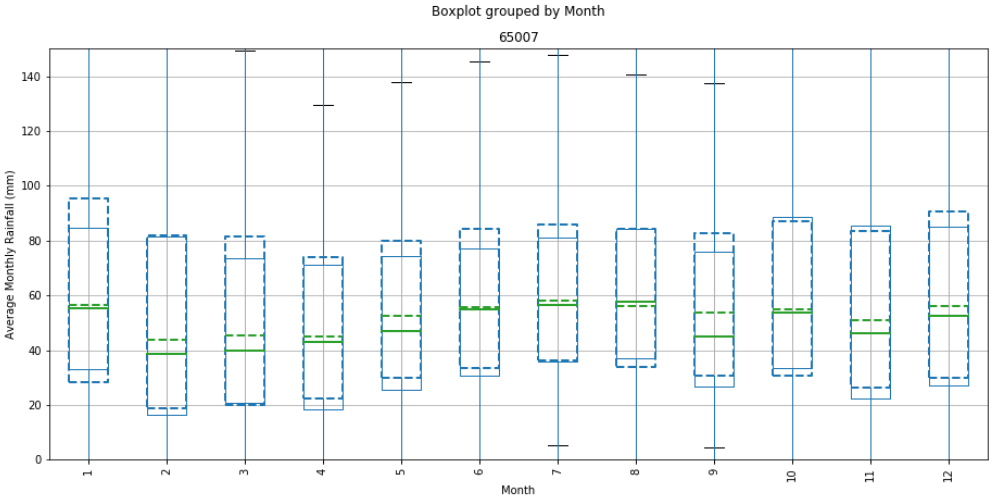
Boxplot grouped by Month
65007
Average Monthly Rainfall (mm)
Month

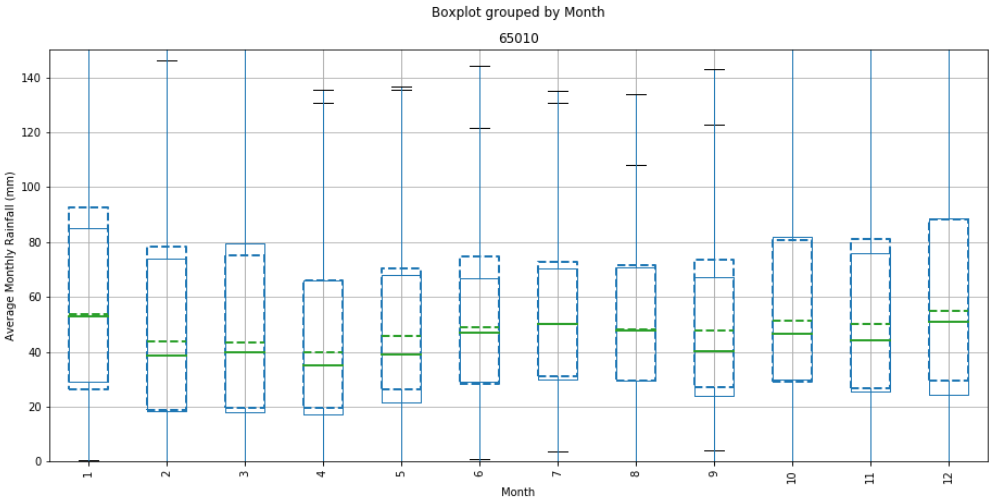
Boxplot grouped by Month
65010
Average Monthly Rainfall (mm)
Month

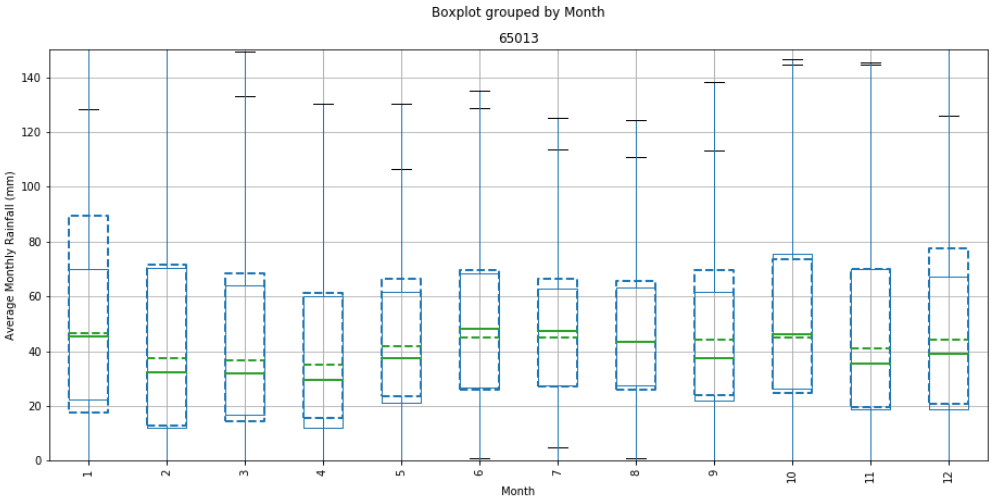
Boxplot grouped by Month
65013
Average Monthly Rainfall (mm)
Month

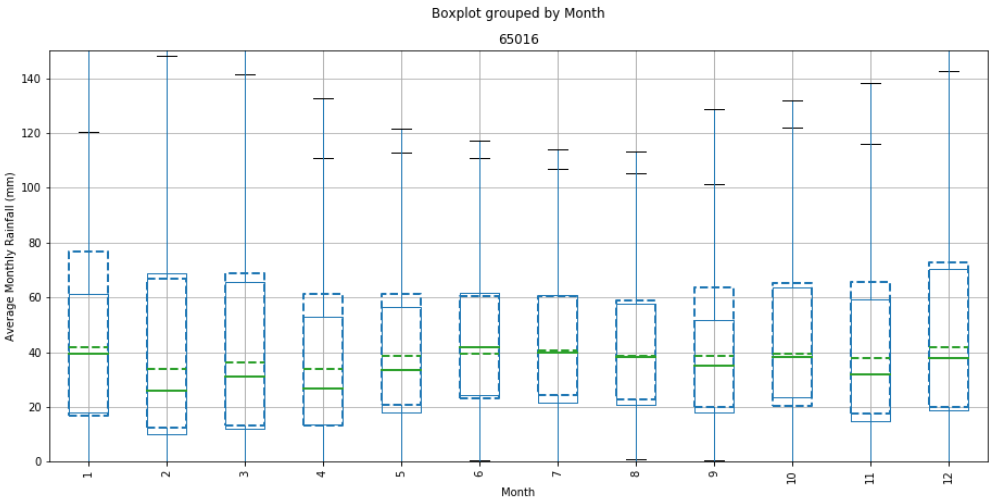
Boxplot grouped by Month
65016
Average Monthly Rainfall (mm)
Month

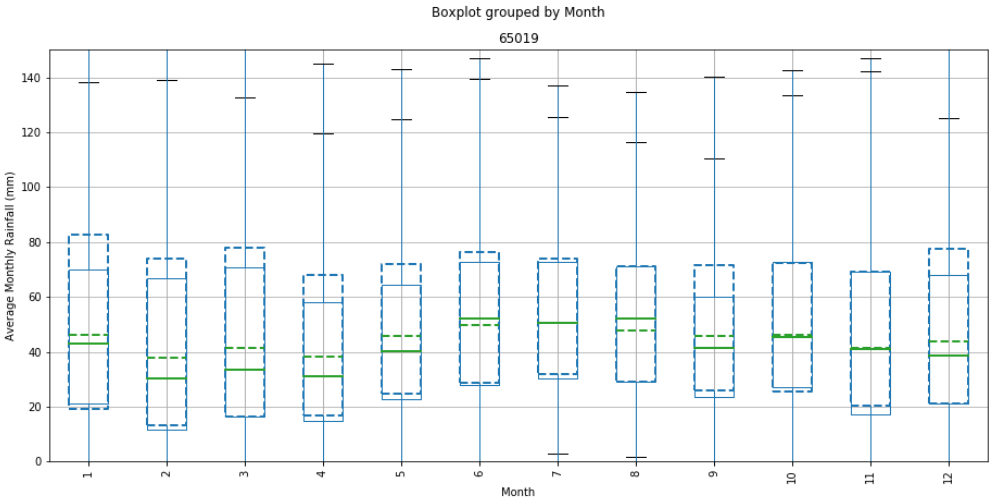
Boxplot grouped by Month
65019
Average Monthly Rainfall (mm)
Month

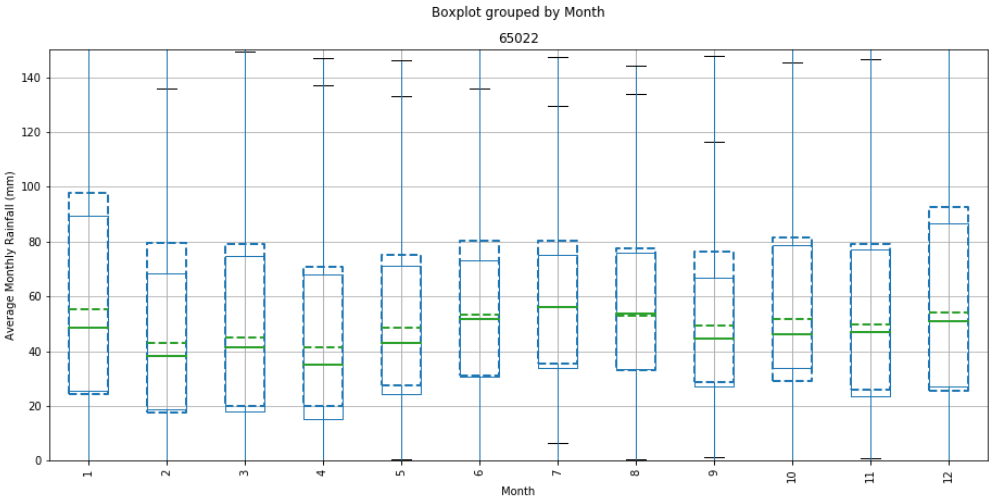
Boxplot grouped by Month
65022
Average Monthly Rainfall (mm)
Month

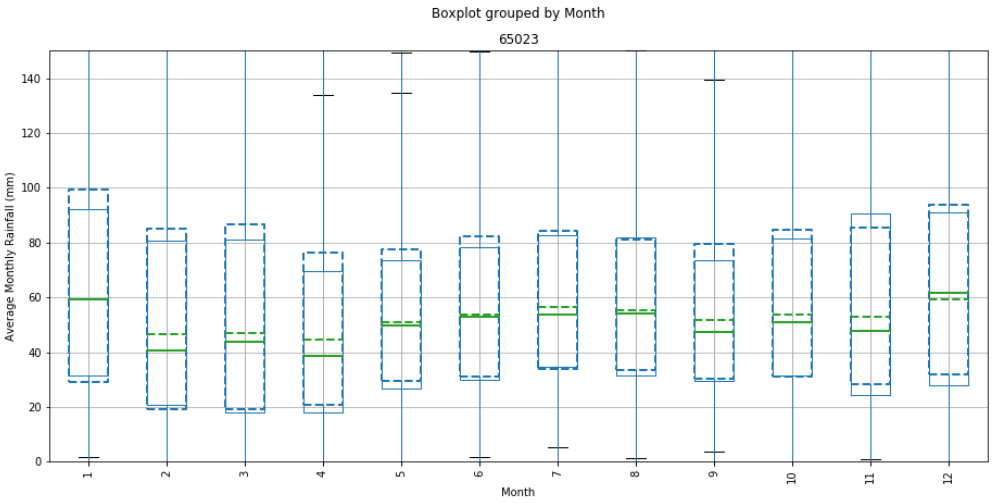
Boxplot grouped by Month
65023
Average Monthly Rainfall (mm)
Month

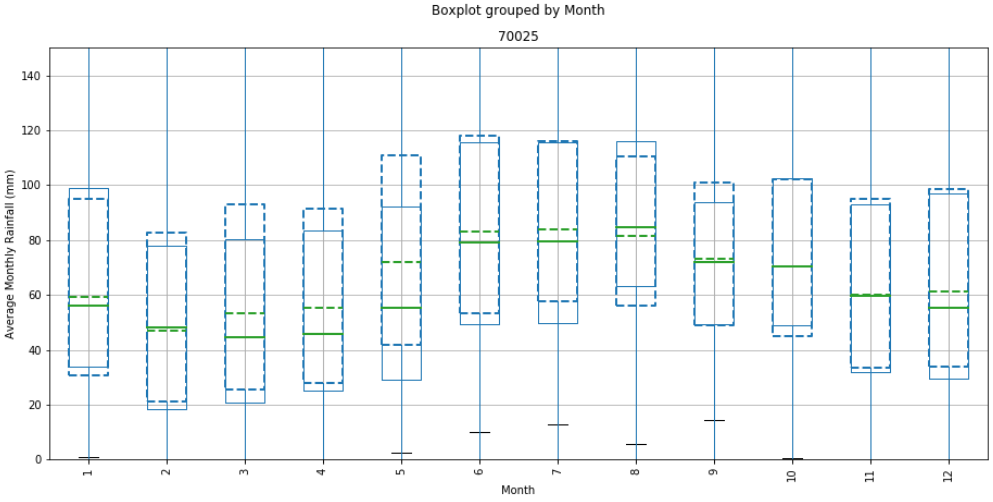
Boxplot grouped by Month
70025
Average Monthly Rainfall (mm)
Month

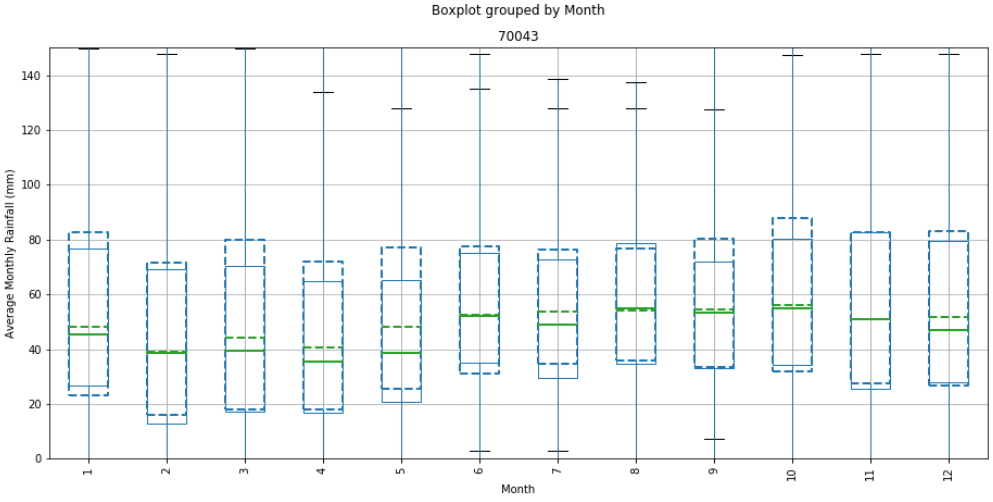
Boxplot grouped by Month
70043
Average Monthly Rainfall (mm)
Month

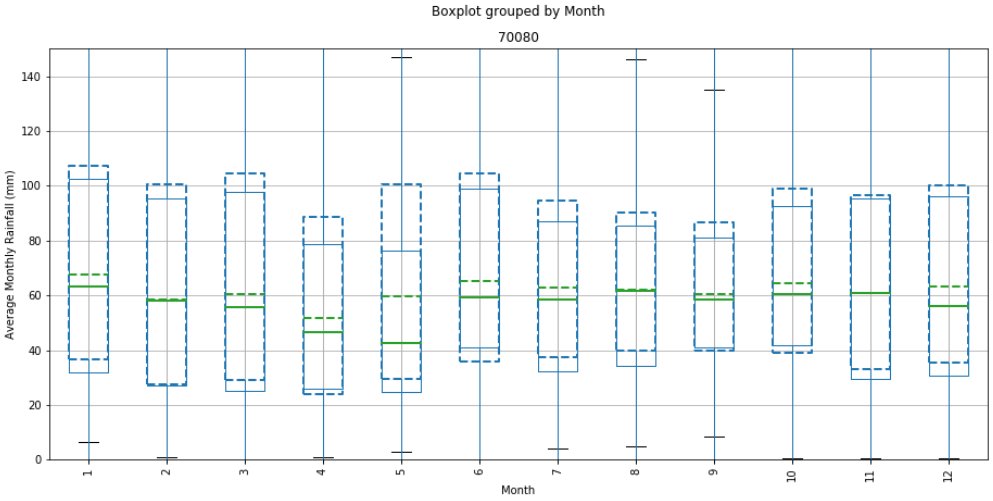
Boxplot grouped by Month
70080
Average Monthly Rainfall (mm)
Month

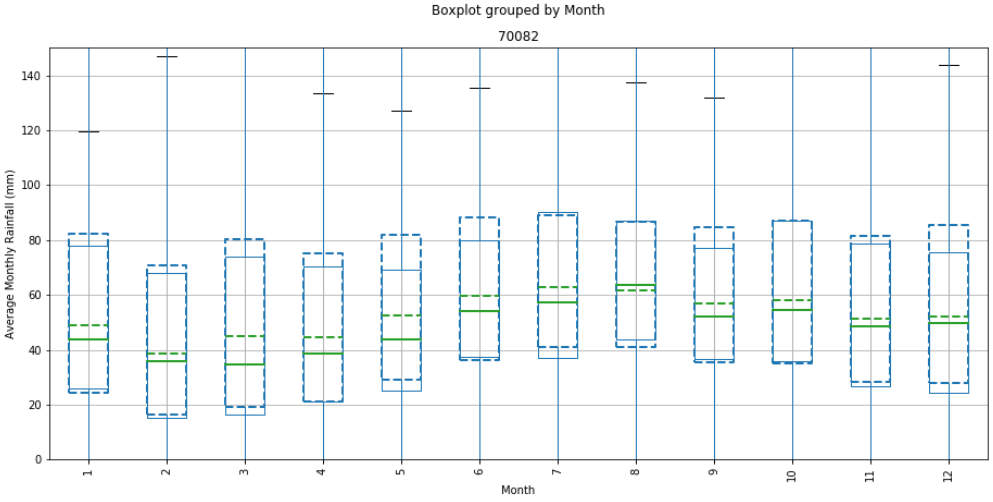
Boxplot grouped by Month
70082
Average Monthly Rainfall (mm)
Month

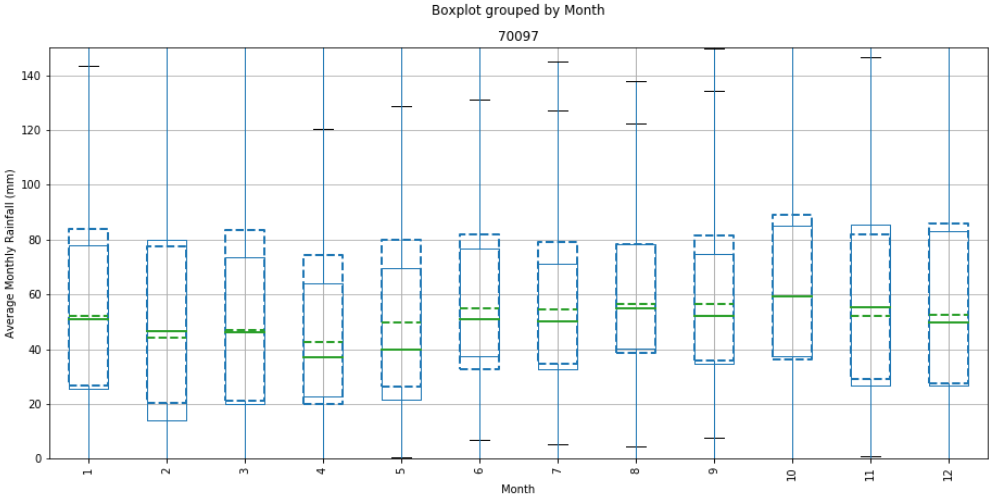
Boxplot grouped by Month
70097
Average Monthly Rainfall (mm)
Month

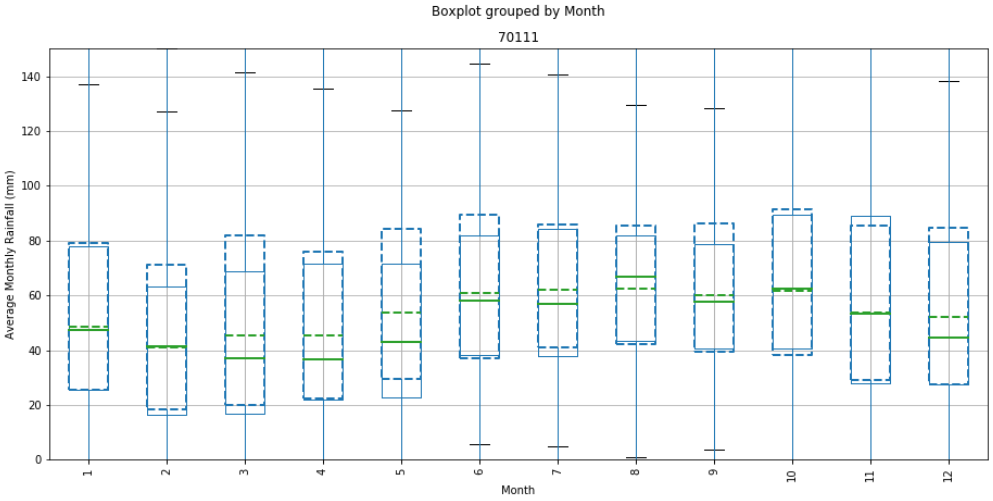
Boxplot grouped by Month
70111
Average Monthly Rainfall (mm)
Month

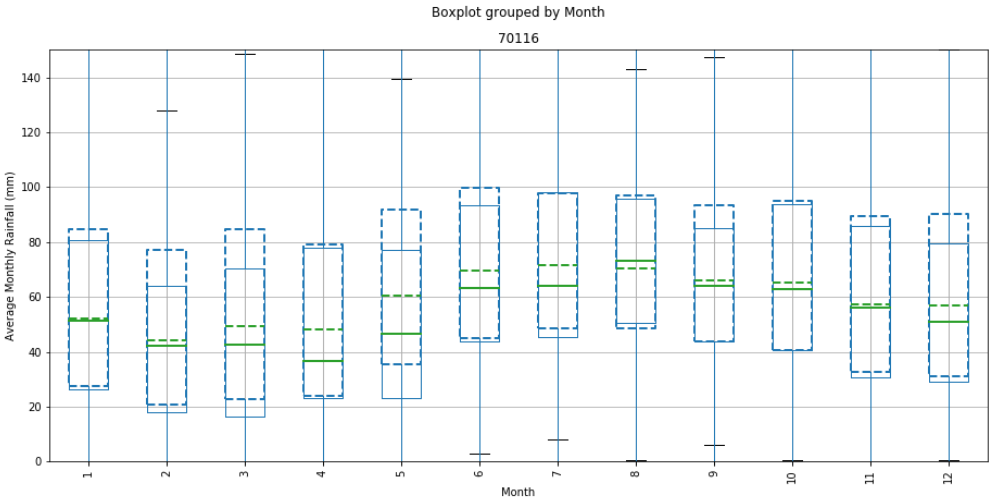
Boxplot grouped by Month
70116
Average Monthly Rainfall (mm)
Month

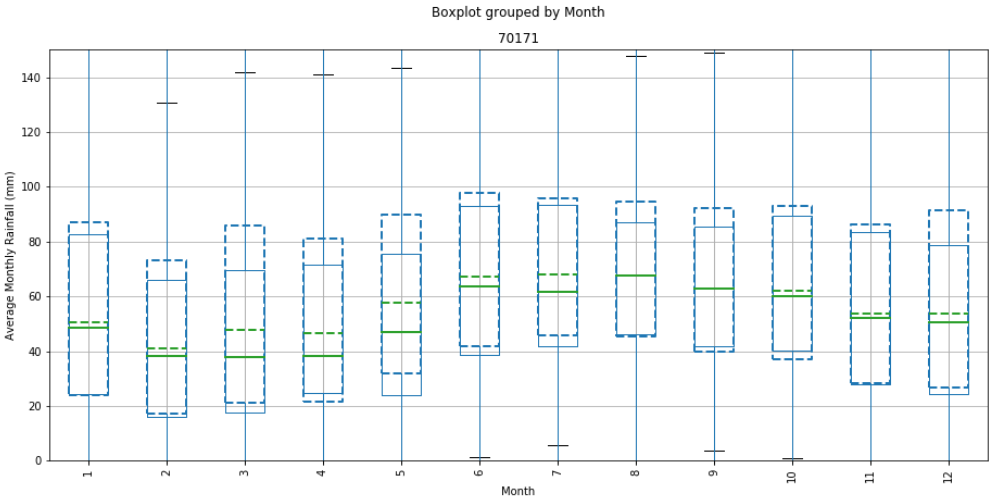
Boxplot grouped by Month
70171
Average Monthly Rainfall (mm)
Month

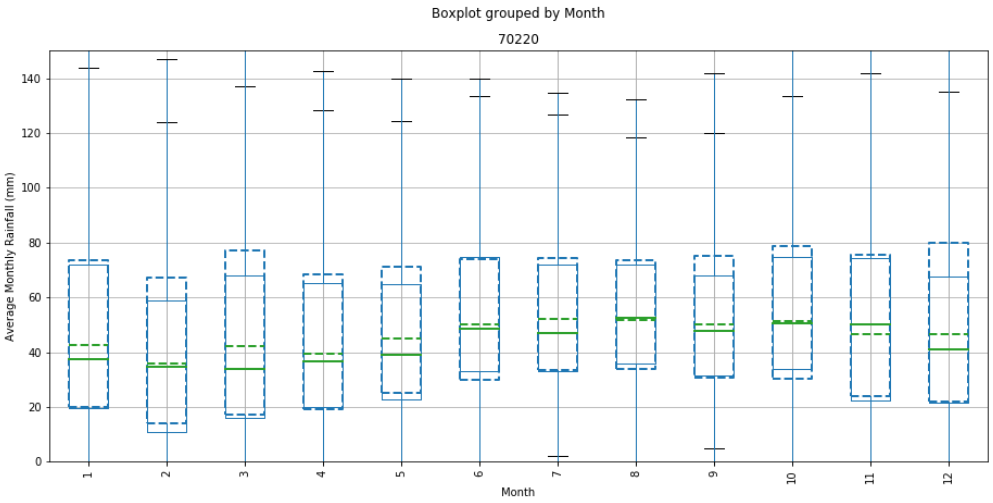
Boxplot grouped by Month
70220
Average Monthly Rainfall (mm)
Month

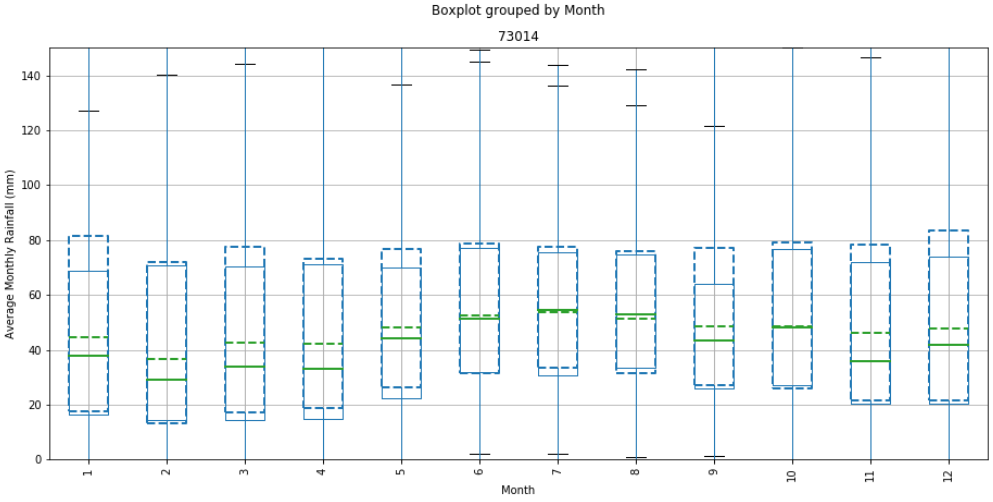
Boxplot grouped by Month
73014
Average Monthly Rainfall (mm)
Month

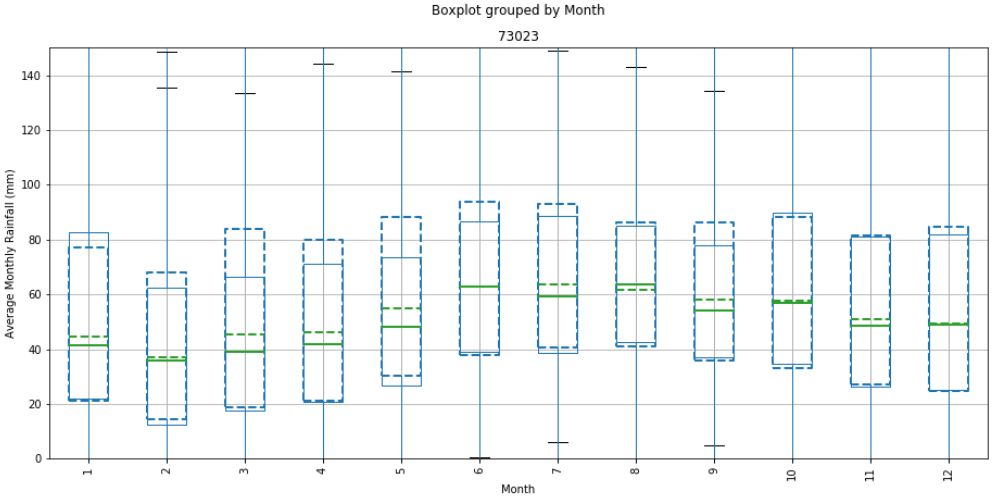
Boxplot grouped by Month
73023
Average Monthly Rainfall (mm)
Month

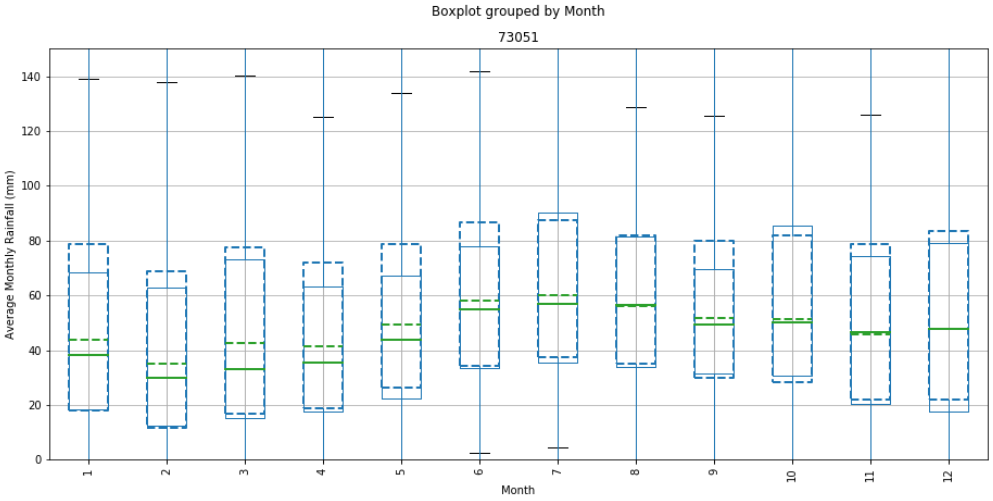
Boxplot grouped by Month
73051
Average Monthly Rainfall (mm)
Month

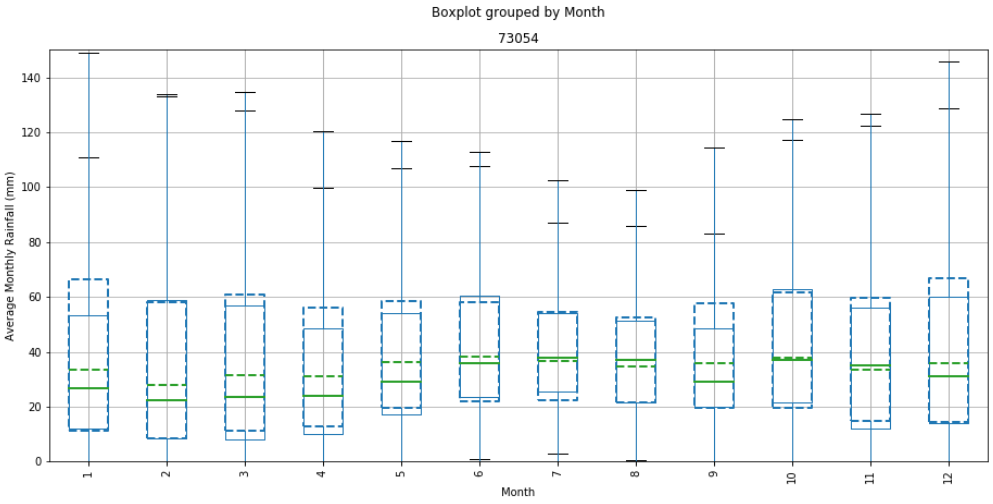
Boxplot grouped by Month
73054
Average Monthly Rainfall (mm)
Month

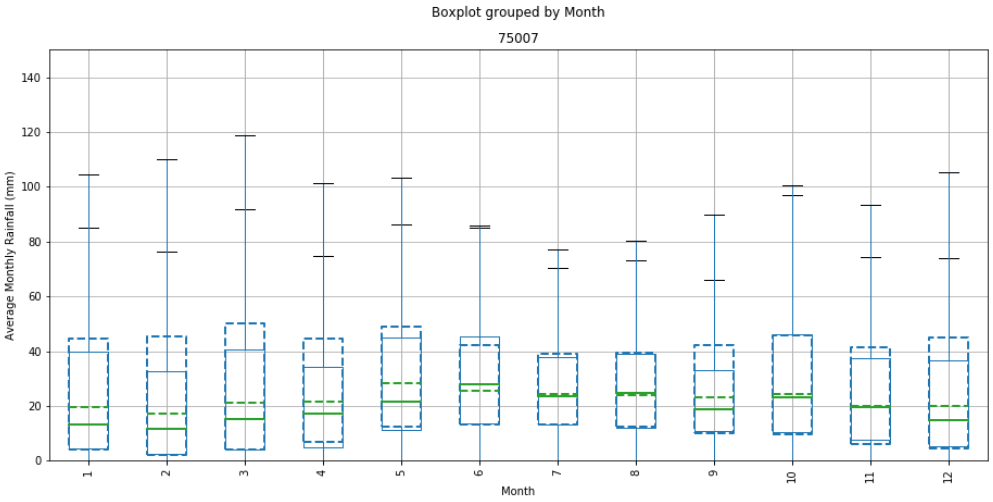
Boxplot grouped by Month
75007
Average Monthly Rainfall (mm)
Month

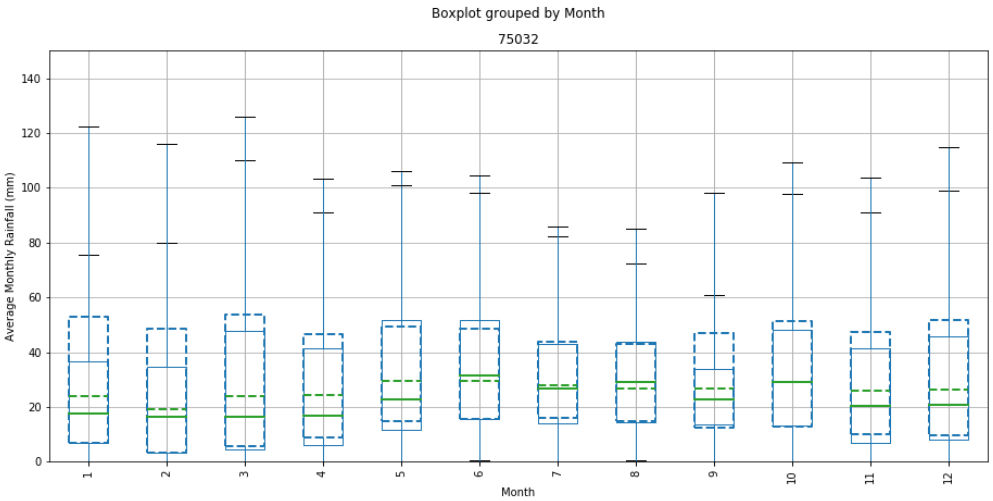
Boxplot grouped by Month
75032
Average Monthly Rainfall (mm)
Month

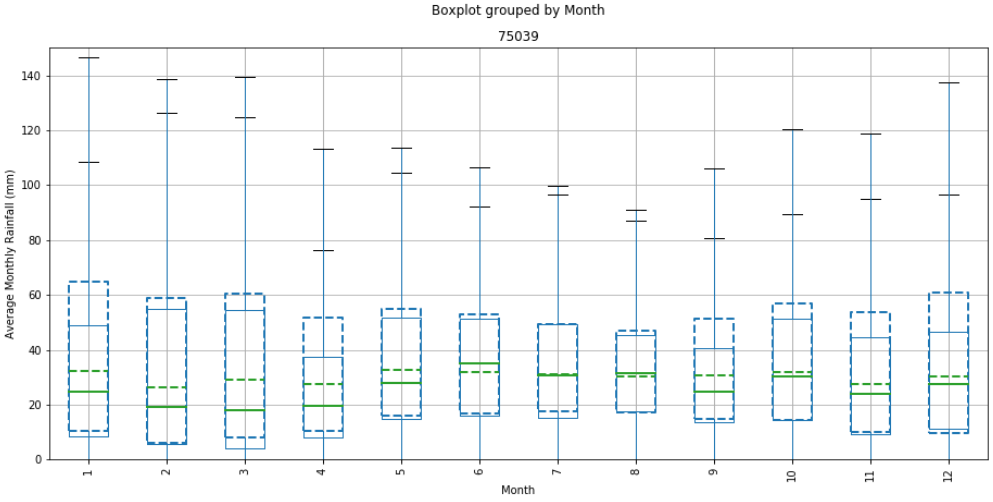
Boxplot grouped by Month
75039
Average Monthly Rainfall (mm)
Month

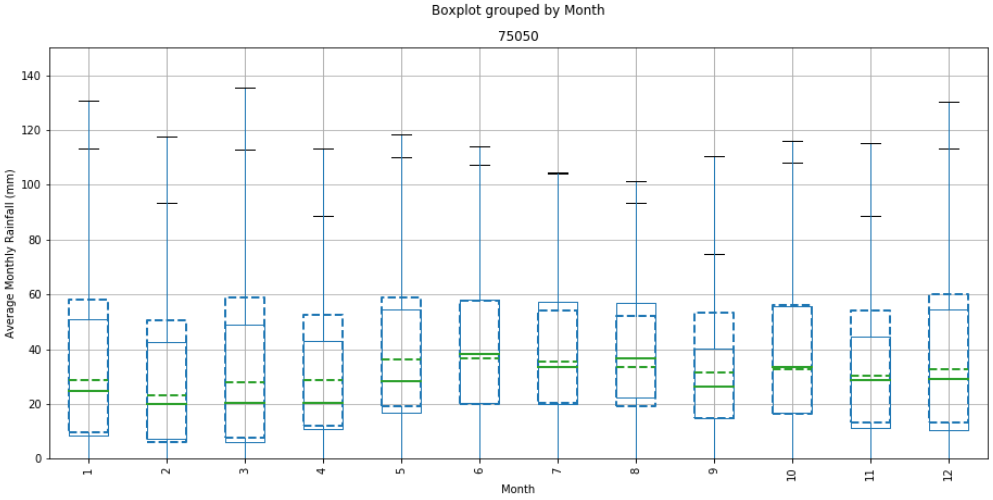
Boxplot grouped by Month
75050
Average Monthly Rainfall (mm)
Month

APPENDIX 5: BEGA REGION PAPER

Incorporating changes in East Coast Low (ECL) behaviour into stochastically generated hydroclimatic data for the Bega River region, New South Wales, Australia by Anthony Kiem

Incorporating changes in East Coast Low (ECL) behaviour into stochastically generated hydroclimatic data for the Bega River region, New South Wales, Australia

ANTHONY S. KIEM

Centre for Climate, Water and Land (CWCL)
School of Environmental and Life Sciences (Earth Sciences)
Faculty of Science
University of Newcastle, NSW, Australia

- Technical Report – DRAFT1
- Prepared for New South Wales Department of Industry – Lands and Water
- 15 August 2019

For further information please contact:
Dr Anthony Kiem
Associate Professor – Hydroclimatology
Centre for Climate, Water and Land (CWCL)
School of Environmental and Life Sciences (Earth Sciences)
Faculty of Science
University of Newcastle, NSW, Australia
T: +61 2 4921 8656
Email: Anthony.Kiem@newcastle.edu.au

Disclaimer
This report has been prepared on behalf of and for the exclusive use by New South Wales Department of Industry – Lands and Water and is subject to and issued in connection with the provisions of the agreement between Anthony Kiem and New South Wales Department of Industry – Lands and Water. No liability or responsibility is accepted for or in respect of any use of or reliance upon this report by any third party.

Table of Contents

List of Figures 3

List of Tables 4

1. Introduction 5
- **1.1 Background** 5
- **1.2 Scope of this study** 6

2. Data 8
- **2.1 Observed daily rainfall and evaporation data (referred to as instrumental data)** 8
- **2.2 Information about projected changes to rainfall and evaporation in the Bega River region (used for ECL Scenario 2)** 8
- **2.3 Information about projected East Coast Low (ECL) behaviour (used for ECL Scenarios 3-8)** 9

3. Methodology 10
- **3.1 Methodology for stochastic data generation** 10
- **3.2 Development of future East Coast Low (ECL) scenarios** 10
  - 3.2.1 ECL Scenario 1 – baseline 10
  - 3.2.2 ECL Scenario 2 – 10 decrease in rainfall, 10% increase in evaporation 10
  - 3.2.3 ECL Scenario 3 – remove one ECL per year 10
  - 3.2.4 ECL Scenario 4 – add one ECL per year 10
  - 3.2.5 ECL Scenario 5 – take one ECL from winter and make it occur in summer instead 11
  - 3.2.6 ECL Scenario 6 – remove five ECLs per year 11
  - 3.2.7 ECL Scenario 7 – add five ECLs per year 11
  - 3.2.8 ECL Scenario 8 – take five ECLs from winter and make them occur in summer instead 11

4. Results 12
- **4.1 Verification that the stochastically generated data accurately reproduces key statistical characteristics** 12
  - 4.1.1 Verification of stochastic model performance at the ANNUAL (January to December) time scale 12
  - 4.1.2 Verification of stochastic model performance at the MONTHLY time scale 15
  - 4.1.3 Verification of stochastic model performance at the DAILY time scale 15
  - 4.1.4 Verification of stochastic model performance at the interannual to multidecadal time scale (i.e. multi-year statistics) 19
- **4.2 Changes to rainfall and evaporation in the Bega River region under different East Coast Low (ECL) scenarios** 22

5. Limitations of this study 23

6. Conclusion 24
- **6.1 Key findings** 24
- **6.2 Recommendations** 24

7. Acknowledgements 25

8. References 26

Appendix A. List of rainfall and evaporation sites used in this study 27

Appendix B. Plots demonstrating that the stochastic model performs satisfactorily at the MONTHLY time scale 28

List of Figures

Figure 1: The eastern seaboard of Australia (ESA) – roughly the area between the east coast of Australia and the Great Dividing Range. 6

Figure 2: Projected impacts of climate change on rainfall along the east coast of Australia (Source: https://www.climatechangeinaustralia.gov.au/en/climate-projections/explore-data/summary-data-explorer/#) 8

Figure 3: Comparison between annual (January-December) MEAN calculated from 130 years of instrumental data (red dot) and the annual MEANS calculated from the 100 replicates of 130 years of stochastically generated data (box plots). 12

Figure 4: Comparison between annual (January-December) STANDARD DEVIATION calculated from 130 years of instrumental data (red dot) and the annual STANDARD DEVIATIONS calculated from the 100 replicates of 130 years of stochastically generated data (box plots) 13

Figure 5: Comparison between annual (January-December) MAXIMUM calculated from 130 years of instrumental data (red dot) and the annual MAXIMUMS calculated from the 100 replicates of 130 years of stochastically generated data (box plots). 13

Figure 6: Comparison between annual (January-December) MINIMUM calculated from 130 years of instrumental data (red dot) and the annual MINIMUMS calculated from the 100 replicates of 130 years of stochastically generated data (box plots). 14

Figure 7: Comparison between annual (January-December) LAG-1 AUTO CORRELATION calculated from 130 years of instrumental data (red dot) and the annual LAG-1 AUTO CORRELATIONS calculated from the 100 replicates of 130 years of stochastically generated data (box plots) 14

Figure 8: Top left = spatial correlations of ANNUAL totals calculated from 130 years of instrumental data. Top right = spatial correlations of ANNUAL totals calculated from the 100 replicates of 130 years of stochastically generated data (box plots). Bottom left = percentage difference in spatial correlations for observed data (top left) and stochastically generated data (top right) [100 x (generated – instrumental)/instrumental]. 15

Figure 9: Scatter plots comparing daily rainfall at Station 1 with daily rainfall at Station 2 for instrumental data (top left), stochastic replicate #1 (top right), stochastic replicate #2 (bottom left), and stochastic replicate #3 (bottom right). 16

Figure 10: Scatter plots comparing daily rainfall at Station 1 with daily evaporation at Station 7 for instrumental data (top left), stochastic replicate #1 (top right), stochastic replicate #2 (bottom left), and stochastic replicate #3 (bottom right). 17

Figure 11: Scatter plots comparing daily evaporation at Station 7 with daily evaporation at Station 8 for instrumental data (top left), stochastic replicate #1 (top right), stochastic replicate #2 (bottom left), and stochastic replicate #3 (bottom right). 18

Figure 12: Percentage difference in spatial correlations for DAILY data at the study sites. Top left is instrumental versus stochastic replicate #1. Top right is instrumental versus stochastic replicate #2. Bottom left is instrumental versus stochastic replicate #3. 19

Figure 13: For replicate #1 at site #1, average (top left), standard deviation (top right), maximum (bottom left), and total over 130 years (bottom right) for daily rainfall under the eight different ECL scenarios. 22

List of Tables

Table 1: Tolerance Limits for differences in key statistics when historical hydroclimatic data is compared with stochastically generated data (based on Srikanthan and McMahon (2003)). 20

Table 2: Stochastic model assessment (based on Srikanthan and McMahon (2003)). Rainfall and evaporation site numbers refer to the sites as they are detailed in Appendix A. 20

1. Introduction

1.1 Background

East Coast Lows (ECLs) are intense low-pressure systems which occur over the subtropical east coasts of Southern and Northern Hemisphere continents. ECLs are typically associated with gale-force winds, large seas, storm surges, heavy rainfall, and flooding. While ECL impacts are often seen as negative, the rainfall associated with ECLs is also very important for water security within the heavily populated eastern seaboard of Australia (ESA) – roughly the area between the east coast of Australia and the Great Dividing Range (Figure 1).

As part of the Eastern Seaboard Climate Change Initiative (ESCCI, www.climatechange.environment.nsw.gov.au/Impacts-of-climate-change/East-Coast-Lows/Eastern-Seaboard-Climate-Change-Initiative), considerable research was conducted into ECLs and the impact of these weather systems on rainfall and water security along the east coast of New South Wales (NSW). One finding from this ESCCI research was that South Coast NSW (where the Bega River region is located) has historically been regularly impacted by ECLs (about 10 times per year on average). Another finding from ESCCI was that small to moderate ECLs are projected to decrease in frequency during the cool season and large ECLs are projected to increase in frequency during the warm season.

The NSW Department of Industry (Department) Regional Water Strategy team requires assistance in defining plausible East Coast Low (ECL) rainfall scenarios to use as a proxy for understanding the potential impacts of climate change on water supply security in the Bega River region.

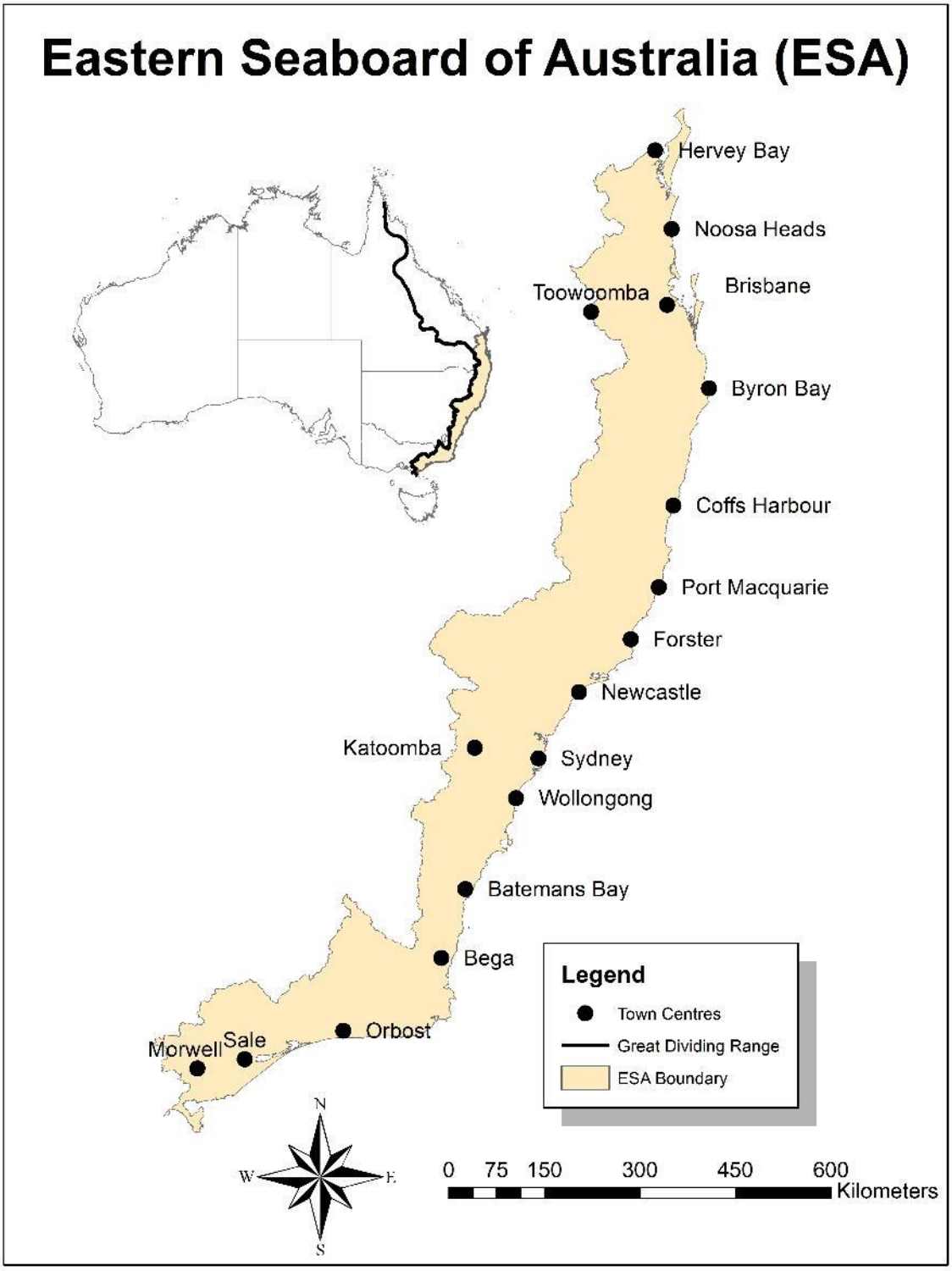

Figure 1: The eastern seaboard of Australia (ESA) – roughly the area between the east coast of Australia and the Great Dividing Range.

1.2 Scope of this study

This study develops eight plausible ECL scenarios for the Bega River catchment and produces stochastically generated daily rainfall and evaporation under these eight ECL scenarios. The stochastically generated daily rainfall and evaporation data will be used as inputs to the Department's hydrological models (e.g. Integrated Quantity and Quality Model (IQQM)) to better understand the

potential impacts of climate change on water supply security in the Bega River region and to assess the adequacy of existing or proposed water supply security infrastructure and/or policy.

This study focusses on:

1. Demonstrating that the stochastic model performs satisfactorily with respect to realistically reproducing the key statistics from the observed record (i.e. number and distribution of rainfall days, multi-site spatial correlation, and multi-variate (rainfall, evaporation) relationships);
2. Illustrating which of the plausible ECL scenarios result in the biggest changes to rainfall and evaporation;
3. Discovering which of the locations in the Bega River catchment are most/least sensitive to changes in ECL behaviour.

2. Data

2.1 Observed daily rainfall and evaporation data (referred to as instrumental data)

Observed (instrumental) daily rainfall and evaporation data for the Bega River region was provided by the Department (see Appendix A for further details on the rainfall and evaporation sites used in this study). In total there were 35 sites (15 rainfall and 20 evaporation). There was no missing data for the period January 1889 to December 2018 (i.e. complete data for 130 calendar years) so this period was defined as the "baseline period" (ECL Scenario 1) and used as the basis for comparison with the other seven ECL scenarios. Summary statistics for annual totals of the 15 rainfall and 20 evaporation sites over the 1889-2018 instrumental period are shown in Appendix B.

2.2 Information about projected changes to rainfall and evaporation in the Bega River region (used for ECL Scenario 2)

ECL Scenario 2 is based on what the "best available evidence" from literature and climate model projections suggests about future (~2050) rainfall and evaporation in the Bega River region. The source of information used to develop ECL Scenario 2 was the Climate Change in Australia resource (https://www.climatechangeinaustralia.gov.au/en/climate-projections/future-climate/regional-climate-change-explorer/sub-clusters/?current=ECSC&tooltip=true&popup=true) – an example of the information available is shown in Figure 2.

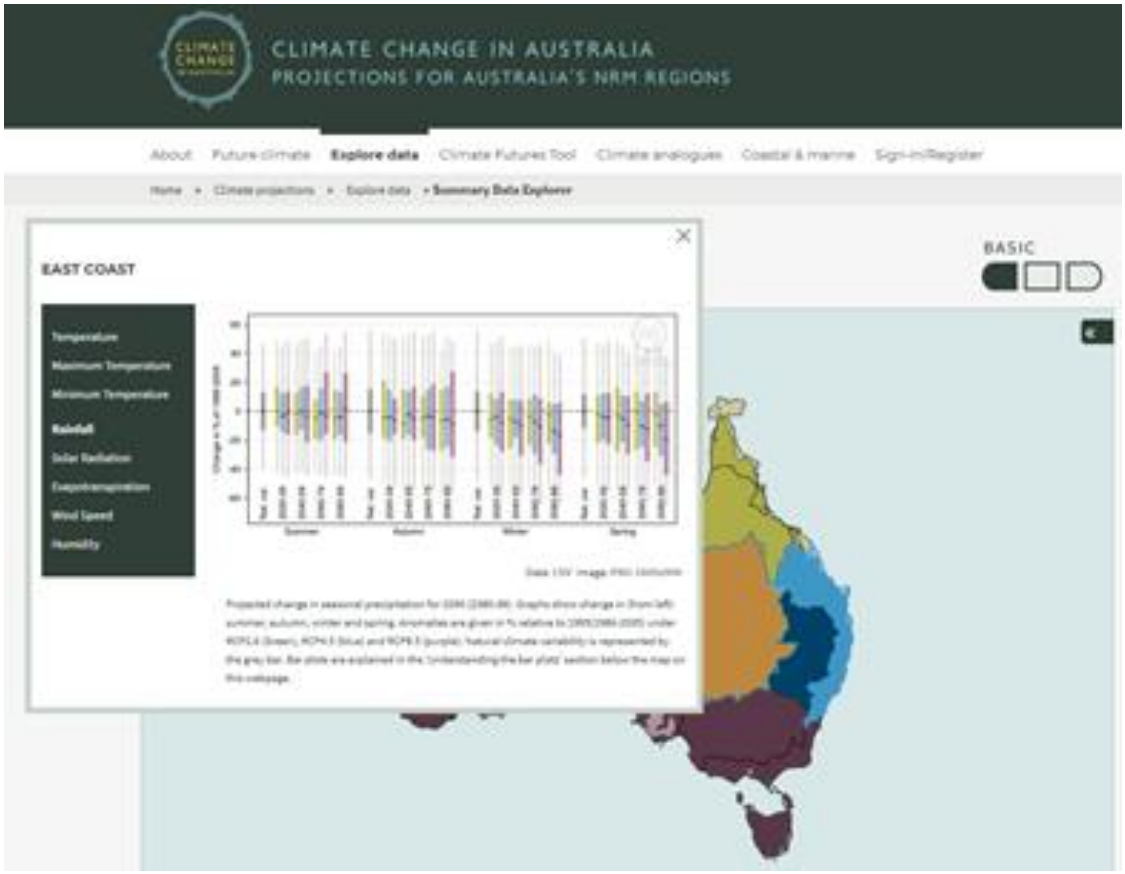

Figure 2: Projected impacts of climate change on rainfall along the east coast of Australia (Source: https://www.climatechangeinaustralia.gov.au/en/climate-projections/explore-data/summary-data-explorer/#).

2.3 Information about projected East Coast Low (ECL) behaviour (used for ECL Scenarios 3-8)

ECL Scenarios 3-8 are based on what the "best available evidence" from literature and climate model projections suggests about how future (~2050) ECL frequency and timing could change in the future. The source of information used to develop ECL Scenarios 3-8 were the reports emerging from Project 2 of ESCCI (www.climatechange.environment.nsw.gov.au/Impacts-of-climate-change/East-Coast-Lows/Eastern-Seaboard-Climate-Change-Initiative).

ESCCI Project 2 used the NSW and Australian Capital Territory (ACT) Regional Climate Modelling (NARCliM, https://climatechange.environment.nsw.gov.au/Climate-projections-for-NSW/About-NARCliM) to downscale climate model outputs and make projections about changes to the frequency, duration and intensity of ECLs.

3. Methodology

3.1 Methodology for stochastic data generation

The daily hydroclimatic data was generated for the required sites using a multi-site stochastic generation based on a lag one autoregressive (AR1) Matalas (1967) model. The multi-site Matalas model was originally developed for application at the annual time scale but this has been adapted in previous work (e.g. McMahon et al., 2008; Mortazavi-Naeini et al., 2015) for application at the daily time scale. The modified multi-site Matalas model uses an AR1 model that preserves the lag-zero and lag-one cross correlations between seasons and locations for all variables (i.e. rainfall and evaporation).

This modified multi-site Matalas model was calibrated (or trained) using the 130 years of historical (i.e. instrumental) daily rainfall and evaporation (January 1889 to December 2018) for the 35 sites (15 rainfall and 20 evaporation) listed in Appendix A. The outputs (100 stochastically generated replicates of 130 years of daily rainfall and evaporation) were then compared with the historical data to determine if the key statistics observed in the instrumental records are accurately reproduced in the stochastically modelled outputs.

3.2 Development of future East Coast Low (ECL) scenarios

3.2.1 ECL Scenario 1 – baseline

ECL Scenario 1 represents the “baseline” case. That is, the inputs for the stochastic generation for ECL Scenario 1 are the observed historical (i.e. instrumental) daily rainfall and evaporation (January 1889 to December 2018) for the 35 sites (15 rainfall and 20 evaporation) listed in Appendix A. ECL Scenario 1 enables quantification of existing (and historical) levels of hydroclimatic variability, and associated risks to water supply security.

3.2.2 ECL Scenario 2 – 10 decrease in rainfall, 10% increase in evaporation

ECL Scenario 2 involves altering the observed historical (i.e. instrumental) daily rainfall and evaporation used for ECL Scenario 1 to incorporate the "best available evidence" from literature and climate model projections suggests about future (~2050) rainfall and evaporation in the Bega River region. For ~2050, the "best available evidence" (see Section 2.2 for details) suggest a 10% decrease in rainfall and a 10% increase in evaporation for the Bega River region. As such, ECL Scenario 2 is developed by applying a 10% decrease to all rainfall and a 10% increase to all evaporation and using the “climate change impacted” time series as inputs for the stochastic generation.

3.2.3 ECL Scenario 3 – remove one ECL per year

The ESCCI research suggests that the frequency and timing of ECLs could change in the future. ECL Scenario 3 is developed by removing one ECL per year from the historical data. This is done by starting with the historical data used for ECL Scenario 1 then, for each year, randomly selecting a day that an ECL occurred and replacing the rainfall that occurred on that day with zero (evaporation remains unchanged). This revised time series is then used as input for the stochastic generation. ECL Scenario 3 (i.e. a decrease of one ECL per year) is considered to be at the lower bound of what is plausible with respect to future changes in ECL frequency.

3.2.4 ECL Scenario 4 – add one ECL per year

ECL Scenario 4 is developed by, for each year, randomly selecting a day and replacing the rainfall and evaporation on that day with the rainfall and evaporation that occurred on a day when an ECL occurred in the historical record. The ECL that is added each time is randomly selected from the full

list of ECLs that have occurred throughout the historical record. This revised time series is then used as input for the stochastic generation. ECL Scenario 4 (i.e. an increase of one ECL per year) is considered to be at the lower bound of what is plausible with respect to future changes in ECL frequency.

3.2.5 ECL Scenario 5 – take one ECL from winter and make it occur in summer instead

ECL Scenario 5 is developed by, for each year, randomly selecting a day during winter (June, July, August) that an ECL occurred and replacing the rainfall that occurred on that day with zero (evaporation remains unchanged). So far this is the same as ECL Scenario 3, however, for ECL Scenario 5 the ECL rainfall removed from winter is inserted on a randomly selected day in summer (evaporation remains unchanged). ECL Scenario 5 (i.e. swapping one ECL per year from winter to summer) is considered to be at the lower bound of what is plausible with respect to future changes in ECL frequency.

3.2.6 ECL Scenario 6 – remove five ECLs per year

ECL Scenario 6 is similar to ECL Scenario 3 except five ECLs per year are removed instead of one. ECL Scenario 5 (i.e. a decrease of five ECLs per year) is considered to be at the upper bound of what is plausible with respect to future changes in ECL frequency.

3.2.7 ECL Scenario 7 – add five ECLs per year

ECL Scenario 7 is similar to ECL Scenario 4 except five ECLs per year are added instead of one. ECL Scenario 7 (i.e. an increase of five ECLs per year) is considered to be at the upper bound of what is plausible with respect to future changes in ECL frequency.

3.2.8 ECL Scenario 8 – take five ECLs from winter and make them occur in summer instead

ECL Scenario 8 is similar to ECL Scenario 5 except five ECLs per year are swapped from winter to summer instead of one. ECL Scenario 8 (i.e. swapping five ECLs per year from winter to summer) is considered to be at the upper bound of what is plausible with respect to future changes in ECL frequency.

4. Results

4.1 Verification that the stochastically generated data accurately reproduces key statistical characteristics

The ability of the stochastic modelling to accurately reproduce key statistical characteristics of the instrumental hydroclimatic data considered important for hydrological modelling and water planning outcomes was objectively assessed at both the annual, monthly, and daily time scale.

4.1.1 Verification of stochastic model performance at the ANNUAL (January to December) time scale

Figure 3 to Figure 7 summarises, for the 15 rainfall and 20 evaporation sites listed in Appendix A, the key annual (January to December) statistics calculated from 130 years of historical data compared with statistics calculated from the stochastically generated data.

Figure 3 to Figure 7 confirms that the differences between the statistics calculated from 130 years of historical data and the statistics calculated from the stochastically generated data is not significant. This demonstrates that the modified multi-site AR1 Matalas stochastic model is satisfactorily replicating key annual statistics of the historical data.

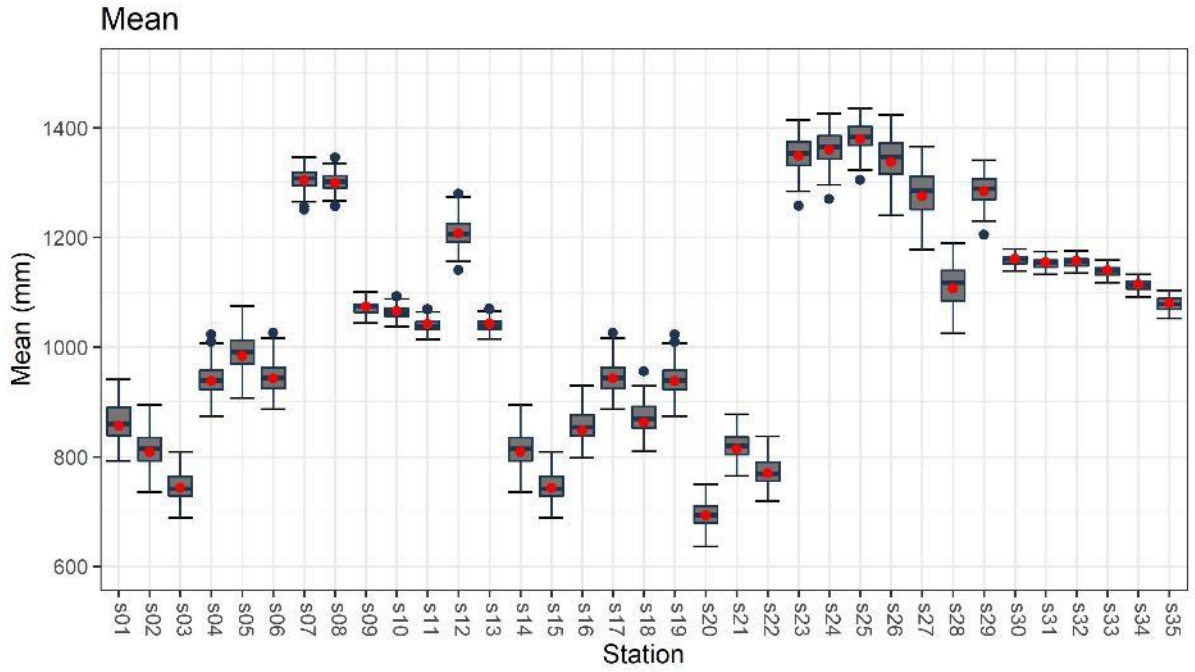

Figure 3: Comparison between annual (January-December) MEAN calculated from 130 years of instrumental data (red dot) and the annual MEANS calculated from the 100 replicates of 130 years of stochastically generated data (box plots).

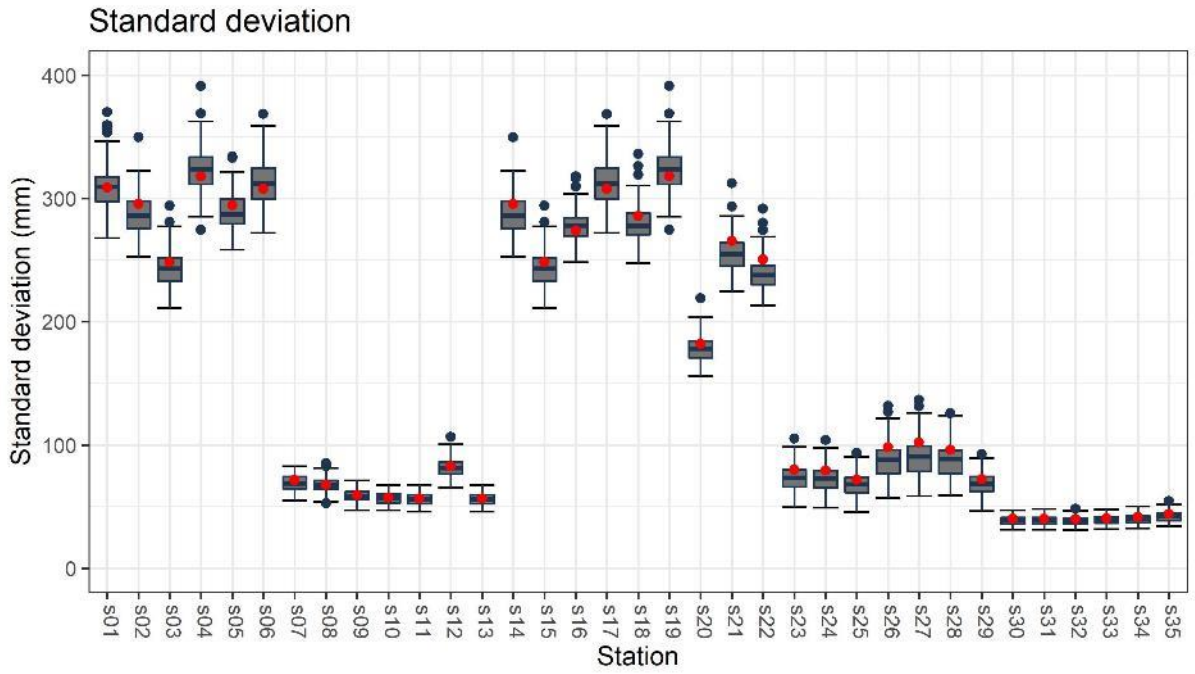

Figure 4: Comparison between annual (January-December) STANDARD DEVIATION calculated from 130 years of instrumental data (red dot) and the annual STANDARD DEVIATIONS calculated from the 100 replicates of 130 years of stochastically generated data (box plots).

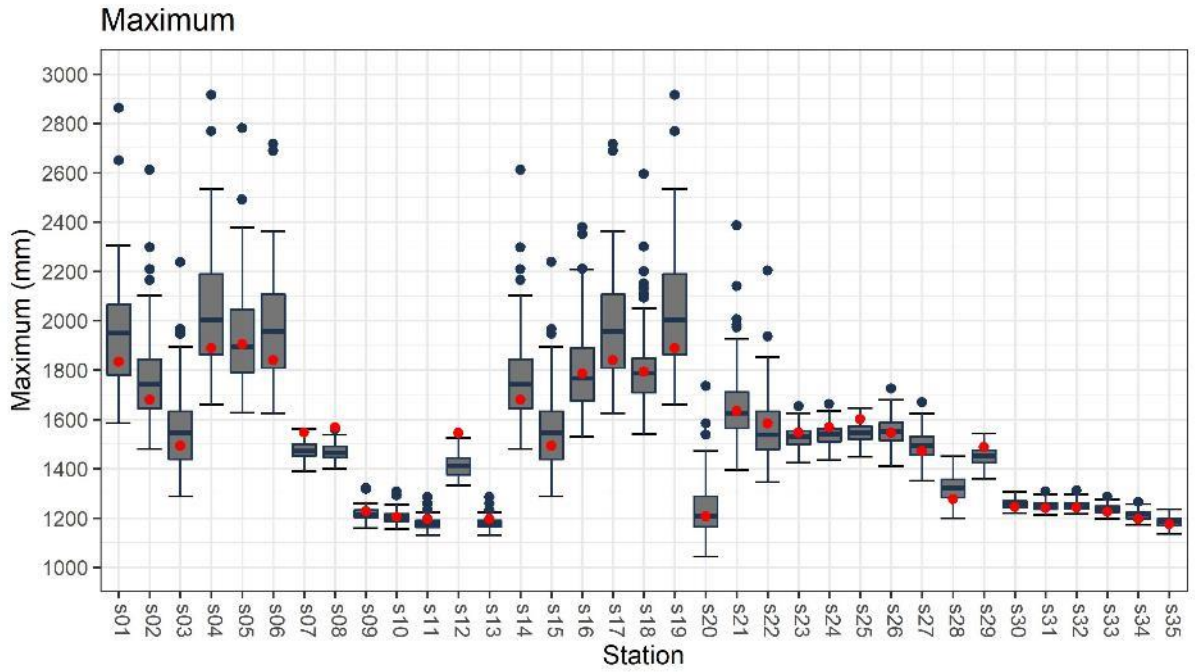

Figure 5: Comparison between annual (January-December) MAXIMUM calculated from 130 years of instrumental data (red dot) and the annual MAXIMUMS calculated from the 100 replicates of 130 years of stochastically generated data (box plots).

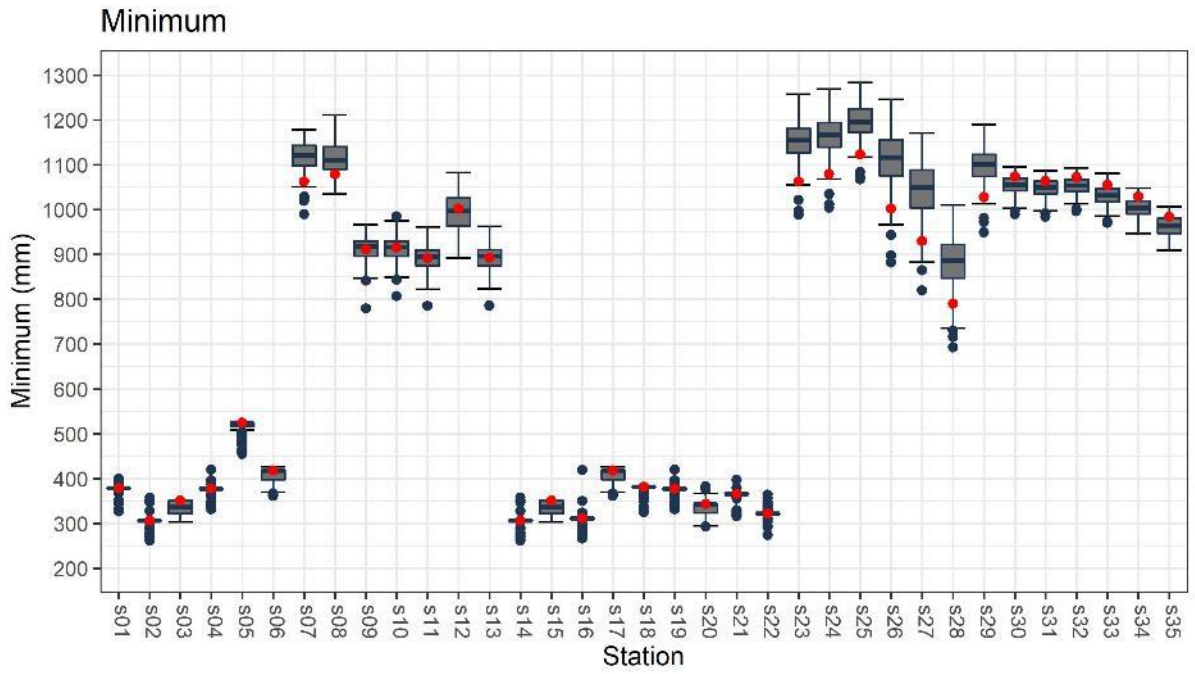

Figure 6: Comparison between annual (January-December) MINIMUM calculated from 130 years of instrumental data (red dot) and the annual MINIMUMS calculated from the 100 replicates of 130 years of stochastically generated data (box plots).

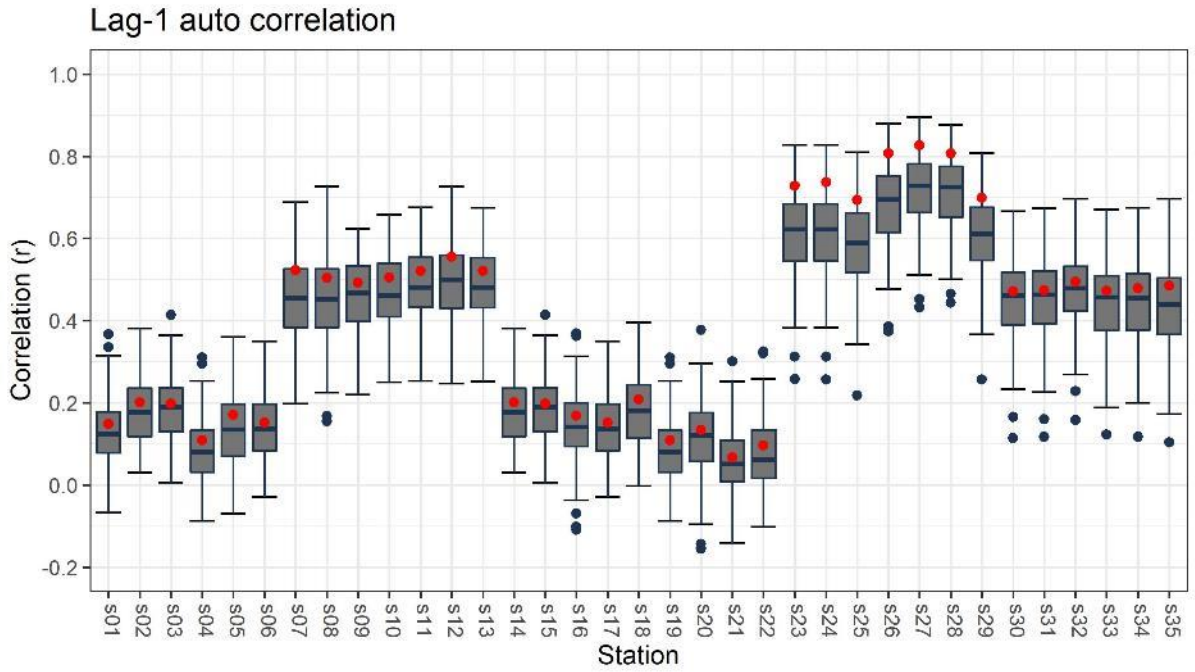

Figure 7: Comparison between annual (January-December) LAG-1 AUTO CORRELATION calculated from 130 years of instrumental data (red dot) and the annual LAG-1 AUTO CORRELATIONS calculated from the 100 replicates of 130 years of stochastically generated data (box plots).

Figure 8 shows the comparison between annual (January to December) lag-zero cross correlations of historical data with those generated by the stochastic model for each of the 15 rainfall and 20 evaporation sites listed in Appendix A (where values for the generated spatial correlations are means of the 100 replicates of 130 years). The average percentage difference (bottom left plot in Figure 8) between historical and the mean of the generated spatial correlations (across all station

combinations) is less than 5% in most cases. This demonstrates that the modified multi-site AR1 Matalas stochastic model is satisfactorily replicating spatial correlations in annual totals that are seen in the historical data.

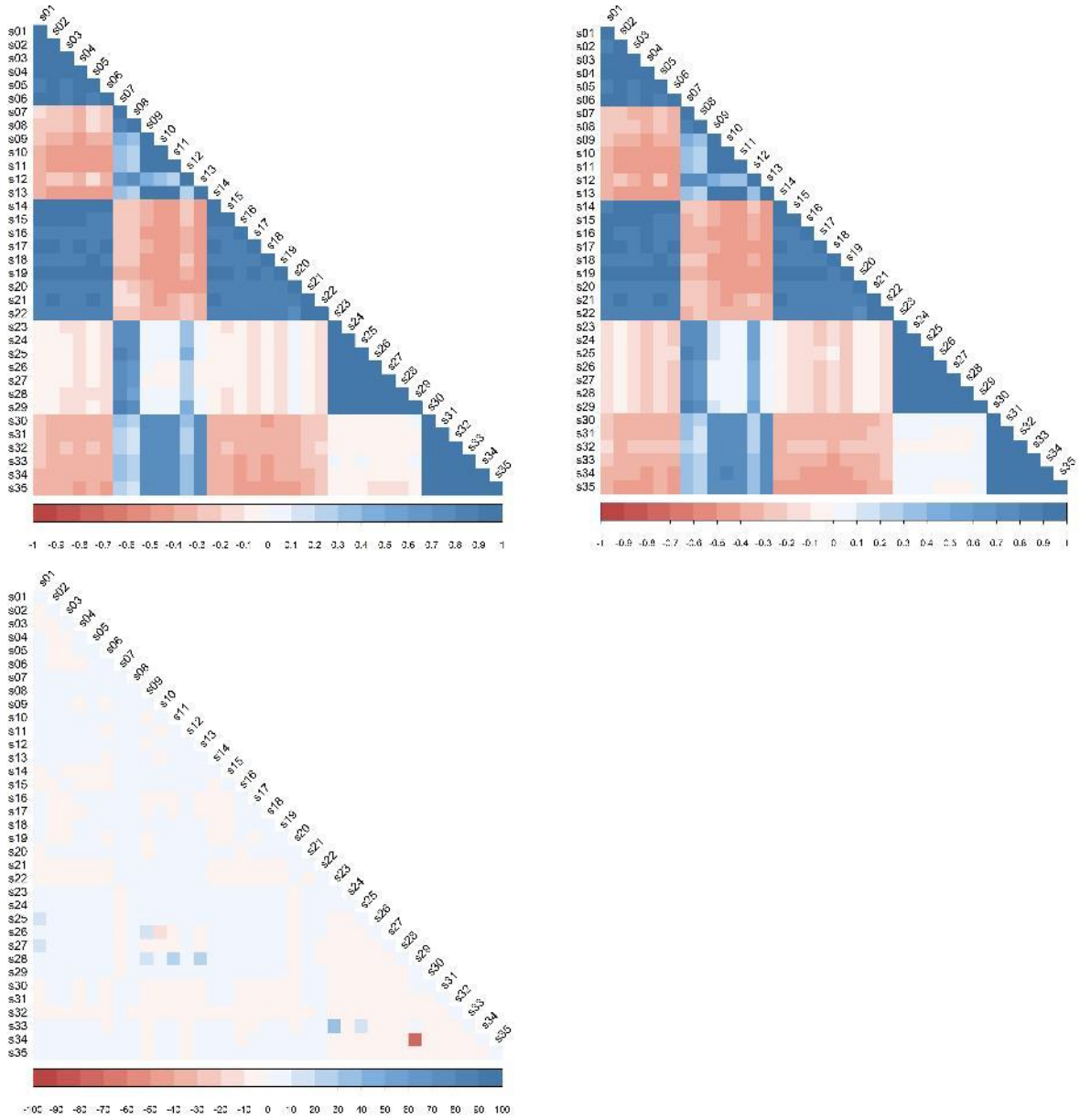

Figure 8: Top left = spatial correlations of ANNUAL totals calculated from 130 years of instrumental data. Top right = spatial correlations of ANNUAL totals calculated from the 100 replicates of 130 years of stochastically generated data (box plots). Bottom left = percentage difference in spatial correlations for observed data (top left) and stochastically generated data (top right) [100 x (generated – instrumental)/instrumental].

4.1.2 Verification of stochastic model performance at the MONTHLY time scale

Appendix B contains plots which demonstrate that the modified multi-site AR1 Matalas stochastic model is satisfactorily replicating key monthly statistics of the historical data.

4.1.3 Verification of stochastic model performance at the DAILY time scale

Figure 9, Figure 10, and Figure 11 demonstrate that the modified multi-site AR1 Matalas stochastic model also satisfactorily replicates historical data at the daily time scale (since the scatter plots for the first three replicates of stochastically generated data (and the associated coefficient of determination

(r^2) are very similar to the scatter plot for the instrumental data (top left in each case)). Note that only the information for the first three replicates is shown in this report but the story is the same for all replicates.

Figure 12 shows that the percentage difference when spatial correlations at the daily time scale for the instrumental record is compared with spatial correlations at the daily time scale for the first three replicates of stochastically generated data is less than 5% in all cases. Note again that only the information for the first three replicates is shown in this report but the story is the same for all replicates. This again demonstrates that the modified multi-site AR1 Matalas stochastic model is satisfactorily replicating spatial correlations seen in the historical data.

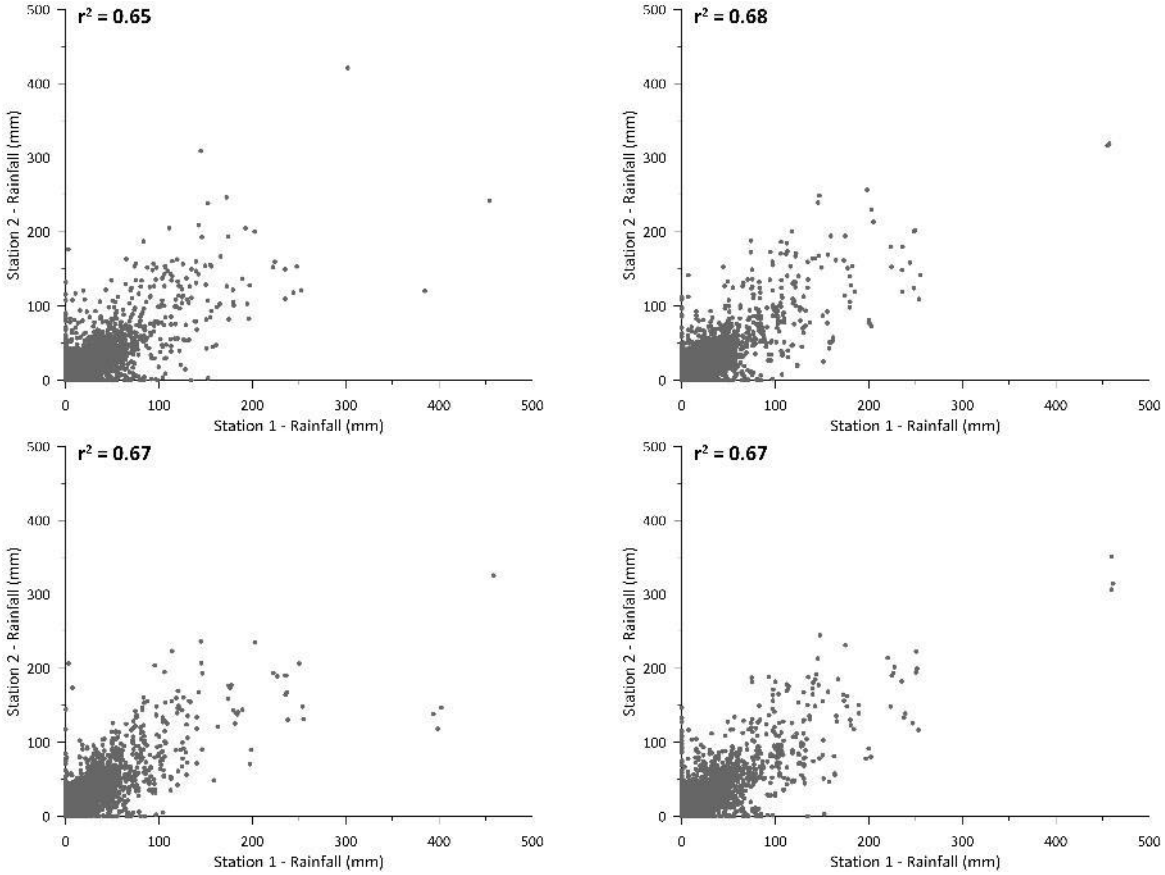

Figure 9: Scatter plots comparing daily rainfall at Station 1 with daily rainfall at Station 2 for instrumental data (top left), stochastic replicate #1 (top right), stochastic replicate #2 (bottom left), and stochastic replicate #3 (bottom right).

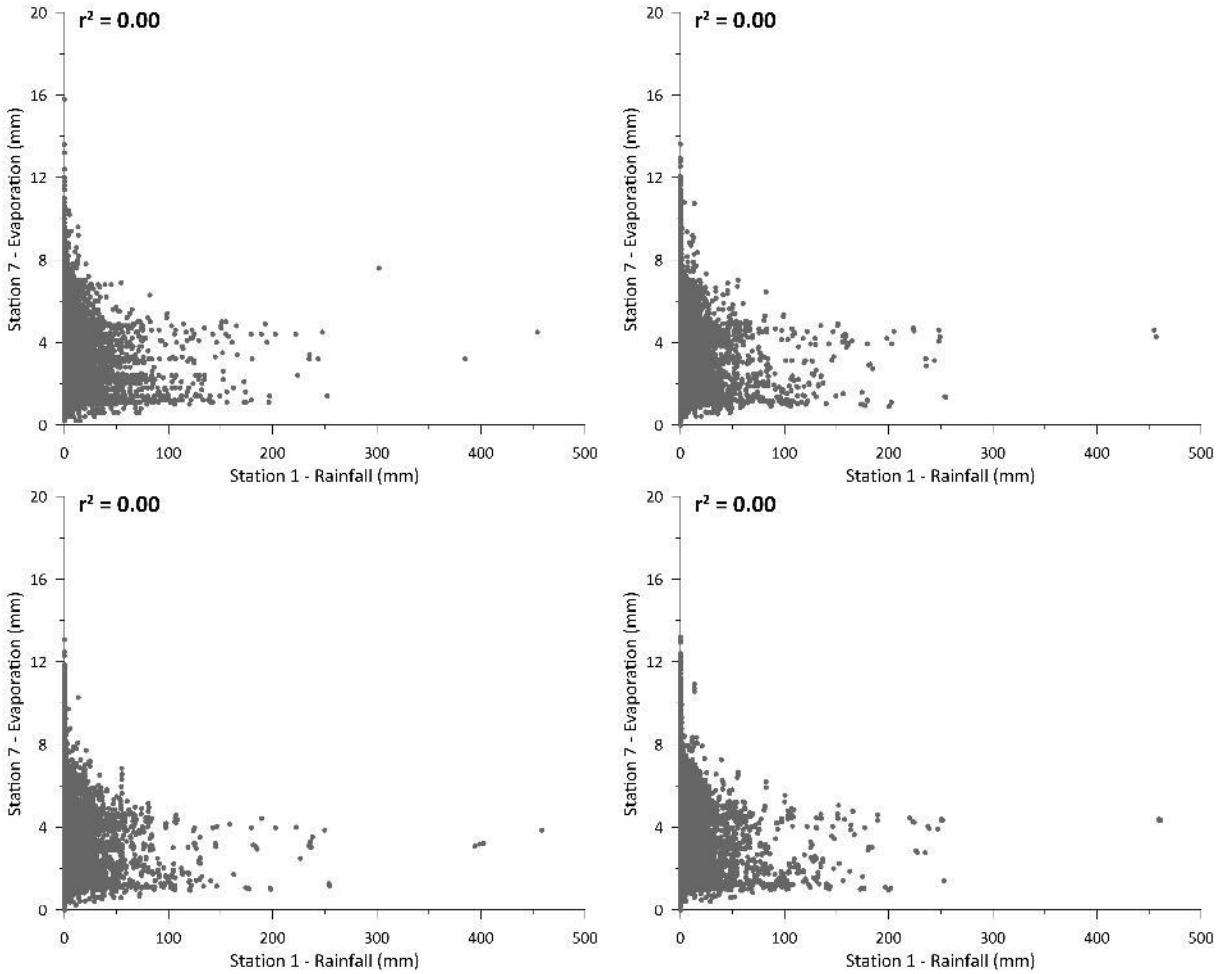

Figure 10: Scatter plots comparing daily rainfall at Station 1 with daily evaporation at Station 7 for instrumental data (top left), stochastic replicate #1 (top right), stochastic replicate #2 (bottom left), and stochastic replicate #3 (bottom right).

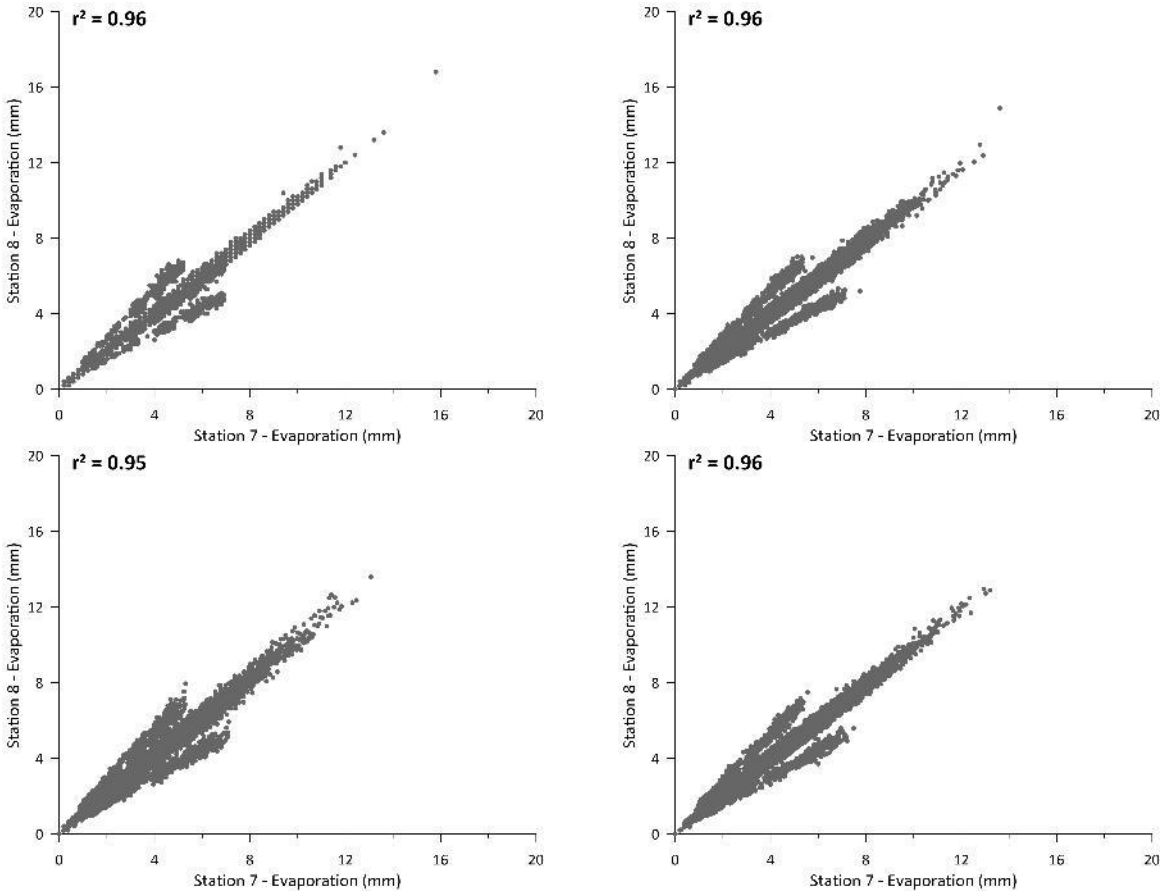

Figure 11: Scatter plots comparing daily evaporation at Station 7 with daily evaporation at Station 8 for instrumental data (top left), stochastic replicate #1 (top right), stochastic replicate #2 (bottom left), and stochastic replicate #3 (bottom right).

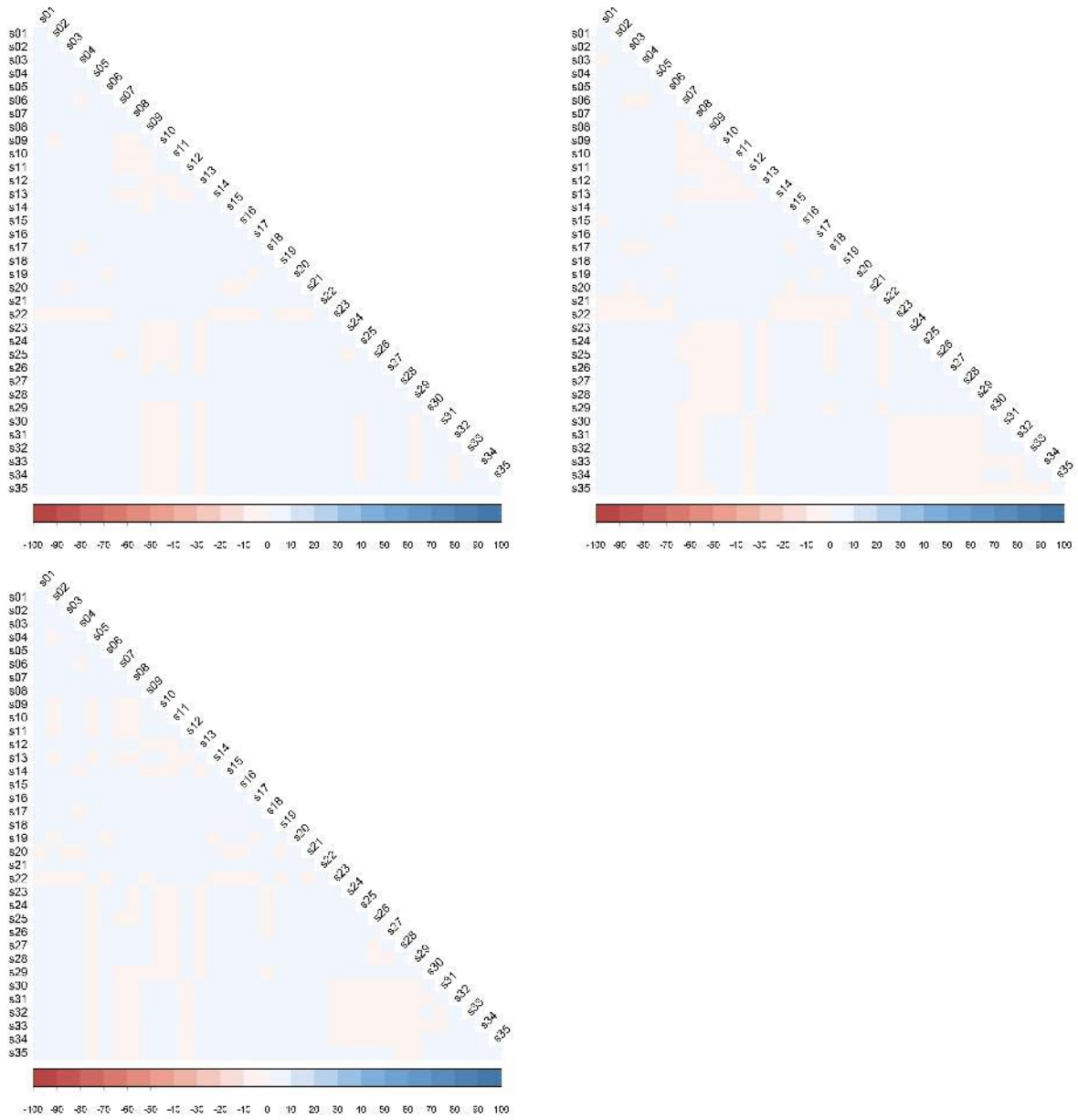

Figure 12: Percentage difference in spatial correlations for DAILY data at the study sites. Top left is instrumental versus stochastic replicate #1. Top right is instrumental versus stochastic replicate #2. Bottom left is instrumental versus stochastic replicate #3.

4.1.4 Verification of stochastic model performance at the interannual to multidecadal time scale (i.e. multi-year statistics)

The results in Section 4.1.1 to Section 4.1.3 are necessary, but not sufficient, validation checks of a stochastic model. Further assessment is required, since as Srikanthan and McMahon (2003) point out, a good stochastic model should preserve other statistics (e.g. maximum, minimum, range, and the minimum 2-year, 3-year, 5-year, 7-year and 10-year sums) as well as the mean, variation, skew and auto-correlation. To assess stochastic model performance (i.e. how well the generated data preserves key statistics of the historical data), Srikanthan and McMahon (2003) developed decision rules covering the number of parameters to be preserved and the tolerance limits on the difference between statistics of the generated and historical data. Following Srikanthan and McMahon (2003), the data generated by the stochastic model are evaluated using the tolerance limits given in Table 1. The number of average annual parameters from all replicates that are within the tolerance limit is counted as follows:

1. *N1 (N2)* is the number of basic model parameters (mean, standard deviation, skewness, lag 1 autocorrelation) that are within Tolerance Limit 1 (Tolerance Limit 2).
2. *M1 (M2)* is the number of the remaining eight validation statistics that are within Tolerance Limit 1 (Tolerance Limit 2).

If $N1 = 4$ and $M1 \geq 6$ the generated data is considered "good". If $N2 = 4$ and $M2 \geq 6$ the generated data is considered "fair". Otherwise the stochastically generated data (and the model that produced it) is considered "poor".

Table 1: Tolerance Limits for differences in key statistics when historical hydroclimatic data is compared with stochastically generated data (based on Srikanthan and McMahon (2003)).

	Parameter	Tolerance Limit 1	Tolerance Limit 2
1	Mean (%)	5	10
2	Standard deviation (%)	5	10
3	Coefficient of skewness	0.5	1
4	Lag 1 autocorrelation coeff	0.15	0.25
5	Maximum (%)	10	25
6	Minimum (%)	10	25
7	Adjusted range (%)	10	25
8	Min 2-yr rainfall sum (%)	10	25
9	Min 3-yr rainfall sum (%)	10	25
10	Min 5-yr rainfall sum (%)	10	25
11	Min 7-yr rainfall sum (%)	10	25
12	Min 10-yr rainfall sum (%)	10	25

Table 2 shows the results of assessment of the performance of the modified multi-site AR1 Matalas stochastic model for the 15 rainfall and 20 evaporation sites listed in Appendix A. Table 2 demonstrates that the stochastic model used here is performing satisfactorily, with the model ranking as "good" for all rainfall and evaporation sites. The stochastic model performance was not classed as "poor" at any of the rainfall or evaporation sites.

Table 2: Stochastic model assessment (based on Srikanthan and McMahon (2003)). Rainfall and evaporation site numbers refer to the sites as they are detailed in Appendix A.

Site	*N1*	*M1*	*N2*	*M2*	Quality
1	4	7	4	8	GOOD
2	4	6	4	8	GOOD
3	4	6	4	8	GOOD
4	4	6	4	8	GOOD
5	4	6	4	8	GOOD
6	4	6	4	8	GOOD
7	4	7	4	8	GOOD
8	4	7	4	8	GOOD
9	4	7	4	8	GOOD
10	4	6	4	8	GOOD
11	4	6	4	8	GOOD
12	4	6	4	8	GOOD
13	4	6	4	8	GOOD

14	4	6	4	8	GOOD
15	4	6	4	8	GOOD
16	4	6	4	8	GOOD
17	4	6	4	8	GOOD
18	4	6	4	8	GOOD
19	4	6	4	8	GOOD
20	4	6	4	8	GOOD
21	4	6	4	8	GOOD
22	4	7	4	8	GOOD
23	4	6	4	8	GOOD
24	4	6	4	8	GOOD
25	4	6	4	8	GOOD
26	4	6	4	8	GOOD
27	4	7	4	8	GOOD
28	4	6	4	8	GOOD
29	4	6	4	8	GOOD
30	4	6	4	8	GOOD
31	4	6	4	8	GOOD
32	4	7	4	8	GOOD
33	4	7	4	8	GOOD
34	4	7	4	8	GOOD
35	4	6	4	8	GOOD

4.2 Changes to rainfall and evaporation in the Bega River region under different East Coast Low (ECL) scenarios

Figure 13 shows, for one site and one replicate, the changes to hydroclimatic conditions associated with each of the ECL scenarios investigated. As expected, the rainfall distributions for each ECL scenario are very different and the impact on runoff (and water availability) under each of these different scenarios is expected to be significant.

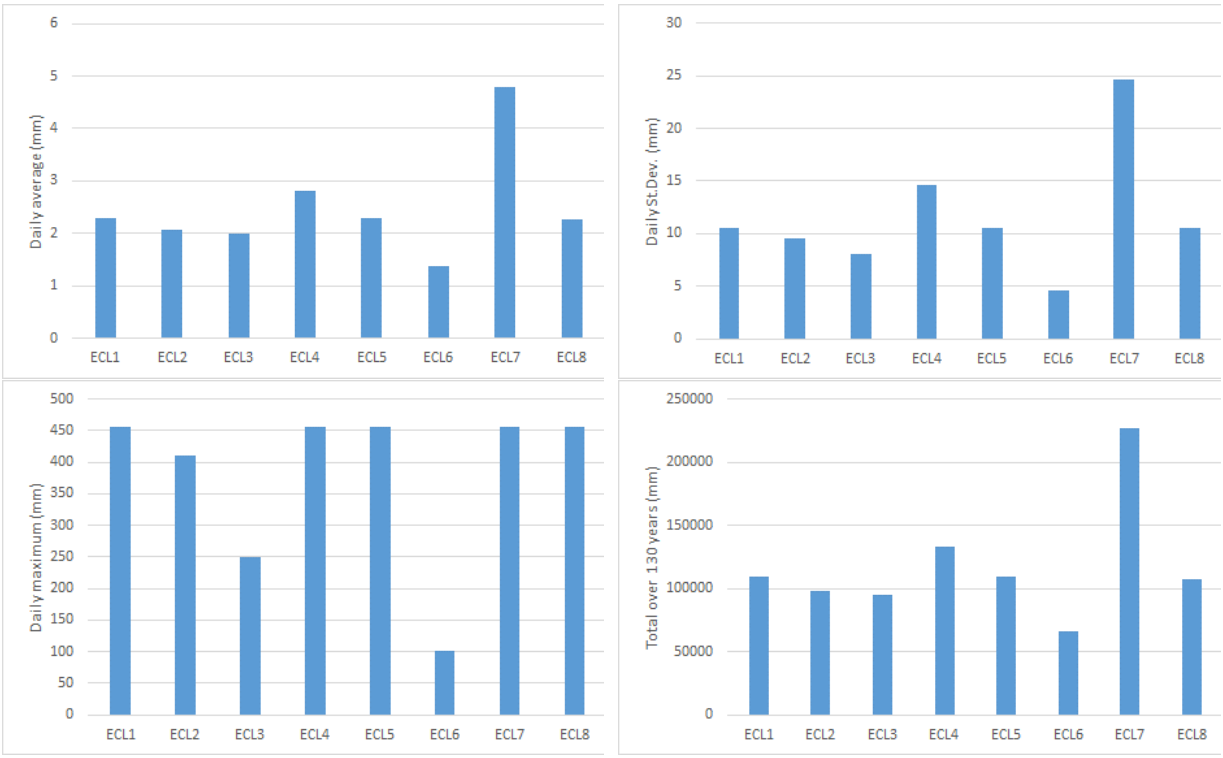

Figure 13: For replicate #1 at site #1, average (top left), standard deviation (top right), maximum (bottom left), and total over 130 years (bottom right) for daily rainfall under the eight different ECL scenarios.

5. Limitations of this study

Limitation 1 is the assumption that the historical/instrumental record (1889-2018) used captures the full range of hydroclimatic variability that has occurred or that is possible due to natural variability. Recent palaeoclimate research suggests this is unlikely and that there are numerous examples of pre-instrumental epochs where the hydroclimatic variability (and associated drought/flood risk) was markedly different to that implied by the historical/instrumental record (1889-2018).

Limitation 2 is that there is an underlying assumption in the multi-site stochastic modelling that the spatial correlations observed in the instrumental period will also apply in the future (and that they also applied in the pre-instrumental period). This is currently no evidence available to determine whether this assumption is valid or not.

6. Conclusion

6.1 Key findings

This study shows that:

1. The modified multi-site AR1 Matalas stochastic model satisfactorily replicates key statistics from the historical data and therefore can be used to generate hydroclimatic scenarios for use as proxies for understanding the potential impacts of climate change on water supply security in the Bega River region.
2. Even small changes to the number and timing of ECL events that occur within a year has a significant impact on rainfall characteristics and these changes to rainfall amounts, timing, and sequencing will likely have even greater impact on runoff, water availability, and associated water supply security.
3. Some locations in the Bega River region are more sensitive to changes in ECL behaviour than others. This is useful information as it could:
    a. help target resources by, for example, focussing first on the locations catchments that are most sensitive to ECL changes and doing what is required to reduce sensitivity and increase resilience;
    b. inform regional water strategies (as opposed to catchment or location focussed) by, where feasible, linking catchments that are most sensitive to ECL changes with catchments that are less sensitive to help improve overall regional resilience in years when there are less ECLs and allow opportunities (i.e. extra water) to be better utilised and capitalised on in years when there are more ECLs.

6.2 Recommendations

Recommendation 1: Address **Limitation 1** by incorporating insights from palaeoclimate research into the hydroclimatic scenarios and associated stochastic modelling.

Recommendation 2: The stochastic data generated here gives insights into the frequency, magnitude, duration and timing of wet/dry phases that are plausible. However, the focus of this report is just on rainfall and evaporation. The next step is to use the stochastically generated hydroclimate data (for each of the eight ECL scenarios) as inputs to hydrological and water supply models to answer questions such as:

- Which locations are the most hydrologically sensitive to changes in ECL behaviour (i.e. which locations show the greatest/least changes in runoff and water availability for each of the different ECL scenarios)?
- What are the socioeconomic and environmental implications of a period wetter/drier than the wettest/driest on record occurring?
- How does the frequency, magnitude, duration and timing of flood/drought indicated by the instrumental record compare with what occurs under ECL Scenarios 2-8?
- How do existing flood/drought risk estimates (i.e. those primarily based on the instrumental record) compare with what occurs under ECL Scenarios 2-8?
- How does flood/drought risk change over time and how vulnerable (or resilient) are existing water resources infrastructure and management strategies to such changes?

7. Acknowledgements

Thanks to Dushmanta Dutta, Aaron Trim, and Katie Brookes from New South Wales Department of Industry – Lands and Water for preparing and supplying the data used as the basis for the stochastic generation described in this report, for double checking the hydroclimatic data reconstructions and stochastic data produced and for discussing the objectives, scope and findings of this project.

8. References

Matalas, N.C. (1967): Mathematical assessment of synthetic hydrology. Water Resources Research, 3(4), 937-945.

McMahon, T.A., Kiem, A.S., Peel, M.C., Jordan, P.W. and Pegram, G.G.S. (2008): A new approach to stochastically generating six-monthly rainfall sequences based on Empirical Model Decomposition. Journal of Hydrometeorology, 9, 1377-1389.

Mortazavi-Naeini, M., Kuczera, G., Kiem, A.S., Cui, L., Henley, B., Berghout, B. and Turner, E. (2015): Robust optimization to secure urban bulk water supply against extreme drought and uncertain climate change. Environmental Modelling & Software, 69, 437-451, doi:10.1016/j.envsoft.2015.02.021.

Srikanthan, R. and McMahon, T.A. (2003): Automatic evaluation of stochastically generated rainfall data. *Proc. 28th International Hydrology and Water Resources Symposium,* Wollongong, Australia, 10–14 November 2003.

Appendix A. List of rainfall and evaporation sites used in this study

Site	Data type	Site Name	Notes
1	Rainfall	069002S.PTO	
2	Rainfall	069003S.PTO	Same as 69003_SILO_Rain.FORS.csv
3	Rainfall	069013S.PTO	Same as 69013_SILO_Rain.FORS.csv
4	Rainfall	069065S.PTO	Same as 69065_SILO_Rain.FORS.csv
5	Rainfall	070237S.PTO	
6	Rainfall	069051S.PTO	Same as 69051_SILO_Rain.FORS.csv
7	Evaporation	069003S.evm	
8	Evaporation	069013S.evm	
9	Evaporation	069002S.F56	
10	Evaporation	069003S.F56	
11	Evaporation	069013S.F56	
12	Evaporation	069051S.e09	
13	Evaporation	069107S.F56	
14	Rainfall	69003_SILO_Rain.FORS.csv	
15	Rainfall	69013_SILO_Rain.FORS.csv	
16	Rainfall	69024_SILO_Rain.FORS.csv	
17	Rainfall	69051_SILO_Rain.FORS.csv	
18	Rainfall	69054_SILO_Rain.FORS.csv	
19	Rainfall	69065_SILO_Rain.FORS.csv	
20	Rainfall	70067_SILO_Rain.FORS.csv	
21	Rainfall	70106_SILO_Rain.FORS.csv	
22	Rainfall	069026_silo_rain.fors.csv	
23	Evaporation	069003_SILO_Evap.FORS.csv	
24	Evaporation	069013_SILO_Evap.FORS.csv	
25	Evaporation	069024_SILO_Evap.FORS.csv	
26	Evaporation	069051_SILO_Evap.FORS.csv	
27	Evaporation	069065_SILO_Evap.FORS.csv	
28	Evaporation	070106_SILO_Evap.FORS.csv	
29	Evaporation	069026_silo_evap.fors.csv	
30	Evaporation	069003_SILO_Mwet.FORS.csv	
31	Evaporation	069013_SILO_Mwet.FORS.csv	
32	Evaporation	069024_SILO_Mwet.FORS.csv	
33	Evaporation	069051_SILO_Mwet.FORS.csv	
34	Evaporation	069065_SILO_Mwet.FORS.csv	
35	Evaporation	070106_SILO_Mwet.FORS.csv	

Appendix B. Plots demonstrating that the stochastic model performs satisfactorily at the MONTHLY time scale

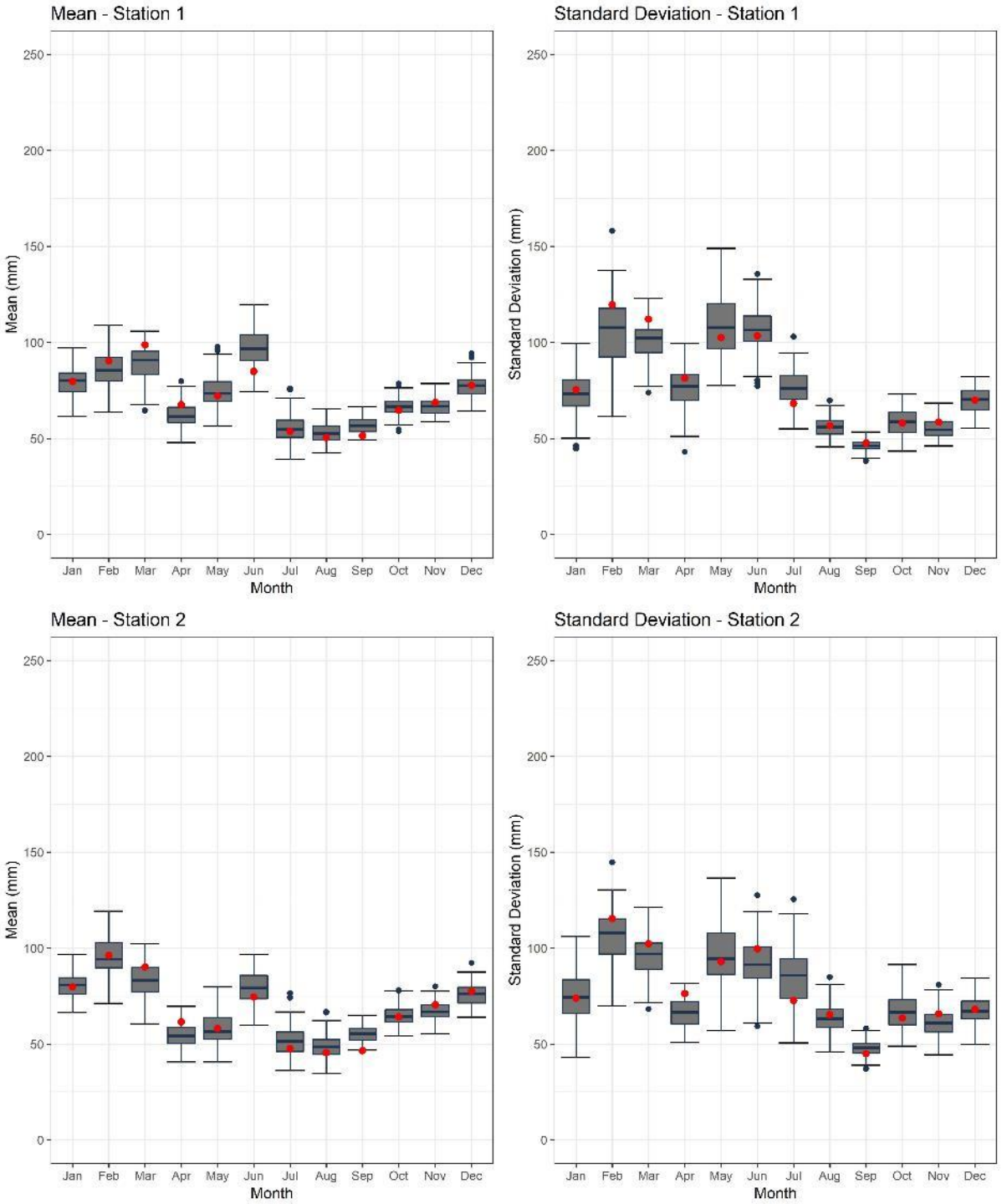

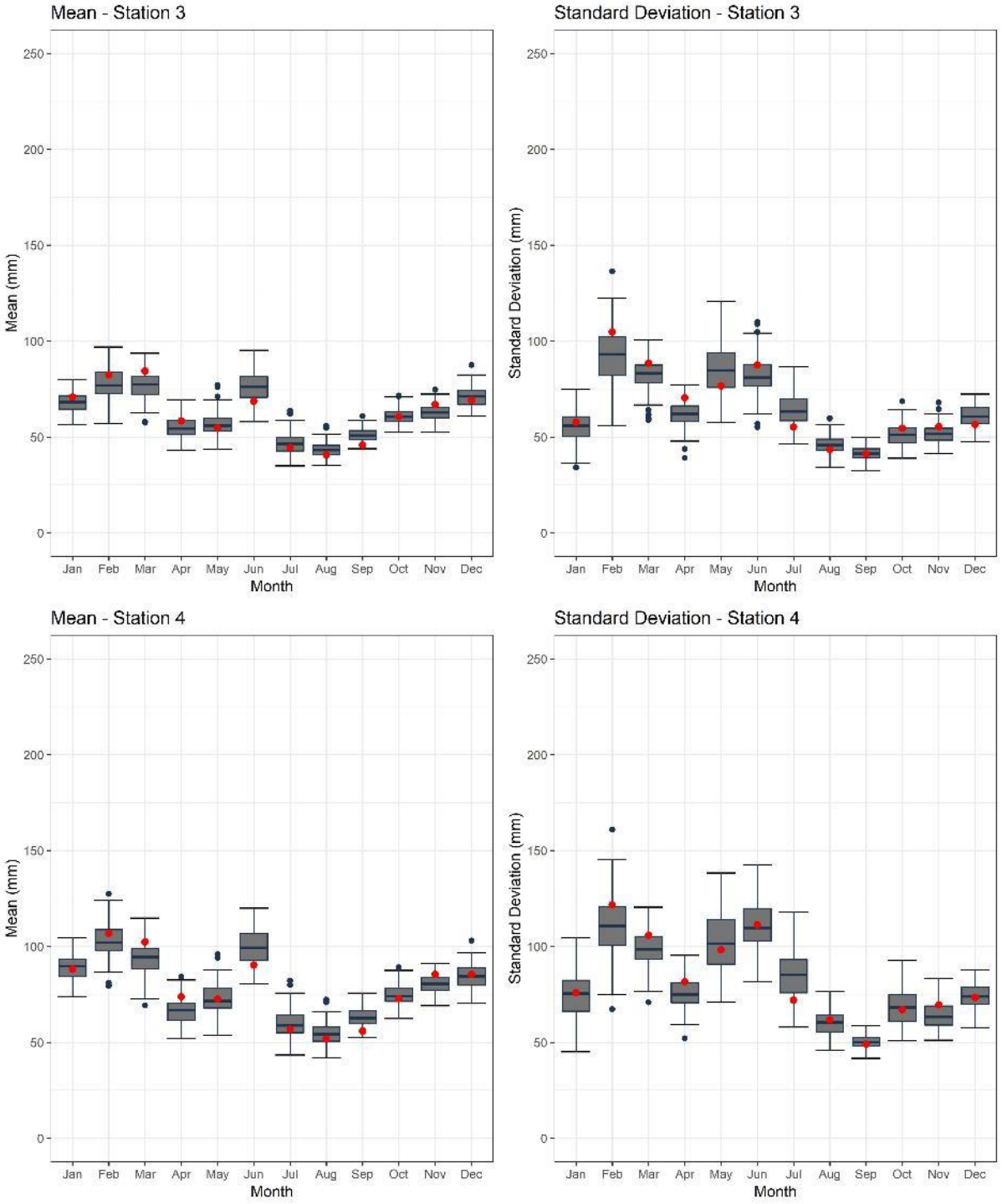
Mean - Station 3
Mean (mm)
Month
Standard Deviation - Station 3
Standard Deviation (mm)
Month
Mean - Station 4
Mean (mm)
Month
Standard Deviation - Station 4
Standard Deviation (mm)
Month
Jan Feb Mar Apr May Jun Jul Aug Sep Oct Nov Dec
0 50 100 150 200 250

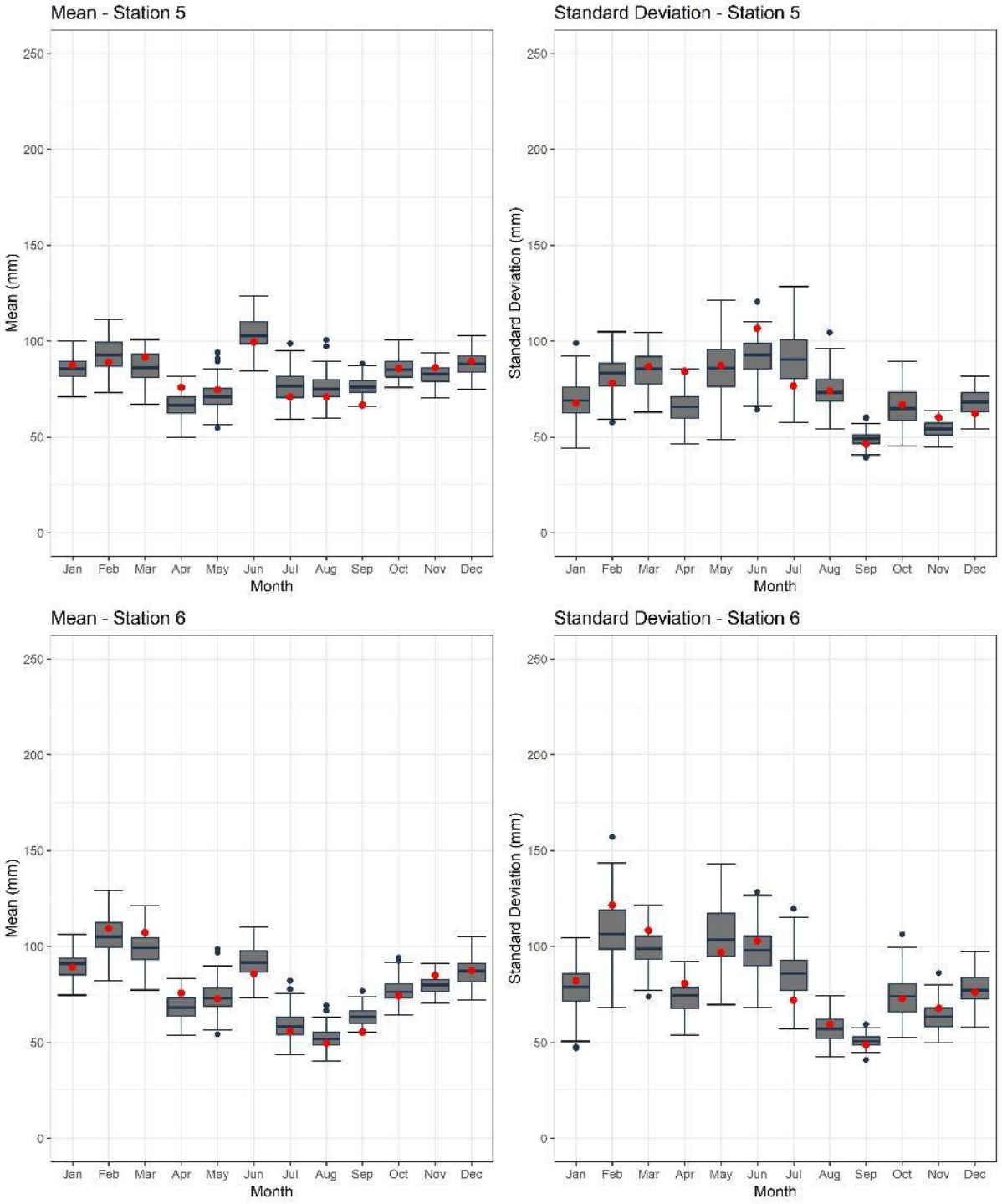
Mean - Station 5
Mean (mm)
Month
Standard Deviation - Station 5
Standard Deviation (mm)
Month
Mean - Station 6
Mean (mm)
Month
Standard Deviation - Station 6
Standard Deviation (mm)
Month
0
50
100
150
200
250
Jan
Feb
Mar
Apr
May
Jun
Jul
Aug
Sep
Oct
Nov
Dec

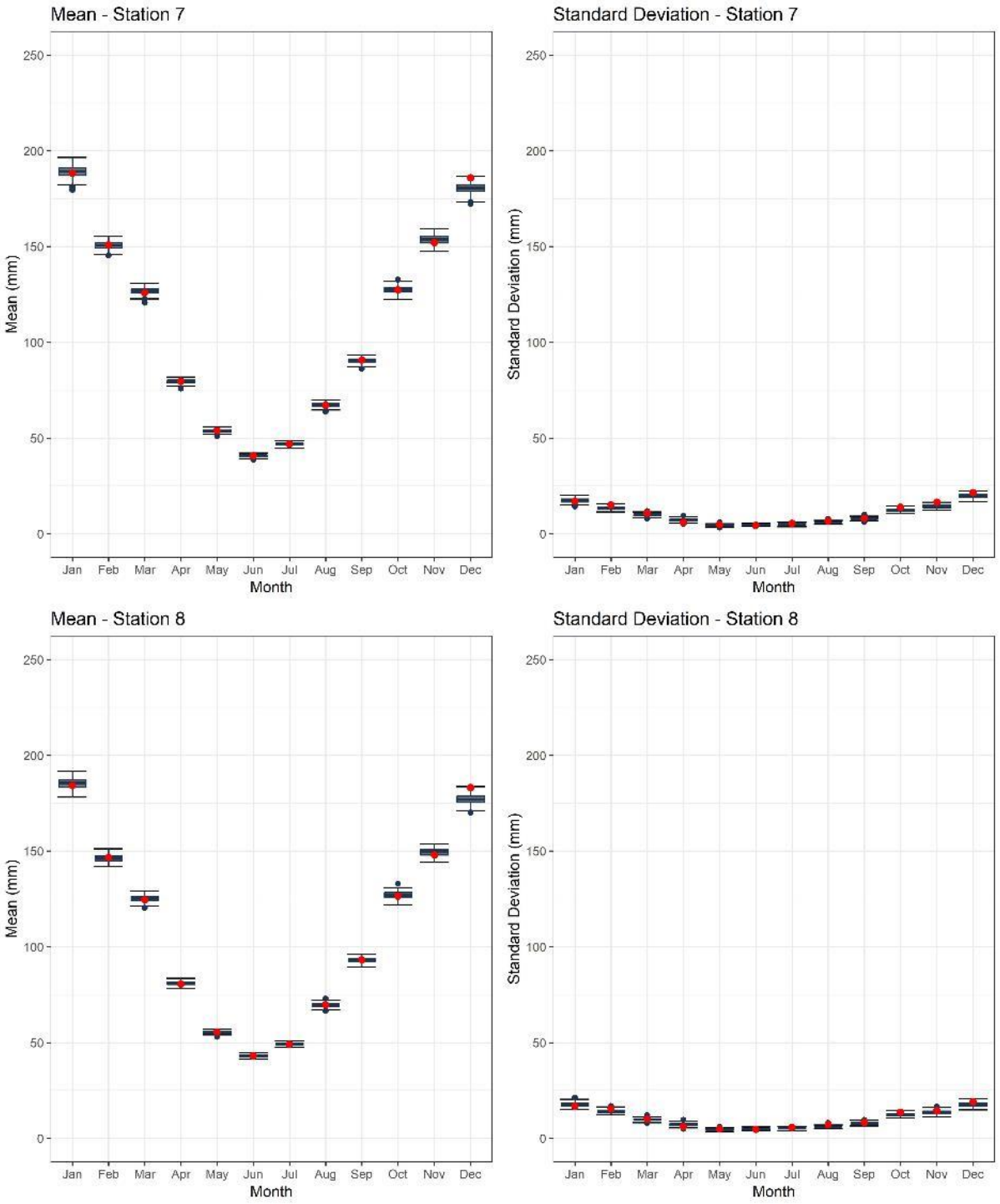
Mean - Station 7
Mean (mm)
Month
Standard Deviation - Station 7
Standard Deviation (mm)
Month
Mean - Station 8
Mean (mm)
Month
Standard Deviation - Station 8
Standard Deviation (mm)
Month
0
50
100
150
200
250
Jan
Feb
Mar
Apr
May
Jun
Jul
Aug
Sep
Oct
Nov
Dec

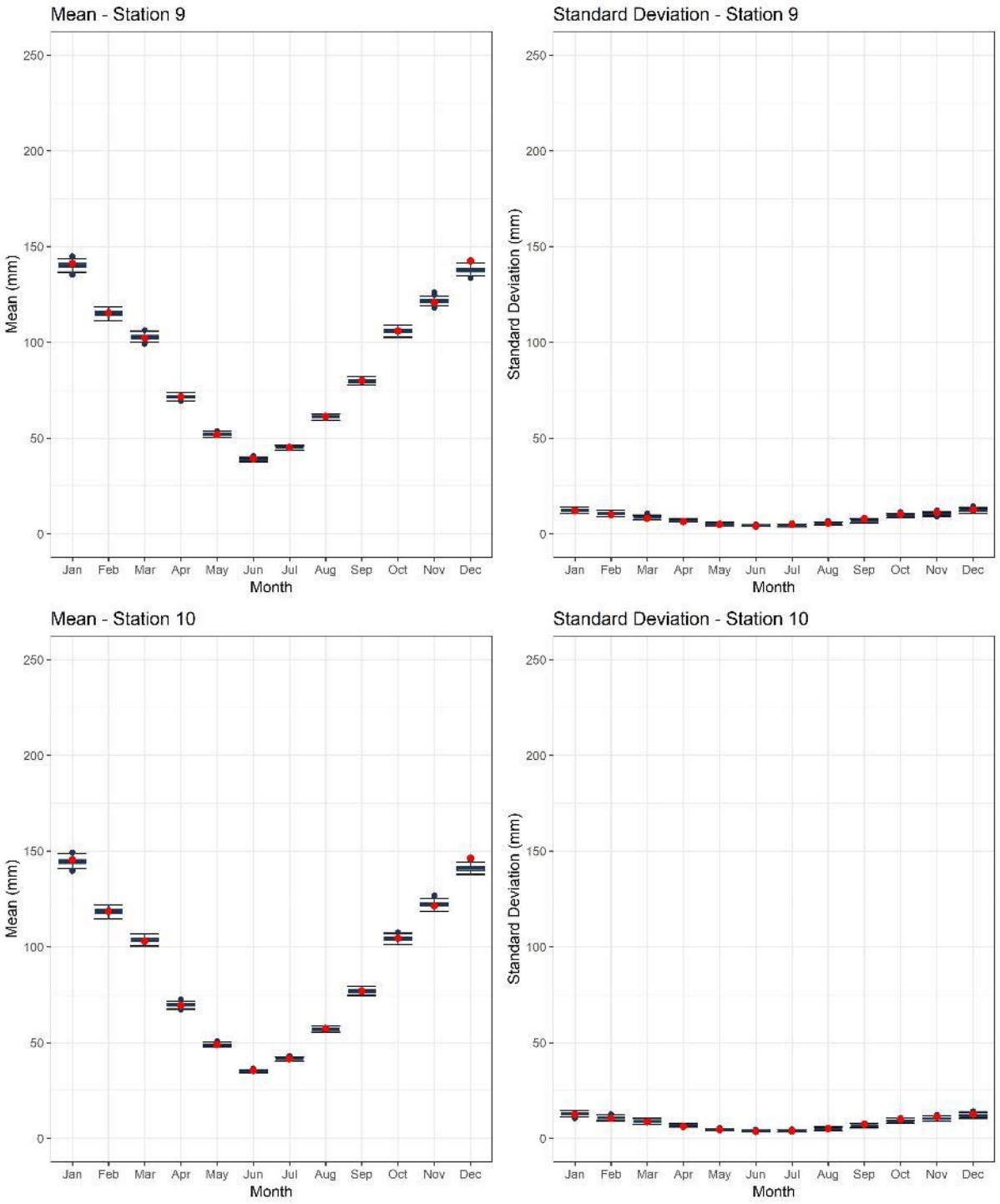
Mean - Station 9
Mean (mm)
Month
Standard Deviation - Station 9
Standard Deviation (mm)
Month
Mean - Station 10
Mean (mm)
Month
Standard Deviation - Station 10
Standard Deviation (mm)
Month
0
50
100
150
200
250
Jan
Feb
Mar
Apr
May
Jun
Jul
Aug
Sep
Oct
Nov
Dec

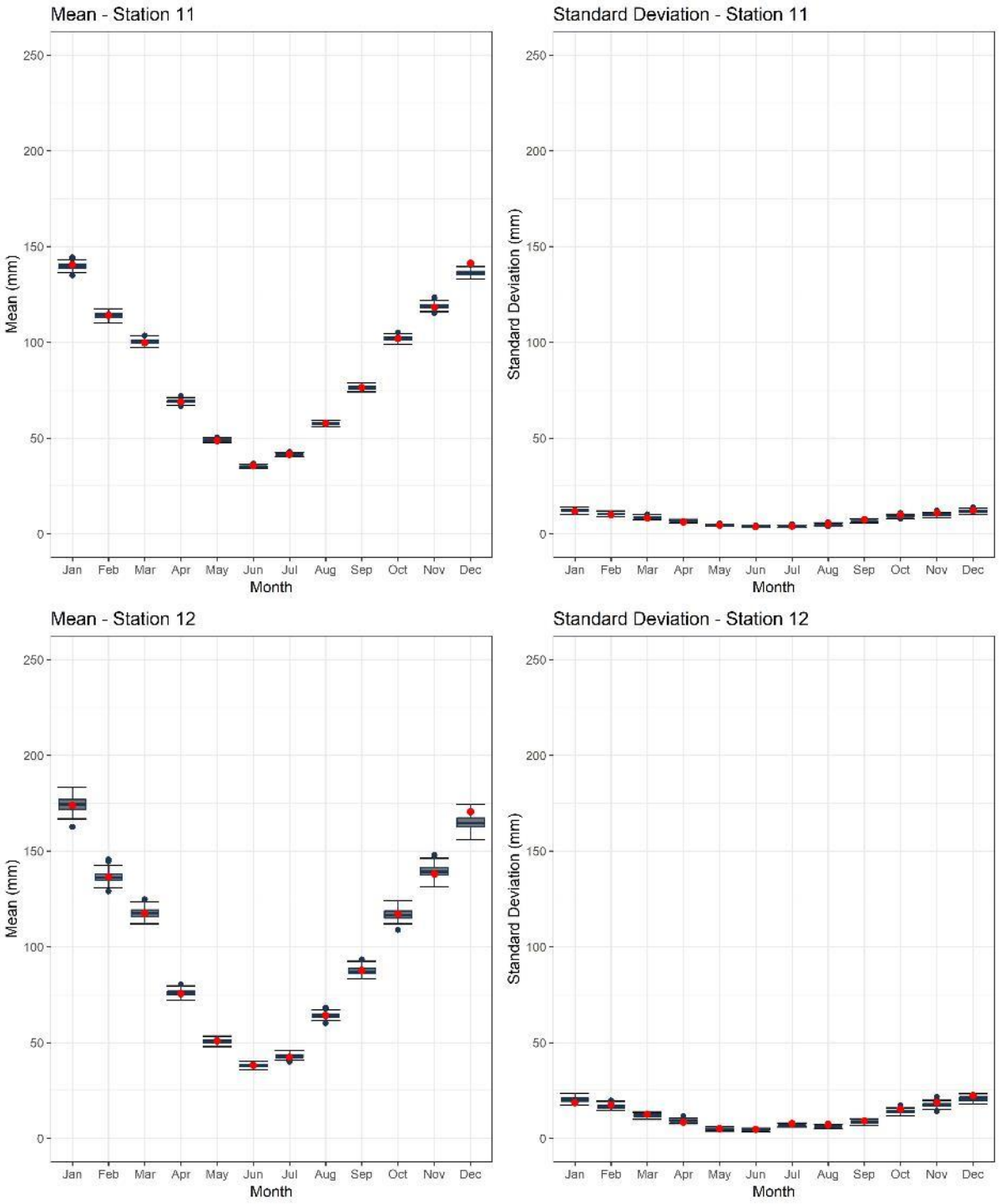
Mean - Station 11
Mean (mm)
Month
Jan Feb Mar Apr May Jun Jul Aug Sep Oct Nov Dec
0 50 100 150 200 250
Standard Deviation - Station 11
Standard Deviation (mm)
Month
Jan Feb Mar Apr May Jun Jul Aug Sep Oct Nov Dec
0 50 100 150 200 250
Mean - Station 12
Mean (mm)
Month
Jan Feb Mar Apr May Jun Jul Aug Sep Oct Nov Dec
0 50 100 150 200 250
Standard Deviation - Station 12
Standard Deviation (mm)
Month
Jan Feb Mar Apr May Jun Jul Aug Sep Oct Nov Dec
0 50 100 150 200 250

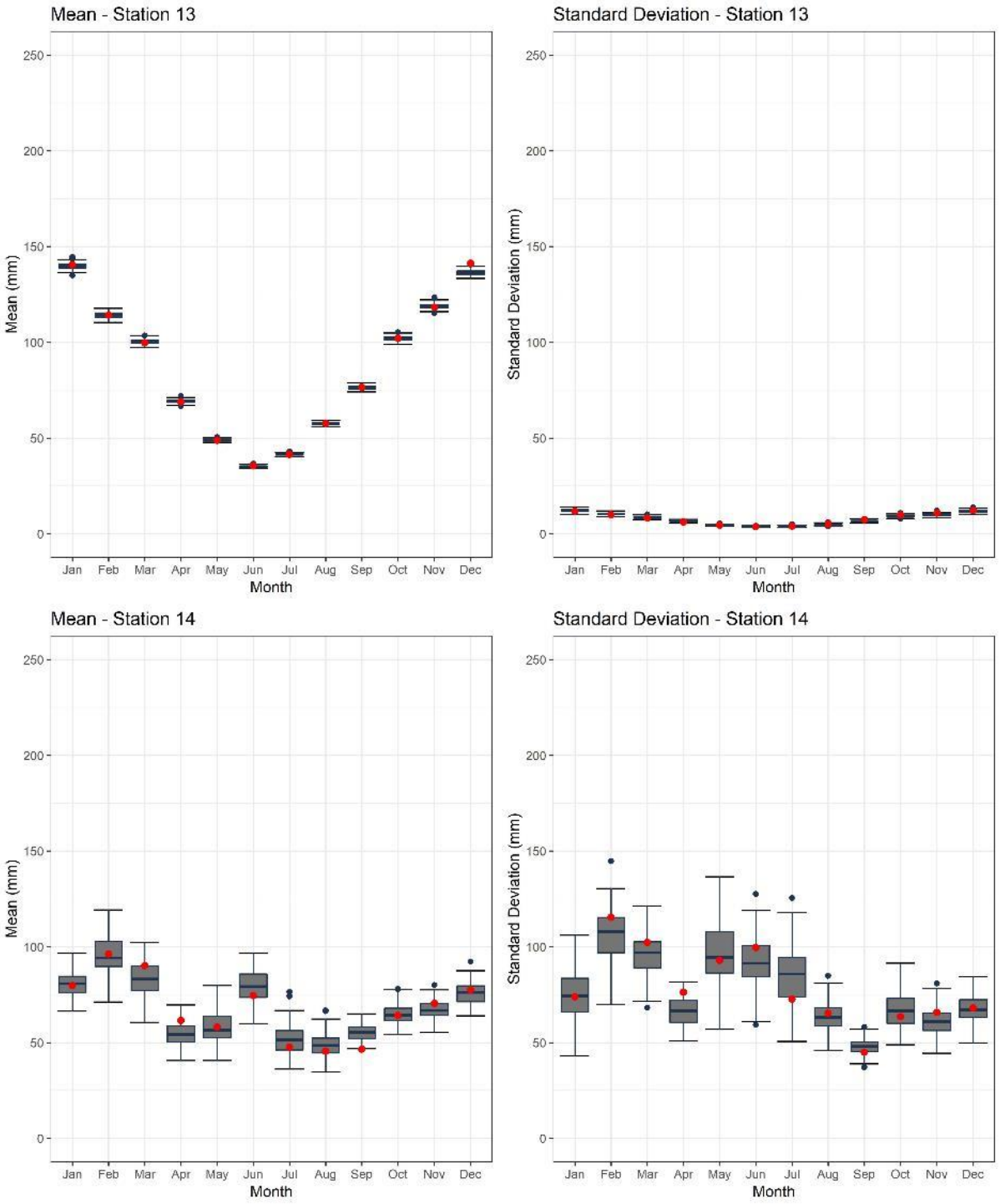
Mean - Station 13
Mean (mm)
Month
Standard Deviation - Station 13
Standard Deviation (mm)
Month
Mean - Station 14
Mean (mm)
Month
Standard Deviation - Station 14
Standard Deviation (mm)
Month
Jan Feb Mar Apr May Jun Jul Aug Sep Oct Nov Dec
0 50 100 150 200 250

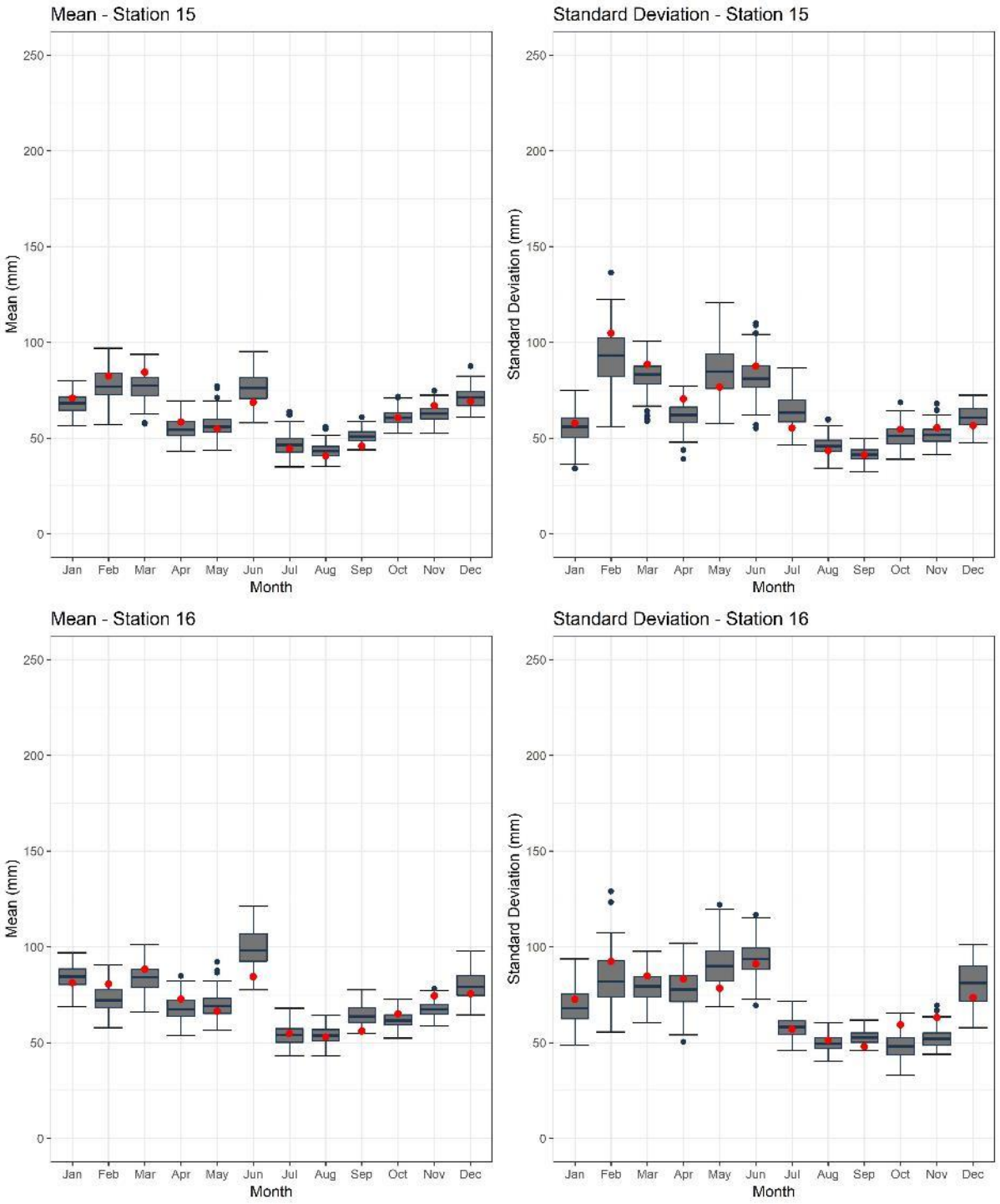
Mean - Station 15
Mean (mm)
Month
Standard Deviation - Station 15
Standard Deviation (mm)
Month
Mean - Station 16
Mean (mm)
Month
Standard Deviation - Station 16
Standard Deviation (mm)
Month
Jan Feb Mar Apr May Jun Jul Aug Sep Oct Nov Dec
0 50 100 150 200 250

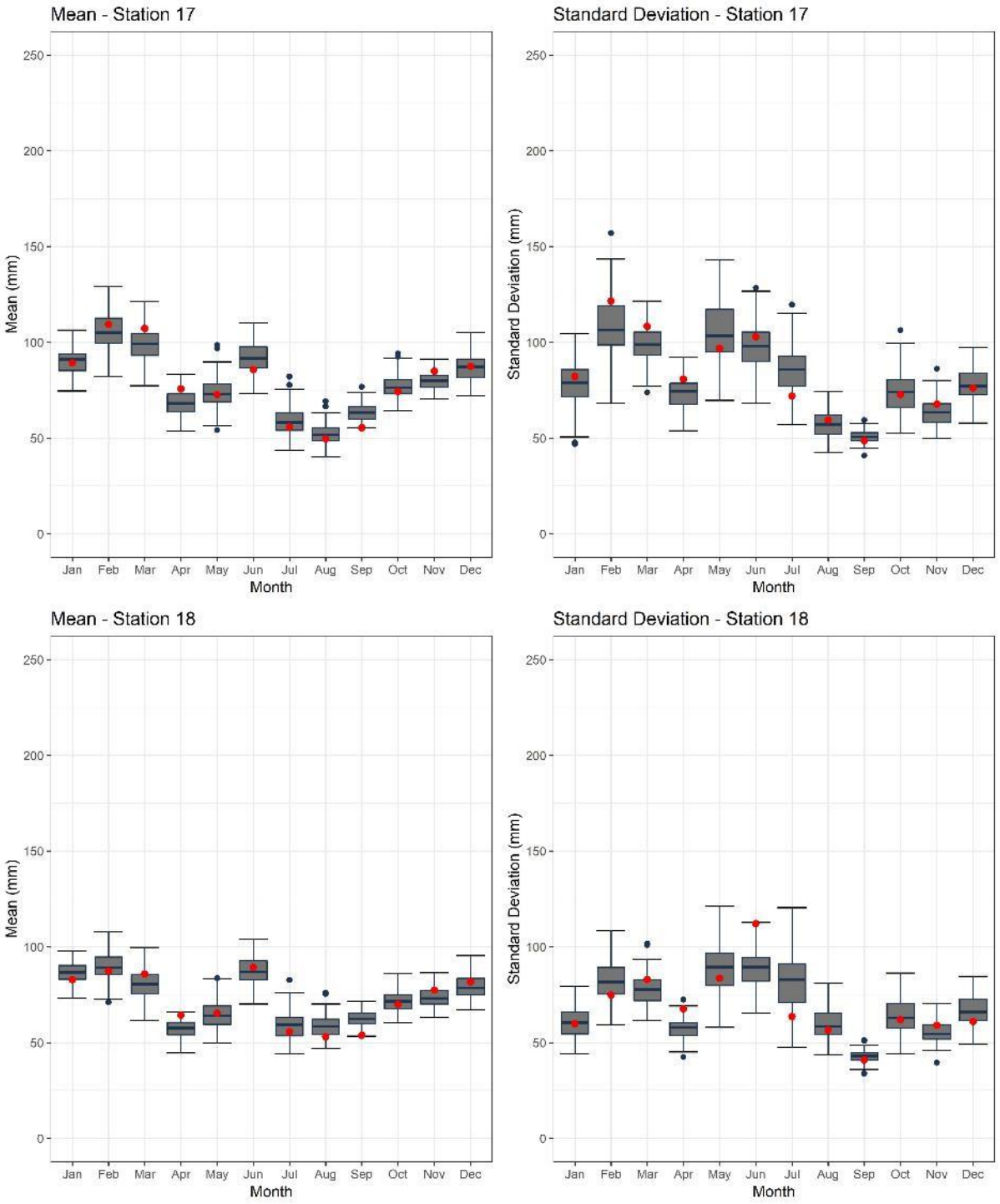
Mean - Station 17
Mean (mm)
Month
Standard Deviation - Station 17
Standard Deviation (mm)
Month
Mean - Station 18
Mean (mm)
Month
Standard Deviation - Station 18
Standard Deviation (mm)
Month
Jan
Feb
Mar
Apr
May
Jun
Jul
Aug
Sep
Oct
Nov
Dec
0
50
100
150
200
250

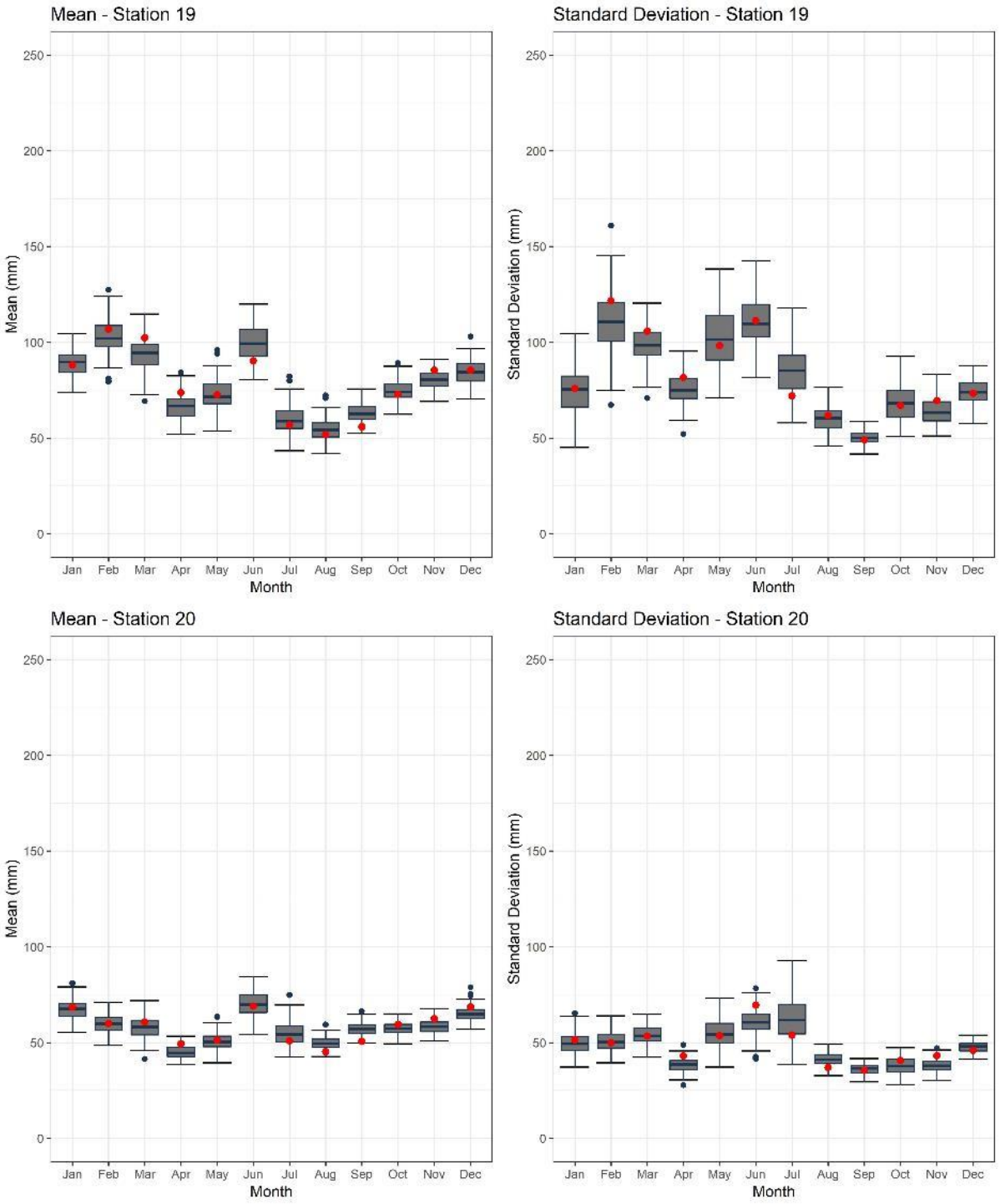
Mean - Station 19
Mean (mm)
Month
Standard Deviation - Station 19
Standard Deviation (mm)
Month
Mean - Station 20
Mean (mm)
Month
Standard Deviation - Station 20
Standard Deviation (mm)
Month
0
50
100
150
200
250
Jan
Feb
Mar
Apr
May
Jun
Jul
Aug
Sep
Oct
Nov
Dec

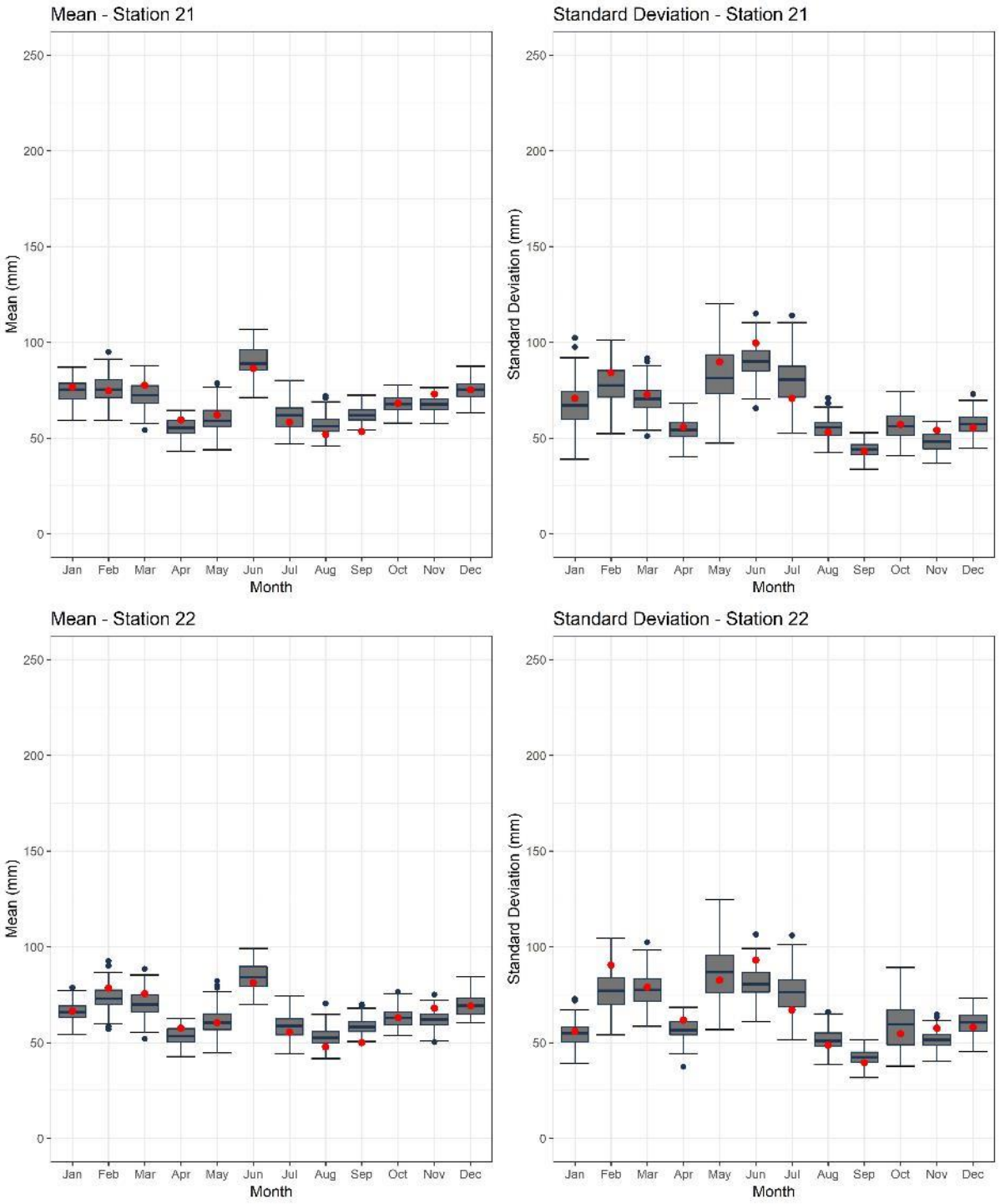
Mean - Station 21
Mean (mm)
Month
Standard Deviation - Station 21
Standard Deviation (mm)
Month
Mean - Station 22
Mean (mm)
Month
Standard Deviation - Station 22
Standard Deviation (mm)
Month
0
50
100
150
200
250
Jan
Feb
Mar
Apr
May
Jun
Jul
Aug
Sep
Oct
Nov
Dec

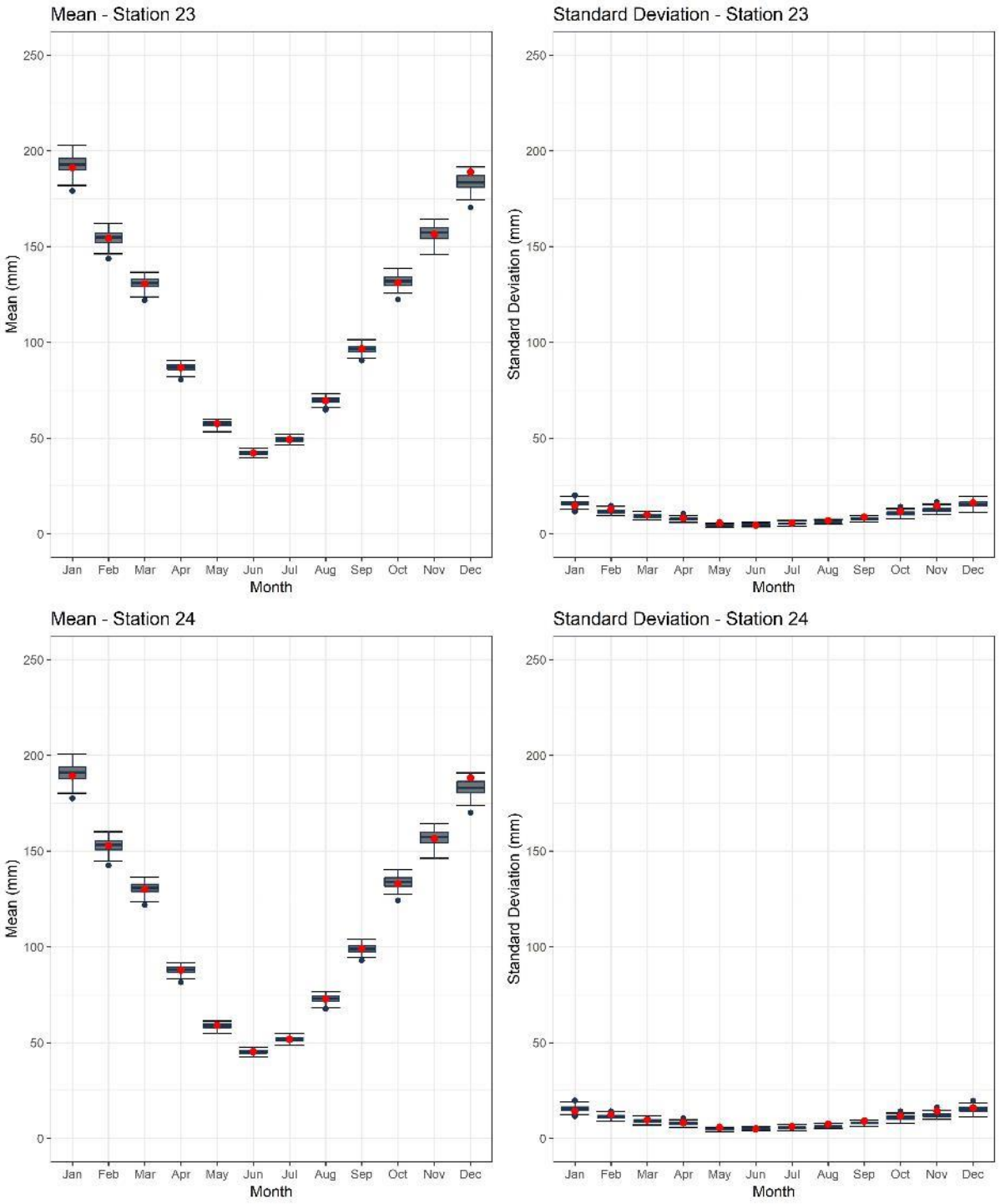
Mean - Station 23
Mean (mm)
Month
Standard Deviation - Station 23
Standard Deviation (mm)
Month
Mean - Station 24
Mean (mm)
Month
Standard Deviation - Station 24
Standard Deviation (mm)
Month
0
50
100
150
200
250
Jan
Feb
Mar
Apr
May
Jun
Jul
Aug
Sep
Oct
Nov
Dec

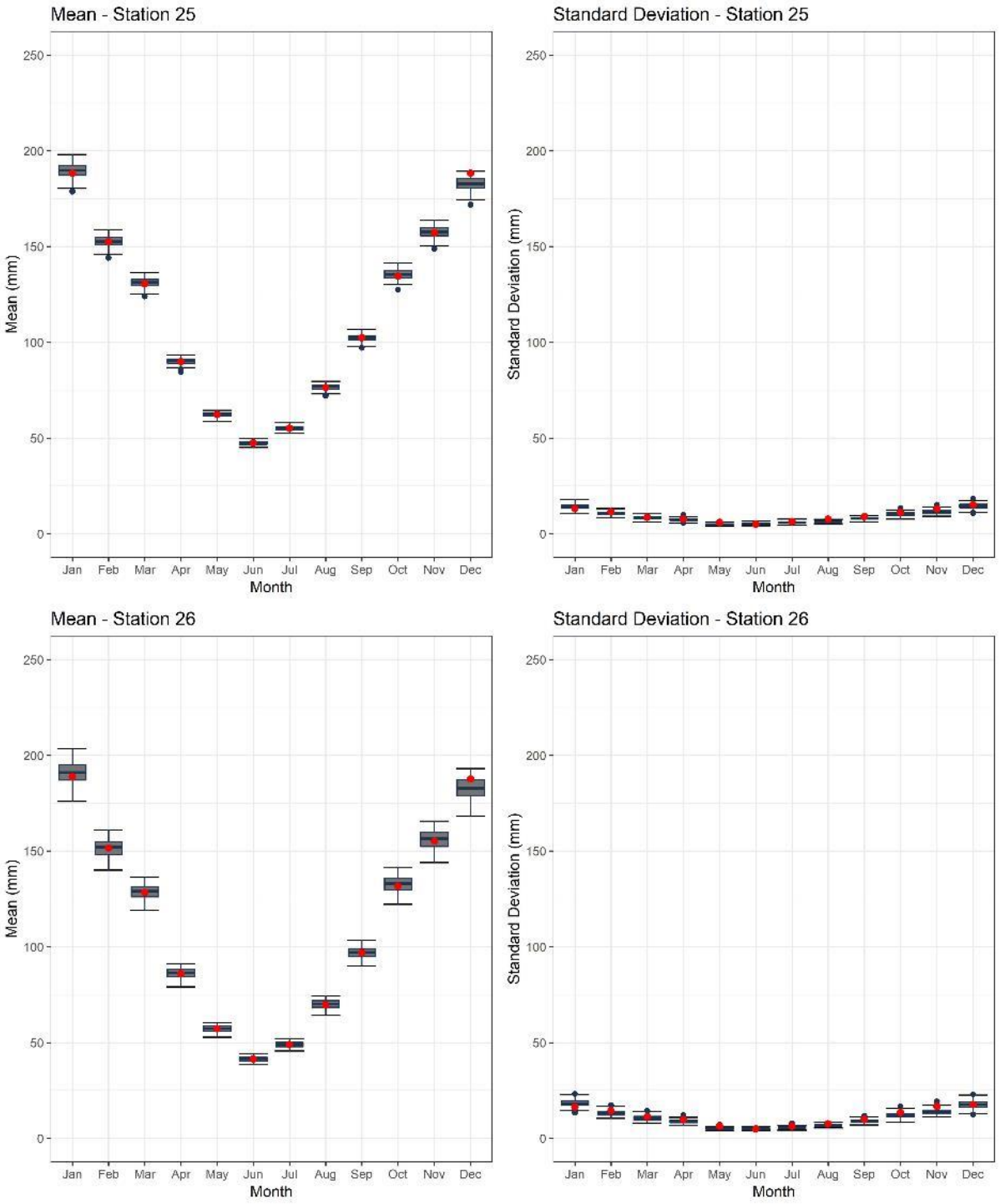
Mean - Station 25
Mean (mm)
Month
Standard Deviation - Station 25
Standard Deviation (mm)
Month
Mean - Station 26
Mean (mm)
Month
Standard Deviation - Station 26
Standard Deviation (mm)
Month
0
50
100
150
200
250
Jan
Feb
Mar
Apr
May
Jun
Jul
Aug
Sep
Oct
Nov
Dec

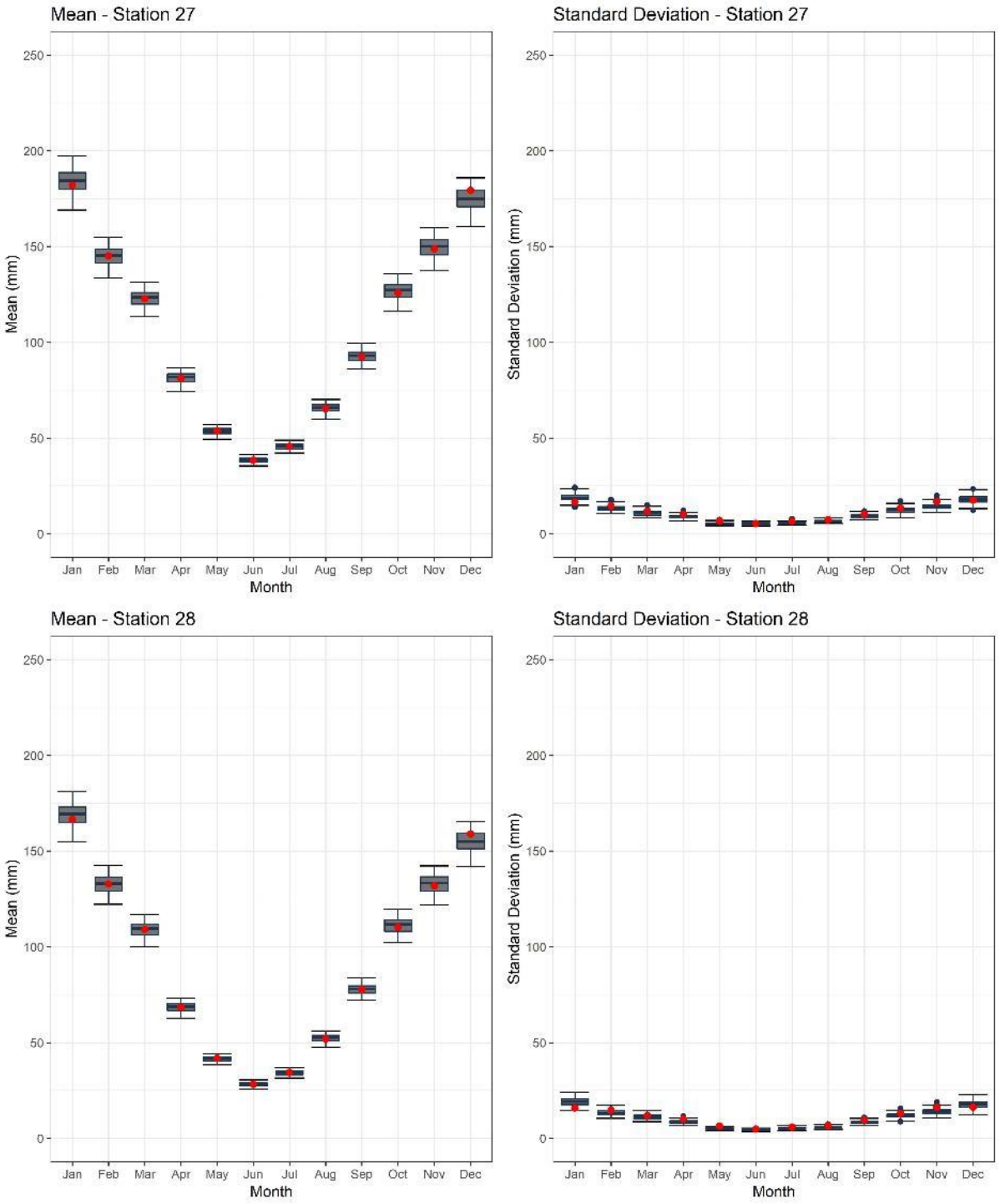
Mean - Station 27
Mean (mm)
Month
Jan Feb Mar Apr May Jun Jul Aug Sep Oct Nov Dec
0 50 100 150 200 250
Standard Deviation - Station 27
Standard Deviation (mm)
Month
Jan Feb Mar Apr May Jun Jul Aug Sep Oct Nov Dec
0 50 100 150 200 250
Mean - Station 28
Mean (mm)
Month
Jan Feb Mar Apr May Jun Jul Aug Sep Oct Nov Dec
0 50 100 150 200 250
Standard Deviation - Station 28
Standard Deviation (mm)
Month
Jan Feb Mar Apr May Jun Jul Aug Sep Oct Nov Dec
0 50 100 150 200 250

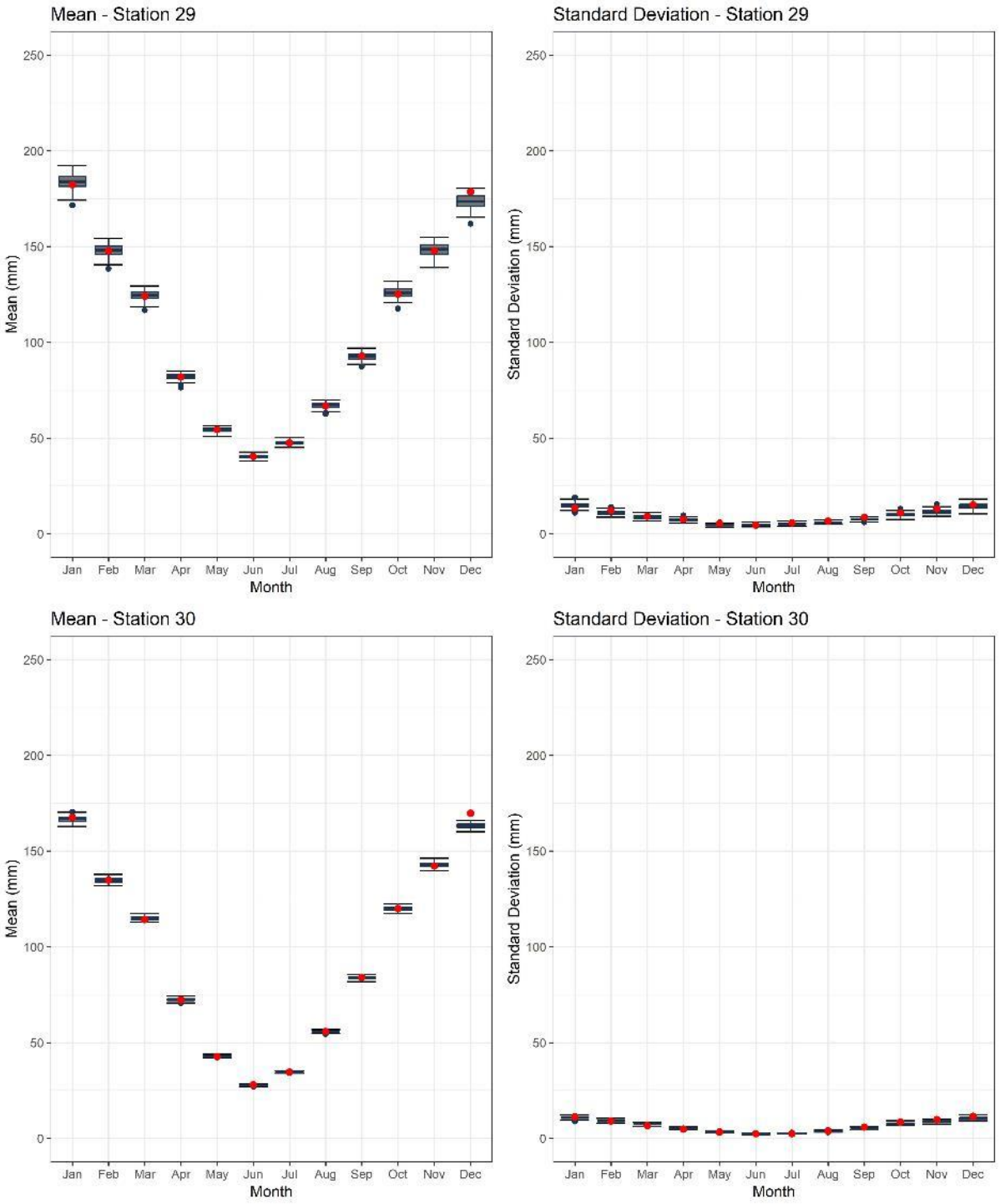
Mean - Station 29
Mean (mm)
Month
Standard Deviation - Station 29
Standard Deviation (mm)
Month
Mean - Station 30
Mean (mm)
Month
Standard Deviation - Station 30
Standard Deviation (mm)
Month
0
50
100
150
200
250
Jan
Feb
Mar
Apr
May
Jun
Jul
Aug
Sep
Oct
Nov
Dec

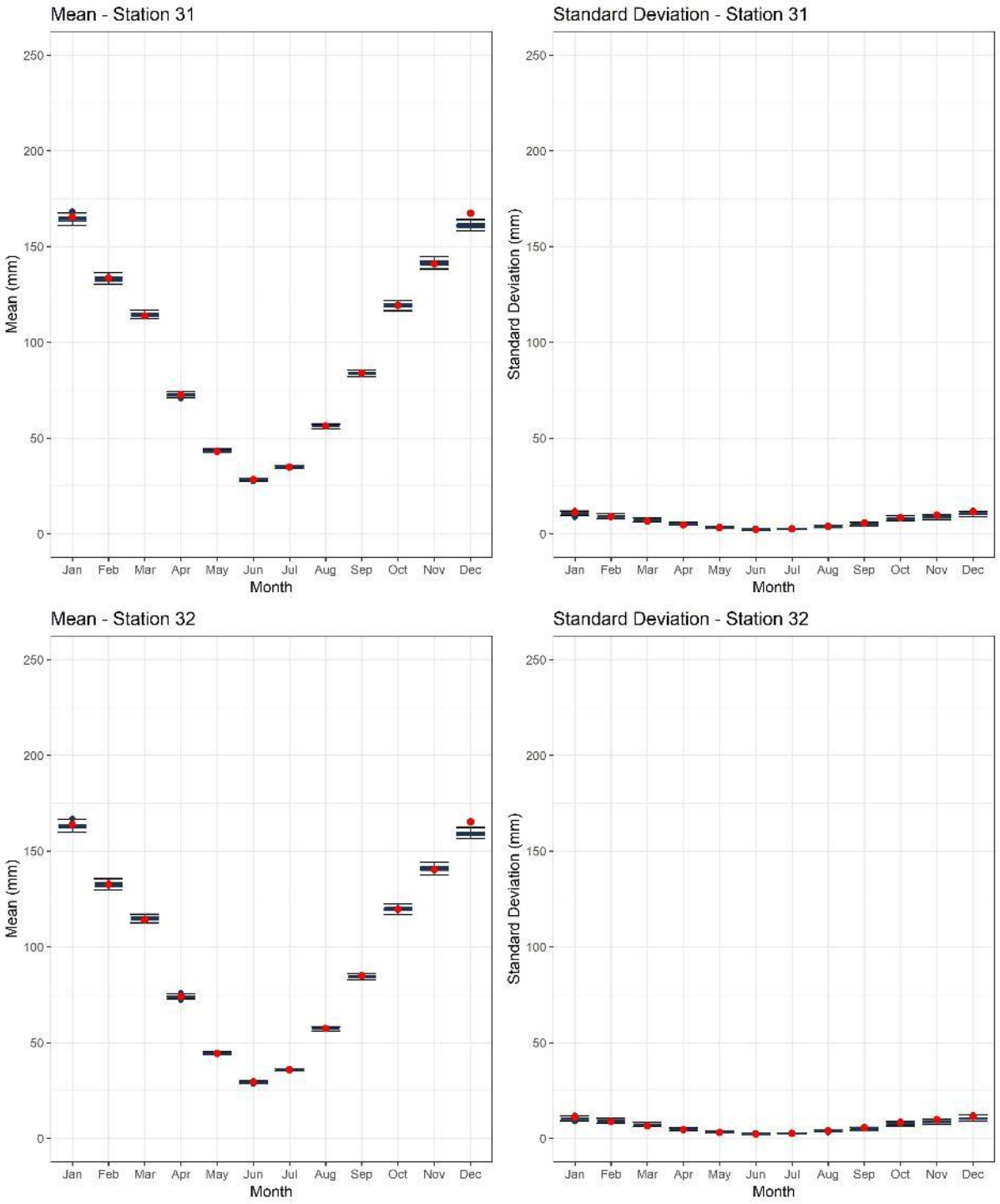
Mean - Station 31
Mean (mm)
Month
Standard Deviation - Station 31
Standard Deviation (mm)
Month
Mean - Station 32
Mean (mm)
Month
Standard Deviation - Station 32
Standard Deviation (mm)
Month
0
50
100
150
200
250
Jan
Feb
Mar
Apr
May
Jun
Jul
Aug
Sep
Oct
Nov
Dec

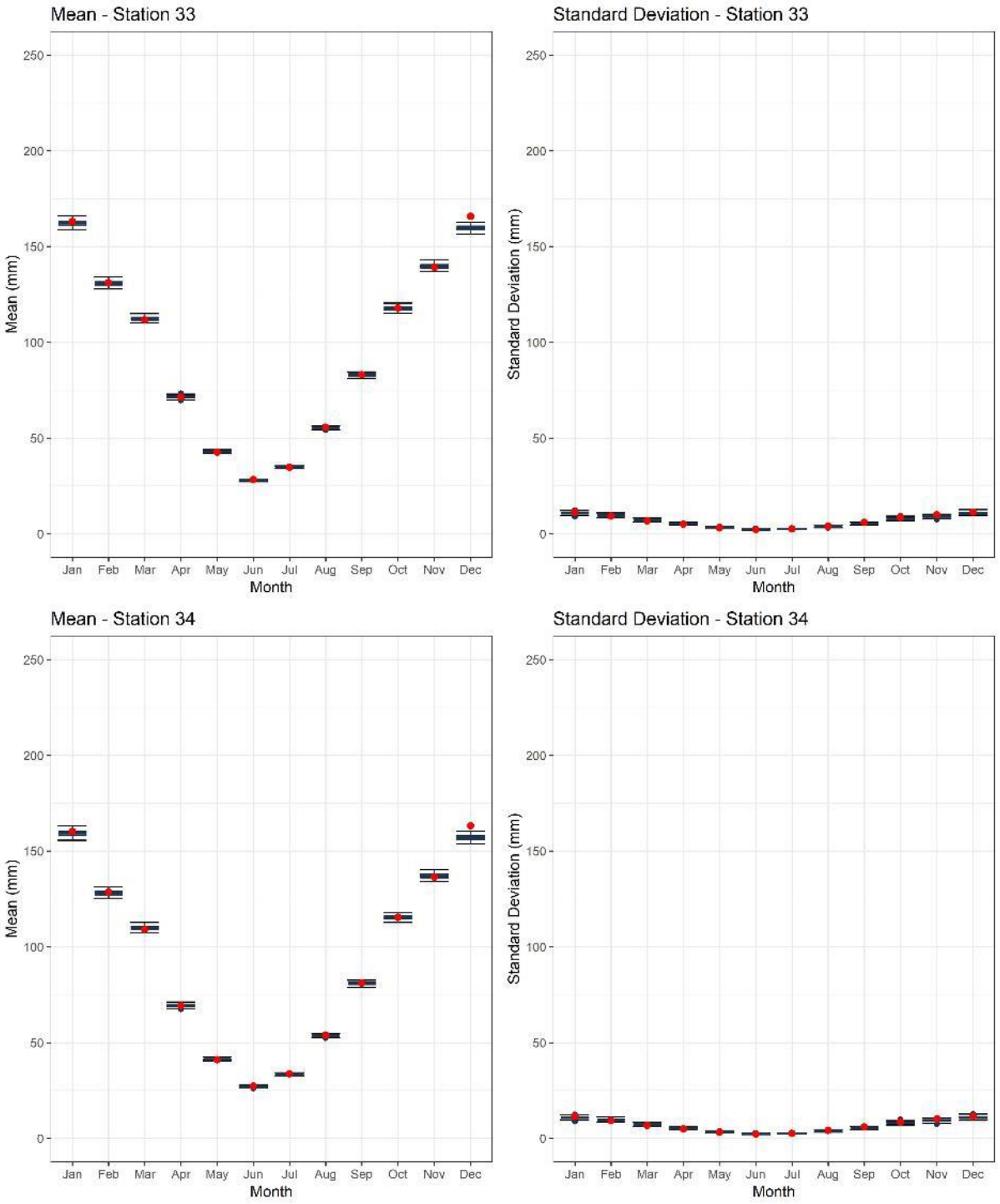
Mean - Station 33
Mean (mm)
Month
Jan Feb Mar Apr May Jun Jul Aug Sep Oct Nov Dec
0 50 100 150 200 250
Standard Deviation - Station 33
Standard Deviation (mm)
Month
Jan Feb Mar Apr May Jun Jul Aug Sep Oct Nov Dec
0 50 100 150 200 250
Mean - Station 34
Mean (mm)
Month
Jan Feb Mar Apr May Jun Jul Aug Sep Oct Nov Dec
0 50 100 150 200 250
Standard Deviation - Station 34
Standard Deviation (mm)
Month
Jan Feb Mar Apr May Jun Jul Aug Sep Oct Nov Dec
0 50 100 150 200 250

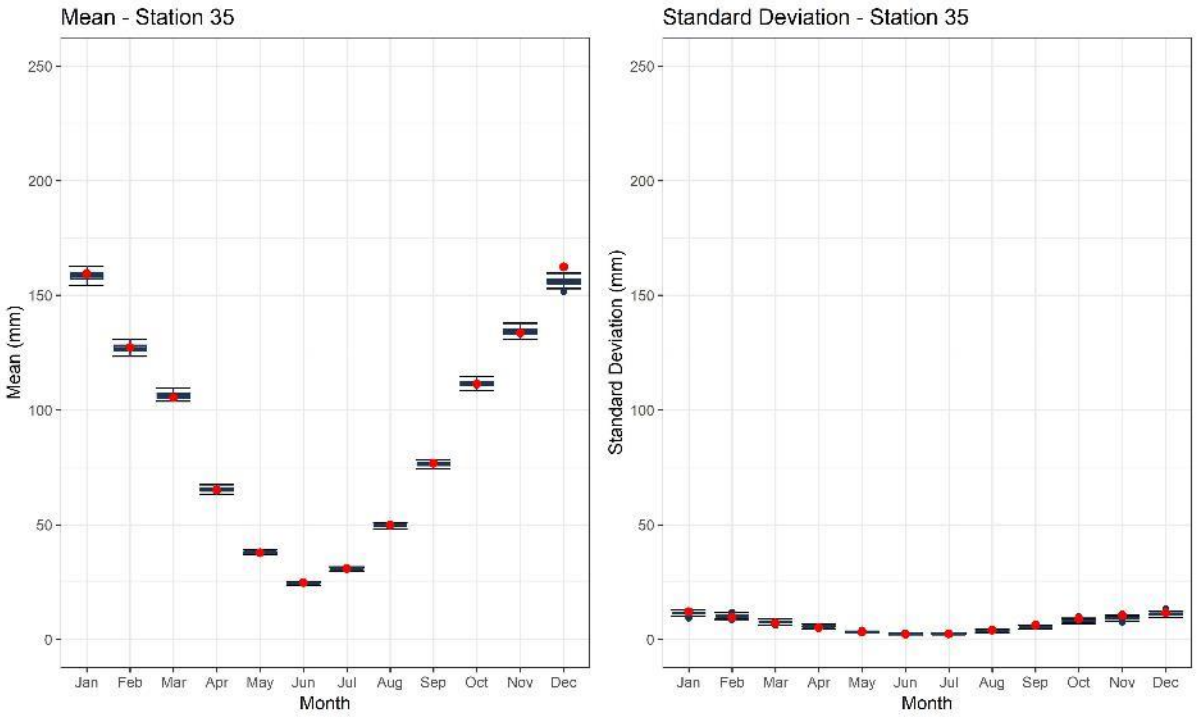
Mean - Station 35
Mean (mm)
250
200
150
100
50
0
Jan
Feb
Mar
Apr
May
Jun
Jul
Aug
Sep
Oct
Nov
Dec
Month
Standard Deviation - Station 35
Standard Deviation (mm)
250
200
150
100
50
0
Jan
Feb
Mar
Apr
May
Jun
Jul
Aug
Sep
Oct
Nov
Dec
Month

APPENDIX 6: DPIE-WATER PRESENTATION

Climate Risk for Regional Water Strategies: Presentation by Mr Richard Beecham

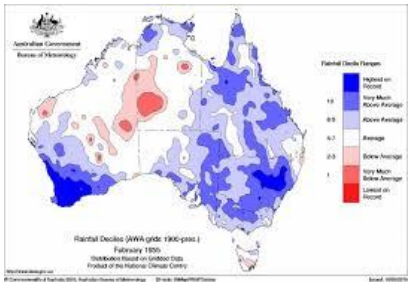

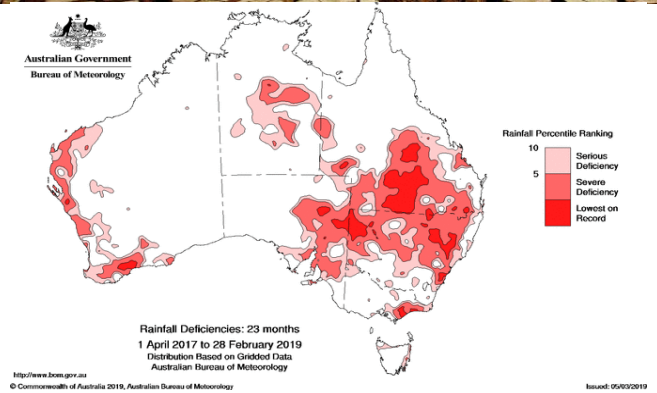

KNOWLEDGE STREAMS SEMINAR SERIES – 18TH JULY 2019

Climate Risk for Regional Water Strategies

Richard Beecham, Water Modelling

Why are we considering climate risk?

Country towns close to reaching 'day zero', as water supplies dry up in the drought

By National Regional Affairs reporter Lucy Barbour

Updated Mon at 1:02pm

PHOTO: Farmers have never known Walcha, in regional NSW, to be so dry. (ABC News: Lucy Barbour)

Across New South Wales and Queensland's southern downs, country towns are approaching their own 'day zero', as water supplies dry up in the drought.

- To provide right level of water security – towns, industry, environment
- Current development, policies developed using historical climate – premise that adaptive responses sufficient.
- Evidence more extreme conditions possible - variability and change
- Need better understanding of plausible future climatic conditions, and modelling tools to understand impacts & outcomes.
- Regional Water Strategies – develop measures (infrastructure / policy)

Regional Water Strategies

Objectives

From Darcy Moar presentation October 2018

- Identify risks to a regions' water resources & opportunities to secure them for the next 30 years
- Includes economic and environmental risk
- Assess infrastructure and policy solutions

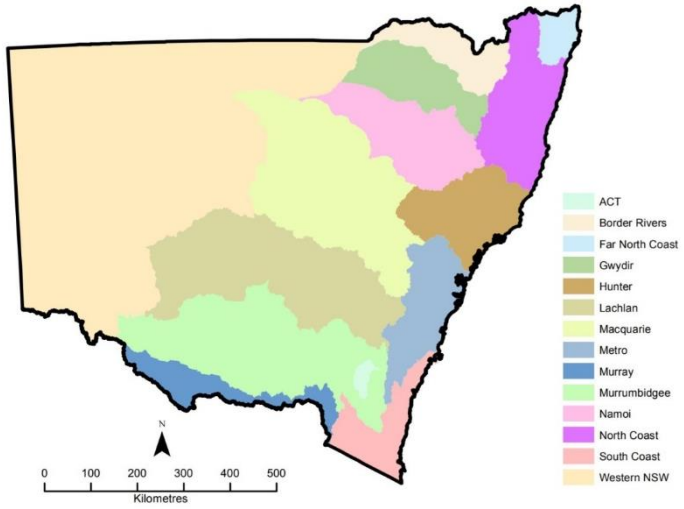

Regional Water Strategies

Outcomes of interest, e.g.

- Security of water supply for water dependent sectors:
  - town water and other critical water needs – importance of high security of supply
  - general security water users – reliability of allocation, sequences of low allocation, long term averages
  - environment water requirements – sufficient volumes and timing provided for
  - Others…

Role of models

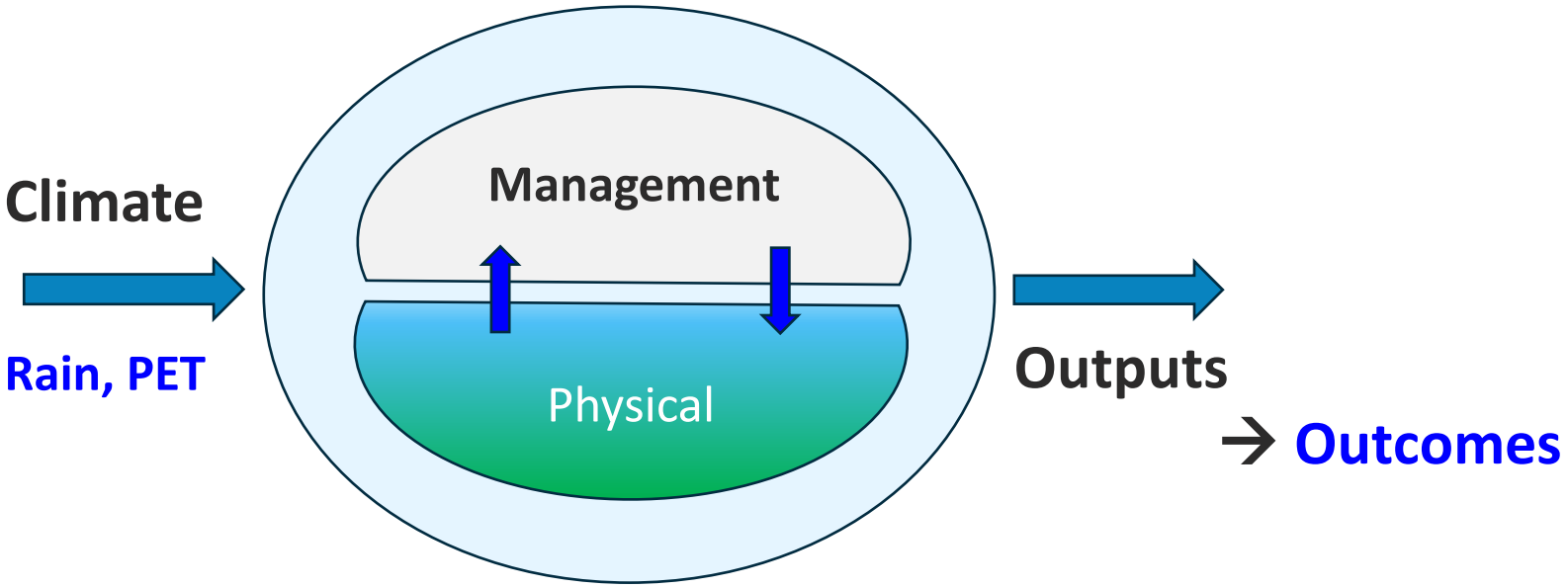

Basis for climate data

Combined variability and change

Natural variability (past)– based on information from observational data and from palaeo climatic studies – statistically extended

Change (future) – based on information from NARCliM regional climate models developed by UNSW and Environment's Climate Science Branch

Data sets combined

Climate information

Historical variability

- Reasonable areal coverage in NSW since 1890
- Characterised by series of wet and dry periods
- 1890's floods → Federation drought → WW2 drought → 1950's floods → 1970's floods → 1980's drought → 1990's floods → Millennium drought → current drought
- Importantly – multi-decadal cycles - 1900-1950 much drier than 1950-2000
- Wet periods in dry cycles and dry periods in wet cycles
- Related to oceanic temperature distribution

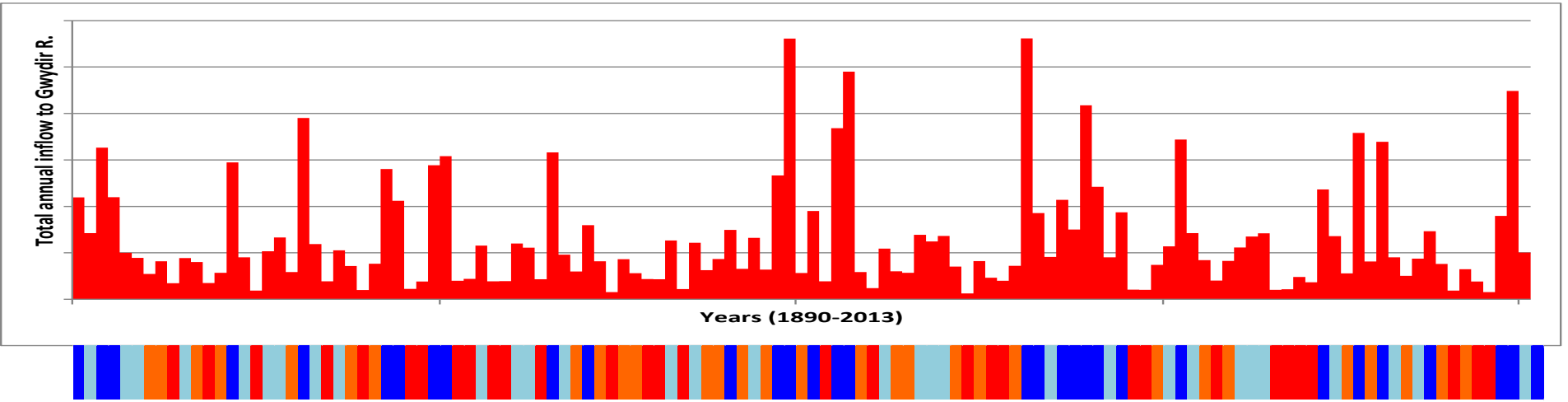

Very dry (0-25%ile)

Dry (25-50%ile)

Wet (50-75%ile)

Very wet (75-100%ile)

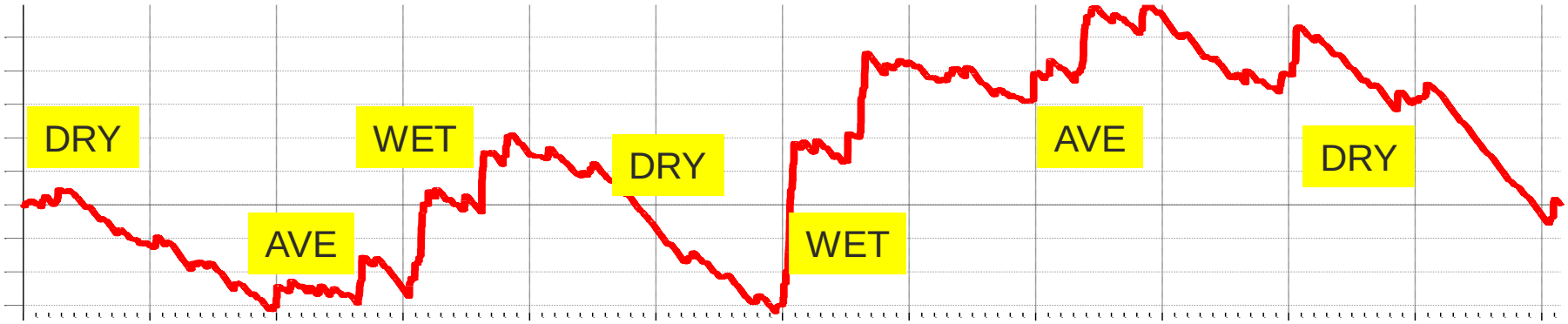

Pacific Ocean temperatures influence rainfall

Interdecadal Pacific Oscillation (IPO)

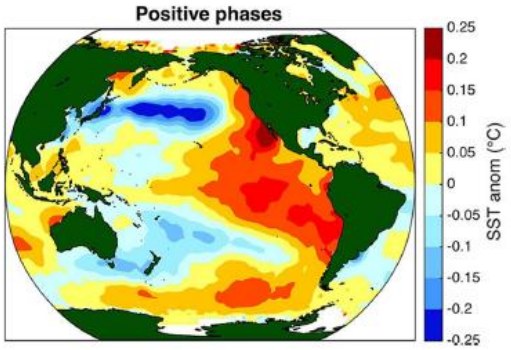

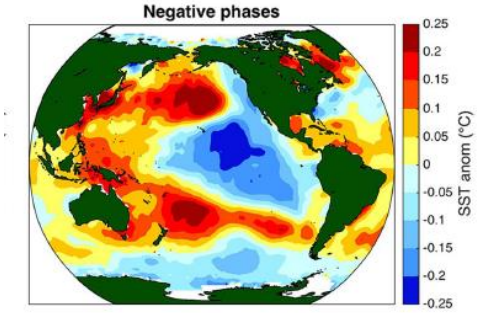

El-Nino Southern Oscillation (ENSO)

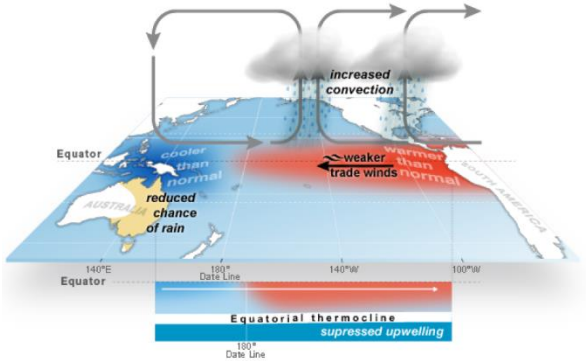

El Niño–Southern Oscillation (ENSO): **El Niño**

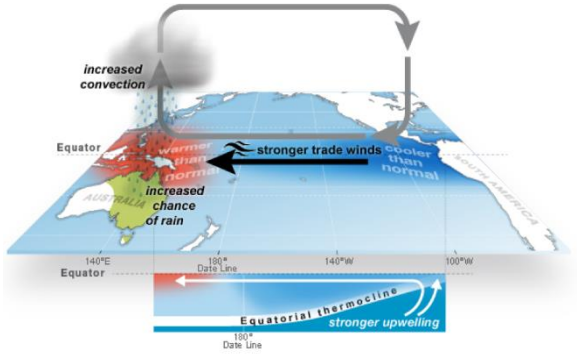

El Niño–Southern Oscillation (ENSO): **La Niña**

Palaeo data – mega droughts in past millennia

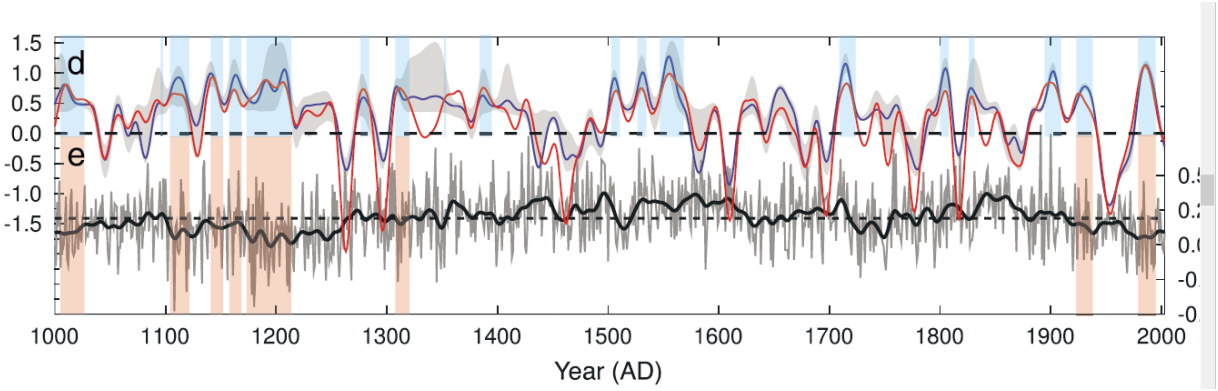

Vance, T. R., J. L. Roberts, C. T. Plummer, A. S. Kiem, and T. D. van Ommen (2015), Interdecadal Pacific variability and eastern Australian mega-droughts over the last millennium, *Geophys. Res. Lett.*, *42*, doi:10.1002/2014GL062447

Building the data set

Analysis of Macquarie climate data

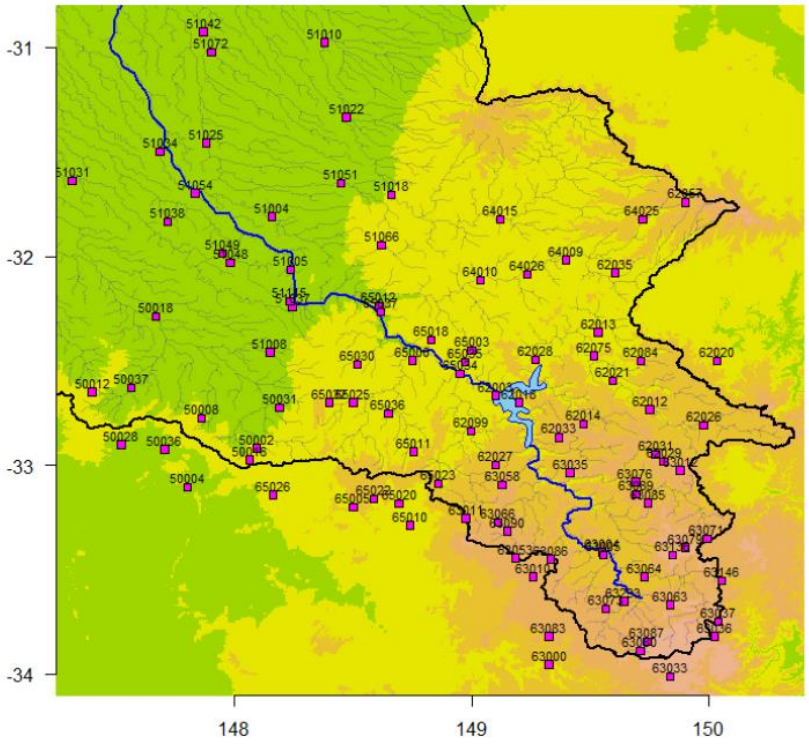

Figure 2 Location of Rainfall Sites (See Appendix A for Site Details)

Comparison of IPO –ve and IPO +ve Mean annual rainfalls

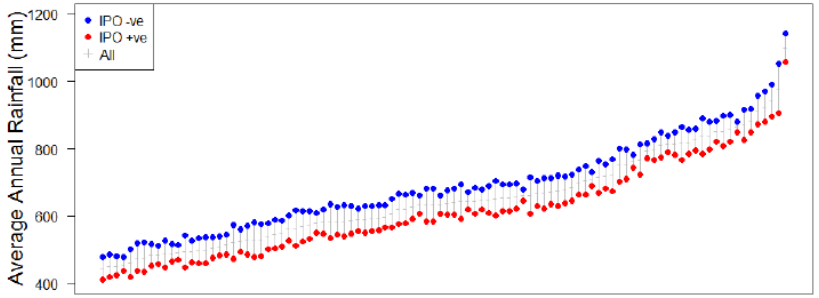

Palaeo-climate analysis - IPO

Observational

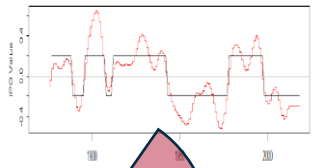

Palaeo

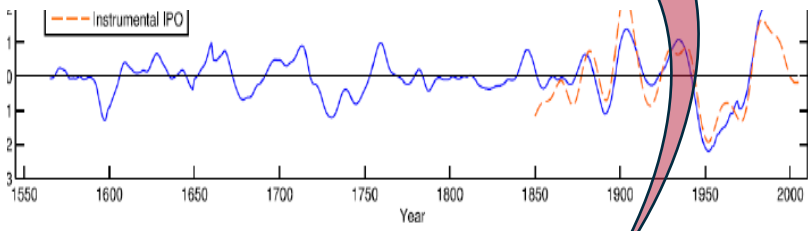

Stochastically generated IPO phase for 10,000 years

10-70 year cycles of –ve and +ve phases

Palaeo-stochastic outputs

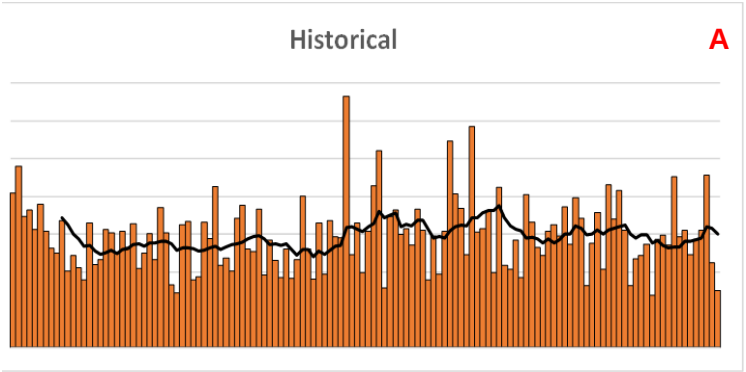

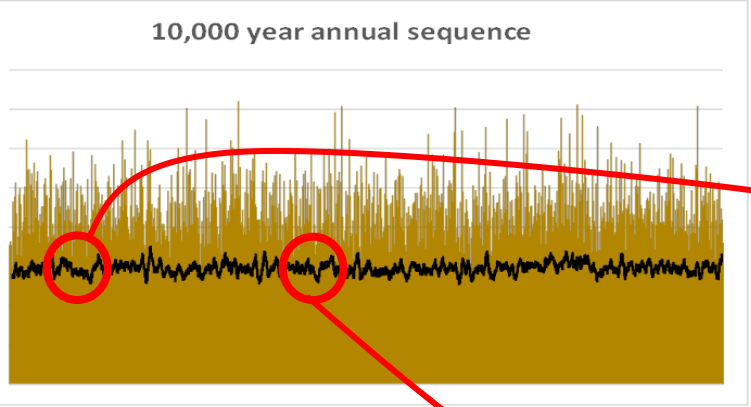

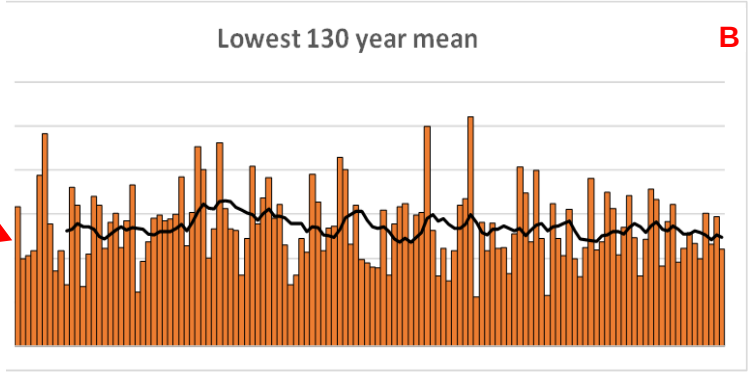

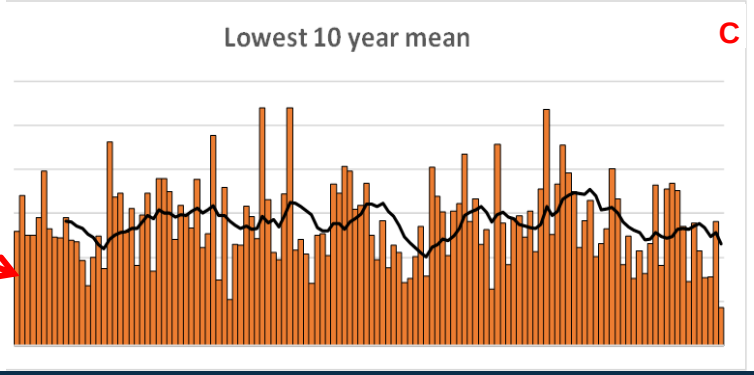

Building the data sets

Global climate models – rainfall and PET changes

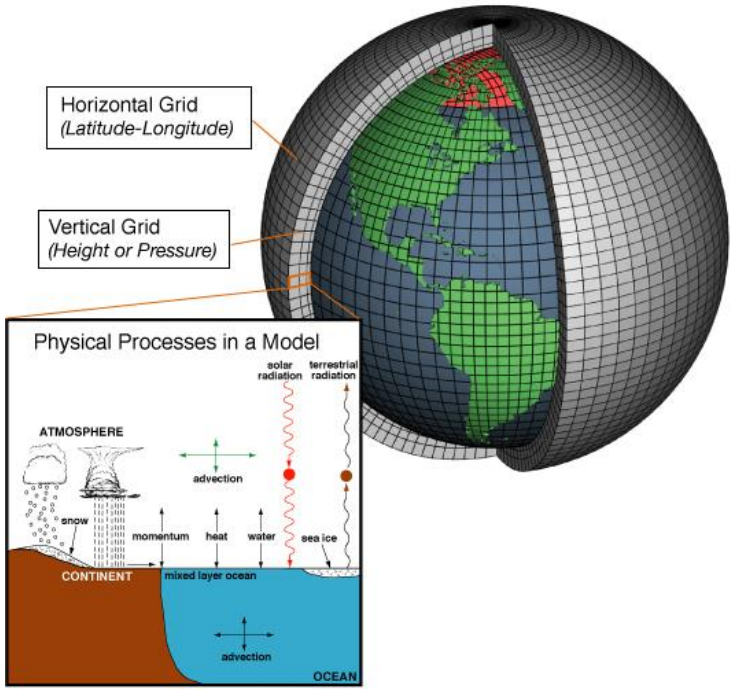

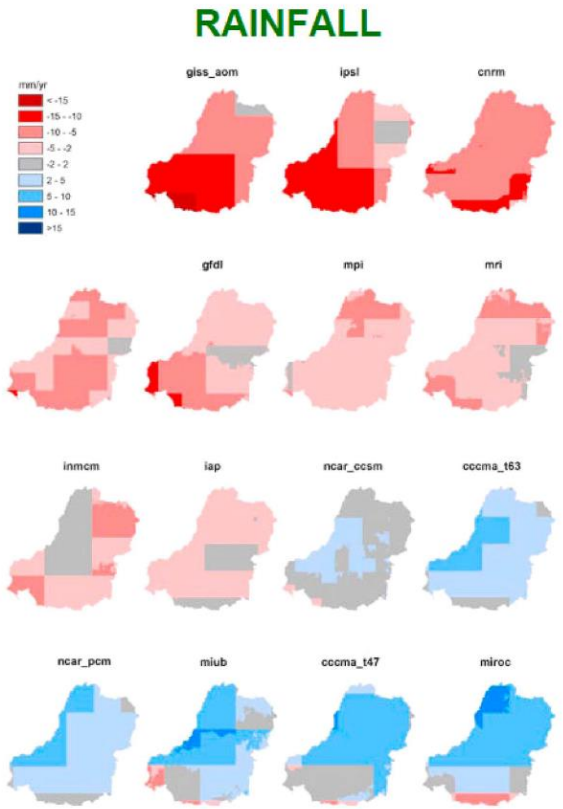

Figure 3. Percentage change in future mean annual rainfall (~2030 relative to ~1990) across the MDB as projected by 15 different climate models [*CSIRO*, 2008a; *Chiew et al.*, 2011].

NSW/ACT Regional Climate Modelling (NARCliM 1.0)

- UNSW – NSW Government joint project led by Environment Group - Climate Science Branch
- 4 Global climate models dynamically downscaled using 3 Regional Climate Models
- 12 regional climate model data sets at 10 km spatial resolution
- Business as usual climate emission scenario
- 3 x 20-year periods:
  - 1990 - 2009,
  - 2020 - 2039,
  - 2060 – 2079
- Publicly accessible data (500TB)
- http://climatechange.environment.nsw.gov.au

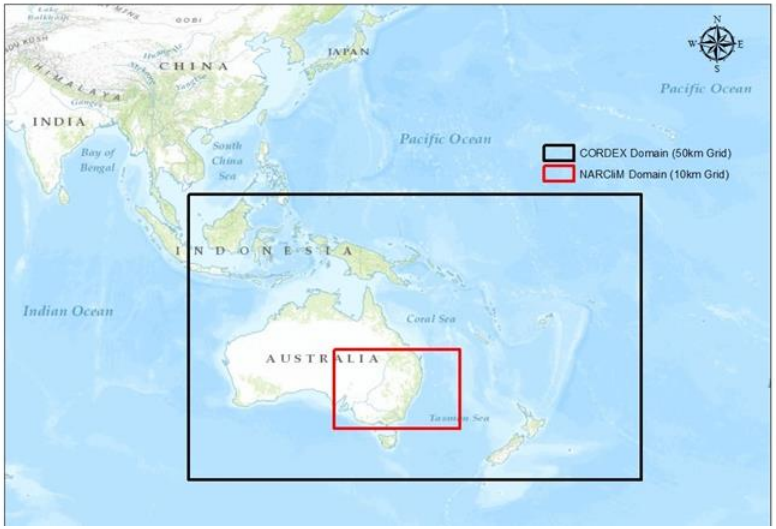

Benefits of NARCliM v Source GCM

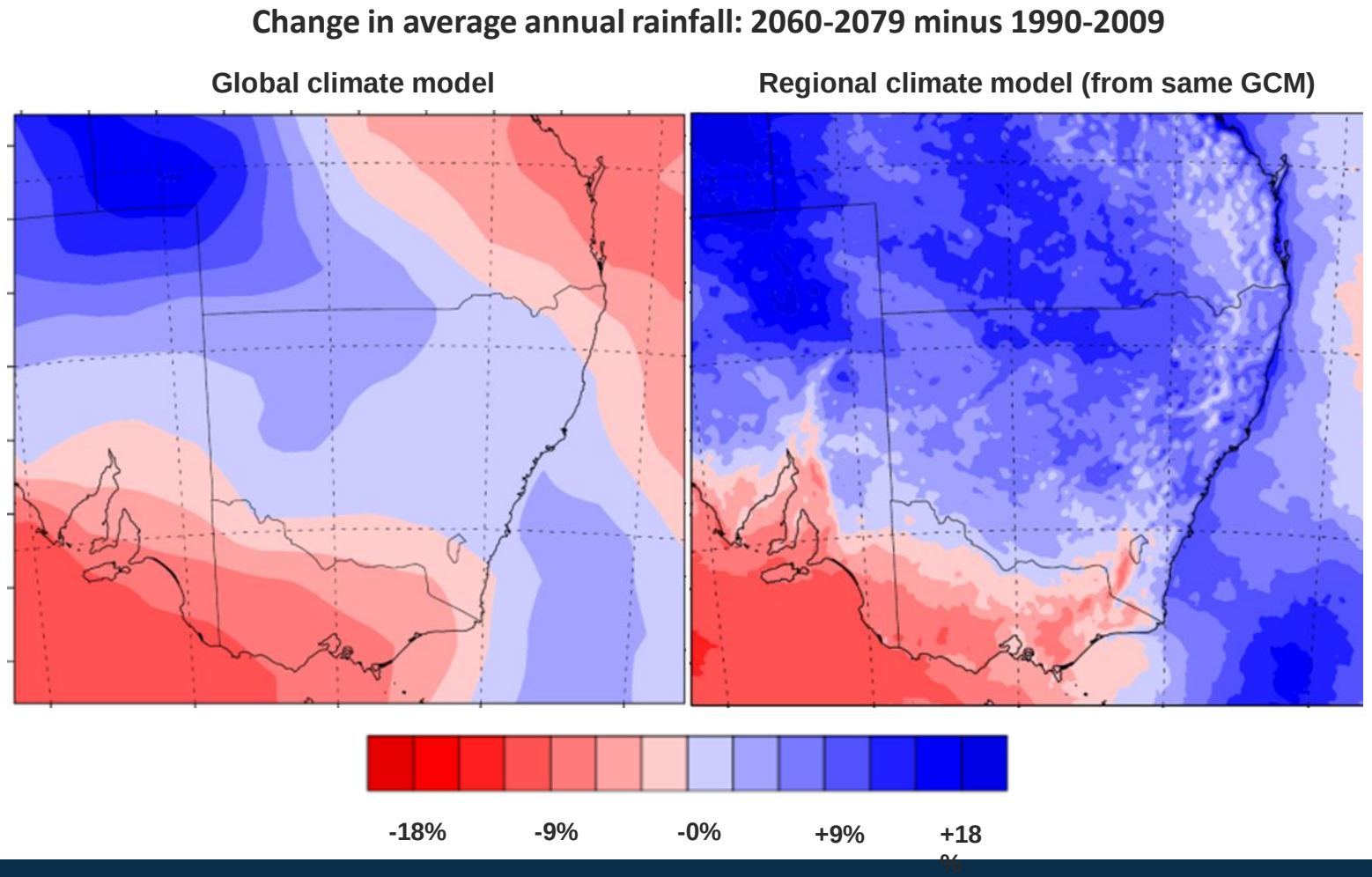

Climate science and water planning

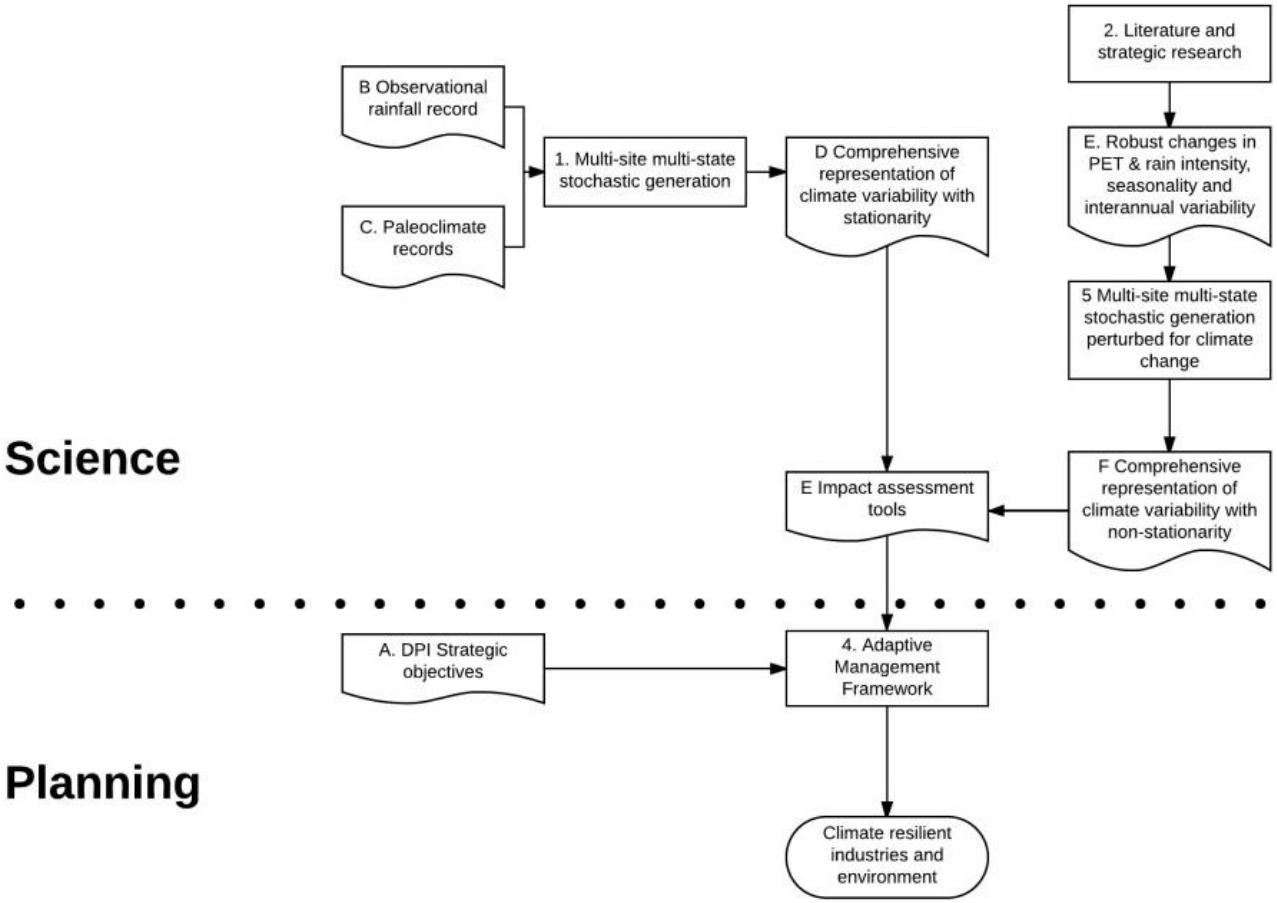

Next steps

- Independent Expert Review
- Complete development of palaeo-stochastic (Northern inland / Coastal / Southern inland nuances)
- Complete RWS modelling
- Have a long break
- Continuous improvement
  - UNSW ARC project outcomes
  - NARCliM 1.5 (and 2.0)
  - Improved palaeo data sets
- Broader application of work
    - Basin Plan, water user risk management

APPENDIX 7: ADDITIONAL ADVICE PROVIDED BY DPIE-WATER: CLIMATE DATA USED

Type of Climate Data used in River System Modelling by DPIE Modelling Unit

The Water Modelling Unit (Water Modelling Unit) of the Department of Planning, Industry and Environment uses daily SILO climate data for Rainfall-runoff and River System Modelling in the recent years. SILO is hosted by the Queensland Department of Environment and Science. The data system began in 1996 as a collaborative project between the Queensland Government and the Australian Bureau of Meteorology (BoM) sponsored by the Land and Water Resources Research and Development Corporation. The datasets are constructed from observational data obtained from BoM. The list of SILO Climate Data is shown in Table A7.1. The data are available in point and gridded formats.

Table A7.1: List of SILO Climate Data – Primary and Derived variables at a daily time step (from 1889-present)

Climate data	Variable	Primary or derived	Short name/code
Rainfall (mm)	Daily rainfall	Primary	daily_rain
	Monthly rainfall	Primary	monthly_rain
Temperature (°C)	Maximum temperature	Primary	max_temp
	Minimum temperature	Primary	min_temp
Vapour pressure (hPa)	Vapour pressure	Primary	vp
	Vapour pressure deficit	Derived	vp_deficit
Evaporation (mm)	Class A pan evaporation	Primary	evap_pan
	Synthetic estimate[1]	Derived	evap_syn
	Combination (synthetic estimate pre-1970, class A pan 1970 onwards)	Derived	evap_comb
	Morton's shallow lake evaporation	Derived	evap_morton_lake
Solar radiation (MJ/m^2)	Solar exposure, consisting of both direct and diffuse components	Derived	radiation
Relative humidity (%)	Relative humidity at the time of maximum temperature	Derived	rh_tmax
	Relative humidity at the time of minimum temperature	Derived	rh_tmin
Evapotranspiration (mm)	FAO56[4] short crop	Derived	et_short_crop
	ASCE[5] tall crop[6]	Derived	et_tall_crop
	Morton's areal actual evapotranspiration	Derived	et_morton_actual
	Morton's potential evapotranspiration	Derived	et_morton_potential
	Morton's wet-environment areal evapotranspiration over land	Derived	et_morton_wet
Mean sea level pressure (hPa)	Mean sea level pressure	Derived	mslp

Source: Queensland Government (2020a)

WMU mainly uses SILO patch point rainfall data and different types of evaporation and evapotranspiration data for different components of river system modelling as summarised below.

- Rainfall-Runoff modelling – Morton's wet-environment areal evapotranspiration overland (Mwet)
- Storage water balance modelling – Morton's shallow lake evaporation (Mlake)
- Crop Water Demand Modelling – FAO56 Evapotranspiration

Morton's method is used by SILO for deriving potential evapotranspiration (PET), actual areal evapotranspiration, wet-environmental area evapotranspiration and shallow lake evaporation (Morton, 1983). As explained by Morton (1983), Morton's Complementary Relationship Areal Evapotranspiration (CRAE) model computes actual evapotranspiration for land environment using climate variables air temperature, net radiation, atmospheric pressure and rate of change of saturated vapour pressure with respect to temperature. The figures below highlight the differences in magnitude (at daily and annual scales), and correlation between PET and Mwet for a selected climate station (station ID: 41100).

The climate data are thoroughly reviewed using a set of quality assessment guidelines prior to selecting suitable datasets for modelling.

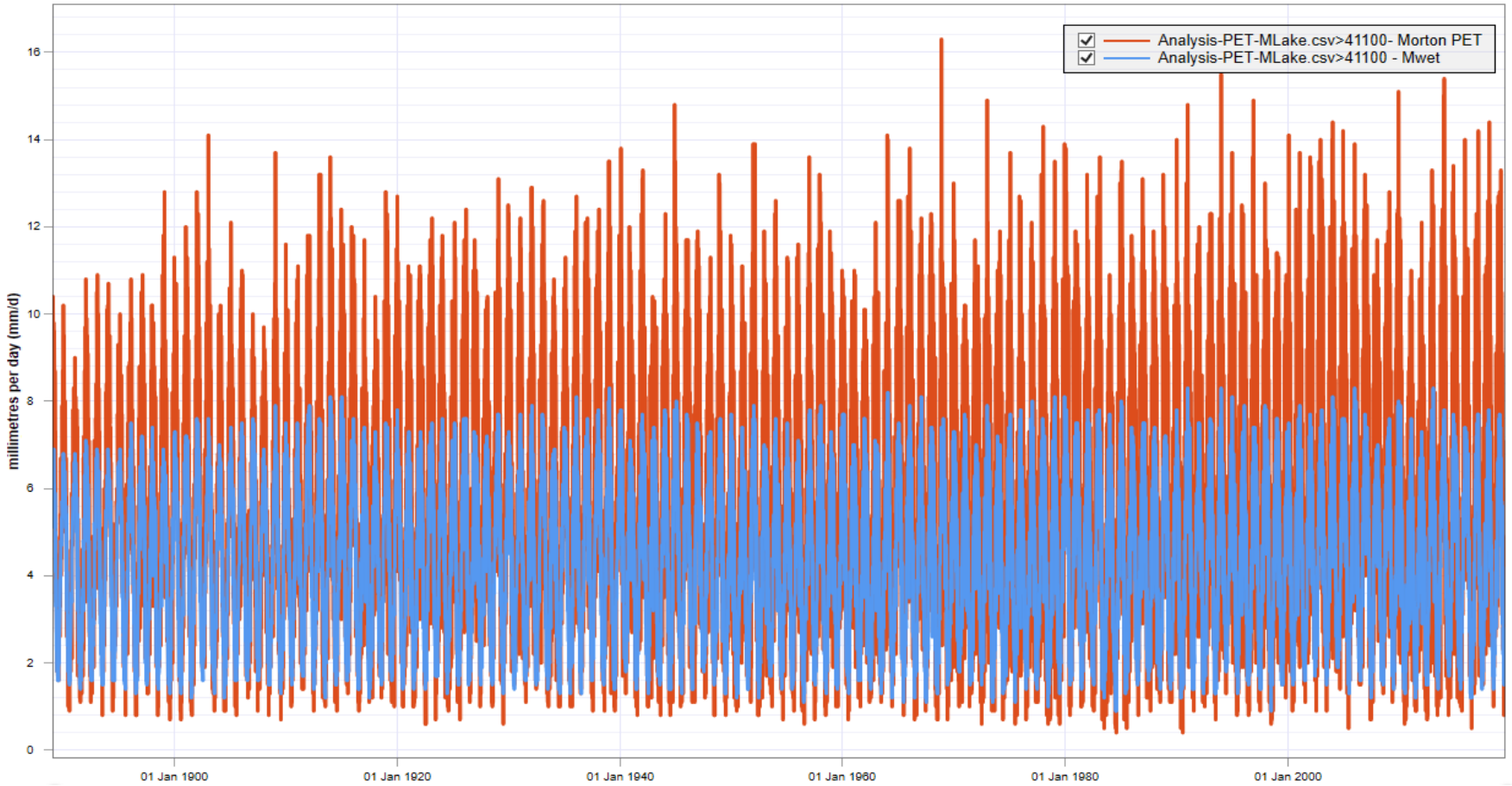

Figure A7.1: Differences in magnitude at a daily scale

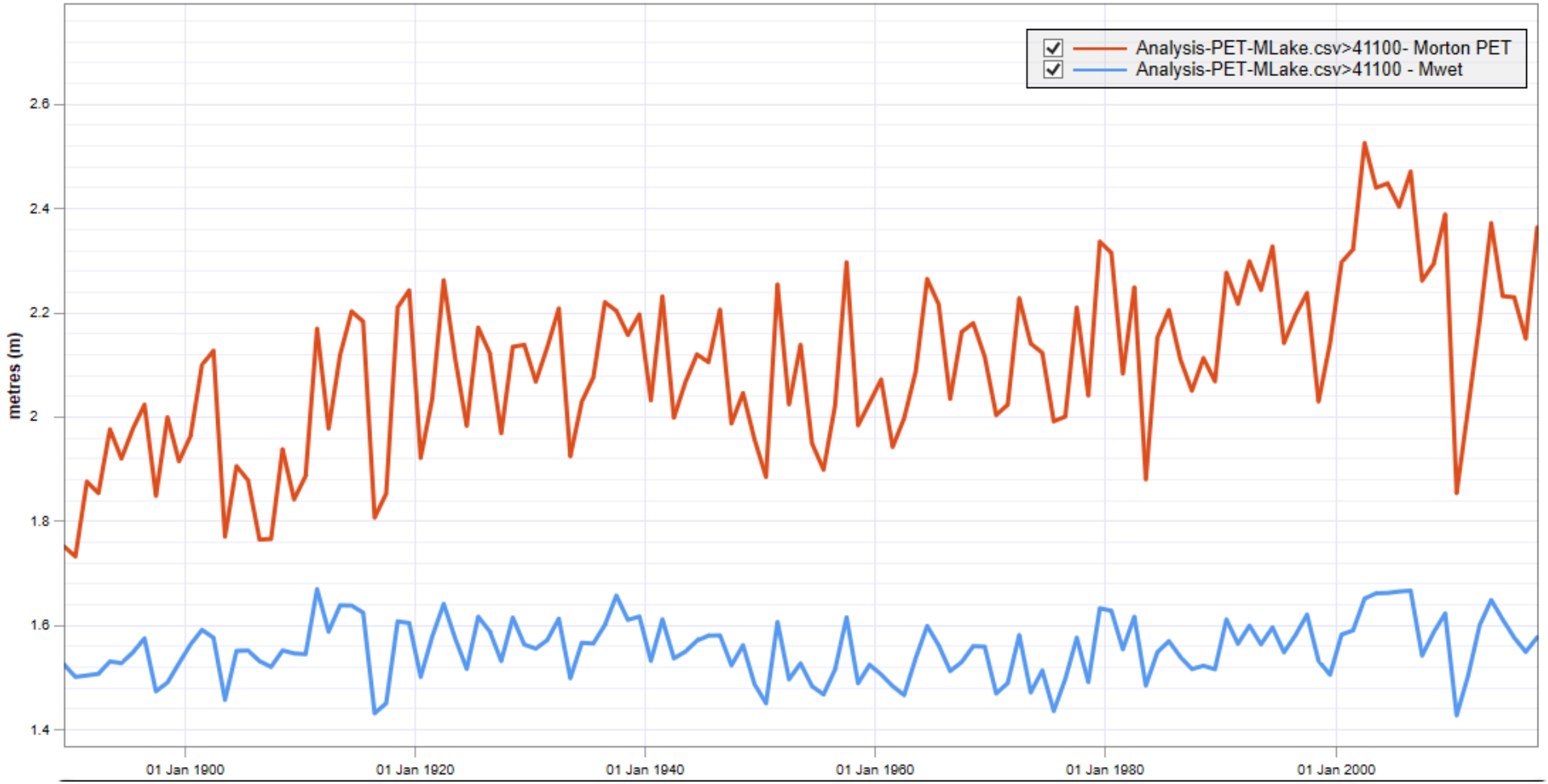

Figure A7.2: Differences in magnitude at an annual scale

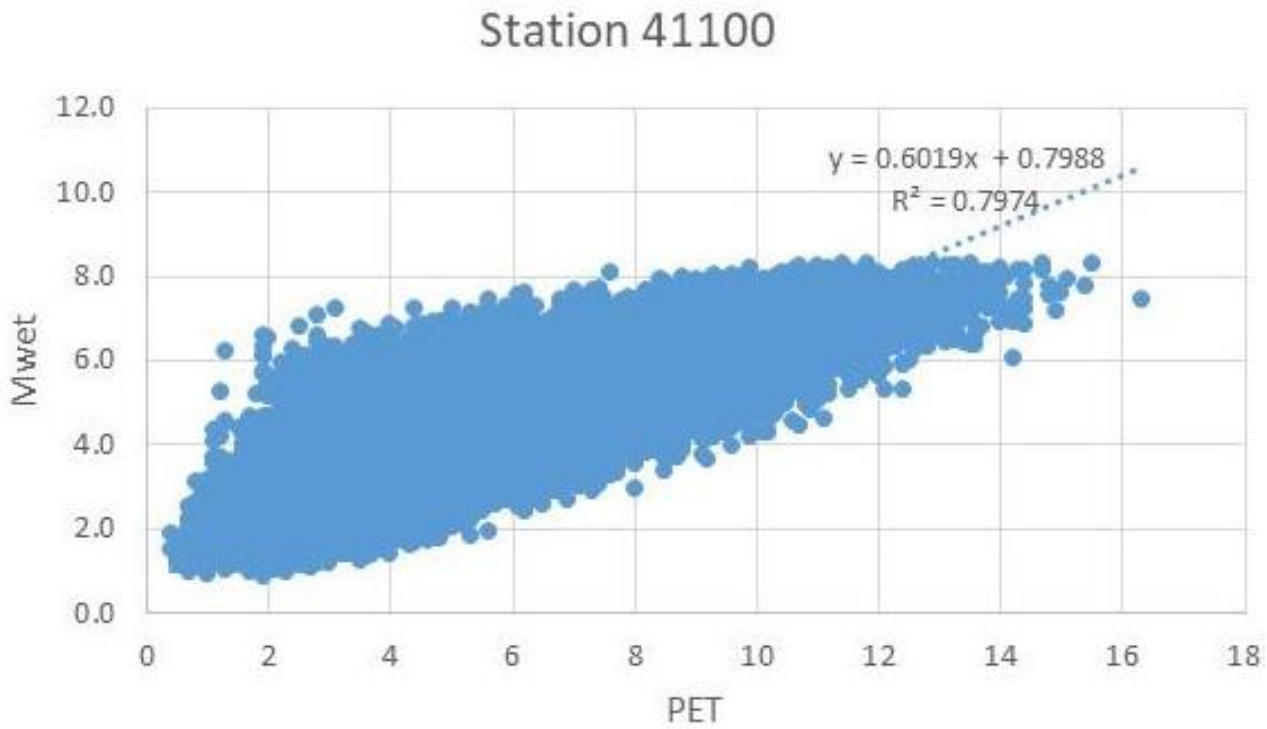

Figure A7.3: Correlation between PET and Mwet for a selected climate station (station ID: 41100)

APPENDIX 8: ADDITIONAL ADVICE PROVIDED BY DPIE-WATER: DATA ASSESSMENT AND HEADWATER CALIBRATION GUIDELINES

In response to questions asked by the Panel, DPIE-Water provided the following documents in relation to the Integrated Quantity and Quality Model (IQQM) software used for surface water modelling:

- Data Assessment and Headwater Calibration Guidelines (undated) – reproduced below
- Streamflow and Climate Data Review - Murrumbidgee Valley (undated) – a report to "review flow and climate data (streamflow, rainfall and evaporation) in the Murrumbidgee Valley for development of headwater rainfall runoff models and flow models for residual reaches. The review covers all available data of streamflow and climate gauges that are used in the Murrumbidgee Source modelling."
- Headwater Flow Calibration Report – Murrumbidgee Valley – Gauging Station 410025 Jugiong Creek (last dated 19 June 2018)
    - a report to "establish the rainfall-runoff model for the headwater catchment above the streamflow gauge 410025 (Jugiong Ck at Jugiong)."
- Headwater Flow Calibration Report – Murrumbidgee Valley – Gauging Station 410061 – Adelong Creek @ Batlow Road (last dated 24 Sept 2018)
    - a report to "establish the rainfall-runoff model for the headwater catchment above the streamflow gauge 410061 (Adelong Creek @ Batlow Road)."

DPIE-Water Data Assessment and Headwater Calibration Guidelines

1. Principles

The guidelines for assessing data and headwater calibration are intended to:

- Demonstrate that the hydrologist has thought about what they are doing and provide a record of that.
- Reflect the fact that this is not a model selection process.
- Produce the best possible model with the resources available. Recognising that one of the resources is time for the hydrologist to spend on calibration.

2. Data Assessment

The guidelines for assessing data vary depending on what type of data is being assessed. Common to all input time-series is the requirement that they are stored in our Time-Series Input Management System (TIMS), so that the exact version of the time-series was used can be established in the future.

3. Rainfall

- SILO Patch Point data has been adopted as the standard for rainfall data. Hydrologists can use other sources if they can't find a satisfactory SILO rainfall site. The patch point dataset has been chosen as it consists of observed data where available and is consistently gap-filled elsewhere.

- Preference is given to sites that have recent (last 30 years) observed data and are still operating. This preference is driven by the need for the models to be compared with observed results (ie: audit runs) over the recent period and to be updated each year.
- Rainfall sites are screened by location and length of record.
- Rainfall time-series should be visually inspected for problems.
- The correlation between the rainfall and runoff is calculated as a guide to which rainfall sites to trial in the rainfall-runoff calibration.
- Candidate rainfall sites are compared to a regional average rainfall series to test for trends that are only present at the candidate site.

4. Streamflow

- Streamflow sites are far rarer than climate stations so the threshold for excluding them from a model is much higher than for other data types.
- Quality codes should be inspected to determine if some parts of the record should be excluded from the calibration.
- The record of gaugings should be inspected to determine: the stability of the station's control, what flow ranges have been gauged, and how often the rating table is updated.
- The station instrument history should be inspected to see how the data was collected and over what period.
- Streamflow record should be visually inspected for problems.
- Streamflow should be checked for unexpected trends by comparing with nearby sites.

5. Evapotranspiration

- Morton's wet environmental evapotranspiration has been adopted based on data availability and McMahon et al. (2013) review. MWet is available through SILO.
- Station choice is based on finding the SILO patch point site that has a mean MWet close to the catchment mean value.
- MWet time-series should be visually inspected for problems.

6. Headwater Calibration

- Flow metrics should be based on the type catchment being modelled. For example, a catchment that is an inflow to a storage the overall total volume is more important.
- The amount of time to expend on calibration should be proportional to the relative contribution of the catchment.
- The decision to represent a catchment with a nested sub-catchment is a model selection decision and should be a calibration-validation comparison exercise.
- Calibration is carried out using FORS (https://qldhyd.atlassian.net/wiki/spaces/MET/pages/524366/Fors).
- The default objective function is SDEB.
- FORS should be run a number of times to explore how stable the model parameters are.
- If more than one rainfall site is available, then different rainfall inputs can be trialled.
- Cumulative model residuals should be checked to see if there is are trends in the results.
- The recession characteristics should be checked and fixing the recession parameters can be tried if they are not satisfactory.

- Model parameters should be compared with other catchments and significant deviations investigated.
- Rainfall scaling factors should be very carefully checked and justified. Factors outside of 20% probably are indicating data problems.

APPENDIX 9: NATIONAL AND STATE INITIATIVES

There are a range of initiatives to develop climate information for decision making. The following provides examples of initiatives at Australian national and state levels.

Climate Change in Australia (CCIA)

The Commonwealth Scientific and Industrial Research Organisation (CSIRO) and BOM have developed an assessment of observed and projected future changes in Australia, using eight GCMs from the CIMP5 and a range of RCPs (RCP2.6, RCP4.5 and RCP8.5). Projections are presented for eight regions with 15 subregions, covering Australia.

The CCIA provide two types of projection data for a range of climate variables, these include:

- *"projected climate changes (relative to the IPCC reference period 1986–2005), based on CMIP5 global climate models judged to perform well over Australia (Model evaluation) plus dynamic and statistical downscaling where appropriate*
- *'Application-ready' future climate data (where projected climate change data are applied to 30 years of observed data (1981–2010) for use in detailed risk assessments)" (CCIA, 2017)*

Victorian Government

CSIRO's Climate Science Centre has developed local-scale climate projections data for Victoria. Six GCMs have been dynamically downscaled based on the Conformal Cubic Atmospheric Model (CCAM) to provide projections at a 5 km by 5 km scale. The GCMs were chosen based on the CCIA as "*representative of the range of projected changes in temperature and rainfall as well as other climate variables*" (Clarke et al., 2019). It is noted that this method is limited by the use of a single downscaling model (CCAM).

The Victorian *Climate Change Act 2017* requires the preparations of sector-based Adaption Action Plans. The Water Sector Climate Change Adaptation Action Plan has been developed by the Victorian Government to ensure a climate change resilient water sector. Actions from the plan include the development of a "*framework to inform consistent and systematics embedment of climate change considerations into water business decisions*" and well as reviewing "*the use of climate change scenarios in water sector planning*" (DELWP, 2018).

Queensland Government

The Queensland Government undertakes water modelling to evaluate the ecological, social and economic impacts of water management. The *Queensland Water Act in 2018* requires that "*water related climate change effects on water availability, water use practices and the risk to land or water resources arising from use of water on land must be considered in the preparation of water plans*".

A 'Critical review of climate change in Queensland water models' report was released in November 2019 (Alluvium, 2019). The report aimed to "*provide an understanding of the science, state of the modelling and future investment needs in order to improve our understanding of existing climate variability and future climate change in Queensland's water models*".

The review found that "*further investment and collaborations is required to ensure climate change effects are considered in all water models, and this is done in a consistent way*". It was concluded that investments should be made for the incorporation of existing climate variability and future climate change in water models to enable better understanding of how water assets are measured now and into the future.

The report provided a range of recommendations, around the development of guidelines, collaboration across government agencies and between states and nationally, reviewing data

gaps, access and availability (e.g. centralisation and sharing of models and data), endorsing the use of a range of climate data (including the development and evaluation of paleoclimate data/research), leveraging climate research and the use of updated climate models, and the development of a consistent approach to modelling climate impacts.

South Australian Government

The South Australian Government, through SA Climate Ready, have developed a set of downscaled climate projections for the development of adaption planning (Enviro Data SA, 2020b). This has been done through the Goyder Institute for Water Research which is a partnership between the SA Department for Environment and Water, CSIRO, Flinders University, University of Adelaide and the University of South Australia.

A subset of GCMs were chosen based on their ability to reproduce the main climate drivers such as the IOD and ENSO. The GCMs were then statistically downscaled (using Nonhomogeneous Hidden Markov Model (NHMM) for daily multi-site rainfall and a statistical weather generator model was used to generate non-rainfall variables) to provide regional projections for a range of climate variables and two emissions scenarios (RCP4.5 and RCP8.5) were used (Enviro Data SA, 2020a).

Bureau of Meteorology

The BOM is currently bringing together hydrological modelling through its land surface model (AWRA-L) with information about future climate change from climate models. It is intended information about future impacts on Australia's water resources will be available by running AWRA-L together with other hydrological models with bias-corrected GCM and RCM data. Analysis of diverse user needs has informed the selection of a suite of bias-correction methods. GCM and RCM data is downscaled to 5 km resolution using simple bilinear interpolation and then bias-corrected to gridded observational reference data before being used to force AWRA-L.

The timeline for the release of a public facing website and a cloud-based data delivery service is scheduled for late 2020.

APPENDIX 10: CLIMATE DATA AND INFORMATION

Measured records – rainfall and evaporation

Rainfall data (collected since the late 19th century) and several data sources of evaporation and potential evapotranspiration (Appendix 7) are accessible through the Queensland Government's SILO database (Queensland Government, 2020c) and more recently, through the Bureau of Meteorology (BOM)(BOM, 2020e).

Several measures of evaporation and evapotranspiration estimates are referred to in the methodology with data in SILO. These include Penman-Monteith (short crop) reference evapotranspiration (FAO56) and Morton's wet environment areal potential evapotranspiration ($Mwet_t$). The methodology also refers to evaporation data from integrated water quantity and quality simulation model (IQQM) sites.

FAO56 evapotranspiration estimates are used mainly for irrigation purposes with evapotranspiration over a "*reference grass surface with height = 0.12m, albedo = 0.23, and a fixed plant-and-surface resistance (Allen et al., 1998)*" (Queensland Department of Environment and Science, pers comm, 13 February 2020).

Mwet provides ET over a large area, assuming unlimited supply of water, with an estimate being an areal average (Wang et al., 2001) (Queensland Department of Environment and Science, pers comm, 13 February 2020). Mwet is similar to FAO56 for wet climates but lower than FAO56 in dry climates (Queensland Department of Environment and Science, pers comm, 13 February 2020). Mwet is similar to FAO56 in coastal areas of south-eastern and eastern Australia (Queensland Department of Environment and Science, pers comm, 13 February 2020).

Potential evaporation (PET) is measured by the amount of water vaporised from a standard Class A pan over 24 hours (Queensland Government, 2020c). Class A pan observations are termed potential evaporation because the measurement is considered the amount of water that could potentially evaporate, but the value may not be representative of the actual evaporation occurring in the area around the pan (Queensland Department of Environment and Science, pers comm, 14 February 2020). Class A pan evaporation data have been collected since the early 1970s (DPIE-Water, 2019).

Synthetic estimates of Class A pan evaporation (Pan_{syn}) are developed to supplement the lack of observed data prior to 1970 and to create a complete data set from 1889 – present. Multiple regression was used to develop a model to estimate evaporation from a linear combination of solar radiation and vapour pressure deficit (Queensland Government, 2020b).

The rainfall data exhibits variability over time. An analysis of the residual mass curve from observed rainfall in NSW typically shows clustering of wet and dry years,

Paleoclimate proxies

Information revealing past climate conditions is contained in climate 'proxies' such as tree rings, carbonate speleothems (stalactites and stalagmites), pollens, corals, ice cores, sediments (ocean and lake) and packrat middens. Proxy records are used for climate reconstruction, which may include signals of severe and prolonged drought and decadal-scale changes in precipitation patterns.

Paleoclimate reconstructions provide a means of obtaining evidence of past climate variability prior to the period when instrumental records became available.

Paleoclimate research *"uses geologic and biologic evidence (climate proxies) preserved in sediments, rocks, tree rings, corals, ice sheets and other climate archives to reconstruct past*

climate in terrestrial and aquatic environments around the world" (USGS, 2019). Reconstructions of rainfall using paleoclimate records indicate sequences of wet and dry periods that have different properties to those observed, including periods of sustained aridity e.g. Vance et al. (2015), (A.D. 1174-1212).

Major climate drivers

The assessment of climate risk in the Methods Paper incorporates the key climate drivers operating in the regions of NSW. These are dominant weather systems operating in and around Australia that either independently or in combination affect the probability of, or amount of rain. The dominant drivers affecting NSW, represented in Figure A10.1, include:

- El-Niño Southern Oscillation (ENSO)/ La Niña
- Inter-decadal Pacific Oscillation (IPO)
- Indian Ocean Dipole (IOD)
- Southern Annular Mode (SAM)
- East Coast Lows (ECL)

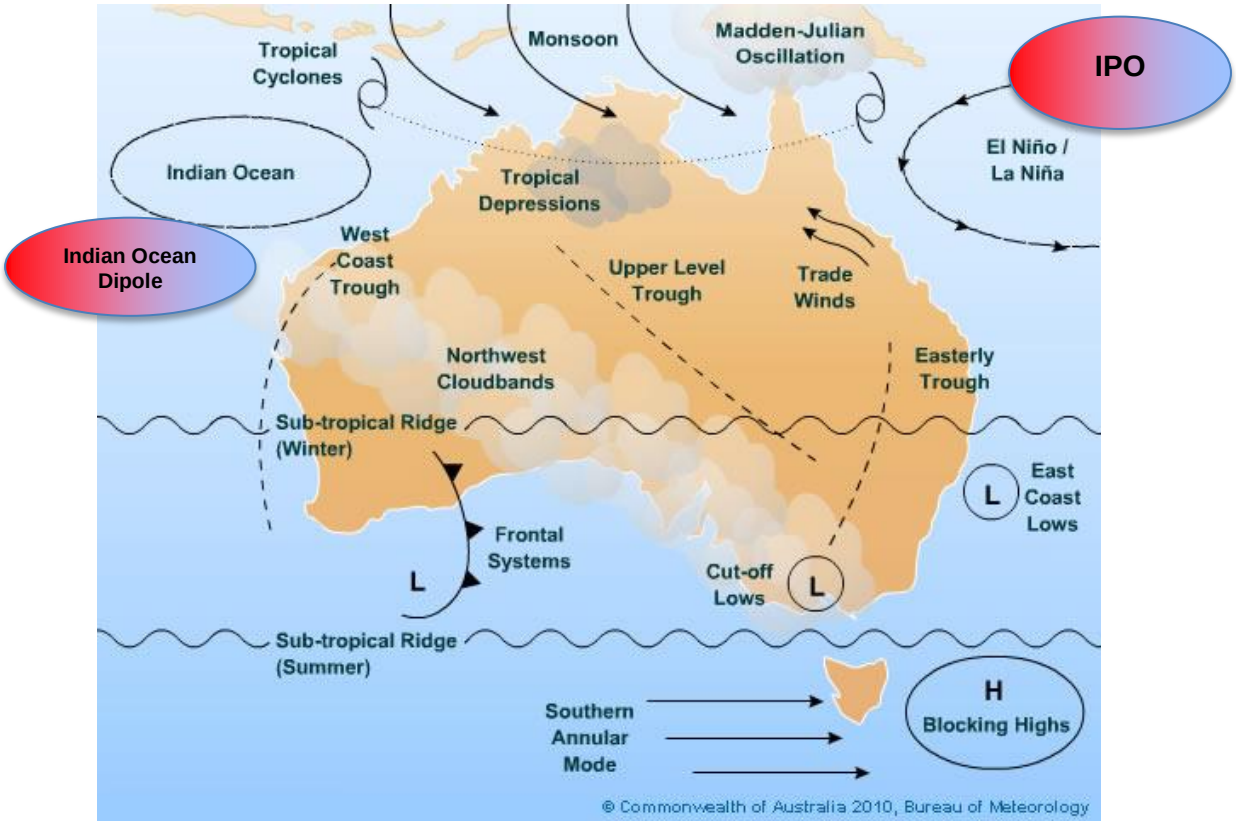

Figure A10.1: Australian climate influences

Source: DPIE-Water (2019) adapted from BOM (2020a)

El-Niño Southern Oscillation (ENSO)

The ENSO is an ocean-atmospheric climate pattern in the Pacific Ocean, which drives sea surface temperatures (SST) within parts of the region. An El Niño results in warming of SST in the central and eastern Pacific, while the reverse is the case with La Niña.

The Southern Oscillation Index (SOI) is calculated through air pressure differences between Darwin and Tahiti and gives an indicator of which cycle will occur and its intensity. Negative SOI usually leads to El Niño periods, resulting in reduced trade winds, cooler SST around northern Australia and dryer and warmer conditions for eastern Australia, including NSW. Positive SOI usually leads to La Niña, which brings wetter and cooler conditions to eastern Australia (OzCoasts, 2020).

El Niño/La Niña cycles, though irregular, tend to follow an autumn to autumn pattern building up to high points in winter/spring and tapering off in summer and autumn. El Niño events tend to last one cycle or year, while La Niña events can occur back-to-back (BOM, 2020g).

BOM reported on 21 January 2020 that ENSO has entered a neutral phase, likely to last until autumn, during which time more local or short-term influences, will have a stronger effect on NSW climate than ENSO (BOM, 2020c).

Inter-decadal Pacific Oscillation (IPO)

The IPO is characterised by SST change in the Pacific Ocean like the ENSO, but an IPO tends to have cycles of 20-30 years rather than much shorter El Niño cycles.

There are varying views on the direction and levels of dependency between the ENSO and IPO. (Queensland study, 2019) notes that the IPO indirectly influences NSW climate by influencing the strength and frequency of the ENSO cycles. Some experts argue that parts of the IPO may be driven by changes in ENSO activity from decade to decade, with the majority of decadal changes in ENSO occurring at random (BOM, pers comm, 14 January 2020). Determining the predictability of variability linked to the IPO, as well as the mechanisms underlying the IPO, are topics of current research.

Alluvium (2019) states the IPO negative periods (cooler) lean toward a La Niña dominance with the reverse for positive IPO (Queensland paper). Rainfall and stream flow tends to be greatest during simultaneous negative IPO and La Niña events with increased flooding risk for Eastern Australia. Further, when IPO is in the positive phase, the connection between ENSO and rainfall in Australia is weakened (Alluvium, 2019).

The period from 1999-2013 was a negative IPO with 2014-2016 a positive IPO (StatsNZ, 2020). However, there is some inconsistency in the literature about the timeframe of the IPO negative phase straddling the New Millennium period, with some reports showing the negative period starting around 1999 (Verdon-Kidd, 2019; StatsNZ, 2020) and some showing 1997 (Leonard, Westra, & Bennett, 2019) as well as some showing the end of the negative phase being around 2013/2014 (Verdon-Kidd, 2019; StatsNZ, 2020) and others showing ongoing at 2018 (Leonard et al., 2019).

Indian Ocean Dipole (IOD)

The IOD occurs in the tropical parts of the Indian Ocean and is the Indian Ocean's version of El Niño with positive, neutral and negative phases. Phases last between one and two years, starting in winter, peaking in autumn and decaying with the northern monsoon season. It has a significant effect on Australia's temperature and rainfall patterns.

The IOD brings lowers sea surface temperatures (SST) to the south-eastern parts of the Indian Ocean during a positive event, with reduced chances of rain across NSW (Figure A10.2).

There is some evidence to indicate increased risk of positive IOD in the future from modelling, but it would be difficult to quantify this risk (pers comm, 14 January 2020).

The positive IOD is more likely to coincide with La Nina and vice versa. BOM noted that Australia's driest year on record (1982) occurred during a simultaneous positive IOD and El Nino, while the wettest (1974) occurred during a negative IOD and La Nina (BOM, 2016).

The BOM issued a notice on 7 January 2020 that the IOD had returned to a neutral phase (from a strongly positive IOD) and is likely to remain so unless the end of autumn. A neutral IOD results in little change to Australia's climate (BOM, 2020d).

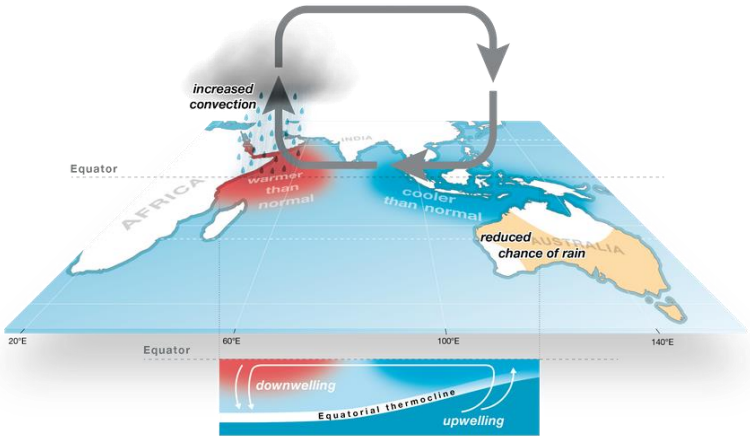

Figure A10.2: Indian Ocean Dipole (IOD) positive phase
Source: BOM (2016)

Southern Annular Mode (SAM)

The SAM, or Antarctic Oscillation, is the north/south movement of westerly rain-bearing winds across middle to higher latitudes of the Southern Hemisphere, which affect rainfall in southern Australia. SAM's influence on a region's rainfall is affected by the season in which it occurs. A 'positive' SAM event during autumn and winter brings storms further south and reduces rainfall in the southern third of Australia. However, during spring and summer, the positive SAM southerly storms cause changes to the local circulation that brings moist air inland, increasing the likelihood of rainfall across most of NSW (Queensland and BOM (below)).

A 'negative' SAM event during summer will bring drier than normal conditions across much of NSW. A negative SAM phase during winter bring wetter than normal conditions to southern parts of NSW but drier conditions to parts of northern NSW (BOM, 2020f).

There has been an increasing trend toward positive SAM events during summer and autumn (BOM, 2020f). Research is underway to better understand whether the positive tendency is a trend or variability as well as to better understand SAM's contribution to climate variability (BOM, 2020f).

A SAM lasts around ten days to two weeks, with a timeframe between events typically between a week and a few months (BOM, 2020f).

East Coast Lows (ECL)

Low-pressure weather systems that form off the east coast of Australia, including NSW, are called East Coast Lows. They are intense storms resulting in high winds, rainfall and heavy surf. ECL intensify quickly over 12 – 24 hours and are most common during autumn and winter, peaking in June (BOM, 2020b).

Overarching influence of the drivers

With the exception of the IPO, the drivers occur in days to months to one- or two-year cycles. The IPO experiences longer cycles lasting up to several decades. As such, the observational data, i.e. daily measurements of rainfall and ET, integrates the positive and negative influences of all the drivers in a single rainfall or ET measurement. The influence of each IPO cycle goes for a longer time period; only a handful of full cycles are captured in the observational data.

Work was done by the Eastern Seaboard Climate Change Initiative (ESCCI) - East Coast Low research program to better understand the impacts from potential changes to future

frequency and intensity of ECLs on the NSW coast. One of the projects considered the effects of future ECLs on water catchments through influence of and timing of heavy rain days. More information about ESCCI is at AdaptNSW (2020a).

Climate models

General circulation models

General circulation ('global climate') models (GCMs) are tools that can be used to project climate change under different greenhouse gas emissions scenarios. These mathematical models represent physical processes in the atmosphere, ocean, cryosphere and land surface and can simulate the response of the global climate system to increasing greenhouse gas concentrations (such as carbon dioxide, CO2) and changes in aerosols. GCM results are used by the Intergovernmental Panel on Climate Change (IPCC) to provide assessments of plausible impacts of climate change under the different emission scenarios. There are a number of models that have been developed by research organisations around the world.

One of the scenarios considered by the IPCC (2014) called RCP8.5 represents a future in which greenhouse gas emissions continue to rise markedly over the coming century. Another scenario called RCP2.6 represents a future in which action is taken to sustainably reduce greenhouse gas emissions over the coming century. RCP8.5 results in global warming (relative to preindustrial values) of approximately 3.2-5.4℃, whereas warming is reduced to approximately 0.9-2.3˚C under RCP2.6 (e.g. Power et al. (2017)). A third scenario called RCP4.5 has greenhouse gas concentrations that are lower than those in RCP8.5 but higher than those in RCP2.6, resulting in global warming that lies between the warming evident under the two more extreme scenarios.

The rate of future global warming will depend on future emissions of greenhouse gases, the feedback processes that dampen or reinforce natural or human-induced disturbances to the climate system, and unpredictable natural forcing factors such as large volcanic eruptions. Uncertain processes that will affect the rate of warming for a given emissions trajectory include cloud formation, water vapour and ice feedbacks, ocean circulation changes and natural cycles of greenhouse gases. Moreover, it is very difficult to assess the impact of climate change on specific locations (AAS, 2019).

This information and knowledge can be used to define an envelope of uncertainty for internally consistent projections of future climate. The width of this envelope expands over time, resulting in increasingly divergent trajectories that may need to be accounted for by planners (Stafford-Smith et al., 2011). The IPCC (2014) note two basic approaches to the handling of this uncertainty:

- the use of a small set of scenarios to characterise the range of impacts on water resources and systems
- the use of a very large number of scenarios to generate likelihood distributions of indicators of impact for use in risk assessments.

While there has been much debate on this issue in the literature, there is yet no consensus on the most suitable approach. This presents a key challenge for water planners who make adaptation decisions that have long lead times or that have consequences through the decades ahead when there will be an interplay between increasing scientific knowledge and persistent if not growing uncertainty and complexity (Bates, 2018).

Regional climate models

The scale of GCMs can limit regional and local scale factors and processes, which can be addressed through regional climate models (RCMs). 'Downscaling' is the process of refining global scale assumptions. This can be achieved through a range of methods, including change factor methods using observed datasets, statistical downscaling and dynamical downscaling.

The NSW and ACT Regional Climate Modelling (NARCliM) Project is a research partnership between the NSW and ACT governments and the Climate Change Research Centre at UNSW Sydney which provides projections of future climate variables like temperature and rainfall for south-east Australia. The NARCliM 1.0 data set was released in 2014 to enable government and local communities plan for the range of plausible future climate scenarios and was used by DPIE-Water in this project.

NARCliM 1.0 projections have been generated from four GCMs dynamically downscaled by three regional climate models (RCMs) to produce a 12-model ensemble at a 10 km horizontal resolution, for the time periods 1990 to 2009 (base-case), 2020 to 2039 (near future) and 2060 to 2079 (far future). This provides 60 years of model output. A further 60 years of model output is obtained by forcing the same three RCMs with 20 years of reanalysis data. Through this process, NARCliM 1.0 provides a total of 900 years of physically plausible data.

Since its release in 2014, the NARCliM developers have collated feedback and are in the final stages of developing an updated version that includes an additional scenario, an updated Global model and longer time series. This iteration (NARCliM 1.5) with updated projections is scheduled for release in the first quarter of 2020. Plans for future iterations are also in train.[1]

The NARCliM website provides guidance around how to use the available data from the 12 GCM-forced simulations and three reanalysis-forced simulations. Guidance from the modellers notes that any assessments of the impacts of climate change should consider the climate data from the range of simulations. A process is laid out to determine how to apply the data:

- Determine the relevant climate variables that will impact the systems under consideration (e.g. rainfall, evaporation, temperatures, etc.)
- Explore a range of future climate changes – different models are projecting different changes to precipitation, temperatures, etc.
- Select the NARCliM simulations to be analysed based on chosen criteria, e.g. which of the twelve simulations captures the largest variability or risk to the area under scope. It may not be practical to run numerical models on the full set of twelve.
- Consider the NARCliM simulation limitations, including bias, in the context of the methodology applied to it and consider how these may affect the results of the model. Bias can be corrected using bias correction or scaling observations. Models using global scale systems like ENSO need to consider what GCMs have been used or how they simulated the global system processes (AdaptNSW, 2020b)

[1] The Climate and Atmospheric Science unit within DPIE, which is leading the NARCliM project upgrades has indicated that NARCliM 1.5 is going through late stage quality assurance but will be available for NSW Government agencies to use prior its anticipated February 2020 release. A comparison of NARCLiM 1.0, 1.5 and 2.0 is at Appendix 8.

APPENDIX 11: STRATEGIC WATER PLANNING UNDER CLIMATE UNCERTAINTY

This appendix provides a discussion of the longer term and is beyond the technical focus of the Review. A key issue raised by the Panel from outset is how information, including uncertainties, is fed into decision making. A statement made by the Panel speaks to this: "*The DPIE report does not address the issue of how the deep uncertainties in the climate risk assessment get incorporated into the decision-making framework*".

Appropriate handling of climate uncertainty in strategic water planning is an active area of research and an evolving process for practitioners. Currently there is a disconnect between the academic literature and practice due to:

- differences in terminology used by the different disciplines involved
- an emphasis on accurate and precise prediction rather than a preparedness and resilience paradigm that evolves to meet emerging threats
- the perceived need to accurately characterise uncertainty (leading to 'decision paralysis by analysis' (Peterson, Cumming, & Carpenter, 2003)) versus the disempowering impacts of large levels of uncertainty and complexity on practical decision making (which can lead to overly conservative decisions such as 'gold plating')
- little synthesis of climate adaptation research findings in terms of their implications for practical decision making (Bates (2018) and references therein).

Concepts of adaptive management in uncertainty

Because of the presence of deep and irresolvable climate uncertainty, decision-makers are being encouraged to look for robust decisions that provide satisfactory performance across a large but not inexhaustible range of plausible futures. That is, to make plans that are flexible and can be adapted over time in response to how future events (such as droughts and heatwaves) unfold. This exercise offers insights into conditions under which problems occur and renders the socio-political, cultural, economic and ecological trade-offs transparent.

Hallegatte (2009) lists five approaches to risk mitigation:

- 'no-regret' strategies that provide benefits in the absence of projected climate change
- reversible options (e.g., adoption of cheap-to-retrofit designs)
- 'safety margins' (i.e., over-design at null or low cost)
- soft adaptation strategies (such as the use of institutional tools to create a long-term prospective, and demand control and water reuse)
- reduction of decision time horizons (e.g., avoiding long-term commitments and choosing short-lived decisions).

The types of strategies listed above provide a reduction in sensitivity to climate model and emissions scenario selection, model error and (probably irreducible) uncertainty. While these strategies may preclude optimal performance, they are more likely to succeed than optimal decision- and policymaking based on unrealistic expectations of predictive accuracy.

Stafford-Smith et al. (2011) have presented a more general framework for reducing complexity and uncertainty that is aimed at helping decision-makers to arrive at better adaptation solutions. It subsumes the five approaches articulated by Hallegatte (2009) and

involves a systematic approach to categorising the interactions between decision lifetime (the sum of lead time and consequence time), the type of driver for uncertainty (e.g., monotonic with an uncertain rate of change or indeterminate) and the nature (type and extent) of adaptation response options. These three factors combine to require different approaches to risk management. In these contexts, the framework provides useful risk mitigation options and describes some available options for reducing decision risk. For these reasons, it has been incorporated into a new set of climate change adaptation guidelines for the Australian urban water industry (WSAA, 2016).

A complementary approach is dynamic adaptive policy pathways (DAPP) which emphasizes dynamic adaptation (iterative risk management) over time. It offers a natural way for handling the vulnerabilities[2] identified through robust decision-making (Kwakkel, Haasnoot, & Walker, 2016; Deltares, 2019).

Many investment and policy decisions in water management have significant and often long-term consequences but often require near-term decisions. Making sound near-term decisions is critical, but individual and societal perspectives differ in terms of competing and changing beliefs, attitudes, values and preferences. When decision makers and analysts face a deeply uncertain future (e.g. due to projected climate change or new information about past climate variability), they need more than traditional prediction or scenario-based decision methods to evaluate alternative policies and actions and make decisions.

The DAPP approach aims to support the development of an adaptive plan that can deal with deep uncertainty. An adaptive plan specifies actions to be taken immediately to be prepared for the near future and actions to be taken now to keep options open if future adaptation is needed. The exploration of adaptation pathways is one of the main ingredients of an adaptive plan and is consistent with the general planning approach of DPIE-Water. As illustrated in Figure A11.1, adaptation pathways describe a sequence of policy actions or investments in institutions and infrastructure over time to achieve a set of pre-specified objectives under uncertain but changing conditions.

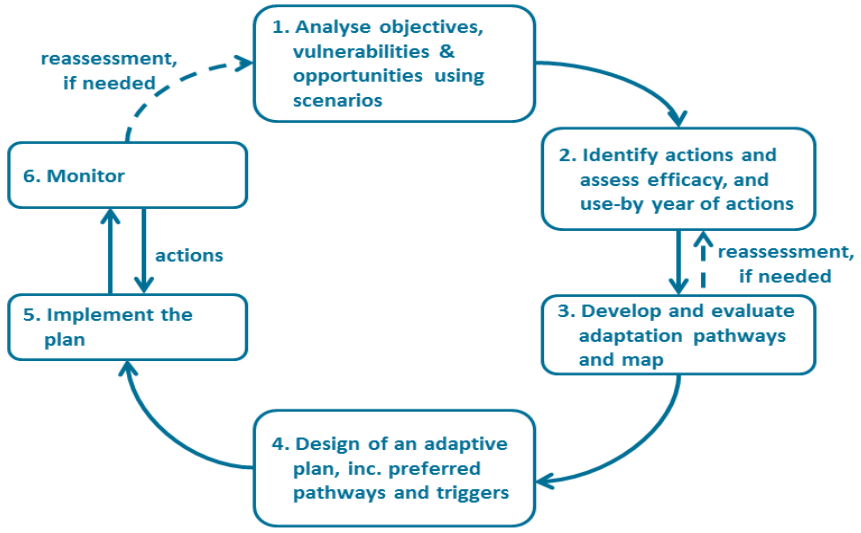

Figure A11.1: Schematic of the dynamic adaptive policy pathways (DAPP) approach

Source: Deltares (2019) modified from Haasnoot et al. (2013)

Adaptation pathway maps can provide insight into policy options, the sequencing of actions over time, potential 'lock-ins', and path dependencies. Figure A11.2 displays an adaptation map and scorecard for a hypothetical example involving a planning horizon of 100 years.

[2] "Vulnerability is a state of susceptibility to harm from exposure to stresses associated with environmental and social change and from the absence of capacity to adapt" (ScienceDirect, 2020)

Starting from the present day (Time 0), planning targets begin to be missed after four years (i.e. when a tipping point is reached). Following the horizontal grey line depicting the current plan, there are four available options (Actions A to D). For the two scenarios considered (low-end and high-end), Pathway 1 (Action A, red line) and Pathway 9 (Action D, blue line) can meet the targets over the planning horizon. However, there is a marked difference in cost (compare the relative costs in the scorecard). Pathway 8 (Action C followed by Action D in approximately 85 years into the future under the high-end scenario) incurs the lowest cost overall. If Action B (yellow line) was chosen initially, a tipping point is reached in about five more years. Then a shift to one of the other three Actions (A, C, or D) would be required to achieve the targets over the planning horizon. Decisions from this tipping point may incur additional but unnecessary costs. For example, Pathway 2 (Action B followed by Action A) incurs the highest cost overall.

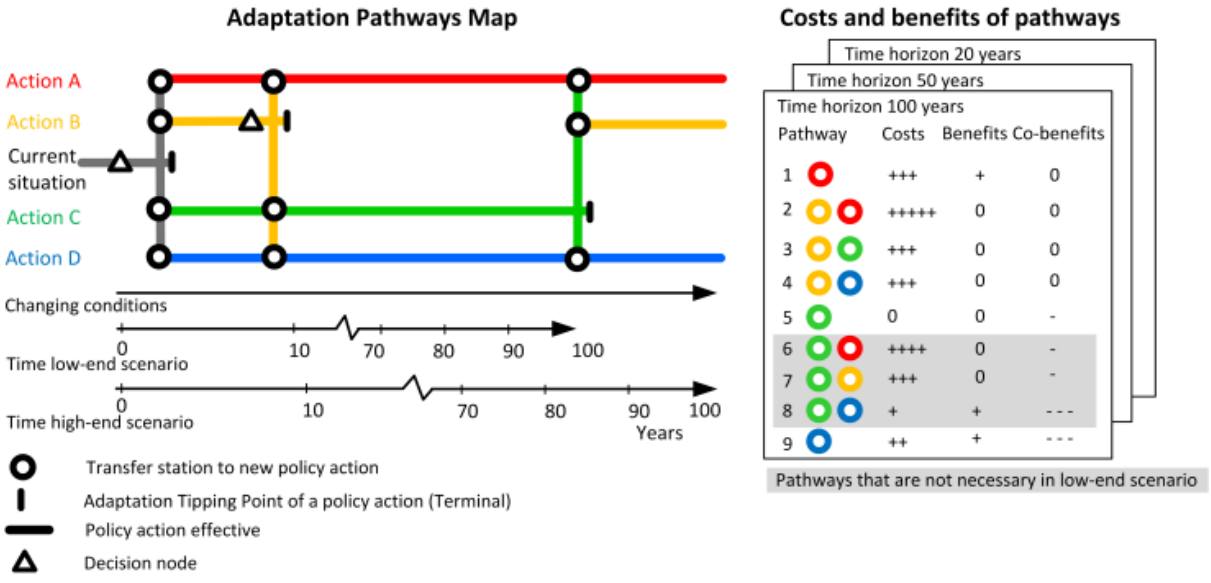

Figure A11.2: Hypothetical example of an adaption pathways map and a scorecard

Source: Deltares (2019) modified from Haasnoot et al. (2013)

'Tipping points' are a key concept in DAPP. They specify the conditions under which an existing policy action or portfolio of actions will fail to meet objectives, and thus will signal when new actions are needed. The timing of a tipping point is scenario dependent (Figure A11.3). The concept of tipping points makes it easier to update plans when new climate information becomes available, or when policy settings change, in which case only the timing of the actions needs to be revised. Thus, the DAPP approach contains elements from a vulnerability bottom-up approach. It differs from the classical top-down approach to adaptation in which the underlying question is: What if climate changes according to a particular scenario? This is followed by analyses of the cause-effect chain from pressures to impact. If the impact is such that policy objectives fail, new adaptation measures are defined to overcome the problem. Then the cause-effect chain is analysed again to answer the question: What if this particular scenario becomes reality and we implement measure X, will the objectives be met?

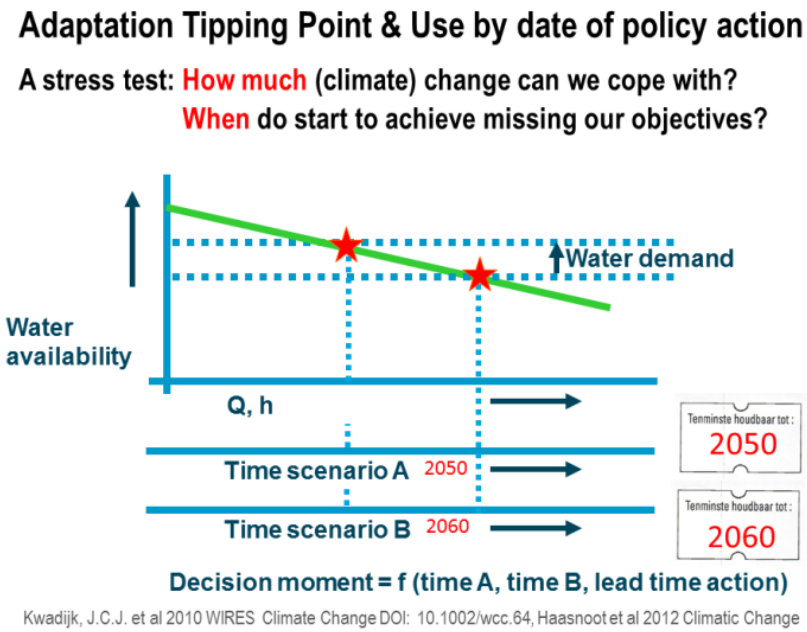

Figure A11.3: Hypothetical example of adaptation tipping points
Source: Deltares (2019)

Communication

Adaptive responses to climate variability and change will be shaped by the geographical, hydrological, socio-economic and political settings confronting planners and the financial resources available. There is a delicate balance to be struck between being too precise about global warming impacts (which can lead to overconfidence in the perceived accuracy of projections) or making openly vague statements that contain less information than that indicated by expert consensus. Subtle changes in the format of communication can affect the way that the message is perceived by the target audience.

Effective communication and knowledge brokering will require ongoing and close contact between scenario developers and stakeholders, and the distribution of science-based information that is tailored to meet their needs (Jacob & van den Hurk, 2009; Ho & Budescu, 2019). The challenge is to identify and validate communication methods that are accurate, transparent, effective and preserve trust in the messenger(s) and their message may benefit from a careful, evidence-based assessment of how to design and tailor communication to the public to increase awareness and promote collective action about the mounting seriousness of climate change impacts.

Summary

There are several key ingredients for successful management of climatic risk (Bates, 2018):

- Climate is only one of many stressors that influence water planning and management decisions and outcomes. Climate-driven hydrological changes will combine with, and possibly amplify, the impacts of other sources of stress, including population growth, economic priorities, infrastructure maintenance/replacement, loss of biodiversity and hence ecosystem services and amenity, invasive exotic species, social behaviour and preferences, and land-use change. These factors could compromise water security and availability if they are inappropriately monitored and managed. Thus, a systematic examination of potential adaptation responses over a wide range of plausible futures will need to consider the interplay between climatic, economic, environmental and cultural factors.

- The primary focus of adaptation planning should be a preparedness and resilience rather than a prediction paradigm. The state of preparedness needs to evolve with emerging threats. The emerging threats are likely to involve unexpected incremental changes in the factors listed above as well as ‘surprises’ (such as rare high-impact events).
- Consideration of a small number but wide range of scenarios to facilitate decisiveness and action rather than ‘paralysis by analysis’. Rare high-impact events should be included in assessments and notions of the ’most likely’ projection or scenario, or the ‘best guess’, abandoned.
- Use of reliability, resilience and vulnerability criteria to assess asset performance under selected scenarios and adaptation responses (e.g. water demand management). Also, the benefits and costs of immediate adaptation and retrofitting infrastructure should also be assessed.
- The DAPP approach lends itself to the adoption of a continuous cycle of planning and evaluation. It leads directly to the development of a set of contingency plans with identified tipping points and alternative courses of action. Planning, resourcing and construction lead times need to be identified, as well as any reasonable means for reducing them
- The adaptation process may involve ‘transformational’ change rather than small, once-off adjustments to existing operating rules and practices. The social acceptability of large-scale change could be problematic.
- Diagnosis of the psychological, social and institutional limits and barriers to adaptation (Jones & Boyd, 2011; Stafford-Smith et al., 2011; Wise et al., 2014). The removal of these barriers may require a preparedness to consider and plan for radical change and consideration of issues such as social equity and justice.
- Engagement with social scientists will be required on issues such as social equity, limits and barriers to adaptation and communication.
- Adoption of adaptive governance arrangements and markets.

REFERENCES

AAS, *Australian Academy of Science*. (2019). *What are the uncertainties and their implications?* Retrieved 14 November 2019, from https://www.science.org.au/learning/general-audience/science-climate-change/8-what-are-uncertainties-and

AdaptNSW. (2020a). *Eastern Seaboard Climate Change Initiative*. Retrieved 25 February 2020, from https://climatechange.environment.nsw.gov.au/Impacts-of-climate-change/East-Coast-Lows/Eastern-Seaboard-Climate-Change-Initiative

AdaptNSW. (2020b). *Guidance on NARCliM Models*. Retrieved 25 February 2020, from https://climatechange.environment.nsw.gov.au/Climate-projections-for-NSW/Download-datasets/Guidance-on-NARCliM-Models

Allen, R.G., Pereira, L.S., Raes, D., & Smith, M. (1998). *Crop evapotranspiration — guidelines for computing crop water requirements*. Food and Agriculture Organization, Rome. Retrieved from http://www.fao.org/3/x0490e/x0490e00.htm

Alluvium. (2019). *Critical review of climate change and water modelling in Queensland - Final Report*. Prepared collaboratively with CSIRO and University of Newcastle on behalf of the Queensland Water Modelling Network, Queensland Government, Brisbane

Bates, B.C. (2018). *From Prediction to Scenario Analysis: A Brief Review and Commentary Bridging Science and Policy Implication for Managing Climate Extremes* (pp. 207-220): World Scientific Series on Asia-Pacific Weather and Climate, World Scientific and APEC Climate Center.

BOM, *Bureau of Meteorology*. (2016). *Indian Ocean Dipole in Australia*. Retrieved 25 February 2020, from http://www.bom.gov.au/climate/iod/images/IOD-in-Australia.pdf

BOM, *Bureau of Meteorology*. (2020a). *Australian Climate Influences*. Retrieved 25 February 2020, from http://www.bom.gov.au/watl/about-weather-and-climate/australian-climate-influences.shtml?bookmark=introduction

BOM, *Bureau of Meteorology*. (2020b). *East coast lows*. Retrieved 25 February 2020, from http://www.bom.gov.au/weather-services/severe-weather-knowledge-centre/eastcoastlows.shtml

BOM, Bureau of Meteorology. (2020c). *ENSO Wrap-Up. Current state of the Pacific and Indian Ocean*. Retrieved 25 February 2020, from http://www.bom.gov.au/climate/enso/wrap-up/archive/20200121.archive.shtml

BOM, Bureau of Meteorology. (2020d). *Indian Ocean influences on Australian climate*. Retrieved 14 February 2020, from http://www.bom.gov.au/climate/iod/

BOM, *Bureau of Meteorology*. (2020e). *Long-range weather and climate*. Retrieved 19 February 2020, from http://www.bom.gov.au/climate/

BOM, *Bureau of Meteorology*. (2020f). *Southern Annular Mode*. Retrieved 14 February 2020, from http://www.bom.gov.au/climate/about/?bookmark=sam

BOM, *Bureau of Meteorology*. (2020g). *When do El Nino and La Nina events occur?* Retrieved 25 February 2020, from http://www.bom.gov.au/climate/enso/history/ln-2010-12/ENSO-when.shtml

CCIA, *Climate Change in Australia*. (2017). *Projections for Australia's NRM Regions*. Retrieved 25 February 2020, from https://www.climatechangeinaustralia.gov.au/en/climate-projections/explore-data/about-data/data-availability/

Clarke, J.M., Grose, M., Thatcher, M., Hernaman, V., Heady, C., Round, V., Rafter, T., Trenham, C., & Wilson, L. (2019). *Victorian Climate Projections 2019 Technical Report*. Melbourne Australia

Deltares. (2019). *Dynamic Adaptive Policy Pathways: supporting decision making under uncertainty using Adaptation Tipping Points and Adaptation Pathways in policy*

analysis. Retrieved 16 November 2019, from https://www.deltares.nl/en/adaptive-pathways/

DELWP, *Victoria Department of Environment Land Water and Planning*. (2018). *Pilot Water Sector Climate Change Adaptation Action Plan*.

DPIE-Water. (2019). *Draft Report of the Water Modelling Unit: Developing climate data sets for use in climate risk assessment for Regional Water Strategies*.

Enviro Data SA. (2020a). *SA Climate Ready. FAQ*. Retrieved 25 February 2020, from https://data.environment.sa.gov.au/Climate/SA-Climate-Ready/Pages/FAQ.aspx

Enviro Data SA. (2020b). *SA Climate Ready. Introduction*. Retrieved 25 February 2020, from https://data.environment.sa.gov.au/Climate/SA-Climate-Ready/Pages/default.aspx

Haasnoot, M., Kwakkel, J.H., Walker, W.E., & ter Maat, J. (2013). Dynamic adaptive policy pathways: A method for crafting robust decisions for a deeply uncertain world. *Global Environmental Change, 23*(2), 485-498. doi: https://doi.org/10.1016/j.gloenvcha.2012.12.006

Hallegatte, S. (2009). Strategies to adapt to an uncertain climate change. *Global Environmental Change, 19*(2), 240-247. doi: https://doi.org/10.1016/j.gloenvcha.2008.12.003

Ho, E.H., & Budescu, D.V. (2019). Climate uncertainty communication. *Nature Climate Change, 9*(11), 802-803. doi: 10.1038/s41558-019-0606-6

IPCC, *Intergovernmental Panel on Climate Change*. (2014). *Freshwater Resources Climate Change 2014 – Impacts, Adaptation and Vulnerability: Part A: Global and Sectoral Aspects: Working Group II Contribution to the IPCC Fifth Assessment Report: Volume 1: Global and Sectoral Aspects* (Vol. 1, pp. 229-270). Cambridge: Cambridge University Press.

Jacob, D., & van den Hurk, B. (2009). *Climate change scenarios at the global and local scales Climate Change Adaptation in the Water Sector* (pp. 23-33): Earthscan.

Jones, L., & Boyd, E. (2011). Exploring social barriers to adaptation: Insights from Western Nepal. *Global Environmental Change, 21*(4), 1262-1274. doi: https://doi.org/10.1016/j.gloenvcha.2011.06.002

Kwakkel, J.H., Haasnoot, M., & Walker, W.E. (2016). Comparing Robust Decision-Making and Dynamic Adaptive Policy Pathways for model-based decision support under deep uncertainty. *Environmental Modelling & Software, 86*, 168-183. doi: https://doi.org/10.1016/j.envsoft.2016.09.017

Leonard, M., Westra, S., & Bennett, B. (2019). *Multisite rainfall and evaporation data generation for the Macquarie Water infrastructure project*. Report prepared for the NSW Department of Industry by the University of Adelaide

McMahon, T.A., Peel, M.C., Lowe, L., Srikanthan, R., & McVicar, T.R. (2013). Estimating actual, potential, reference crop and pan evaporation using standard meteorological data: a pragmatic synthesis. *Hydrology and Earth System Sciences, 17*, 1131-1363.

Morton, F.I. (1983). Operational estimates of areal evapotranspiration and their significance to the science and practice of hydrology. *Journal of Hydrology, 66*, 1-76.

OzCoasts. (2020). *Climate Change*. Retrieved 25 February 2020, from https://ozcoasts.org.au/indicators/coastal-issues/climate_change/

Peterson, G.D., Cumming, G.S., & Carpenter, S.R. (2003). Scenario Planning: a Tool for Conservation in an Uncertain World. *Conservation Biology, 17*(2), 358-366. doi: 10.1046/j.1523-1739.2003.01491.x

Power, S.B., Murphy, B., Chung, C., Delage, F., & Ye, H. (2017, 9 February). Droughts and flooding rains already more likely as climate plays havoc with Pacific weather, *The Conversation*. Retrieved from https://theconversation.com/droughts-and-flooding-rains-already-more-likely-as-climate-change-plays-havoc-with-pacific-weather-71614

Queensland Government. (2020a). *Climate Variables*. Retrieved 25 February 2020, from https://www.longpaddock.qld.gov.au/silo/about/climate-variables/

Queensland Government. (2020b). *Open data portal: SILO climate database - evaporation - synthetic*. Retrieved 19 February 2020, from https://www.data.qld.gov.au/dataset/silo-climate-database-evaporation-synthetic

Queensland Government. (2020c). *SILO - Australian Climate Data from 1889 to Yesterday*. Retrieved 19 February 2020, from https://www.longpaddock.qld.gov.au/silo/

ScienceDirect. (2020). *Vulnerability*. Retrieved 25 February 2020, from https://www.sciencedirect.com/topics/earth-and-planetary-sciences/vulnerability

Stafford-Smith, M., Horrocks, L., Harvey, A., & Hamilton, C. (2011). Rethinking adaptation for a 4 °C world. *Philosophical Transactions of the Royal Society A: Mathematical, Physical and Engineering Sciences, 369*(1934), 196-216. doi: doi:10.1098/rsta.2010.0277

StatsNZ. (2020). *Interdecadal Pacific Oscillation*. Retrieved 25 February 2020, from http://archive.stats.govt.nz/browse_for_stats/environment/environmental-reporting-series/environmental-indicators/Home/Atmosphere-and-climate/interdecadal-pacific-oscillations.aspx

USGS, *United States Geological Survey*. (2019). *Paleoclimate research: Lessons from the Past, Roadmap for the Future*. Retrieved 13 November 2019, from https://www2.usgs.gov/landresources/lcs/paleoclimate/

Vance, T.R., Roberts, J.L., Plummer, C.T., Kiem, A.S., & van Ommen, T.D. (2015). Interdecadal Pacific variability and eastern Australian megadroughts over the last millennium. *Geophysical Research Letters, 42*(1), 129-137. doi: 10.1002/2014gl062447

Verdon-Kidd, D.C. (2019). *Development of multi-site rainfall and evaporation data for the Lachlan Regional Water Strategy*. Report prepared for the NSW Department of Industry by the University of Newcastle

Wang, Q.J., Chiew, F.H.S., McConachy, F.L.N., James, R., de Hoedt, G.C., & Wright, W.J. (2001). *Climatic Atlas of Australia Evapotranspiration, Bureau of Meteorology, Australia,*.

Wise, R.M., Fazey, I., Stafford Smith, M., Park, S.E., Eakin, H.C., Archer Van Garderen, E.R.M., & Campbell, B. (2014). Reconceptualising adaptation to climate change as part of pathways of change and response. *Global Environmental Change, 28*, 325-336. doi: https://doi.org/10.1016/j.gloenvcha.2013.12.002

WSAA, *Water Services Association of Australia*. (2016). *Climate Change Adaptation Guidelines*. Project Report WSA 303 - 2016 v1.2